The Great Glen Caledonian Igneous Suite: New geochemical and geochronological insights into the final stages of the Caledonian Orogeny

Eilidh Jean McLaren Milne BSc (Hons)

Submitted in fulfilment of the requirements for the degree of Master of Science by Research

School of Geographical and Earth Sciences

College of Science and Engineering

University of Glasgow

August 2019

Abstract

The Caledonian Orogeny is responsible for the consolidation of British and Irish crust and the intrusion of an extensive suite of granite (sensu – lato) plutons and dykes. Said intrusions are collectively known as the Newer granites and are a natural laboratory for studying mid-crustal petrogenetic processes in a post-collisional setting. Recent workers have highlighted inconsistencies in the timeline of events for the final stages of the orogeny (the so-called 'Scandian phase'), particularly regarding the timing and geodynamic processes associated with Newer granite magmatism. New single grain U – Pb zircon data from three undated Newer granite bodies (Glen Loy, Cluanie and Loch Linnhe), and whole rock geochemical data from five (Glen Loy, Cluanie, Loch Linnhe Clunes and Scaddle) will facilitate new insights into said issues.

Intrusions at Glen Loy, Cluanie and Loch Linnhe return ages of 433.6 +/- 3.9, 437.7 +/- 3.3 and 439.4 +/-3.1 respectively (+/- 2σ). Their emplacement therefore predates estimates for slab break-off, usually invoked as the mechanism behind Newer granite melt generation, which requires some explanation. The geochemical profiles for Scaddle and Loy strongly suggest a mantle source, which requires explanation given their emplacement coincides with what is traditionally accepted as peak crustal thickening - another contradictory set of circumstances. As detailed, the newly acquired data is largely inconsistent with previously accepted geodynamic timelines for so called 'Scandian' events and supports a growing array of data suggesting the demarking of Caledonian orogenic events has been erroneous. A new model is presented, which includes Baltica - Laurentia collision occurring far earlier than traditional estimates of c. 430 Ma; instead occurring at c. 450 Ma. All subsequent events and processes are associated with crustal thickening, slab rollback, and eventual slab break-off.

Table of Contents

List of Tables

List of Figures

List of Accompanying Material

GLEN LOY

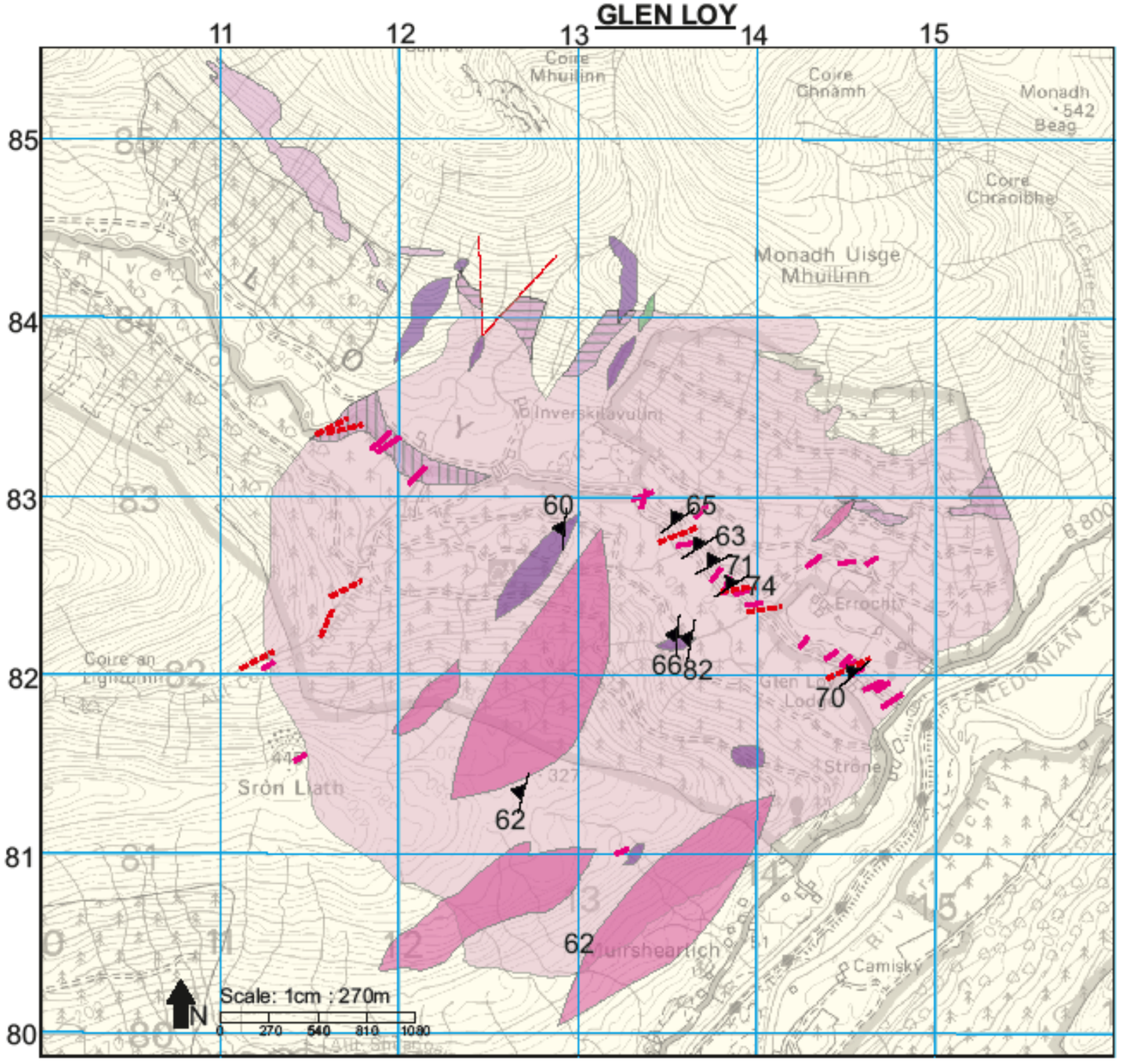

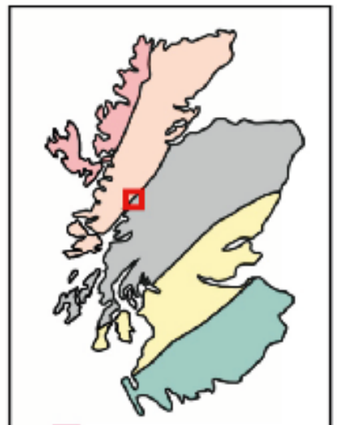

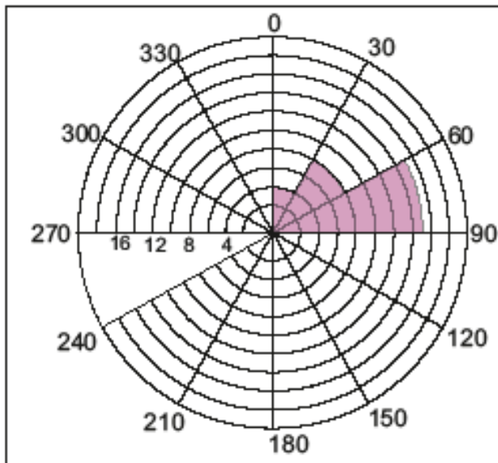

Rose diagram showing the orientation of the pegmatite intrusions observed throughout the Glen Loy body. The intrusions were predominately vertical/near vertical.

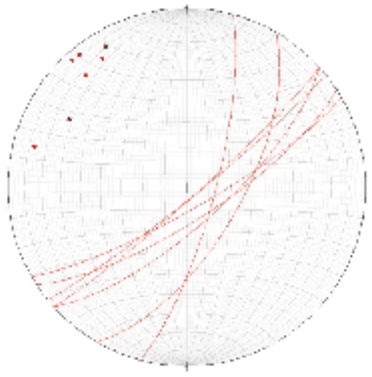

Stereonet visualising the strike and dip of the fabric observed in the shear zones. Stereonet produced via the program visible geology: https://app.visiblegeology.com.

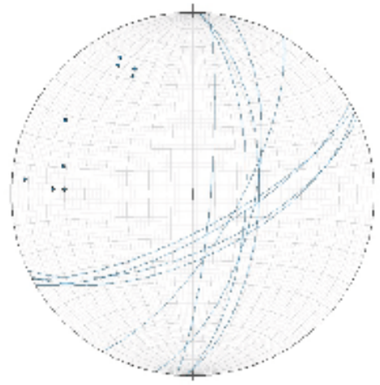

Stereonet visualising the strike and dip of the primary magmatic fabric. Stereonet produced via the program visible geology: https://app.visiblegeology.com.

Legend

Igneous Facies:

Diorite: Medium grained (~3mm). Typically 50 - 70% plagioclase; 15 - 30% hornblende; 0 - 10% biotite; 0 - 5% pyroxene, 0 - 15% quartz.

Hornblende Gabbro: Coarse grained (~5mm). Typically 5 - 30% plagioclase, 25 - 45% hornblende 5 - 15% biotite; 20 - 40% pyroxene.

Granite Pegmatite: Medium - coarse grained (3 - 5mm). Typically 50 - 70% K-feldspar; 5 - 25% plagioclase; 10 - 20% quartz; 0 - 15% muscovite; 0 - 5% biotite.

Mafic Intrusions: Very fine grained (<0.5mm). Typically 40% clinopyroxene; 25% hornblende; 25% biotite.

Garnet and biotite rich diorite: Diorite with garnet content of up to 25%. Biotite content >20%.

Biotite rich diorite: Diorite with biotite content of up to 30%.

Sedimentary facies:

Loch Eil Facies: Quartz and feldspar dominated granulite with occasional biotite rich calc silicate lenses.

Measurements and Structural Info:

Fault zone (unobserved).

Shear zone.

62 **Strike and dip of magmatic fabric:** Defined by alignment of hornblende grains.

GLEN SCADDLE

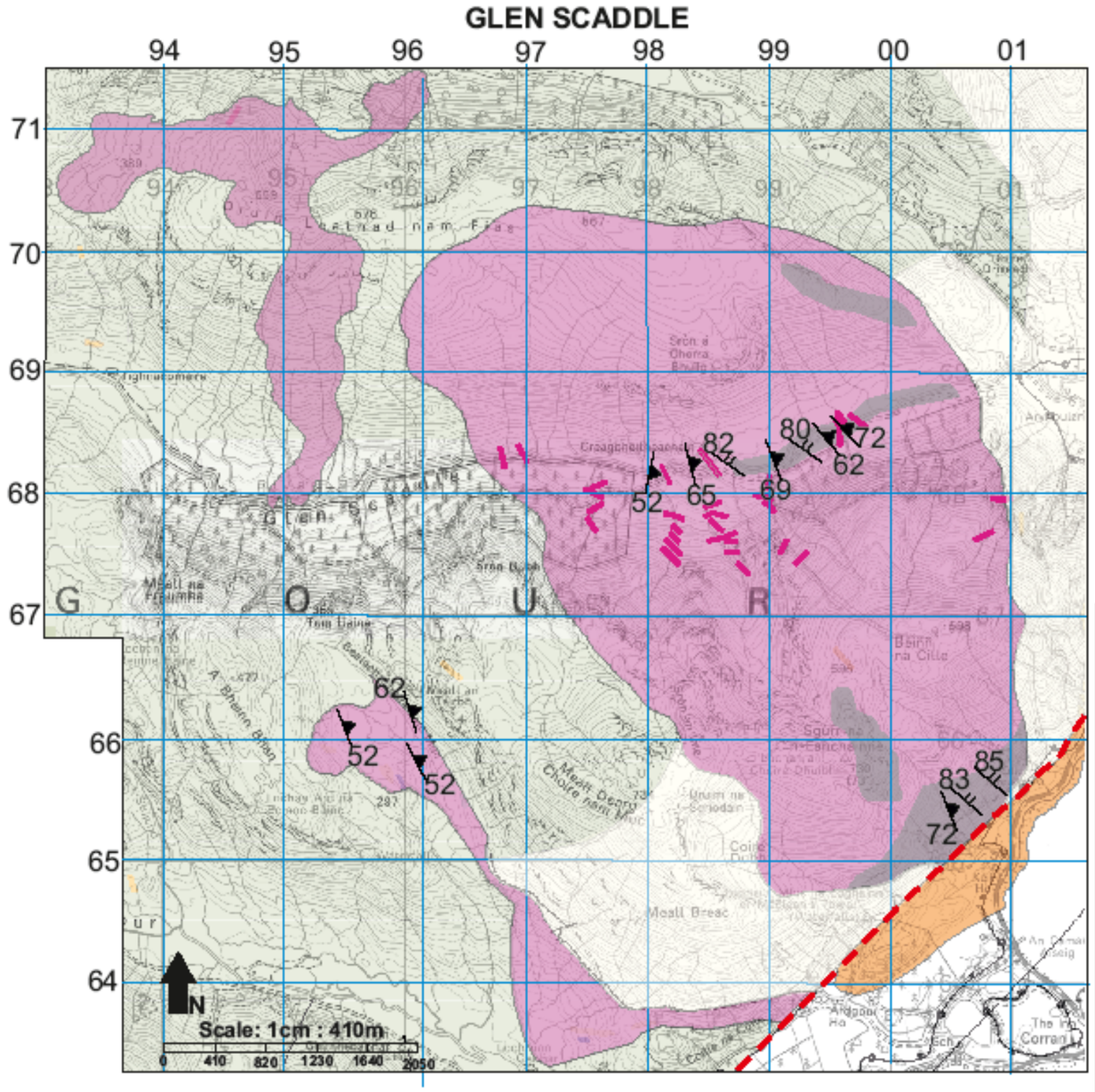

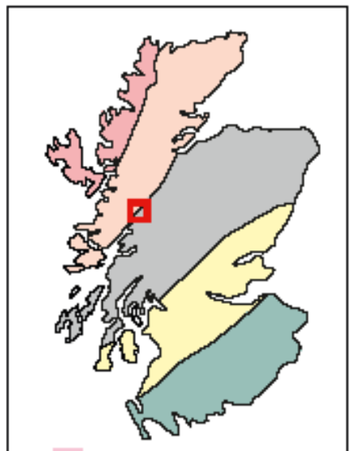

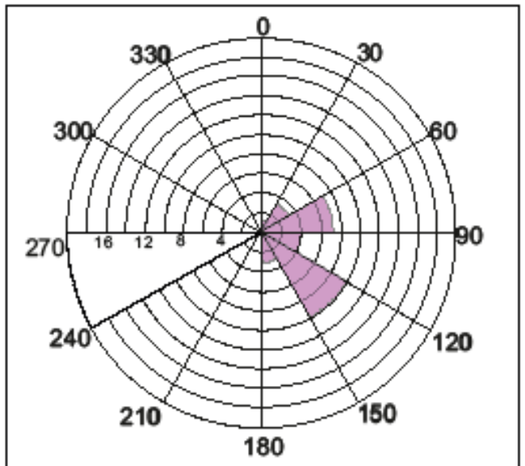

Rose diagram showing the orientation of the pegmatite intrusions observed throughout the Glen Scaddle body. The intrusions were predominately vertical/near vertical.

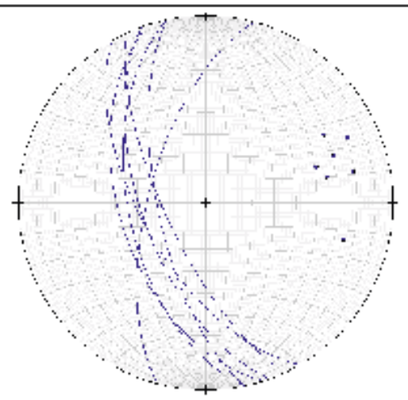

Stereonet visualising the strike and dip of the primary magmatic fabric, where observed. Stereonet produced via the program visible geology https://app.visiblegeology.com/profile.html.

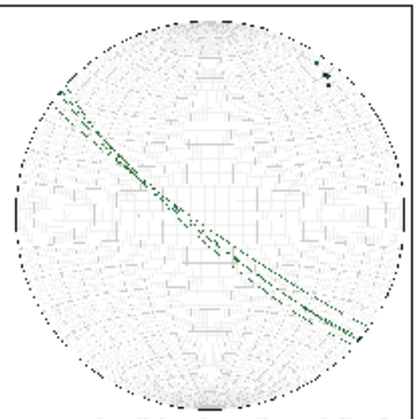

Stereonet visualising the strike and dip of the secondary tectonic fabric, where observed. Stereonet produced via the program visible geology https://app.visiblegeology.com/profile.html.

LEGEND:

Igneous Facies:

Gabbro - Diorite: Medium grained (~3mm). Typically 25 - 50% plagioclase; 0 - 30% hornblende; 0 - 15% biotite; 10 - 40% pyroxene; 0 - 5% epidote, 0 - 5% chlorite.

Meta-gabbro: Medium - coarse grained (3mm - 5mm). Typically 5 - 30% plagioclase; 24 - 45% hornblende; 5 - 15% biotite; pyroxene 20 - 50%,0 - 5% epidote, 0 - 5% chlorite.

Granite Pegmatite: Medium - coarse grained (3 - 5mm). Typically 5 - 30% plagioclase 50 - 70% K - Feldspar; 10 - 20% Quartz; 5 - 25% Plagioclase; 0 - 15% Muscovite; 0 - 5% Biotite.

Loch Linnhe Granite: Fine - medium (~3mm) granite body. 40% K-Feldspar, 30% plagioclase,15% quartz.

Sedimentary facies

Loch Eil Group : quartz and feldspar dominated granulite, with occasional abundant biotite and calc-silicate lenses.

Loch Eil Group (Upper Garry formation): quartz and feldspar dominated granulite, with occasional abundant biotite and calc-silicate lenses.

Measurements and Structural Info.

72 **Strike and dip of tectonic fabric:** Defined by secondary phase of mafic mineral alignment.

72 **Strike and dip of primary magmatic fabric:** Defined by alignment of mafic minerals along their long axis.

Fault Zone (unobserved).

Acknowledgements

First and foremost, I would like to thank Iain Neill for his outstanding supervision throughout the course of this project. His enthusiasm for and knowledge of highland geology and the earth sciences is inspiring. His patience and willingness to help with all matters, academic and otherwise, has been greatly appreciated, and without it my masters would undoubtedly have been a far less constructive experience. His approach to supervision and research has led me to have a hugely positive experience and feel I have accomplished far more on both an academic and personal level than I could have anticipated.

Thank you also to John Macdonald, my second supervisor, for his excellent insights into U – Pb zircon dating, and also for his help in the field, which were both greatly appreciated. My warmest regards to the technical staff John Gileece, Robert Macdonald and Peter Chung, each of whom guided me through the practical elements of the research with patience and top-notch expertise. An additional thank you to Cristina Persano and Eammon McKenna for all their help with LA – ICPMS analysis and sample preparation. My thanks also to the staff at SUERC and Edinburgh and Manchester University for their analytical expertise, and to the Inverness Field Club for subsidizing my fieldwork. Further, all the postgraduate staff in 414/418 were a fantastic group to celebrate and lament the ups and downs of academic life with.

On a personal level, I would like to thank my parents and family for all their support (a special mention also to my Aunt Patricia). Thanks to my flatmates Eimear and Jack for being excellent friends, and to Andrew and Alexander for their great company and conversation. In that regard, Victoria and Amy also deserve a special thank you, as do many of my colleagues and climbing partners at the Glasgow Climbing Centre.

Author's Declaration

I declare that, except where explicit reference is made to the contribution of others, that this dissertation is the result of my own work and has not been submitted for any other degree at The University of Glasgow or any other institution.

Printed name:

Signature:

Date:

Definitions/Abbreviations

AFC	Assimilation Fractional Crystallization
BSE	Back Scattered Electron
CA-ID-TIMS	Chemical Abrasion Isotope Dilution Thermal Ionization Mass Spectrometry
CL	Cathodoluminescence
DCHZ	Deep Crustal Hot Zone
EPMA	Electron Probe Micro-Analysis
GGFZ	Great Glen Fault Zone
HFSE	High Field Strength Elements
HREE	Heavy Rare Earth Elements (Gd – Lu)
LREE	Light Rare Earth Elements (La – Gd)
LOI	Loss On Ignition
LA – ICPMS	Laser Ablation Inductively Coupled Plasma Mass Spectrometry
MASH	Melting, Assimilation, Storage, Homogenisation
NHT	Northern Highlands Terrane
SCLM	Sub Continental Lithospheric Mantle
SEM	Scanning Electron Microscope
SNG's	Scottish Newer Granites
TIP	Turkish Iranian Plateau
XRF	X – Ray Fluorescent Spectrometry

1. Introduction

The late Ordovician – early Devonian Caledonian Orogeny encompasses the events associated with the final closure of the Iapetus Ocean, and the resultant amalgamation of the British and Irish crust into the pattern of fault bounded terranes seen today (Atherton and Ghani, 2002; Chew and Strachan, 2013; Fowler et al., 2008; Holdsworth et al., 2007; Kinny et al., 2003; Oliver et al., 2008; Reavy, 1994; Soper, 1988; Strachan and Evans, 2008).

The Newer Granites are traditionally considered to be magmas emplaced in the Northern highlands terrane (NHT), Grampian, and Midland valley terrane from c. 435 Ma – c. 390 Ma (Oliver et al., 2008; Kocks et al., 2014; Fowler et al., 2008; Mendum, 2012). It is generally accepted that their emplacement is associated with the final closure of the Iapetus Ocean and the collision of the Baltica with the Laurentian margin – a phase of the Caledonian orogeny traditionally referred to as the Scandian event (Atherton and Ghani, 2002; Dewey et al., 2015).

The extensive suite of Newer granite plutons and associated dykes have been well studied in Scottish Caledonian discourse (e.g. Oliver et al., 2008; Kocks et al., 2014; Neilson et al., 2009; Atherton and Ghani, 2002). While several geodynamic models have been presented, there remains a lack of consensus as to the source of melt (lower crustal vs. subduction modified lithospheric mantle (SCLM); e.g. Stephenson et al., 2000); the timing and duration of volcanic and plutonic activity (e.g. Neilson et al., 2009); the relationship of activity relative to major structural events such as orogen-parallel strike slip faulting (e.g. Hutton, 1992; Jacques and Reavy, 1994) and the occurrence of geodynamic triggers such as subduction, slab roll-back and slab break-off (e.g. Atherton and Ghani, 2002).

Recent advances in single grain zircon U – Pb dating through methods such as isotope dilution-thermal ionization mass spectrometry (ID-TIMS), sensitive high-resolution ion microprobe (SHRIMP) and laser-ablation inductively coupled mass-spectrometry (LA – ICP-MS) are considered robust methods for dating igneous rocks of Newer Granite age. These methods have been applied to many of the Newer granites (e.g. Oliver et al., 2009; Strachan and Evans, 2008; Miles et al., 2016), but many bodies remain either undated, or dated via unsatisfactory, now disrepute methods (e.g. Rb-Sr, K-Ar dating methods). New single grain U – Pb

zircon data is presented for the Newer granite intrusions at Glen Loy, Cluanie and Loch Linnhe.

Analysing whole rock major and trace element geochemical profiles is a robust method for accessing the petrogenetic history of magmatic bodies. Geochemical profiles can provide insights into the genesis, ascent and evolution of magma body, allowing inferences to be made about the wider tectonic setting at the time of emplacement. Geochemical datasets for many Newer granite bodies are incomplete. Some plutons have published U-Pb zircon ages, but no whole-rock or mineral-scale geochemical data exists. Whole rock geochemical data is presented for Newer granite intrusions at Glen Loy, Glen Scaddle, Cluanie, Clunes and Loch Linnhe. Major element characterisation was investigated via XRF, while trace elements were investigated through ICP – MS.

The methods outlined above, combined with field investigation of the intrusions at Loy and Scaddle and mineral chemistry data for Loy and Clunes, are employed with the intention of fulfilling the following **aims** and *objectives*:

- **Determine crystallization ages for the Glen Loy, Cluanie and Loch Linnhe intrusions of the NHT** *(U-Pb zircon dating via La-ICPMS).*

- **Establish the source of melt, evolutionary pathway and emplacement method for the intrusion at Glen Loy, Glen Scaddle, Clunes and Cluanie** *(through interpretation of major and trace elemental datasets acquired via XRF and ICP MS respectively).*

- **Explore the previous geochemical classification of the Clunes and Cluanie intrusion as TTG-like or adakitic, and further unravel the implications of these classifications with regards to the model for their genesis and evolution** *(through modelling specific aspects of genesis, ascent and evolution using major and trace element data).*

- **Assess the coherence of the newly acquired data to the currently accepted timeline of the geodynamic events associated with final Baltica – Laurentia (Scandian) collision.** *This will involve a discussion of the implications of recent literature invoking the need to revise the timeline (e.g. Bird et al., 2013; Cawood et al., 2015).*

2. Previous Work

2.1 Caledonian Terrane Amalgamation

The Caledonian orogeny refers to the Ordovician – Silurian collision of the continental blocks Laurentia, Baltica and Avalonia, as the Iapetus Ocean was consumed beneath the SE margin of the supercontinent Laurentia (Stephenson et al. 2000; Dewey et al. 2000). Only slivers of Iapetus ocean crust remain in Scotland today, in ophiolite complexes such as Unst, Shetland and Ballantrae in the Southern Uplands (Spray and Williams, 1980; Flinn et al., 2005; Crowley et al., 2015), and the Highland Border Complex (Chew and Strachan, 2013). Most workers have, until recently, judged the Caledonian Orogeny in terms of two collisional events (Neilson et al., 2009; Atherton and Ghani., 2002; Oliver et al., 2008); the Grampian Orogeny, representing the collision of an Avalonian island arc with Laurentia, and the subsequent Scandian Orogeny, a continent-continent collision between Baltica and Laurentia. Recently, new evidence for an additional phase of metamorphism has cast doubt upon this 'two – stage' model for orogenic events (Bird et al., 2013; Cawood et al., 2015).

The Caledonian orogenic belt may have been equivalent in scale to today's Alpine-Himalayan orogen (Chew and Strachan, 2013). The western margin of the Caledonides extends from Arctic Svalbard through Greenland and the NW of Scotland, NW Ireland, and across the Atlantic to Greenland, Newfoundland and ultimately to the Appalachian Mountains of North America. In Europe, the eastern margin extends through W Norway, N England and Ireland (Stephenson et al., 2000). The British Caledonides must thus be understood in the context of, and seen as an extension of, the Appalachian orogen of eastern North America and the Caledonides of Scandinavia and East Greenland (Chew and Strachan, 2013). The British Caledonides encompasses an orthotectonic zone and a paratectonic zone. These ortho/para-tectonic zones are defined by the degree of deformation and metamorphism; the orthotectonic zone being significantly metamorphosed and deformed, the paratectonic zone having only bearing structures synonymous with low grade metamorphism (Atherton and Ghani, 2002). The orthotectonic zone is bounded by the Moine Thrust (N) and the Highland Boundary Fault (S). The paratectonic zone is bounded by the the Midland Valley terrane (N) and the

Leinster - Lakesman terrane of N England and Isle of man (S). Between the terranes of S Scotland and N England lies the buried Iapetus Suture.

Collision between Laurentia and Baltica is generally described as ‘soft’, due to the oblique angle at which continents collided (i.e. not a ‘head on’ collision). Owing to the ‘soft’ collision, deformation and metamorphosis of Moine sediments and the development of large scale deformation structures is recorded in the NHT and Grampian terranes (the orthotectonic zones), the Siularian sediments of the Midland Valley terrane and Southern Uplands (paratectonic zone) are ony weakly defomed (Chew and Strachan, 2014). The identification of terranes with non-contiguous metamorphic histories separated by strike slip faults, has led to the understanding that fault movement was a key component in transporting the terranes to their present positions (see *Figure 1*) (Stephenson et al., 2000; Oliver et al., 2008).

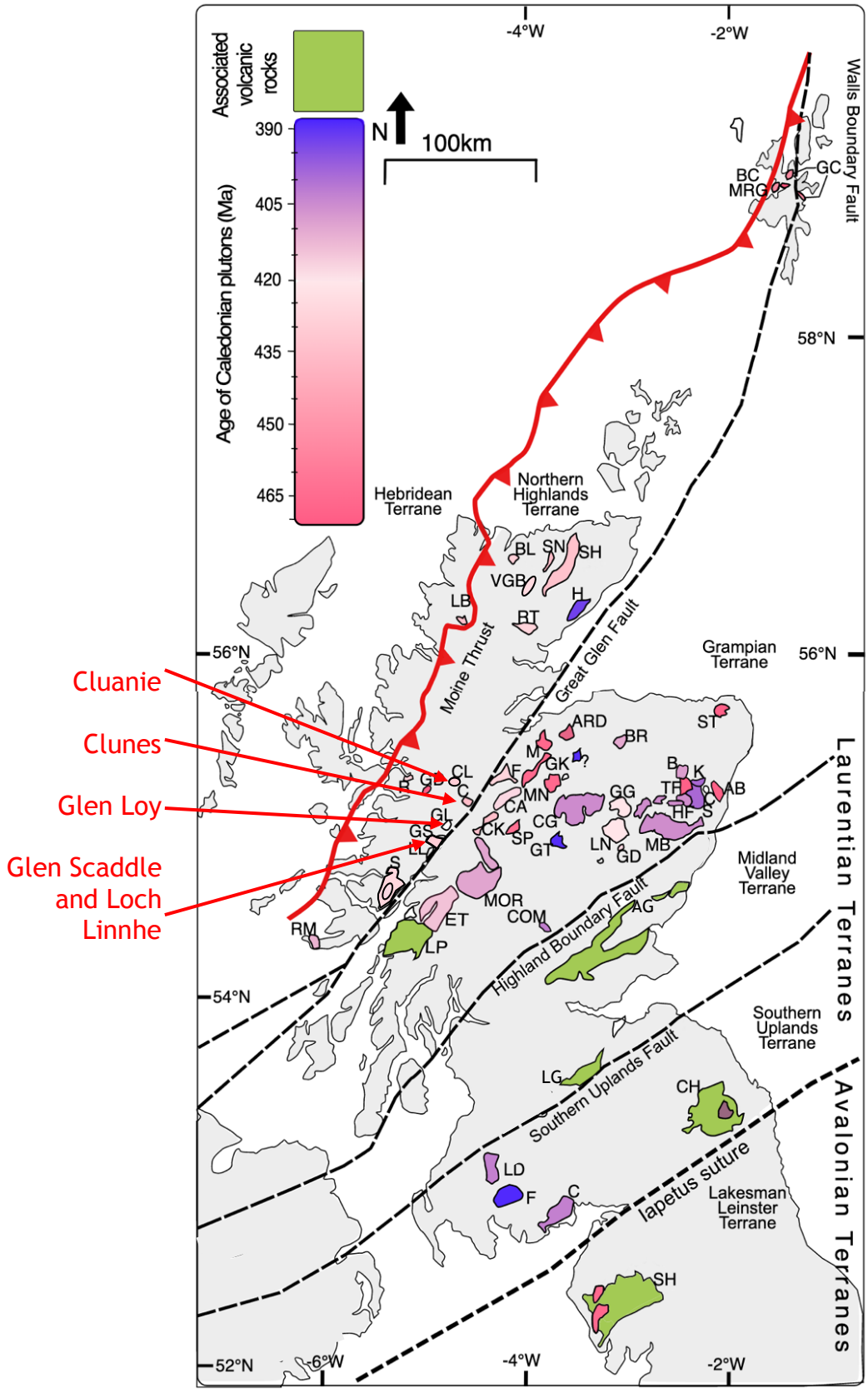

Figure 1: Terrane map of Scotland with Caledonian age plutons and other relevant volcanic bodies annotated. The colour coding is a schematic representation of the reported ages as listed in Table 1. Pluton outlines are taken from BGS diGiMapGB-625. Plutons without age data (Glen Loy and Loch Linnhe) are left uncoloured.

Table 1: Table containing ages and dating methods for plutons/volcanic bodies presented in Figure 1.

	ID	Pluton Name/Location	Method	Age (Ma)	Error (2σ)	Reference
Northern Highlands Terrane	GD	Glen Dessary Syenite	U – Pb Zircon	448	2	Goodenough et al., 2011
	LB	Loch Borrolan Syenite	U – Pb Zircon	430	4	Millar et al., 2008
	SN	Strathnaver Granite	U – Pb Zircon	429	11	Kinny et al. 2003
	C	Clunes Tonalite	U – Pb Zircon	428	2	Stewart et al. 2001
	GS	Glen Scaddle Intrusion	U – Pb Zircon	426	3	Strachan and Evans, 2008
	BL	Ben Loyal Granite	U – Pb Zircon	426	9	Halliday et al. 1987
	SH	Strath-Halliday Granite	U – Pb Monzanite	426	*n/a*	Kocks and Strachan, 2006
	R	Rogart Igneous Complex	U – Pb Zircon	425	1.5	Kocks et al. 2014
	S	Strontian granodiorite (outer)	U – Pb Zircon	425	3	Rogers and Dunning 1991
	RT	Ratagain Granite	U – Pb Badellyite	425	3	Rogers and Dunning 1991
	VGB	Vagastie Bridge Granite	U – Pb Zircon	424	8	Kinny et al. 2003
	RM	Ross of Mull Granite	U – Pb Zircon	418	5	Oliver et al. 2008
	S	Strontian Granite (inner)	U – Pb Zircon	418	1	Paterson et al. 1993
Grampian Terrane	S	Strichen	U – Pb Zircon	473	n/a	Oliver et al. 2000
	TF	Tillyfourie	U – Pb Zircon	471	12	Oliver et al. 2008
	Ab	Aberdeen	U – Pb monzonite	470	n/a	Kneller and Aftalion, 1987
	K	Kennethmont	U - Pb Zircon	457	1	Oliver et al. 2000
	SP	Strathspey	U – Pb Zircon	449	6	Oliver et al. 2008
	ARD	Auldearn Granite	U – Pb Zircon	432	10	Oliver et al. 2008
	F	Foyers	U – Pb Zircon	424	4	Oliver et al. 2008
	LN	Lochnagar	U – Pb Zircon	420	2	Oliver et al. 2008
	GD	Glen Doll	U – Pb Zircon	419	5	Oliver et al. 2008
	GG	Glen Gairn	U – Pb Zircon	415	1	Oliver et al. 2008
	ET	Etive	U – Pb Zircon	415	6	Oliver et al. 2008
	BR	Ben Rinnes	U – Pb Zircon	411	5	Oliver et al. 2008
	MOR	Moor of Rannoch	U – Pb Zircon	409	8	Oliver et al. 2008
	B	Bennachie	U – Pb Zircon	408	5	Oliver et al. 2008
	B	Ballater	U – Pb Zircon	406	5	Oliver et al. 2008
	MB	Mount Battock	U – Pb Zircon	406	5	Oliver et al. 2008
	CG	Cairngorm	U – Pb Zircon	404	18	Oliver et al. 2008
	COM	Comrie	U – Pb Zircon	404	6	Oliver et al. 2008
	HF	Hill of Fare	U – Pb Zircon	403	8	Oliver et al. 2008
	GT	Glen Tilt	U – Pb Zircon	390	5	Oliver et al. 2008
Southern Uplands	LD	Loch Doon	K - Ar	408	2	Stephens and Halliday, 1979
	C	Criffel	Rb - Sr	397	2	Stephens and Halliday, 1979
	F	Fleet	Rb – Sr	392	2	Stephens and Halliday, 1979
Associated Volcanics	SH	Shap	U – Pb Zircon	415	1	Miles et al. 2018
	LP	Lorn Plateau	Rb - Sr	400	5	Clayburn et al. 1983
	CH	Cheviot Lava	Rb - Sr	395	4	Jhingran, 1942
	AG	Arbuthnott Group	Devonian (undated)			Thirlwall, 1988
	LG	Lanark Granite	Devonian (undated)			Thirlawall, 1988

2.2 Terranes of Scotland and their relationship to the Caledonian Orogeny

2.2.1 The Hebridean Terrane

The Hebridean Terrane (to the NW of the Moine Thrust) is underlain by a basement of Archean and Paleoproterozoic Laurentian continental granulites and gneisses, and represents the Laurentian foreland (Chew and Strachan, 2013; Rainbird et al., 2001). The Lewisian Gneiss complex ranges in age from 3100 Ma to 1800 Ma and contains some of Europe's oldest rocks (Rainbird et al., 2001; Park et al., 2002).

Mesoproterozoic to Neoproterozoic sedimentary successions known as the Torridonian successions lie unconformably upon this Lewisian Gneiss basement. These successions can be subdivided into three distinct units: the Stoer Group, the Sleat Group and the Torridon Group (Rainbird et al., 2001). The Stoer group has been dated at c. 1200 Ma, and consists of continental sandstones, siltstones, basal breccia and conglomerates thought to have been deposited in a narrow NNE trending rift (van de Kamp & Leake 1997). The Sleat group consists of 3.5km of fluvial sandstone and siltstone deposited in local rift systems and can only be seen at Kishorn Nappe (Park et al., 2002).

The 6km thick Torridon sequence (deposited 1200 – 970 Ma; Chew and Strachan 2013) is predominantly a course red arkose and subarkose sandstone. The sequence overlies the Stoer Group with an erosional unconformity and is believed to be a deposit of two large alluvial aprons (Rainbird et al., 2001).

Lewisian and the Torridonian are in turn overlain unconformably by Cambrian/Ordovician transgressive sedimentary sequences, clastic in nature lower in the sequence (the Ardvreck Group), the younger strata being predominantly carbonate (the Durness Group) (Park et al., 2002).

2.2.2 The Northern Highland Terrane

East of the Moine Thrust and north of the strike-slip Great Glen Fault Zone (GGFZ), the NHT comprises largely of the Moine Supergroup – metasediments originally deposited in a shallow subsiding sea as thick beds of sandstones and shales (1000 – 870 Ma) (Chew and Strachan, 2013; Holdsworth et al., 1994). The Moine Supergroup rest unconformably on a Lewisian-type basement (Chew and Strachan, 2013; Strachan et al., 2010) and as such, was deposited on the eastern margin of Laurentia. The sediments of the Moine thus represent the Laurentian cover sequence (Chew and Strachan, 2013). The maximum depositional age for the Moine successions is given at c. 950Ma (Kinny et al., 1999; Friend et al., 2003). The lower age for deposition is defined by the intrusion of the West highlands Granite Gniess at c. 870Ma (Friend et al., 1997). This age range has led to correlation between the Moine and Torridon sequences (Peach and Horne, 1930). However, more recent detrital zircon work indicates deposition in two separate sedimentary basins (Friend et al., 2003; Cawood et al., 2004), although some workers maintain the upper Torridon is equivalent to the lower Moine (Krabbendam et al., 2008).

Three divisions of the Moine Supergroup are recognized; the Morar group, the Glenfinnan group and the Loch Eil group (Holdsworth et al., 1994). The Morar group consists of 6 – 9km of marine and fluvial psammites (the succession records a marine – fluvial regression followed by a fluvial – marine transgression; Bonsor et al., 2012). This succession is the most westerly of the Moine successions (Strachan et al., 2010). The Glenfinnan division comprises of a series of strongly deformed psammites and pelites, metamorphosed to a higher grade than the others in the Moine Group (Strachan et al., 2010). The Loch Eil group consists of gently dipping psammites, deposited in a shallow marine tidal environment (Strachan et al., 2010).

The metamorphic evolution of the Moine is complex and is thought to include at least one (if not more) events prior to the closure of the Iapetus Ocean (Bird et al., 2013; Cawood et al., 2015). A general summary of the metamorphic history of the Moine is presented in *Table 2*. Traditional models for Caledonian events outline two main phases of metamorphism, while more recent work has identified a third phase. These events are detailed below.

470 – 460 Ma; deformation associated with Grampian orogenic events. This is evidenced by activation of the Sgurr Beag and Naver Nappes and the presence of metamorphic mineral assemblages (Strachan et al., 2010). Titanite dating of the West Highland Granite Gneiss gives an age of c. 470Ma for regional amphibolite-facies metamorphism (Rogers et al., 2001). Prograde garnets (dated using Lu – Hf methods) of Grampian age (c. 470 Ma) are reported by Bird et al. (2013). The Sgurr beag and Naver nappes record deformation correlated with Grampian Orogenic events (Chew and Strachan, 2013). The Sgurr Beag thrust carries the Glenfinnan group over the Morar group, and is thought to have been activated by Knoydartian deformation (Tanner and Evans, 2003) and reactivated by the Grampian (Krabbendam et al., 2008).

456 – 443Ma. The '450Ma event'; first identified by Bird et al. 2013, through Lu – Hf dating of prograde garnets from the Moine Nappe, giving ages for prograde metamorphism occurring at c. 450Ma. This has since been supported by U-Pb ages from the Glenelg pegmatite reported by Cawood et al., 2015 (c. 456 - 446Ma). Both workers propose that the high grade metamorphism recorded at c. 450Ma is a separate, previously unrecognized metamorphic experienced by the Moine (i.e. not related to Grampian or Scandian events)

435 – 425 Ma; deformation and metamorphism associated with the Scandian orogenic episode. Field evidence for this event is recorded in the form of the regional scale NW trending thrust belt; the Moine Thrust, and widespread folding and fabrics symptomatic of amphibolite to greenschist facies conditions (Holdsowrth et al. 2007; Chew and Strachan, 2013). The dating of metamorphic mineral assemblages has also been used to constrain Scandian deformation. C. 435 - 425 Ma Rb/Sr, K/Ar and $^{49}Ar/^{30}Ar$ mica ages from Moine mylonites and schists at Knocken and Dundonnel are presented by Freeman et al. (1998). U-Pb dating of monzanite grains from the Kirtomy Nappe migmatites was carried out by Kinny et al. (1999), and returned metamorphic ages of 431 +/-10.

Table 2: Summary of the pre-Caledonian and Caledonian history deformation history of the Moine Supergroup.

Pre-Caledonian and Caledonian deformation of the Moine Supergroup of the NHT (including deposition)	
Deposition (1000 – 870Ma)	*Sediments derived from the erosion of the c .1.1 – 1.0 Ga Grenville orogenic belt and deposited in a basin on the margin of the Laurentian sector of the Rodinian supercontinent (Strachan et al., 2010).*
Knoydartian Event (c. 830 – 725 Ma)	*This event is still poorly understood. Extensional tectonics and orogeny are both cited as potential mechanism behind deformation (Cutts et al., 2009).* **Associated features:** Garnet grade metamorphism, minor isoclinal folding, the intrusion of pegamtites, formation of pervasive foliation and S1 schistocity, first movement on the Sgurr Beag fault (Strachan et al., 2010).
Grampian (c. 470 – 460)	*Deformation associated with the collision of the Grampian Taconic arc with the Laurentian continental margin. Deformation is localised in the eastern sector of the NHT, above the Sgurr Beag and Naver Nappe.* **Associated features:** Mid – upper amphibolite facies metamorphism, tight isoclinal folding (recumbent), formation of the Loch Coire migmatite and pervasive NW trending lineations. D2 phase of Moine deformation. Also associated with the formation of a composite S0/S1/S2 foliation (Strachan and Evans, 2008)
Scandian (c. 435 – 425)	*Deformation associated with the collision of Baltica and Laurentia. Deformation pervasive throughout the NHT.* **Associated features:** Mid – low amphibolite facies metamorphism, major upright folding, development of S3 shistocity, activation of the Moine Thrust. D3 - 4 phase of deformation (D3 folding are upward facing and plunge towards the Great Glen; D4 folds are gentle – open) (Strachan and Evans, 2008).

The NHT is dominated by Newer granite magmatism (see *Figure 1* and *Table 1*). The Newer granite suite in the NHT covers a huge variety of rock types and scales of intrusion, from quartz-feldspar vein complexes (e.g. Glen Garry, Fettes & MacDonald, 1978), less evolved minor intrusions such as microdiorites and appinites (Fowler et al., 2008), and stocks and larger plutons (e.g. Fowler et al., 2008; Oliver et al., 2008).

The intrusions studied in this work (at Glen Scaddle, Glen Loy, Cluanie, Clunes and Loch Linnhe) all lie within the NHT, and in close proximity to the Great Glen and associated faults. A total of 17 bodies are acknowledged by Oliver et al. (2008) in their extensive compilation of Scottish granitoids; this total admittedly omitting several (at the time) unstudied intrusions (the intrusions at Loch Linnhe, Glen Loy and Cluanie included).

The majority of previously dated intrusions within the Northern Highlands terrane return ages within the range of c. 430 +/- 2 Ma (e.g. the Glen Dessary Syenite) and c. 418 +/- 1 Ma (e.g. the Strontian Granite; Patterson et al. 1993; Oliver et al. 2008). Many workers associate their emplacement with a regime of sinistrally transpressive faults such as the GGFZ (Oliver et al., 2008; Stewart et al., 2001).

There are several temporal inconsistencies in the reporting of the Newer granites and, by association, the Scandian orogeny. Firstly, the association of the granites with what most authors consider to be the 'middle' of the Scandian Orogeny, is unusual. Many of the 'granite' (sensu lato) bodies have significant mafic facies and/or mafic parental magmas (e.g. Fowler et al., 2008) and are thus indicative of mantle melting, which is normally suppressed when orogenic belts are at their thickest (Song et al., 2015). Dated bodies such as Strathnaver granite (429Ma) overlap with the generation of migmatites in Sutherland in the Northern Highlands (431 +/- 10Ma; Kinny et al., 1999) which most authors understand as a time of 'peak metamorphism' (e.g. Chew and Strachan, 2013). It may be that these dates reflect maximum heating of the Scottish crust, but this heating may long post-date the main phase of mountain-building activity during the Scandian. A delay in maximum heating of the crust can be a result of post collisional radiogenic heating by the decay of K – U and Th, as is reported by Sylvester, (1998) in the Alps and Himalayas.

2.2.3 The Grampian Terrane

South of GGFZ lies the Grampian terrane, dominated by Dalradian sediments (Stephenson et al., 2013). Similar to the Moine, the Dalradian Supergroup comprises a package of complexly deformed meta-sediments (with some meta-volcanic additions) initially deposited on the SW margin of Laurentia between ~800 and 510 Ma (Chew and Strachan, 2013; Stephenson et al., 2013). There are 6 main divisions of the Dalradian (the Trossachs, Southern Highlands, Argyll, Appin, Grampian and Badenoch groups). Of these, the Badenoch Group is cut by the so-called Grampian Shear Zone at ~806 Ma (Noble, 1996), and shares similar detrital zircon patterns with the Moine Supergroup of the Northern Highlands, suggesting they are equivalent (Cawood et al., 2014; Stephenson et al., 2013).

Deformation and metamorphism have been extensively studied in the Dalradian rocks, after Barrow's (1893) pioneering work in correlating different mineral assemblages with conditions of metamorphism. Four phases of regional deformation are recognized in the Dalradian Supergroup (D1 – D4) (Chew and Strachan, 2013; Tanner, 2014; Stephenson et al., 2013). The D1/D2 phases describe the main phase of ductile deformation experienced by the Dalradian, initiating early folds at the Tay Nappe, Loch Awe Syncline and the Islay Anticline (Tanner, 2014; Stephenson et al., 2013). The D3 phase is restricted to the SW of the Grampian terrane, and is not responsible for any major structures in the SW highlands.The D4 phase resulted in the formation of large upright regional scale structures (e.g. the Highland Border Downbend) and is responsible for the widespread development of crenulation cleavage (Tanner, 2014). All of the dated Caledonian deformation in the Grampian Highlands is associated with the Grampian Orogeny. Ordovician-Silurian sinistral movement on the GGFZ meant that only the Northern Highlands were far enough north to experience significant Scandian deformation and metamorphism (Underhill and Brodie, 1993; Mendum and Noble, 2010).

Igneous activity in the Grampian terrane is widespread and well documented (Oliver et al., 2008; Rogers and Dunning 1991; Dempster et al., 2002; Neilson et al., 2009) (See *Figure 1* and *Table 1)*.

The newer Gabbro's (e.g. the Portsoy Gabbro) are thought to represent the root of the continental arc formed during Grampian collision (Carty et al., 2012). They are interpreted as mantle melts produced by extensional thinning of the lithosphere and decompression melting of the asthenosphere (Carty et al., 2012).

The granites of the far North East (e.g. Aberdeen and Strichen intrusions) are dated at around 470 Ma (Oliver et al. 2000; Kneller and Aftalion, 1987), their emplacement associated with Grampian collisional events (Oliver et al., 2008; Neilson et al., 2009) and the convective removal/delamination of the Iapetus ocean crust below as it was subducted beneath the Laurentian margin. This subdivision of the Caledonian granites are termed 'Group 1 granites' are distinct from the Newer granites (Pankhurst and Sutherland 1982; Oliver et al., 2008), and tend to be foliated with typical S – Type geochemical signatures (Oliver et al., 2008). These S - type granites are studied in detail by Appleby (2007). They are proposed to be generated as a result of the melting of Dalradian country rock and are notable due to their apparent isotopic heterogeneity. This heterogeneity is interpreted by Appleby (2007) as being a result of the melt being assembled incrementally from multiple melt batches of different composition, source and petrogenetic evolution.

Unfoliated granites associated with decompression melting were intruded around 455 Ma (e.g. Kenneth-mont, Moy, and Inzie granites; Oliver et al., 2008). Exhumation driven by erosion allowed the rise of hot asthenosphere and the genesis of S - type granites from melting of Al – rich meta-sediments (only a low melting temperature was achieved, meaning higher temperature igneous protoliths remained unmelted) (Oliver et al. 2008). I - type (calk-alkaline) magmatism in the Grampian terrane began at 430 Ma, and persisted for around 22 Ma (Neilson et al., 2009). Neilson et al. (2009) invokes crustal melting with a metasomatically hydrated mantle component as a petrogenetic model, citing the compositional diversity of intrusions within the Grampian terrane.

2.2.4 The Midland Valley Terrane

The Midland Valley terrane is associated with early Palaeozoic (late Cambrian – early Ordovician) oceanic crustal and island arc material from the northern margin of the Iapetus Ocean. Several supra-subduction ophiolite complexes were obducted prior to the Grampian Orogeny (Unst, Shetland and Bute ophiolite complexes; Chew et al., 2010) (Chew and Strachan, 2013). There are two belts of obducted material in the Midland Valley terrane; one in proximity to the Highland Boundary Fault and another further south containing the Ballantrae ophiolite (Stone, 2014). The Midland Valley Terrane extends into Ireland where there are proposed remnants of the Grampian arc and forearc basin (e.g., the South Mayo Trough). The terrane is otherwise dominated by younger post-orogenic cover (Chew and Strachan, 2013). There are no exposed Caledonian granites in the Midland Valley terrane (Bluck et al., 1983).

2.2.5 The Southern Uplands Terrane

Finally, the Southern Uplands Terrane (lying south of the Southern Uplands Fault and north of the buried Iapetus suture) is an early Palaeozoic (Silurian – Ordovician) accretionary prism of Iapetus Ocean sediments (Oliver et al. 2008; Trewin and Rollin, 2002; Waldron et al., 2008). Deposition occurred between c. 490 and 425 Ma on the Laurentian margin of Iapetus; the dominant lithologies being coarse grained greywackes with finer grained siltstone/mudstone beds. Turbidites are a major feature of the stratigraphy. The sequences are all steeply dipping and folded, with a generalised younging direction being to the NW - consistent with their involvement with the NW dipping subduction zone beneath the Laurentian continental margin (Chew and Strachan, 2013; Waldron et al., 2008). Sediment provenance has been constrained as being from continental a landmass to the North, and volcanic island to the southwest (Stone, 2014; Waldron et al., 2008). With the subduction of Iapetus Ocean crust, the sedimentary packages were deformed (both folded and faulted) and stacked against the Laurentian margin before being thrust over continental basement (Chew and Strachan, 2013).

2.3 Caledonian Geodynamic framework

Until recently, a two - stage (Grampian – Scandian) model for Caledonian orogenic events was generally accepted (Oliver et al., 2008; Atherton and Ghani; Dewey et al., 2015). Recent workers have identified evidence for an additional third phase of deformation experienced by the terrane (Bird et al., 2013; Cawood et al 2015).

2.3.1 The Grampian Phase

The Grampian event refers to the 'hard' collision of the Laurentian passive margin with the Midland valley supra-subduction island arc complex at c. 475 Ma (Neilson et al. 2009; Dewey 2005; Chew and Strachan, 2013) (see *Figure 3*). This collision resulted in the deformation of 15km of Dalradian sediments via the formation of nappes, and the obduction of ophiolites such as the Highland Border Ophiolite (Dewey, 2005; Chew et al., 2010). Evidence for deformation is widespread and seen throughout Shetland and the NHT and Grampian terrane (see *Section 2.2.2)* (Chew and Strachan, 2013). The entire orogenic episode is inferred to have lasted 18 Ma (Dewey, 2005). Field evidence for the collision in the form of obducted oceanic crust, deformation structures (predominantly found within the Appalachian sector of the orogeny) and temporally well constrained conformable stratigraphic sequences from the South Mayo Trough (Ireland) have delivered consensus as to the nature and timing of the Grampian orogenic sequence (Chew and Strachan, 2013).

It is generally accepted that subduction polarity reversal (i.e. change in direction of movement of subducting slab, from towards the continent to away from it) was a component of the Grampian collision (Dewy and Strachan 2003; Dewey, 2005). This is thought to have occurred due to the attempted subduction of the young, buoyant midlands valley crust beneath the Laurentian margin. This arc/margin collision is distinct from continent/continent collision, where buoyancy impedance rarely occurs (Dewy, 2005). The buoyancy impedance is overcome by the forced subduction of what was initially the overriding slab - slab break off being a prerequisite factor in allowing the 'flipped' subducting slab entry to the asthenosphere. In the case of the Grampian event, attempted subduction of the Midlands Valley Arc occurred for 8Ma resulting in extensive crustal shortening and thickening. The resulting subduction flip (from continent bound to away),

hypothesized to have taken place at 467Ma, would have relieved this this progressively tight collision zone via slab roll back and extensional collapse. Said extensional collapse is thought to have taken only 1.6Ma. This polarity reversal facilitated both the continued consumption of Iapetus ocean crust, and the development of an Andean-type continental margin.

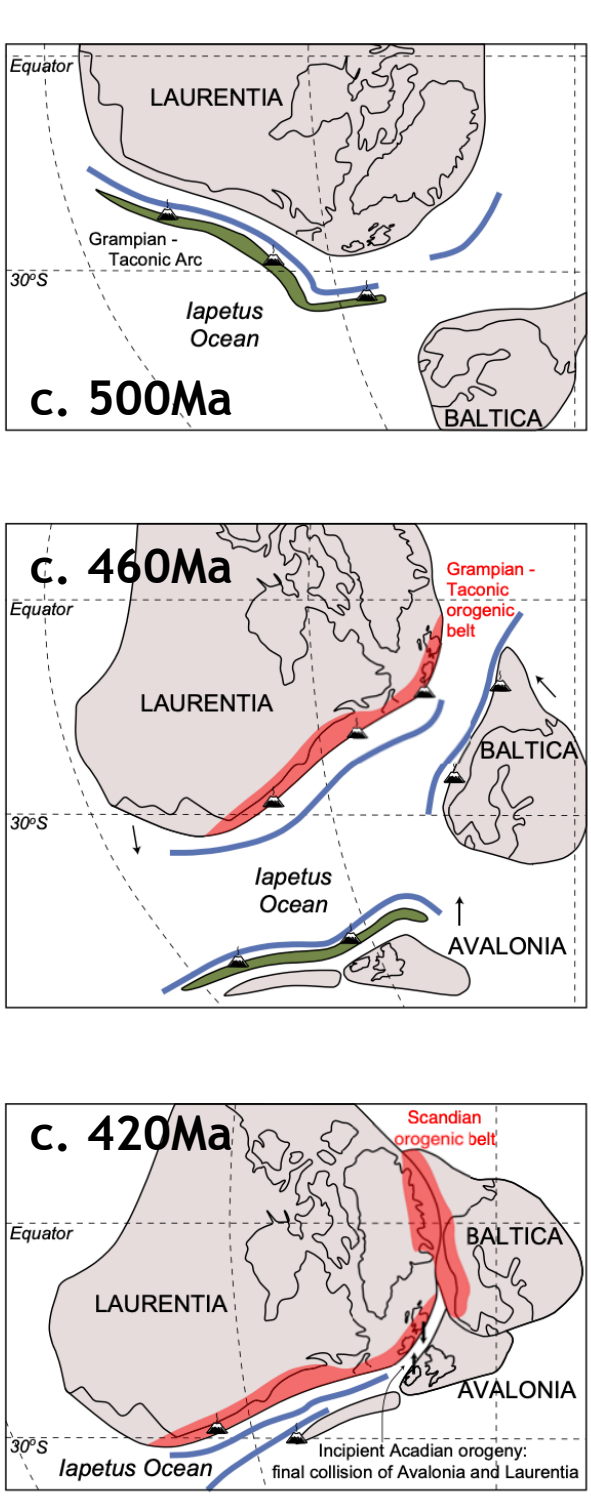

S directed subduction outboard of Laurentia creates the Midland valley/Grampian Taconic arc in the Iapetus ocean.

The Midland Valley/Grampian Taconic arc collides with Laurentia, an event known as the Grampian Orogeny.

N directed subduction begins under Laurentia while S directed subduction begins under Avalonia, resulting in Iapetus ocean closure.

The Iapetus Ocean closes with the collision of Baltica and Laurentia (resulting in the so-called 'Scandian Orogeny') and the highly oblique collision of Laurentia and Avalonia – The Acadian orogeny.

Figure 3: Schematic diagram showing the evolution of the Caledonian orogenic cycle and the closure of the Iapetus Ocean. The three traditionally accepted stages Volcanic arcs are shown in green; trenches are shown in blue and indicate the 1599 polarity of subduction; collisional orogens are shown in red. Figure modified from 'The Laurentian Caledonides of Scotland and Ireland', Chew and Strachan (2013). Published online at: https://doi.org/10.1144/SP390.16.

2.3.2 The Scandian Phase

The Scandian phase of the Caledonian Orogeny describes the collision of Baltica with the Laurentian margin. (Dewey and Strachan 2003; Mendum, 2012; Chew and Strachan, 2013) (See Figure 3). Paleomagnetic evidence from Cocks and Torsvik (2006) points to a rotation of the Baltican continent prior to collision with the Laurentian margin. Evidence for regional deformation and metamorphism related to the Avalonia – Laurentia collision is largely lacking, and such it has been inferred to have been 'soft' (due to the highly oblique nature of the closure) (Chew and Strachan, 2013).

The Scandian Event (the collision of Baltica with the Laurentian margin) is responsible for major regional deformation and has been cited as the mechanism behind the reactivation of the Sgurr Beag and Naver thrust systems, the formation of the Moine thrust zone, as well as the development of several orogeny parallel sinistral displacements (e.g. GGFZ) (Goodenough et al., 2010; Dewy and Strachan 2003; Mendum 2012). These displacements were a result of the sinistrally transpressive nature of the Scandian Orogenic phase (Oliver et al. 2008; Mendum 2012) and are generally accepted to have acted as pathways for channelling melts into the mid-crust (Hutton, 1992; Jacques and Reavy, 1994). This relationship has been used to understand the timing of fault motion via U – Pb dating of Zircons found within Newer granite intrusions found in proximity to fault zones (Stewart and Strachan, 2000; Oliver et al., 2008; Hutton, 1992; Jacques and Reavy, 1994).

This event is also responsible for the formation of regional scale fabrics, as detailed in *Section 2.2.2*.

The Scandian orogenic phase is associated with the intrusion of several granitoids bodies (sensu lato), termed the Newer granites. The timing of their emplacement largely falls within the window of 430 – 380 Ma (Chew and Strachan, 2013; Oliver et al. 2008), meaning intrusion post-dates subduction according to the currently accepted timeline for Scandian events. Their chemistry is in general calk-alkaline, typically a subduction influenced signature (Fowler et al. 2008; Miles et al., 2016, respectively) or (See *section 2.2.2)*. Isotope compositions and inherited zircon populations indicate a significant component of crustal recycling, as well as a

lithospheric mantle derived component, typical indicators of post-suduction emplacement (Miles et al., 2016).

One of the foremost hypotheses for the generation of the Newer granites (and lateral equivalents in Ireland) comes from Atherton and Ghani (2002), who propose a slab break-off of the Baltican slab beneath Laurentia as an initiating factor (see Figure 4). Slab break-off occurs as a subducted slab is weakened and eventually ruptured by rifting induced by asthenospheric flow following continental collision.

After slab break-off, it is assumed that hot asthenosphere will 'flow' into the vacancy left by the ruptured slab, perhaps inducing thermal erosion of the lithosphere above and triggering melting of the lowermost lithosphere by conduction (e.g. Keskin, 2003). Given the likelihood of the lithospheric mantle and asthenosphere already being metasomatically altered by subduction, the melts produced will be broadly calk-alkaline and arc like, but usually of smaller volume and at lower degrees of partial melting.

This template is considered compatible with Caledonides, a conclusion supported by comparison to the Tertiary Alps – a well described orogen for which the evidence for geodynamic events (including slab break-off) remains intact (Atherton and Ghani, 2002).

Other possible explanations for the calk-alkaline signature and post-subduction explacement of the Newer granites are explored by Miles et al. (2016). They include the dehydration of a stationary slab of subducted oceanic crust, and partial melting of previously metasomatized lithospheric mantle in response to lateral post subduction shear. These hypotheses are generally overlooked in favour for the slab break-off hypothesis of Athertone and Ghani, (2002).

Miles et al. (2016) also report on the apparent absence of magmatism during the period associated with subduction prior to Scandian collision (c. 40Ma – 430Ma). They consider a shallow subduction angle (which supresses melt generation) and extensive erosion and tectonic removal of intrusions (aided by the tropical climate of the Grampian terrane at this time (Bluck 2000; 2013)). The latter concept, while difficult to prove, is reported in subduction regimes globally (Hawkesworth et al., 2009; 2013). Miles et al. (2016) and Bluck (2000; 2013) do however note

the apparent absence of material of this age in sedimentary basins adjacent to where intrusions would have been anticipated. This leaves the hypothesis unsubstantiated, but the poor preservation of arc material generally mean it is still considered plausible.

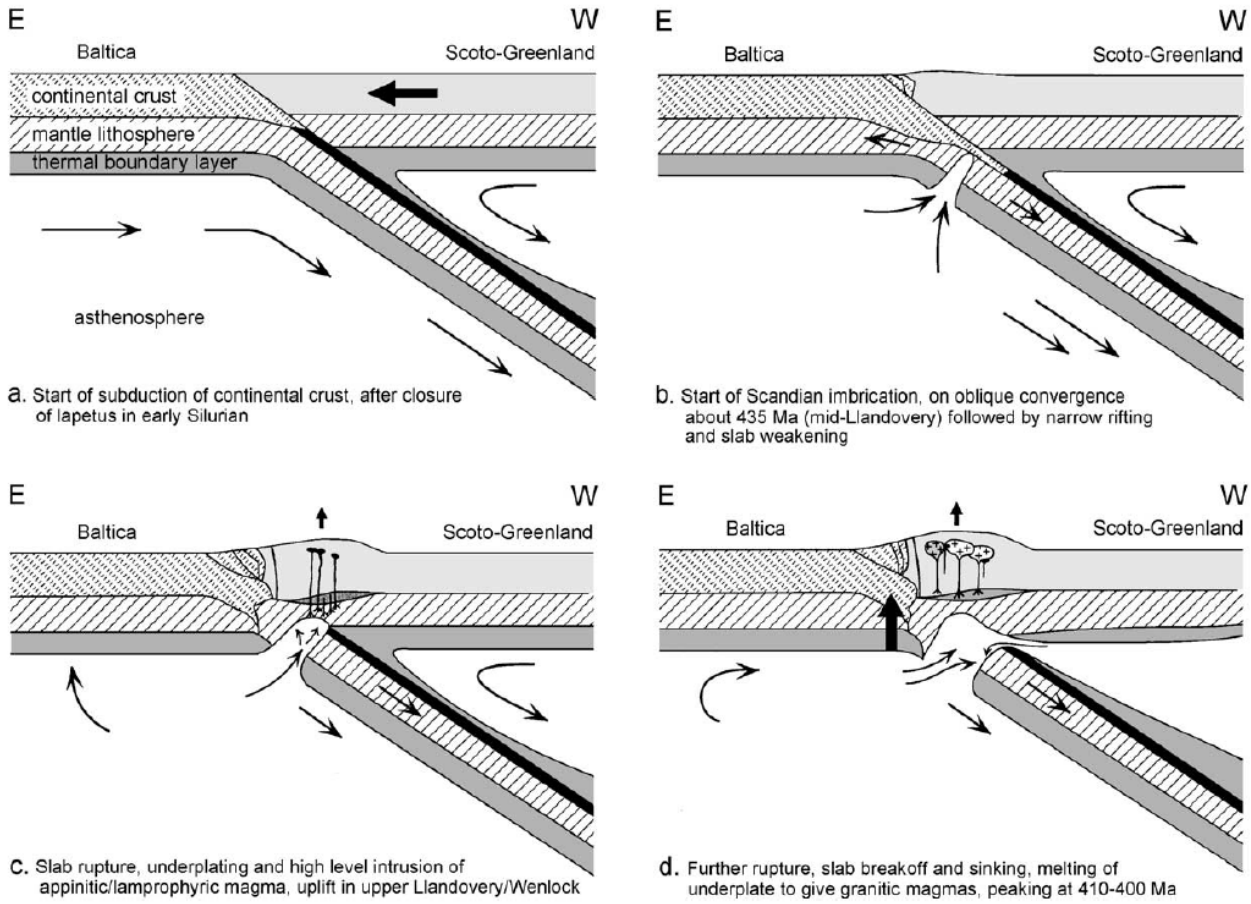

Figure 4: Schematic diagram showing the stages of slab break following Scandian events (from Atherton and Ghani, 2002). The timing of the events (e.g. collision at c. 435 Ma) remains uncertain.

2.3.3 The '450Ma event'

An additional phase of regional metamorphism recorded in the NHT has recently been identified. The event was first recognized by Bird et al., (2013), via the identification of Moine Nappe garnets recording prograde metamorphism at c. 450Ma. The Moine nappe is thought to represent the Moine metasediments thrust over the Laurentian foreground during Caledonian orogenesis (Holdsworth et al., 2007). The Lu – Hf ages from the Moine Nappe garnets range in age from 458.7+/- 4.5Ma – 448.7+/- 5.0Ma (Bird et al., 2013). This data points to a further phase of regional deformation thus far not named or well documented in Scottish geological discourse. Further evidence for said additional phase of metamorphism is presented by Cawood et al. (2015), who provides U – Pb ages from the Glenelg pegmatite, found in the Morar group of the Moine. The ages range from c. 458 – 446Ma and indicate that high grade metamorphism and pegmatite formation was taking place at this time.

Both workers interpret the mechanism behind this regional tectonothermal metamorphic event as an arc accretion event similar in style to the Grampian orogeny (Bird et al., 2013; Cawood et al., 2015). However, with the absence of field evidence of arc material, both authors acknowledge that this hypothesis is difficult to substantiate.

2.3.4 The Acadian Event

The Acadian Event is considered by some workers to be the final transpressional stage of the Caledonian orogenic timeline (Mendum et al., 2012). This is disputed by some workers (e.g. Woodcock et al., 2007), who characterise the event as proto-varsican as opposed to Caledonian. The event is traditionally thought to have occurred between c. 400Ma and c. 390 Ma (Mendum et al., 2012), as evidenced by radiometric dating of igneous bodies emplaced associated with the final stages of the event (e.g. the Shap, Skiddaw intrusions of the Lakesman and Leinster terrane) and by constraining cleavage development through illite/mica dating (Merriman et al., 1995). New evidence presented by Woodcock et al. (2016) suggests said time constraints may require further work.

The Acadian event occurred due the northward migration of the Amorican micro-continent (the Midlands craton) with the rest of the Avalonian continent and its sedimentary basins (See Figure 3). The event is responsible for the large-scale deformation of Lower Palaeozoic sediments in N England, Wales and S Ireland. The N directed collision of the Midlands valley craton created a sinistrally transpressive tectonic regime, initiating widespread folding and cleavage formation. In Scotland, deformation was focused at existing terrane bounding faults (Southern Upland fault, Highland boundary fault and the GGFZ), decreasing in intensity with distance from the fault zones. Scottish Devonian stratigraphy (e.g. the old red Sandstone) also show some deformation structures thought to be produced by the event.

2.4 Summary of problems in reconstructing the geodynamic setting of the Late Caledonian Orogeny

Reconstructing a plate tectonic model for Late Caledonian collisional events is inherently problematic; as is acknowledged by Mendum (2012), who states 'presently exposed evidence (for the orogenic phases) is limited — unsurprising, given that subduction, faulting, uplift, exhumation and erosion all combine to either conceal or destroy it'. Issues with the timing of magmatic events in relation to geodynamic events are raised consistently in the literature (Atherton and Ghani, 2002; Oliver et al., 2008; Neill and Stephens., 2009; Miles et al., 2016), as is the attempt to reconcile the varied whole rock chemistry of the plutons with geodynamic events (Fowler et al. 2008; Neill and Stephens, 2009). Generally accepted features of Late Caledonian magmatism include the importance of strike-slip faulting in channelling melts to the surface (Mendum, 2012; Stewart et al. 2001; Holdsworth et al. 2015; Hutton 1988), and the involvement of a slab break-off event following Scandian collision, as a driver for asthenospheric upwelling and mantle or crustal melting (after Atherton and Ghani, 2002; Neilson et al. 2009).

2.4.1 Timing of Newer granite emplacement

The Newer granites of the NHT are worth revisiting given that their emplacement coincides with or shortly postdates peak regional metamorphism as it is currently understood (lasting 435 to 425Ma; Chew and Strachan, 2013; Friend et al 2003). Given that magmatism, some of which is evidently mantle-derived (e.g. Loy and Scaddle, given their mafic bulk composition), temporally coincides with migmatite generation and the termination of large-scale movement on the Moine thrust Zone (Kinny et al., 1999), it is possible that previously accepted 'Scandian' deformation features do not represent maximum thickness of the Scottish crust shortly postdating collision. Rather they may represented heating of that crust some millions of years after crustal thickening had taken place (such a phenomenon has been reported in other orogenic belts globally, where the radiogenic decay K – U and Th heats the crust long after collision (as is reported by Sylvester, 1998, in

the Alps and Himalayas)). If this is the case, then the traditional temporal framework for Baltica – Laurentia collision may be erroneous.

With improvements being made to the global understanding of post-collisional magmatism in orogenic belts, it is clear that the geodynamic framework in for Scandian events in Scotland has several inconsistencies. The consideration that collision and crustal thickening could not have occurred contemporaneously with the formation of previously identified metamorphic fabrics and structures has yet to be addressed. As discussed in *Section 2.3.3*, the possibility that our understanding of the temporal framework of the orogeny has been erroneous has been raised by rencet workers Bird et al. (2013) and Cawood et al. (2015).

2.4.2 Caledonian Terrane Amalgamation

Understanding positioning of the terranes prior to Caledonian amalgamation is imperative if the spatial distribution of magmatism is to be understood. The positioning of the Northern highlands terrane in Silurian time is still regarded a contentious issue (Dewey and Strachan 2003; Dewey et al., 2015). The northern boundary of said terrain - the Moine Thrust - represents the northern extent of Baltica – Laurentia collision (Mendum, 2012). For the NW highlands terrane to be involved in Baltica – Laurentian collision, it is implied to have been situated 500 – 700km north by orogenic strike, being brought into its current positioning by the movement along sinistral displacements such as the GGFZ. The Grampian terrane thus shows no evidence of involvement in Scandian Orogenic events (Oliver et al. 2008) (See Figure 5). The matching of ages and geodynamic events across the major Scottish terrane boundaries must be done with care as oblique collision will potentially result in events such as slab break off being recorded at different times in different terranes (i.e. diachronous collision or slab tearing).

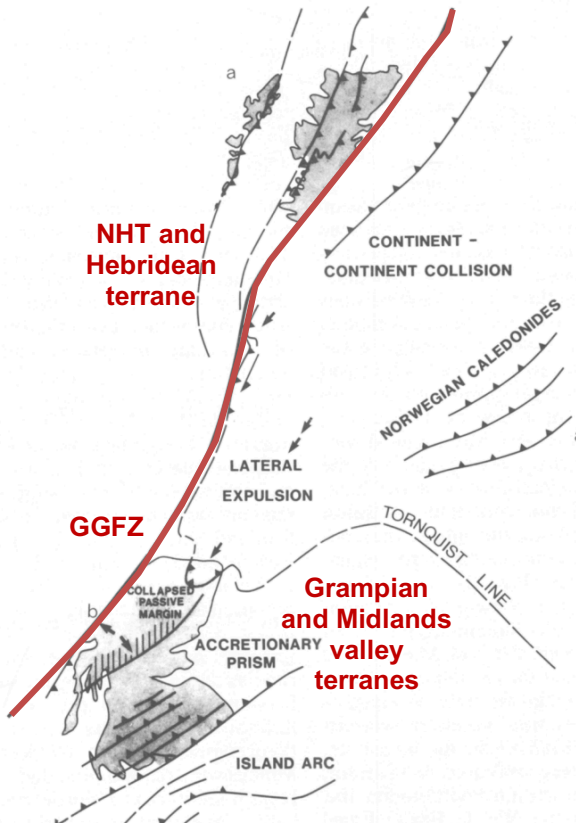

Figure 5: Schematic diagram showing the suspected arrangement of Scottish terranes prior to sinsitral strike slip movement on the GGFZ. Adapted from Coward (1990), The Precambrain, Caledonain and Varsican framework to NW Europe. Available online at https://sp.lyellcollection.org/content/specpubgsl/55/1/1.full.pdf

2.5 Newer Granites of the study area

The Cluanie, Clunes, Glen Scaddle, Linnhe and Glen Loy plutons or intrusions have been selected for detailed geochronological and geochemical reasons.

Firstly, only Clunes and Scaddle have reliable U-Pb zircon ages, Clunes being dated at 427.8+/- 1.9 Ma, and Glen Scaddle at 426+/- 3 Ma (Stewart et al., 2001 and Strachan and Evans, 2008, respectively) (see Table 3). Adding geochronological data from Cluanie, Glen Loy and Loch Linnhe will allow advances in the temporal framework of the orogeny to be made. Data from Loy and Linnhe is particularly important in this regard considering their emplacement in proximity to the GGFZ (Linnhe being found within the fault zone itself). Emplacement ages will therefore give insight into the timing of the first movement of this major lithological feature, in itself an important consideration in understanding the timeline of Scandian orogenic events.

Secondly, Glen Loy and Scaddle contain mafic facies which strongly indicate the occurrence of mantle melting. This is incompatible with peak crustal thickness associated with Scandian collision. Thus, an emplacement age from Glen Loy is important in defining the timing and/or duration of mantle melting in relation to Scandian collision and peak crustal thickness. Such data may also be used to infer the timing of slab break-off in the Caledonides, a possible mechanism for generating mantle melting (Atherton and Ghani, 2002).

Third, a cluster of plutons in this region of a similar age could mean they are evolved a common parent magma. This is best investigated through the geochemical study of the mafic facies. Naturally, if the plutons are genetically related to one another, then it will be possible to test whether the most evolved bodies (e.g. Clunes, which is tonalitic, and Cluanie, which is trondhjemitic) could be the product of extensive fractionation of mantle-derived melts. This work will test the crustal melting hypothesis for the Cluanie trondhjemite of Neill & Stephens (2009).

Table 3 summarises the data available in the literature for the Scaddle, Clunes, Cluanie, Glen Loy and Loch Linnhe pluton

Table 3: Summary of the data available in the literature form the Glen Saddle, Clunes, Claunie, Loy and Loch Linnhe plutons.

	Geochronology	Geochemistry	Structural Observations
Glen Scaddle	426+/- 3 Ma – U/Pb zircon. A 'Structural' age for Scaddle is suggested to be between D2 and D3 stages of regional Loch Eil (Moine) deformation. (Strachan and Evans, 2008)	N/A	The pluton occupies major D3 fold (Glen Scaddle synform). Emplaced prior to D2 stage and deformed by D3 stage of regional deformation. Margins of the pluton are broadly parallel to the regional composites for D2. (Strachan and Evans, 2008)
Clunes	427.8+/- 1.9Ma – U/Pb zircon. Stewart et al. (2001)	N/A	No reported evidence for regional scale deformation structures associated with D2 or D3 events. Fabrics are magmatic, reflecting processes that occurred during cooling. (Stewart et al. 2001)
Cluanie	417 Ma - U-Pb zircon (Pidgeon and Aftalion, 1978) 425+/-4 Ma – Rb – Sr (Powell 1983).	Major and trace element profiles published. Key features include: **- High Ba -Sr:** Poorly understood but thought to be related to subducted pelagic material in the melt source. **- High light REE's and relatively low HFSE's:** Typical markers of subduction related magmatism (Neill and Stephens, 2009; Fowler et al., 2008)	No reported evidence for regional scale deformation structures associated with D2 or D3 events.
Glen Loy	N/A	N/A	No reported evidence for regional scale deformation structures associated with D2 or D3 events, but there is a suggestion that the body has been folded (Johnstone and Mykura, 1989).
Loch Linnhe	N/A	N/A	N/A

2.5.1 Glen Scaddle Intrusion

The Glen Scaddle Intrusion is found on the northern shore of Loch Linnhe, the geomorphological expression of the GGFZ. Scaddle intrudes the Moine rocks of the Loch Eil Group (Strachan and Evans 2008) (See Figure 1).

The Glen Scaddle Intrusion was first described by Wilson and Drever (1940), who classify the intrusion as a 'gabbrodiorite with appinitic affinities'. Evidence for metamorphism was noted by Drever (1940), who described several instances of shearing and granulitisation.

The intrusion was revisited by Strachan and Evans (2008), who describe the Glen Scaddle intrusion as a medium to coarse grained foliated metagabbro. Enclaves of unmetamorphosed rock are described as consisting of hypersthene (opx), cpx and plagioclase, with amphibole and minor quartz and biotite. They also note a change from ultrabasic rocks at the margins of the intrusion to basic/felsic rocks in the centre. Crude layering between melanocratic and leucocratic gabbroic types on scales of up to several metres was observed by Stoker (unpublished PhD thesis, Univ. of Liverpool, 1980). Foliation is described as being largely parallel to the contact with the Moine.

Strachan and Evans match deformation structures identified in the intrusion to those described elsewhere in the Loch Eil Group in order to constrain a 'structural' age for emplacement. Drawing on the work of Stoker (1983), they conclude that the intrusion was intruded in the between the D2 and D3 stages of deformation in the area. This is based on the correlation between metamorphic foliation and the axial plane of the D3 Glen Scaddle syncline (D3 being associated with major upright folds elsewhere in the region). They further assert that the intrusion was emplaced as a series of sills, the gradation from ultrabasic to basic/acidic representing differentiated layers of a sheet intrusions. It is highlighted the Glen Scaddle intrusion can be used effectively to constrain lower limit for the timing of upright folding and amphibolite facies metamorphism Caledonides.

Homogenised crystal U – Pb dating of zircon grains was carried out using a VG 354 mass spectrometer, giving ages of 426+/- 3 Ma (Strachan and Evans (2008). This

age corresponds well with those of other nearby Late Caledonian Granites (See Table 1).

Geochemical data for the Glen Scaddle metagabbro has yet to be produced, and thus no petrogenetic model for genesis or ascent has been put forward. The proximity of the intrusion to the GGFZ implies emplacement was likely initiated by fault movement (Strachan and Evans 2008).

2.5.2 The Cluanie Pluton

The Cluanie pluton, a small 20km^2 body described by Neill and Stephens (2009) as a granodiorite or trondhjemite, is intruded into the Moine rocks of the NHT (see Figure 1). The body lies just 30km east of the Moine thrust, 15km NW of the GGFZ and, notably, at the intersection of a mapped strike slip faults; a NW/SE trending fault west of the intrusions and a NE/SW trending fault to the east. The trends of these fault are significant: the NE/SW trend is that of the Loch Shin Line, the NE/SW trend the GGFZ. The unnamed NE/SW trending fault found to the found to the east of the body is a splay of the Strathglass fault. If said fault was dextral in nature, then the body would have been emplaced in a pull apart zone at the conjunction of the two faults.

Cluanie is described as a largely homogenous porphyritic granodiorite, the main variable being the concentration of alkali feldspar megacrysts (Neill and Stephens, 2009). Accordingly, 4 subdivisions are recognized; a megacryst-rich hornblende diorite (c.15% alkali feldspar megacryst), megacryst rich hornblende diorite (megacrysts content <10%), megacryst-free hornblende granodiorite and a megacryst-free biotite granodiorite. The alkali feldspar content of Cluanie is anomalous according to its sodic bulk composition (An_{15-30} plagioclase dominates typical assemblages (60%); Neill et al. 2016), its presence in such abundances justifying classification as a trondhjemite (Barker, 1979). The body has itself been intruded by several minor microdiorite dykes, the north east sector being particularly well populated.

Geochemically, Cluanie can be classified as a high Ba –Sr granitoid (Neill and Stephens 2009). This classification places it within an enigmatic category of high Ba-Sr Caledonian granites and syenites emplaced in the Northern Highlands. Their

petrogenesis is a contentious issue, Harmon et al. (1984) suggesting their geochemical characteristics can be attributed to mantle derived appinitic parent magma, more recent investigations suggesting they are related by differentiation via crustal contamination and crystal fractionation (Fowler et al. 2001; Fowler and Henney, 1996). The mechanism behind melt generation also remains inconclusive (Fowler et al., 2008).

Similar to the nearby plutons Ratagain, Strontian, Rogart and Helmsdale, Cluanie has high light REE's and relatively low HFSE's. Despite being the most depleted pluton with regards to Nd and Sr, when plotted, the isotopic elemental data forms consistent arrays with other associated intrusions, which project towards the plot of the Moine. This stands as robust evidence for incorporation of Moine host rocks during the evolution and ascent of the melts.

Two ages have been proposed for the Cluanie pluton; a U-Pb age of 417 Ma (Pidgeon and Aftalion, 1978), and a Rb – Sr age of 425+/-4 Ma (Powell 1983). Advances in geochronology, particularly with new methods for single grain U-Pb lead dating of zircons (i.e. TIMS, SHRIMP of LA-ICPMS) has cast many of these older dating methods into disrepute, and as such these are not relied heavily upon in recent publications (Oliver et al. 2008). This is particularly true of Rb – Sr ages which, due to the lower closure temperature of the system (400 – 525 °C) and the ability of the system to be reset, are generally not thought to give reliable crystallisation ages for granite plutons (Miles et al., 2016). The closure temperature of the U – Pb system is >900°C, generally thought to be higher than the granite liquidus (although this is H_2O dependant) (Miles et al., 2016). Recent advances have been made in re-interpreting Rb – Sr data to account for this low closure temperature. As reported by Miles et al., 2016, a revised decay constant allows for ages to recalculated to the estimate crystallisation age of a body. The decay constant is lowered by 1.9%, which in turn adds c. 8Ma to the the age of the pluton. Thus, the 425+/-4 Ma age acquired for the Cluanie pluton by Powell (1983) can be converted to a crystallization age 433 +/-4 Ma.

2.5.3 The Clunes Tonalite

The Clunes tonalite is a small, poorly exposed (and thus little studied) intrusion NW of Loch Lochy, occupying only 4km^2 (see Figure 1).

The intrusion is deemed compositionally homogenous and is made up of sodic plagioclase (An37 – An31), quartz, hornblende and biotite (Stewart et al. (2001); modal proportions are omitted). The majority of the intrusion is tonalitic, but small granitic/granodioritic zones are present, defined by modal variability of quarts and mafic minerals, as well as the occasional local occurrence of K feldspar. A fabric is reported, defined by plagioclase mineral alignment. This thought to be associated with deformation of the melt as it cooled, rather than being introduced post emplacement (Stewart et al. 2001). This is inferred by the presence of sub-solidus deformation structures (dissolution of the outer rims of plagioclase/hornblende/biotite grains, sutured boundaries of quartz). The fabric has been closely studied by Stewart et al. (2001), particularly within the context of the GGFZ. The fabric is aligned with the SW and NE margins of the intrusion and is suggested to have been a result of magma chamber contraction, or magma buoyancy forces interacting with the chamber walls i.e. not due to regional tectonothermal activity. The orientation and shape of the body is suggested to have been controlled by pre-existing fabrics in the Moine, a theory already applied to Caledonian emplacements such as the Loch Loyal Syenite and the Foyers Granite (Holdsworth et al. 1999; Stewart et al. 2001)

U – Pb zircon geochronology was carried out by Stewart et al. (2001), returning a crystallization age of 427.8+/- 1.9Ma. This plots very close to the age of the Ratagain granite (425+/-3Ma; Rogers and Dunning 1991). The emplacement of both of the Ratagain granite is associated with compressional strike slip faulting, highlighting the importance of said structural regimes at this time (420 – 430 Ma) (Stewart et al. 2001). In the absence of any evidence for major deformation, it can be assumed that emplacement post-dated major regional Caledonian tectonothermal activity.

The model put forward by Stewart et al. (2001) regarding the emplacement of the body highlights the significance of early movement on the GGFZ and the associated ductile rotation of the regional NNW trending Moine foliation. A ‘stick point’ (the

product of rheological contrast between the faulted units; Hutton 1982), inferred by the presence of the Coire Lochain shear zone, eventually developed into a 'tectonic void', which was subsequently infilled by tonalitic melt. This is very much in compliance with the tectonic context of the emplacement, with regards to the Scandian orogenic phase and the relationship between strike slip faulting and plutonism. However, the interpretation of Stewart et al. (2001) omits any detail of the petrogenesis of the Clunes melt, focusing solely on structural aspects of emplacement. No geochemical analysis has been carried out on Clunes. Confirming the classification as a tonalite would require the body to satisfy a specific set of geochemical characteristics (Condie, 2004).

2.5.4 The Glen Loy Complex

Glen Loy is poorly studied relative to other Newer Granites. It is briefly described by Johnstone and Mykura (1989) in their investigation of early basic and intermediate rocks of the Caledonides. The intrusion is small, outcropping over only 4 km^2, and intrudes the Moine rocks of the Loch Eil division (see Figure 1). There are numerous petrological similarities between the Glen Loy intrusion and the nearby Glen Scaddle intrusion (lying just 50 km to the SW); the key difference being in the degree of alteration – Glen Scaddle being extensively sheared and metamorphosed, Glen Loy showing little sign of alteration.

The Glen Loy complex has been classified as a hornblende gabbro, consisting primarily of labradorite feldspar and well-developed prismatic hornblende. The variable modal proportions of said minerals define rhythmic banding on a decimetre scale. Gradation of mineral size is also described, inferred to be a result of gravitational settling of crystals within the melt (Johnstone and Mykura, 1989).

There is, as of yet, no geochemical or geochronological profile for Glen Loy. No detailed structural mapping has been carried out, and such the relation to Caledonian structural and geodynamic events is unknown. Johnstone and Mykura (1987) suggest the pluton may have been involved in two separate phases of regional deformation/folding but no evidence is volunteered to substantiate this claim.

2.5.5 The Loch Linnhe Granite

The intrusion at Loch Linnhe is poorly studied, with no prior field, analytical or structural investigation. The body is located in proximity to the Scaddle intrusion, almost at the heart of the GGFZ (see Figure1). The main intrusion is elongate in shape, stretching roughly 4.5km along the Northern shore of Loch Linnhe at Corran. Other areas of exposure are found 3.5km to the SW, at Inversanda Bay.

2.5.6 Other intrusions of the NHT: general features

The geochemical characteristics of the newer granite intrusions of the NHT are explored by Fowler et al., 2008. His extensive datasets of whole rock major and trace element chemistry and Sr- Nd isotopic compositions are used invoke a source of melt and provide constraints on the degree of crustal contamination and the extent of fractional crystallization. Key features of the NHT intrusions are described in Table 4.

2.5.6.1 Strontian

The Strontian pluton is found just north of both the GGFZ and Loch Linnhe (to the southwest of the Scaddle intrusion), within the Loch Eil subdivision of the Moine. Covering 200km^2, Strontian is amongst the largest SNG intrusions, followed by Strath-Halladale, at 175km^2 (Fowler et al. 2014). Strontian, like Rogart, is a composite intrusion, with an outer foliated hornblende granodiorite and an inner biotite granodiorite. Appinitic enclaves are described at various localities in the pluton, a relatively common feature of many of the Newer Granites.

2.5.6.2 Ratagain

The Glenelg-Ratagain pluton of northern Inverness-shire is a 20km^2 body of significant compositional variability, emplaced in close proximity to the Moine thrust. The body is dated at 425+/-3Ma (Hutton and McEarlean, 1991). Fowler et al. 2008 describe a variety of lithologies; a pyroxene-mica-diorite, olivine gabbro, monzodiorite and quartz monzonite. Syenitic zones, mafic enclaves and metasedimentary xenoliths are also described. Emplacement is thought to be associated the sinistral Strathconan fault, thought to be an important second order structure to the GGFZ (Watson, 1984; Hutton and McEarlean, 1991). Emplacement mechanisms associated with regional strike slip faulting (Hutton and McEarlean, 1991).

2.5.6.3 Rogart

The Rogart Pluton of Sutherland is a 70km^2 centrically zoned monzodiorite – granodiorite- granite body, with appinitic enclaves (Fowler et al. 2008; Kocks et al. 2014). The body was dated at 425+/-1.5 Ma using U-Pb zircon methods, placing

it in the same age bracket as Ratagain, Strontian and Clunes. The range of magma types represented in the Rogart Igneous Complex has been linked to variation in emplacement mechanisms associated with large scale tectonic controls (Kocks et

al. 2014). Also associated with Rogart are a range of leucogranites and injection migmatites, thought to be the result of partial melting of the Moine country rock following the intrusion of the magmas of the main pluton. Kocks et al. 2014 conclude that the monzodioritic component was emplaced during crustal thickening associated with the D2 stage of Caledonian deformation and is related

to the ductile deformation of the Navel thrust. The granitic-granodioritic central pluton developed later (although there is no evidence for a significant hiatus in emplacement) and has been linked to the formation of the Loch Shine Line (a steeply dipping dextral shear zone). The Navel thrust and Lock Shin line are thus both inferred to have been of crustal scale, and responsible of the channelling of mantle derived melts during their deformation (Kocks et al. 2014).

2.5.6.4 Helmsdale

The Helmsdale pluton of Glen Elg in the far North East is a large intrusion, covering 98km^2. It is a composite body, the outer section being described as coarse-grained porphyritic granodiorite, the inner a fine-grained adamellite. The age of the pluton is given as 420Ma. (Fowler et al. 2008).

Table 4: Geochemical characteristics of the NHT intrusions as detailed in the literature.

Characteristic	Explanation
High Ba – Sr content	This signature is attributed to the influence of subducted pelagic sediments (naturally rich in Ba and Sr) in the mantle source (Andersson et al., 2016; Fowler et al., 2008)
Caledonian Parental Mantle Array	Fowler et al., (2008) identify the CPMA (the Caledonian Parental Mantle Array) as a melt source. The CPMA is thought to have been heterogeneous in terms of levels of isotopic enrichment, largely influenced by subduction.
Subduction signature (E.g. Low Nb-Ta)	NHT magmatism is associated with the northern-directed subduction of Iapetus oceanic lithosphere during the amalgamation of Baltica and Laurentia, so typical markers of subduction related magmatism are present (e.g. Soper et al., 1992).
Evolution by fractional crystallization and limited crustal assimilation	The Nd–Sr isotope covariations for the newer granites form arrays that project towards the composition of the Moine host rocks. This implies significant incorporation of Moine rocks during melt evolution, in mid-upper crustal magma (Fowler et al., 2008). Fractional crystallization is thought to have been a major control on Newer Granite evolution. Inconsistency with the geochronological data make the concept of a single batch of melt evolving via fraction crystallization untenable. Fowler et al., invokes discrete batches of melt evolving independently.
Association with appinites/mafic facies	Mafic facies (e.g. hornblende meladiorites and gabbros) are a common feature of NHT, often found in association with more evolved bodies. These bodies are incontrovertibly mantle derived and are thought to represent a parent to the more evolved intrusions (Fowler et al., 2008).

2.6 Global Analogues for the SNG Suite

2.6.1 TTG and Adakite Genesis

Previous geochemical investigation into the Clunes and Cluanie plutons have noted similarities to the adakite/TTG suite. Stewart et al. (2001) classify Clunes as a Tonalite, albeit without any supporting geochemical data. Cluanie is characterised as 'granodiorite of trondhjemitic affinity' by Neill and Stephens (2009). The data acquired in the work classifies Clunes and Cluanie as 'adakite-like'. This geochemical classification infers a specific set of processes in operation, as described below.

2.6.1.1 The Trondhjemite, Tonalite, Granodiorite Suite

Tonalites (e.g. Clunes) and granodiorites (e.g. Cluanie) belong to a suite of rocks known as TTG's (Tronjhemites, Tonalities and Granodiorites) (Barker, 1979). TTG's dominate Archean terranes, meaning significant interest surrounds establishing the conditions required for their formation, which would shed light on the nature of geodynamics on the Early Earth (Martin, 1999). Typical TTGs are defined as sodic granitoids with having Al_2O contents >15%, SiO_2 > 70%, Sr > 300ppm, Y > 20 ppm, Yb < 1.8 ppm, Nb >/= 10 ppm (Condie, 2005).

Many authors (Condie, 2005; Martin, 1999) have noted the geochemical similarity between the TTG suite and Adakites – a modern day magmatic or volcanic rock associated with volcanic arcs and collision zones, and initially proposed to be intrinsically linked to slab melting (Defant and Drummond, 1990).

2.6.1.2 Adakites

Adakite characterisation is based on elevated LREE and LILE contents and low HREE and Y content. As a result, the Sr/Y and La/Yb ratios are high. Characrtersation can also be carried out based on the modal proportion of feldspars in hand specimans (Defant and Drummond 1990). Adakites have andesitic - rhyolite compositions, with >56% SiO_2 (Defant and Drummond 1990; Castillo et al., 2006). Defant and Drummond (1990) were the first to link these geochemical parameters with 'derivation by melting of young subducted lithosphere' (Defant and Drummond, 1990). The identification of intrusions and volcanic rocks

seemingly produced by slab melts marked significant progress in the study of arc magmatism and the fate of the oceanic slab post-subduction. Further, slab melting and subsequent crustal recycling was seen as a viable mechanism for the formation of the Archean TTG (trondhjemite - tonalite - granodiorite) suite, thus giving an insight into magmatic processes of early Earth (Castillo et al., 2006). Since the high Sr/Y ratio has been linked to highly economic quantities of copper and gold, bolstering understanding of how, why and where they are formed is of significant interest for economic reasons (Castillo et al., 2006; Chiaradia et al., 2012).

Since their initial identification, the geochemical parameters required for adakite classification have been significantly revised and expanded (Castillo et al., 2006; Ribeiro et al., 2016). Further, the intrinsic link to melting of the descending oceanic crust has been questioned, with many workers identifying adakitic rocks in environments where slab melting is not viable (Ribeiro et al., 2016; Macpherson et al., 2005; Kolb et al., 2013). In these scenarios, melting of the thickened lower crust is often invoked (Atherton and Petford, 1993; Chung et al., 2003; Wang et al 2005). Other workers have suggested that extensive differentiation of parental basaltic magma is sufficient to produce the adakitic geochemical signature (Ribeiro et al., 2016; Macpherson et al., 2005; Kolb et al., 2013). These scenarios are outlined in more detail below and summarised in Table 5.

2.6.1.2.1 Modern Adakite genesis via slab melting

The relationship between adakite magma production and melting of subducted basaltic crust is based on both experimental and observation data (Sen et al., 1994; Defant and Drummond 1990). Modern adakite genesis via slab melting is linked to the forced subduction of ‘young, hot crust’ (Peacock et al., 1994). Defant and Drummond (1990) originally suggested that adakite genesis can only take place in convergent margins where the subducting material is >25 Ma. This was revised in later literature, with a number of other conditions that are conducive to slab melting being added. These include scenarios where older crustal material (>25ma) melts during subduction initiation, subduction collision, tearing of the slab leading to the opening of an asthenospheric window or a shallowing of the subduction angle (Sajona et al., 1993 & 1994; Yogodzinski et al., 2001; Calmus et al., 2003).

2.6.1.2.2 Adakite genesis via melting of the thickened mafic lower crust

By contrast, the adakites of southern Tibet are commonly cited as being the result of melting of the thickened lower crust, with additional input of enriched mantle and/or upper crustal components (Chung et al., 2003). In the case of Tibet, melting is proposed to have been triggered by the mantle melting and advection of heat into the lower crust, initiated by slab break off (Hou et al., 2004). In orogenic environments where the lithosphere is thickened to 50 – 40 km, melts formed from the mafic lower crust will be in the garnet amphibolite stability field, fulfilling the common variable identified for adakite classification (Chung et al., 2003). Crustal melts will further interact with lower to middle crust, which initiates assimilation and homogenization processes. High Sr/Y ratios are commonly interpreted as an indication of deep melting.

2.6.1.2.3 Adakite genesis via extensive differentiation of mantle melts

Many workers have otherwise proposed that adakites can be produced by high pressure fractionation of mantle melts (Ribeiro et al., 2016; Macpherson et al., 2005; Kolb et al., 2013).

Macpherson et al. (2005) studied the Surigao adakites of the southern Philippines. They concluded that the adakitic signature of the Surigao rocks was produced either by a) high pressure crystal fractionation of a garnet bearing assemblage from a basalt sourced in the metasomatized mantle wedge, or b) melting of a solidified garnet bearing basalt. They conclude that ‘any subduction zone has the potential of produce adakitic magma if basalt crystalizes at sufficient depth’ (Macpherson et al., 2005).

Ribeiro et al. (2016), also working in the Philippines, illustrates how water rich mantle melts that are stalled in the lower crust can fractionate a garnet and high-pressure Mg-rich amphibole to produce an evolved residual melt with an adakitic fingerprint. They find that their genesis is controlled by the magma mixing and fractionation of high-pressure phases - the depth of storage is thus an important feature in their formation. Crustal assimilation is thought to be a minor process in the formation of their signature.

Kolb et al. (2013) explores the importance of amphibole fractionation in the development of the adakite signature through studying the adakitic rocks of the

East Serbian section of the Balkan – Carpathain Arc. They investigate whether normal arc and adakitic signatures may both be produced from a single parental magma, through a process that involves multiple stages of minor assimilation and fractional crystallization in the lower and upper crust.

Kolb et al. (2013) find that adakitic and normal arc melts can be formed from a single parental magma, in the Serbian case, a mantle-derived hydrous basaltic andesite. The emergence of the adakite signature involved extensive high-pressure amphibole fractionation in the lower crust, followed by plagioclase dominated upper crustal fractionation.

In all scenarios, the melting or evolution of basalt at high pressure, where garnet and/or amphibole are both stable and present as a residual or fractionating phase, has been identified as a key variable (Castillo et al., 2006). Garnet and amphibole stability are key to adakite formation, but an additional factor is the absence of plagioclase as a residual or fractionating phase. This is an important control on Sr and Y content of a melt. Plagioclase (which incorporates Sr) is stable at lower pressures, whereas garnet (which incorporates Y) is stable at higher pressures. The result of this relationship is a dramatic increase of the Sr/Y ratio with increasing depth of melting. La and Yb have comparable behaviours. Fractionation or melting in the absence of plagioclase thus results in Sr enrichment, while the stability of garnet and amphibole leads to Y depletion (Kolb et al., 2012).

Investigation into the relationship between high Sr/Y melts and economically significant porphyry deposits demonstrate the importance of the mid-crustal fractionation pathway (Chariada et al., 2015). As outlined above, extensive mid-crustal fractionation (and a degree of crustal assimilation) can yield suitable conditions for high Sr/Y melts (i.e. higher pressures lead to the fractionation of assemblages of amphibole and garnet) (Kolb et al., 2012; Macpherson et al., 2005). It is understood that critical factors in the formation of porphyry deposits include high water content (>4 wt. %), high sulphur content (1000ppm) and a highly oxidised magma (Chariada et al., 2015). An andesitic oxidised magma crystalising in the mid-crust has also been demonstrated to exsolve a sulphur rich fluid, into which copper can effectively partition (if it is present in abundance in the melt). The ascent of these copper rich fluids into the the lower crustal magma chambers is the mechanism behind porphyry formation (Chariada et al., 2015).

Table 5: Summary of three main models for adakite petrogenesis.

Process		Example	Reference
Slab melting	Adakite genesis via slab melting predominantly occurs where young, hot crust is subducted (initially thought to be strictly <25 Ma). A number of other conditions have been shown to facilitate melting in older slabs e.g. during subduction initiation, subduction collision, a shallow subduction angle (oceanic crust is far more likely to reach its wet-solidus in hot geotherms). Slab melts formed percolate thought the mantle wedge, before fractionating in a magma storage region.	Southern Andes Experimental Aleutian Islands	Kay et al., 1993, 1999 Sen et al., 1994 Kay et al., 1978; Yogadzinski et al., 1998
Melting of the thickened mafic lower crust	Melting of mafic lower crust, itself typically formed of previous arc-basalt, can produce the adakitic signature, should the overlying crust be sufficiently thickened for the lower region to be in the garnet amphibolite stability zone (typically 40 – 50m depth). The melts then further interact with and fractionate in the middle to lower crust.	Tibet The Philippines	Chung et al., 2003; Hou et al., 2004 Yumul et al., 1999
Extensive differentiation of mantle melts	Mantle melts have been shown to be able to acquire adakitic signatures under certain condition. High pressure crystal fractionation in the lower crust is a key feature of this process, while the melts themselves are commonly cited to be source from a water-rich metasomatized mantle wedge.	Mindano Arc, Phillipines Serbia	Macpherson et al., 2005 Kolb et al., 2013.

2.6.1.3 TTG's and adakites of the Southern Andes: Are they related by fractional crystallization?

In his robust investigation of Adakite and TTG geochemistry and petrogenesis, Condie (2004) explores whether TTG's and Adakites could be sourced from the same parental melt, undergoing different fractional crystallization pathways prior to emplacement. Condie (2004) cites the southern Andes, where both rocks with adakitic and TTG geochemical profiles are found in close proximity (see *Table 6)* (Kay et al., 1993, 1999; Stern and Kilian, 1996; Petford and Atherton, 1996). This led many workers to question the possibility that TTG's and adakites are both slab melts, invoking that subsequent fractional crystallization reduced the compatible element components (Castillo, 2016). Condie (2004) concludes that Adakites and TTG's are not related by fractional crystallization, suggesting that Adakites are slab melts, and TTG's the result of partial melting of the lower crust in arc systems, or in the roots of oceanic plateaus.

Table 6: Description and interpretation of the geochemistry of the Andean TTGs and Adakites (geochemistry after Kay et al., 1999; interpretations after Kay et al., 1999 and Condie, 2005).

	Geochemistry	Interpretation
Southern Andean / Patagonian Adakites	High La/Yb ratio High Mg numbers (50 – 70) Enriched in Ni (>40ppm), Cr (>80ppm) and Sr (1800ppm).	These characteristics interpreted to imply the interaction of slab melts with the ultramafic material of the mantle wedge (rich in MgO, Ni, Cr and Sr). The adakites are invoked to be slab melts that incorporated compatible elements as the percolated through the mantle wedge (Kay et al., 1999).
TTGS of the Central Volcanic Zone	High La/Yb ratio Lower Mg numbers (<55) Low values for Ni (5ppm), Cr (50ppm) and Sr (300ppm)	Kay et al. (1999) invokes that delamination resulted the production of basaltic magmas that pooled at the base of the thickened lower crust, facilitating melting (i.e. the TTG's are lower crustal melts, that had no interaction with the ultramafic material of the mantle wedge).

2.6.2 Orogeny and Post- Orogenic Magmatism

To build a hypothesis regarding the relationship between Caledonian geodynamic and magmatic events, the spatial and temporal evolution of similar orogens should be studied. The Tibetan Plateau and the Turkish Iranian Plateau can be studied in this regard.

2.6.2.1 The Tibetan Plateau

The Cenozoic collision of the Indian and Asian plates along the Indus – Tsangpo zone (associated with the closure of the Neo-Tethyan Ocean) is generally accepted as the mechanism behind the rise of the Tibetan Plateau and the associated Himalayan mountain range (Molnar et al. 1993; Royden et al., 2008). Some controversy remains concerning the timing of initial collision (Yin and Harrison, 2000; Aitchison et al., 2002; Rowley, 1998). The model of Lee and Lawver (1995) – soft collision at 69Ma, hard collision at 45Ma – is used by Chung et al. (2005) in their examination of Cenozoic magmatism in Tibet.

Post collisional magmatism is well documented and seen as one of the key methods for tracing the geodynamic evolution of the plateau (Chung et al. 2005). Mapping out magmatism spatially and temporally enables Chung et al. (2005) to synthesize an understanding of the timing of; 1) the underthrusting of Indian continental lithospheric mantle under Asia, 2) rollback and subsequent break off of the subducted Neo-tethyan slab, and 3) the removal of the Lhasa lithospheric root. Chung et al. (2005) identify four pulses of magmatism. These stages are summarised in *Figure 6* and *Table 7*.

The work of Chung et al. (2005) and other workers in Tibet is of keen interest when studying the Caledonides in that it informs on the timescales mountain belts evolve, and the magmatic expression that might be expected at each stage.

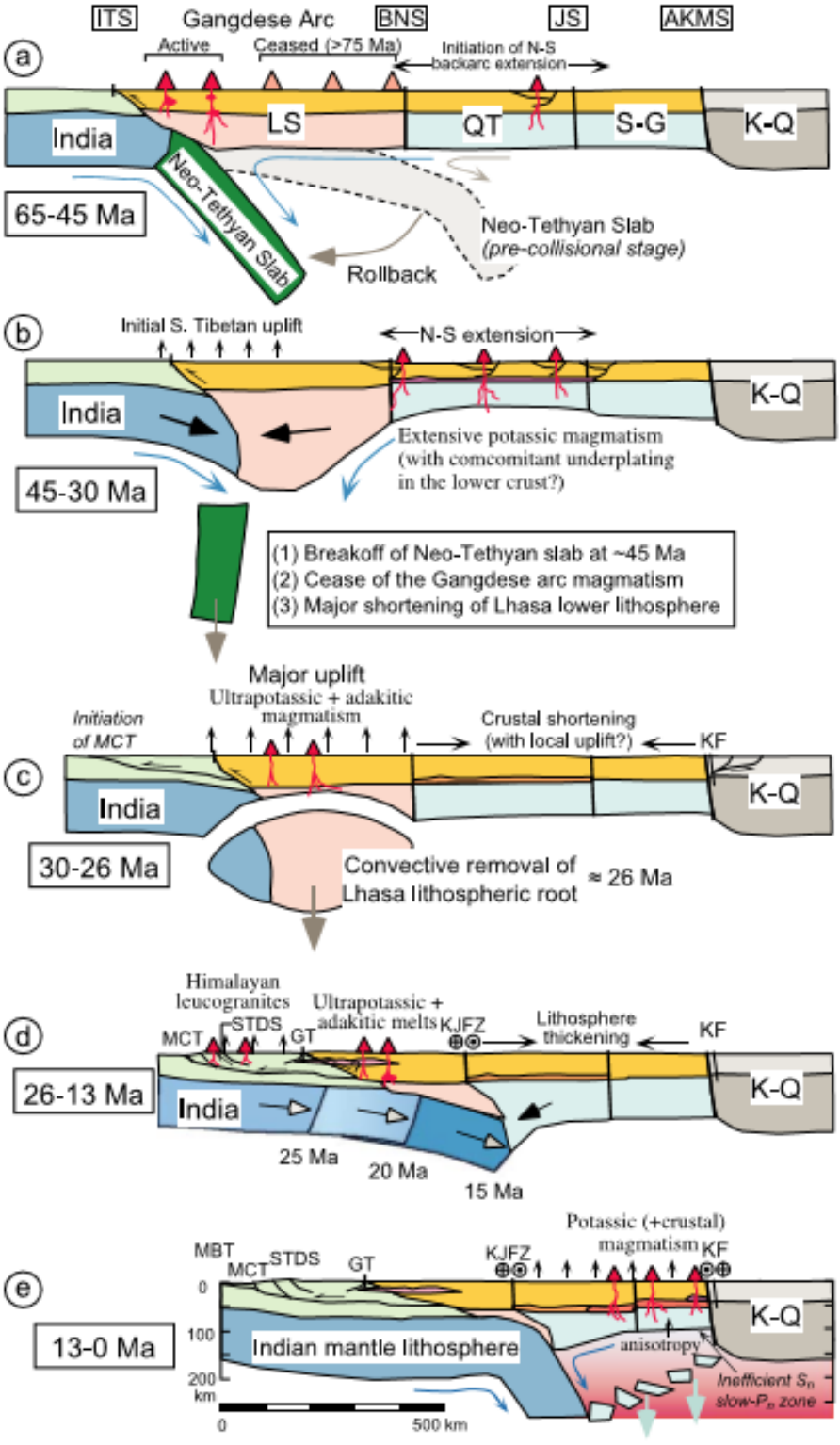

Figure 6: From Chung et al. (2005). Schematic diagram showing each stage of orogeny and associated magmatism. These are detailed further in Table 7.

	Period	Style of magmatism and associated tectonic environment
A)	**65 – 44 Ma**	Magmatism in the intermediate aftermath of the collision (c. 65Ma) is restricted to the southern part of the Lhasa terrain (close to the sutre zone) and resembles typical continental arc magmatism i.e. calk-alkali in nature. Sr and Nd isotope data implies significant involvement of juvenile mantle component during the magma generation process, suggesting a **source in the mantle wedge**.
B)	**45 – 30 Ma**	Neo-Tethyan oceanic slab is proposed to have detached from the Indian continental lithospheric mantle at c. 45 Ma – 20 Ma after proposed collision (Zhang et al. 1987). Magmatic activity was expressed immediately and was widespread, the defining feature being high to very high alkali contents (ultrapotassic and shoshonitic suites). The more felsic bodies have characteristics indicative of small volume melts from an **enriched lithospheric mantle source**.
C)	**30 – 13 Ma**	The third phase of magmatism is markedly different from those prior, occurring as dyke swarms and small volume plugs. The intrusions are classified as either ultrapotassic or adakites, the latter containing Cu and Mo – Au deposits in certain localities. These are suggested to have been derived from **melting of the thickened lower crust** (likely >50km), which consisted of mafic eclogite and/or garnet amphibolite. Melting is presumed to have occurred due to the removal of the crustal root beneath the Lhasa terrane (Chung et al. 2003; Chung et al. 2005). Chung et al. 2005 highlight that the adakites could not have been sourced from the Neo-Tethyan slab, due inconsistency's with Nd and Sr isotope signatures and the timing of evets (the Neo-tethyan slab was likely already detatched from the orogenic system by this stage).
D)	**15 Ma – recent**	Widespread potassic magmatism reoccurred in Tibet at 15Ma. At this time, Tibet was transformed into an east west extensional environment.

Table 7: Summary of magmatism and associated tectonics in the Tibetan plateau, after Chung et al., 2005.

2.6.2.2 The Turkish Iranian Plateau

The Turkish Iranian Plateau (TIP) of Eastern Turkey, Northern Iran and the Caucuses is similarly well intact analogue by which the temporal and spatial effects of orogeny and slab break off can be studied, especially with regards to their magmatic expression (e.g. Neill et al., 2015; Keskin, 2007; Pearce et al., 1990). Adakite generation can also be studied here (Lechmann et al., 2008). The Arabia-Eurasia collision is also of interest as, similar to the Scandian event, collision was oblique and the magmatic expression was staggered in accordance.

The TIP was uplifted following the Cenozoic continent - continent collision of the Arabian plate and Eurasian plates, associated with Neo – Tethyan ocean closure (the same ocean closure discussed with regards to the Tibetan Plateau) (Pearce et al., 1990).

The timing of Arabia - Eurasia collision is remains uncertain, with a spectrum of ages being reported in the literature; from the Late Cretaceous (70 – 60 Ma e.g. Mazhari et al., 2009), Late Eocene – Oligocene (c. 35 Ma; Allen and Armstrong, 2008), or Early – middle Miocene (c. 12Ma; Guest et al, 2006). Post-collisional surges in magmatism and uplift following a magmatic gap has been used to infer the timing of slab break – off (Lechmann et al., 2018). Many studies (e.g. Allen and Armstrong, 2008; van Hunen and Allen, 2011) now favour a model of arc collision occurring in the late cretaceous, with hard Arabia - Eurasia occurring in the early Oligocene (c. 33Ma), and slab break off occurring in the late Miocene (c. 10 – 5 Ma, initiating magmatism across the collision zone that prevails to this day (Neill et al,. 2015).

The magmatism experienced in the TIP is either calc-alkaline, with a subduction related signature and source in the SCLM, or adakitic (see *Figure* 7). The calc-alkaline signature show ubiquitous negative Nb – Ta anomalies, enrichment in the LILE's as is typical of melts source form the metasomatized mantle wedge or SCLM. The adakites of the TIP are studied by Lechmann et al., 2018, who attempts to model the source of the adakitic fingerprint.

Lechmann et al. (2018) favour a scenario that involves the re-melting of a mafic underplate consisting of Eocene/Oligocene age subduction related cumulates

(eclogite or garnet – clinopyroxene – hornblende). This would explain the clear mantle peridotite signature of the adakites (high Mg#, Cr and Ni). This signature cannot be explained by melting of the subduction-modified mantle alone, due to the evolved, high SiO_2 nature of the samples. The high SiO_2 contents seen in the adakites would require approximately 40% removal of olivine, inconsistent with the elevated Cr and Ni contents observed.

The two distinct pulses of magmatism in NW Iran (c. 16.2 – 10.6 Ma and c. 5.5 – 0.4 Ma), with a clear 5 Ma magmatic gap, can be used to infer the time slab break-off was experienced in NW Iranian Azerbyjan. It is of note that the suites of adakitic character are emplaced following this magmatic gap and the proposed time of slab break off. As stated previously, it is also important to note that given the oblique nature of the collision, the timing of slab break-off and its associated magmatic expression will also vary across space (Lechmann et al., 2018).

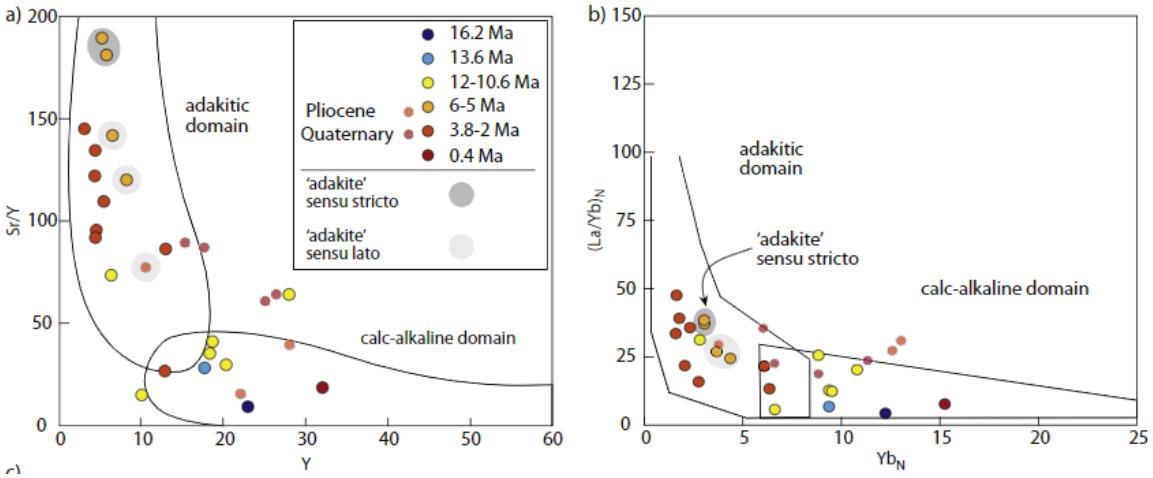

Figure 7: From Lechman et al., 2018. (A) Sr/Y versus Y diagram with adakitic and calc-alkaline domains after Defant and Drummond (1990). (B) Chondrite normalized La/Yb versus Yb diagram with adakitic and calc-alkaline domains after Martin (1986). The suites are aslo colour coded to display their U – Pb zircon age.

3. Methodology

3.1 Thin section Preparation

Normal thin sections for optical microscopy were prepared from rock chips using standard techniques, as discussed in *Appendix A – Thin section Preparation*. Samples for electron microscopy and microprobe analysis were polished further using a 0.3μm wetted alumina powder for 10-20 minutes.

3.2 Electron Probe Micro-Analysis (EPMA)

EPMA is a micro-analysis technique highly effective for in-situ, minimally destructive characterization of the chemical composition of materials. The instrument was used to establish calcic-amphibole compositions in samples from Glen Loy and Clunes, such that the aluminium-in-hornblende geobarometer could be used to establish depth of crystallisation. Plagioclase feldspar compositions were also analysed in order to establish their albite-anorthite ratio.

For depth/pressure estimations to be carried out accurately, a specific mineralogy must be observed (plagioclase, hornblende, biotite, K-feldspar, quartz, sphene, magnetite or ilmenite, + epidote (Hammersrom & Zen, 1986). The barometer also assumes that the amphibole crystallised at the granite solidus, and thus textural analysis of the samples must be carried out to ensure amphiboles selected for analysis are in equilibrium with surrounding minerals (Hammersrom & Zen, 1986).

3.2.1 EPMA Acquisition parameters

EPMA analyses was performed at the University of Manchester with Cameca SX100, using 5 crystal wavelength dispersive spectrometers. Calibration was carried out using a mixture of natural and synthetic minerals and oxides; with crystals of known composition being used as secondary standards. The secondary standards are detailed in *Appendix E*. The analytical set-up used is detailed in *Table 8* and *Table 9*.

Table 8: Crystal wavelength dispersive spectrometer set up used for elements measured.

	Crystal wavelength dispersive spectrometer:				
	LIF	**PET**	**LPET**	**TAP**	**TAP**
Elements measured	Fe	Ti	K	Rb	Sr
	Mn	Cr	P	Na	Al
	Co		Ca	Mg	Si

Table 9: EPMA acquisition parameters

	EPMA acquisition parameters
Beam Intensity	15nA
Beam Size	5µm
Kilivolts	15

3.3 Rock Crushing and Powdering

Powdered rock samples were prepared for whole rock major and trace elemental analysis.

Samples were cut into blocks no bigger than 3cm by 3cm in order to fit into the rock crusher. Care was taken to remove as much as possible of the weathered outer surface as possible so that the whole rock geochemistry represented the un-weathered parent rock. A Powerglide Hydraulic Drive saw was used to cut medium to large blocks, and E-Bueller Geocut used for small to medium sized blocks.

The un-weathered blocks were crushed into chips using a Retch Jaw crusher. The jaws of the crusher were adjusted using the wheel on the side of the instrument. Once a sample had been run through the crusher and reduced to chips, the jaws were wound closer together to further reduce the size of the chips. To prevent cross contamination, the Retch jaw crusher was cleaned extensively between samples. The cleaning routine involved dismantling the jaws or the crusher, and the inside of the chute brushed and wiped down with acetone.

Milling was carried out in the crushing room using the Vibratory disk mill. This step was carried out once the sample was in consisted of chips no greater than 1cm by 1cm. The plates of the mill were adjusted using the wheel on the back of the instrument. The crushed material is fed into the instrument via the hopper.

3.4 X-Ray Fluorescent Spectrometry (XRF)

XRF was used to measure major element compositions of powdered samples from Clunes, Glen Loy, Glen Scaddle and Loch Linnhe. The technique was carried out at Edinburgh University, by lab manager Nic Odling.

3.4.1 Glass Disc Preparation

Major element concentrations were measured on fused glass discs of homogenous composition. Unignited rock powders were dried at 110°C overnight to remove residual moisture. 1g of each sample powder was ignited at 1100°C in order to decompose carbonates and hydrous silicates.

0.95g of each sample was weighed into a platinum crucible and mixed thoroughly with a borate flux (Johnson and Mathey Spectroflux 105) in a ratio of 1:5 sample: flux ratio. Spectroflux 105 is a mixture of Lithium tetraborate, Lithium oxide which acts as an x-ray heavy absorber.

The mixture was fused in a muffle furnace (1100°C for 20 minutes) and cooled to room temperature to form a glass. The samples were re-weighed and the weight loss measured (due to de-volatilisation of hydrous silicates and carbonates). The lost weight was replaced with additional flux to regain the initial 5:1 sample: flux ratio. The sample was fused for a second time over a Meker, which was swirled thoroughly to produce homogenous compositions. The molten mixture was poured onto a graphite plate, and a glass disc formed by compression with an aluminium plunger. This casting operation was carried out on a hot plate at 220°C. The glass disc was left on the hotplate for ten minutes to slow the cooling process, preventing fragmentation.

3.4.2 Spectrometer set up

The XRF spectrometer was calibrated for major element analysis using international standard samples. In terms of precision, three runs of standard JB1-A returned a first relative standard deviation of better than 0.7%. Instrumental settings are presented in *Table 10*.

Table 10: XRF acquisition parameters

Element	Line	Tube voltage	Tube current	Analysing crystal	Angle of crystal	Collimator (μm)	Detector	Time (s)
Si	Kα	50	50	InSb	144.63	300	Flow	20
Al	Kα	50	50	PE	144.82	300	Flow	20
Na	Kα	50	50	TlAp100	55.16	300	Flow	50
Mg	Kα	50	50	PX1	22.99	700	Flow	20
P	Kα	50	50	Ge	140.98	300	Flow	20
K	Kα	50	50	LIF200	136.71	300	Flow	20
Ca	Kα	50	50	LIF200	113.12	300	Flow	6
Ti	Kα	50	50	LIF200	86.14	300	Flow	14
Mn	Kα	50	50	LIF200	62.99	300	Flow	20
Fe	Kα	50	50	LIF200	57.49	300	Flow	8

3.4.3 Inductively coupled plasma mass spectrometry (ICP-MS)

Powdered samples were dissolved via acid digestion for analysis. A mixture of hydrofluoric acid (HF) and Nitric acid (HNO_3) was used for the first stage of digestion. 0.15g (+/-0.05g) of sample was added to the acid and left on a hot plate for 24 hours. 0.1ml of HNO_3 was then added to the mixture and left for another 24 hours. 0.2ml of perchloric acid was then added to the solution, which was left on a heated hotplate for a further 24 hours. 5% HNO_3 was then added to complete the digestion process.

Trace element characterisation was carried out at the Scottish Universities Environmental Research Centre (SUERC). The ICP-MS used was an Agilent 7500ce fitted with a double loop spray chamber and self-aspirating Teflon nebulizer tuned for a flow of 0.1mn/ml.

The reference material used was SRM USGS BCR-2 (British Columbia river basalt). Errors were calculated by the ICP-MS software at SUERC, based on the first relative standard deviation of repeat runs of USGS standard reference material BCR-2 (n=25). In terms of precision, the laboratory quoted first relative standard deviations for trace elements of better than 4% for all elements.

3.5 Preparation of Zircon Grains

Zircon grains from Glen Loy, Cluanie and Loch Linnhe were isolated in preparation for dating using U – Pb isotope decay.

3.5.1 Sieving

Milled material was separated into size fractions using sieves of different mesh sizes. The mesh sizes used were 710μm, 500μm, 250μm, 212μm. The sieves were stacked with the mesh sizes decreasing from the top of the stack to the bottom. A collecting tray was placed at the base stack and the milled material entered into the top sieve. The stack was placed on a vibrating plate and left for 30 minutes. The material separated by each mesh size was bagged up separately.

3.5.2 Washing

The sub 500μm and 250μm fraction was washed with water to remove lighter minerals e.g. clay particles. The sub 500μm material was added to a beaker of water. The heavier minerals settled to the bottom of the beaker while the lighter clay particles remained in suspension. The water and suspended particles were carefully poured off. This process was repeated until there were no particles in suspension (until the water added to the beaker ran clear).

3.5.3 Zircon grain isolation - vertical magnetic separation

Zircon is a nonmagnetic mineral. Frantz isodynamic magnetic separator was used to isolate nonmagnetic minerals in the sample. Only the strongly magnetic grains are removed here, as the grains flow past the magnet too rapidly to effectively remove all moderately magnetic minerals. The grains were loaded into the closed hopper above the magnet. The magnet strength and the distance of hopper from the magnet were set. These settings were changed twice to maximise the possibility of removing magnetic grains, and to prevent the flow of grains becoming blocked by the accumulation of strongly magnetic minerals at the top of the magnet. The settings are displayed in *Table 11*.

Magnetic minerals stick to the magnet while non-magnetic minerals fall into the tray beneath. Once all of the grains were passed through the hopper, the non-magnetic material in the tray was removed and placed in a clean beaker. The magnet is turned off and the magnetic grains allowed to fall into the clear tray below. This magnetic material was removed and bagged up. The non-magnetic material was passed through the separator with the same settings a further two times to remove as many magnetic grains as possible.

Table 11: Operation parameters for vertical separation. *Distance of magnet from hopper.

	Distance* (cm)	Current (Amps)
1st run:	2	1
2ND run:	1	1.5
3RD run:	0.5	2

3.5.4 Zircon grain isolation - gravity separation using heavy liquids

The material remaining after vertical magnetic separation consists of a mixture of non - or weakly magnetic minerals. Zircon is a heavy mineral, with a density of ~3.93-4.73 g/ml. Other non- or weakly magnetic minerals are comparatively lighter e.g. quartz has a density of 2.65g/ml, feldspar a density of 2.62 – 2.75g/ml. Heavy minerals such as zircon can thus be isolated through the using density separation. This was carried out by immersing the grains in the heavy liquid lithium heteroolytungsate (LST), density 2.8+-0.02g/ml. Since this value falls between that of the target mineral zircon and the lighter mineral components, immersion facilitates the separation of the sample into heavy and light mineral components.

The density of LST must first be checked before use. At the correct density, 10ml of LST should weigh 28+-0.02g.

750ml of LST was added to a separator funnel. 200g of grams of the sample was added, and the grains stirred thoroughly with a stirring rod. The mixture was left

for two hours to allow the heavy minerals to settle to the bottom of the separator funnel. After two hours, the funnel was opened carefully, allowing only the heavy grains at the bottom of the separator funnel to run into the filter paper on the buchnel funnel below before it was closed. The filter paper and grains were removed and placed in an aluminium petri dish in the fume cupboard to dry. Once dry, the grains were carefully transferred into a small vile or petri dish, and labelled.

Pure LST was collected at each stage in the process and recycled. All pieces of apparatus that come into contact with LST were rinsed down with deionised water and the runoff captured and stored for distillation.

3.4.5 Horizontal magnetic separation

Any remaining magnetic minerals were removed by passing the samples through a horizontal Frantz magnetic separator. The instrument consists of a chute that runs past an electromagnet of user-set field strength. The chute is tilted and rolled at a shallow angle and has two distinct separation tracks. Magnetic grains will be drawn to one track of the chute, while nonmagnetic grains will continue down a separate track. The samples were stored in a hopper above the chute of the separator which can be opened to release a steady stream of grains. Each sample was run four times to remove as many magnetic grains as possible. The electromagnetic field strength was increased by increasing the intensity of the current by increments of 0.4amps after each run (i.e. 0.4amps, 0.8amps, 1.2amps, and 1.8amps).

This was the final stage of mineral separation. The remaining non-magnetic grains were transferred into a vial labelled ready for mounting.

3.4.6 Grain mounting

Resin was prepared by combining 7.5ml of epoxy and 1ml of hardener. Each liquid was carefully transferred via syringe into a glass beaker where the mixture was stirred slowly for five minutes and left to settle for a following five minutes. Care was taken at each stage of this process to avoid the incorporation of bubbles into the mixture, which can stick to the grains and disrupt analysis.

A glass slide (7.5cm x 5cm) was wiped clean with acetone and coated with a quick release agent. Two rubber washers, coated on all sides with quick release agent, were placed on the slide. A smaller washer was placed within each of these, and the grains carefully poured onto the glass exposed within the washers to give a thin cover. The smaller inside washer was removed with tweezers, and the resin poured carefully onto the glass within the larger washer. A sheet of plastic was placed over the resin filled washers, and a weight placed on top. The samples were left for 48 hours to allow the resin to set. After 48 hours, the weight was removed from the samples and a scalpel or razor blade used to carefully prise the rubber washer and resin mount from the glass slide. The excess resin was carefully clipped from round the side of the washer. The washer was broken apart with clippers, and carefully peeled away, leaving the circular epoxy mount. The sample ID was inscribed onto the back of the sample using a diamond pen.

Three resin grain mounts were made for Cluanie and Glen Loy (CL1, CL2, CL3 and GL1, GL2, GL3 respectively), while a single resin mount was made for Loch Linnhe (LL). The zircon grains in each sample from Glen Loy and Cluanie are sourced from identical blocks.

3.4.7 Grinding and Polishing

The epoxy mounts were ground down to expose the grains at the surface of the resin using silicon carbide abrasive paper. Paper of grade P800 (European P-Grade) was used first. The paper was wet, and the samples ground over it in a figure of 8 motion. The sample was checked at short intervals to minimise the chance of over-grinding and loss of grains.

Once the majority of the grains were exposed at the surface of the resin, the P1200 paper was used briefly, followed by P2400 and P4000. These papers were used for as little as 30 seconds each, the aim simply to minimise the imperfections introduced by the previous step of grinding.

Polishing was carried out in order to remove scratches and imperfections introduced by the grinding. The sample was mounted onto a Kemet 300 series polishing device with a polishing pad wetted with 1µm alumina powder and water. The mounts were polished until the grain surfaces were clear and unscratched.

3.4.8 Cathodoluminescence imagery

The grains were imaged using the Cathodoluminescence (CL) detector on the Scanning Electron Microscope (SEM). CL imagery of zircon grains enables identification of compositional zoning in zircon grains. Compositional zoning is an indication of different phases of growth throughout the 'life' of the grain and is thus an important feature to consider when selecting targets for the laser. Each grain was imaged using the CL and backscattered electron (BSE) detector, and its position in the resin mount and sample ID noted. Following this analysis, the samples were polished gently on the 1µm alumina to remove any remaining carbon coating applied for the SEM. Once wiped down, they were handled with gloves to avoid contamination.

3.4.9 Mapping and target selection

Once the CL images of the grains were acquired, targets of 30µm spot size were determined based on the zoning patterns seen in the grains. These positions were recorded in a format that could be imported into the LA-ICPMS. This was done using the FT. Stage application, linked to a petrographic microscope. The grid references were saved and exported to csv file format, ready to be imported into the laser.

3.5 Laser Ablation Inductively Couple Plasma Mass Spectrometry (LA-ICPMS)

LA – ICPMS is a widely used tool in microanalysis and U – Pb geochronology. It involves lasing the surface of a mineral and measuring the ablated aerosols with a mass spectrometer. Analysis was carried out in-house at Glasgow University. The laser component of the system used was a RESOlution laser made by Australian Scientific Instruments. The mass spectrometer used to ionize and collect the sample was a single collector iCAPRQ model made by thermoscientific. The instrument uses an Argon (Ar) carrier gas. The control software used to operate the laser was Geostar, developed by Norris Software specifically for use with the RESOlution instruments. The instrument was calibrated using the standard glass NIST 610 and a secondary reference material Plesovice (see *Appendix B*).

3.5.1 Set up

The samples were loaded into the sample holder which was scanned on an Epson flatbed scanner and the image file imported into Geostar. Before loading the sample holder into the cell, the cell was flushed of the Argon carrier gas. Once the sample holder was loaded, a live video display of the holder in the cell was calibrated against the image acquired from the Epson flatbed scanner to allow navigation around the samples.

The coordinates of the zircons targeted for analyses were imported into the Geostar. A calibration procedure was repeated for each sample, in order to check that the points selected for analysis were well positioned on the zircon grains. The same was done for the secondary reference material Plesovice, and the standard glass NIST 610. These points were distributed through the set zircon data points (one NIST610 and one Plesovice per 10 Zircon grains, with two NIST610 points at the start and end).

The acquisition parameters are displayed in *Table 12*.

Table 12: LA – ICPMS acquisition parameters

Acquisition parameters	
Fluence:	4.5
Resolution rate:	10Hz
Ablation time:	30 Seconds
NZ:	11
Spot size:	30µm
Isotopes measured:	133Cs, 198Hg, 204Pb, 207Pb, 207Pb, 208Pb, 232Th, 235U, 238U

3.5.2 Data reduction using Iolite Software

The software Iolite was used to process and reduce the data produced from the mass spectrometer. Iolite was used to normalize values to the secondary reference materials and standard glass and correct for analytical limitations (e.g. downhole fractionation; the evolution of U-Pb readings over time). The data reduction scheme (DRS) 'VisualAge' was used to process the data (Petrus and Kamber, 2012).

3.5.3 Establishing a crystallization age

The datasets produced by iolite and the VisualAge DRS were interrogated in Excel using the add-in Isoplot 3.7 (developed by Berkeley Geochronological Centre) to construct U-Pb Concordia plots.

3.5.3.1 Percentage discordance

In order to interrogate the data set and remove discordant readings, percentage discordance was calculated using *Equation 1*.

$$D1: (206Pb/238U\ age)/(207Pb - 206Pb\ age)*100$$

$$D2: (206Pb\text{-}238Uage)/(207Pb\text{-}235U\ age)*100$$

Equation 1: Equations for calculating percentage discordance (D1 and D2).

The resulting percentages acts as a qualitative assessment of whether there has been disturbance to the isotopic ratios within the zircon following crystallization (generally due to Pb migration within the zircon crystal lattice). Applying these formulas gives a numerical evaluation concordance, where 100 is perfectly concordant and values higher or lower are progressively more discordant. Only points with a discordance of <5% were plotted and considered when establishing a crystallization age each pluton (Horstwood et al., 2016).

3.5.3.2 Screening for common lead

Common lead (or non-radiogenic lead) must be accounted for in a system in order to calculate an accurate date. 204Pb is the least abundant Pb isotope present in

zircon but can be introduced by contamination. Screening for common abnormally high common lead readings was carried out manually (the ratio with 204Pb with 206Pb, 207Pb and 208Pb was compared to those of the reference material). No values were significantly higher than that of the reference material (by an order of magnitude greater than 2). (Horstwood et al., 2016).

3.5.3.3 Final Crystallization age

The final ages were calculated using the 'Mean Age' function in isoplot. The 206Pb/238U age was used, as this is considered the most accurate isotopic ratio for grains of this age (Horstwood et al., 2016). Where analysis was carried out over two separate sessions, the data was first interrogated separately, before the selected grains were combined to calculate a final age. The texture of the grain was considered when selecting grains for the final crystallization age. Grains that appeared strongly metamict were discarded.

4. Results

4.1 Fieldwork, petrography and mineral chemistry

Fieldwork was carried out at Glen Loy and Glen Scaddle. Petrologic and structural observations from the field are presented here, at all times referencing maps presented in the supplementary material (see Page 18 and 19). Measurements taken in the field are given in *Appendix E*. Petrographic thin section work is also presented for Glen Loy, Scaddle, Cluanie and Clunes.

Crystal chemistry investigation via EPMA was carried out on samples from Glen Loy and Clunes. The chemical classification of plagioclase grains was calculated, followed by that of amphibole, such that the Al – in – hornblende geobarometer could be applied. The amphibole composition from Glen Loy was found to be incompatible with the geobarometer.

4.1.1 Glen Loy

4.1.1.1 Field description

The Glen Loy complex covers approximately 4km^2 and is intruded into the Loch Eil division of the Moine. The intrusion is roughly circular with a fragmented western margin, where numerous isolated smaller bodies are exposed (see Supplementary Item 1 and Figure 1). The lithologies associated with the Glen Loy Complex are described below and in more detail in *Table 13*.

4.1.1.1.1 Diorite

Although variable, the Glen Loy complex consists in the most part of a hornblende-rich diorite with an occasionally well-developed primary magmatic fabric. This fabric is parallel throughout the body, as opposed to being in line with the walls of the pluton and defined by the alignment of elongate hornblende grains. Magmatic fabric measurements are presented in stereonet format on the Glen Loy map (see *Page 17*). In general, the fabric strikes between 0 – 65 degrees and dips steeply to the NW. There appear to be two distinct sets of fabrics, one set striking at 0 – 30 and the other at ~60. In sectors where this magmatic fabric is well developed, there is often centimetre scale rhythmic layering of zones richer and poorer said hornblende grains.

4.1.1.1.2 Hornblende Gabbro

At the western extent of the pluton, the diorite grades into a hornblende gabbro (NG 1260 to 1340 to 8300) which is also seen outcropping in small isolated patches west of the pluton (NG1240 8375, NG 1235 8430 and from NG1215 8375 in the south to NG 1230 8423 in the north). These outcrops were characterised by their high mafic mineral component (60 – 95%) and well-developed pyroxene and hornblende grains. Pyroxene grains of up to 1cm x 1cm and bladed hornblende of up to 1.5cm x 0.5cm are a characteristic part of the mineral assemblage.

4.1.1.1.3 Granite Pegmatite

The main body is crosscut by numerous granite pegmatite intrusions, sharing a similar trend (average orientation: 58°). A total of 19 substantial bodies (>1m wide) were counted crosscutting the river Loy from Loy Bridge at NG 1480 8180 to NG 1330 8300. These pegmatites range in size from centimetre scale, vein like intrusions to several metres wide. Larger zones of the granite pegmatite are found

at the southern extent of the pluton. Here, they are seen to cover areas of up to 2km x 500m (e.g. from NG 1230 8130 – 1315 8260).

4.1.1.1.4 Mafic Intrusions

A number of small lamprophyre intrusions were also identified (NG 1190 8325, 1226 8310 and at 1340 8395). These bodies were very fine grained and consisted entirely of mafic minerals. Classification as lamprophyre would require further geochemical characterisation.

4.1.1.1.5 Structural Observations

Several small shear zones were found throughout the body, characterized by zones of intense fracturing (see Figure 12). The zones are no greater than 2m wide and are often exploited by the River Loy or its tributaries. All shear zones were steeply dipping to the NW, typically with a strike of between 0° and 60°. Due to poor levels of exposure, the shear zones were difficult to follow laterally. Any primary magmatic fabric is lost in these zones. The orientation of the fabric in these shear zones are given in *Appendix E*.

4.1.1.1.6 Contact with Country rock

The contact with the Loch Eil Psammite is complex. It can be well studied in the River Loy, where both the far western and eastern contacts with the Loch Eil Psammite are exposed. There is a transitional zone of around 20 – 30 metres at both sides, where bedrock material has been incorporated into the pluton. To the west, there are prominent rafts of garnet bearing psammite - psammitic material found within the hornblende rich diorite. Here, the garnets are euhedral and well-developed and 1mm x 1mm in size.

Similar rafts of psammitic – semi-pelitic bedrock material are found to the northern extent of the pluton. These xenolith rafts are surrounded by diorite with a biotite component of up to 30%.

Lithology	Mineralogy/characteristics	Modes
Diorite	Medium-grained (0.3 x 0.3cm). Primary magmatic fabric defined by the alignment of elongate hornblende grains. (*See Figure 8*)	Plagioclase: 50 - 70% Hornblende: 15 - 30% Biotite: 0 – 10% Pyroxene: 0 – 5% Quartz: 0 - 15%
Hornblende Gabbro	Coarse-grained (0.5 – 0.5cm). Very occasional magmatic fabric defined by alignment of elongate hornblende grains. (*See Figure 8*)	Plagioclase: 5 - 30% Hornblende: 25 - 45% Biotite: 5 – 15% Pyroxene: 20 - 50%
Granite pegmatite	Medium-Coarse grained (0.3 – 0.5cm). No fabric observed. Bodies range in thickness from half a metre to a several 10's of metres. (*See Figure 10*)	K- feldspar: 50 – 70% Quartz: 10 – 20% Plagioclase: 5 – 25% Muscovite: 0 – 15% Biotite: 0 – 5%
Mafic Intrusions	Very fine grained. (0.5mm x 0.5mm). Dark grey to black in colour. No fabric observed	Clinopyroxene: 40% Hornblende: 25% Biotite: 25% Plagioclase: 10% (Estimates)

Table 13: Glen Loy complex lithologies.

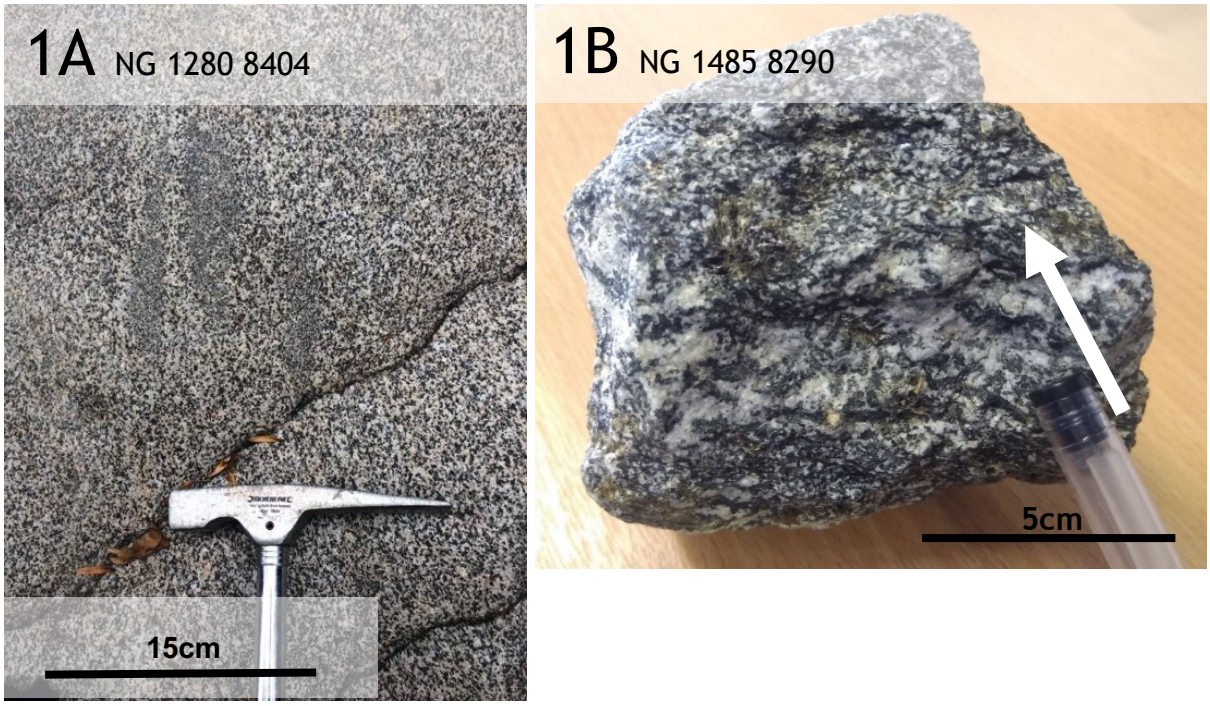

Figure 8: Field and hand specimen photographs of the diorite lithology. 1a) Mafic, fine-grained blobs within the diorite. There is no obvious reaction rim. 1b) Hand specimen showing primary magmatic fabric defined by elongate of elongate hornblende minerals. An approximately 3cm band of relatively plagioclase rich/hornblende poor is marked by the pen/arrow.

Figure 9: Field and hand specimen photographs of the hornblende gabbro. 2a) large hornblende grains of up to 3cm in length in a matric of mostly plagioclase. 2b) The plagioclase content is comparatively low (<5%), with the large hornblende crysts still being visible.

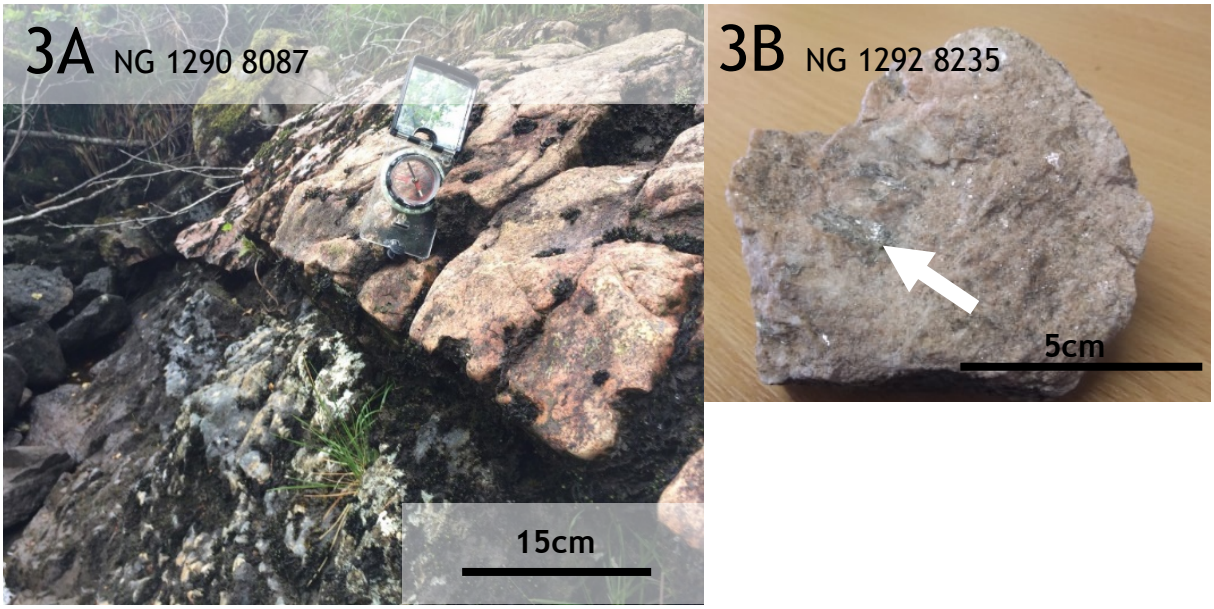

Figure 10: Field and hand specimen photographs of granite pegmatite. 3a) Contact between granite pegmatite and diorite is shown. These boundaries are sudden and there is little change in the diorite up to the boundary. 4b) Hand specimen of granite pegmatite showing large muscovite grains.

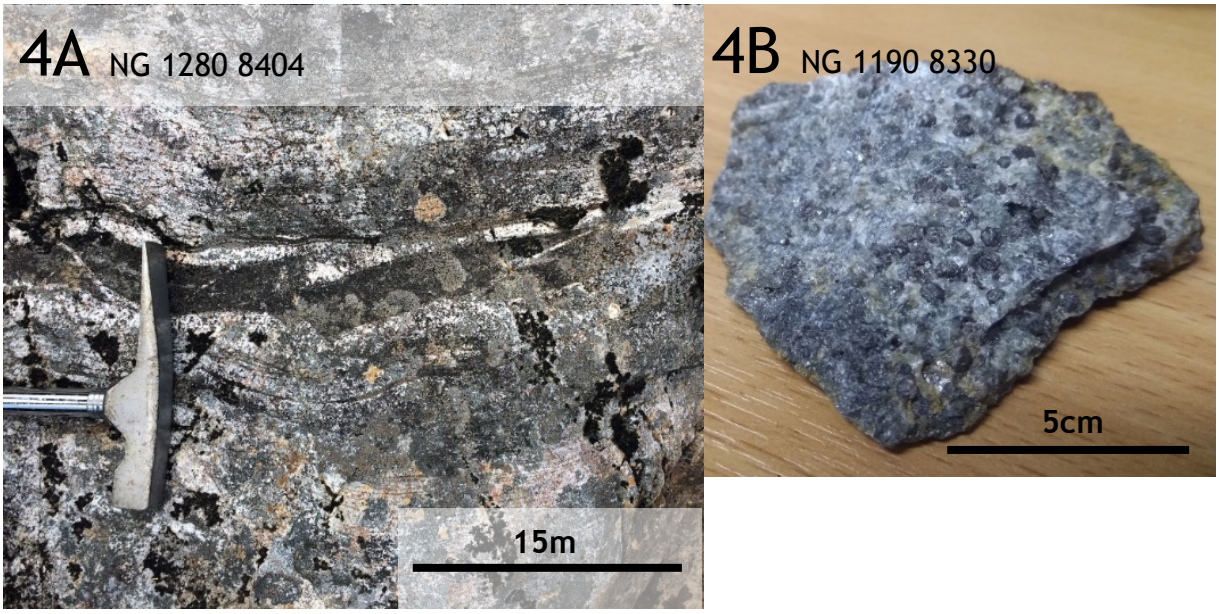

Figure 11: 4a) Metasedimentary Loch Eil psammite xenolith found close to the contact. The dimensions of the xenolith raft were not apparent - the material appears to have been partially incorporated into the diorite. 4B) Garnet - and biotite - rich hand specimen.

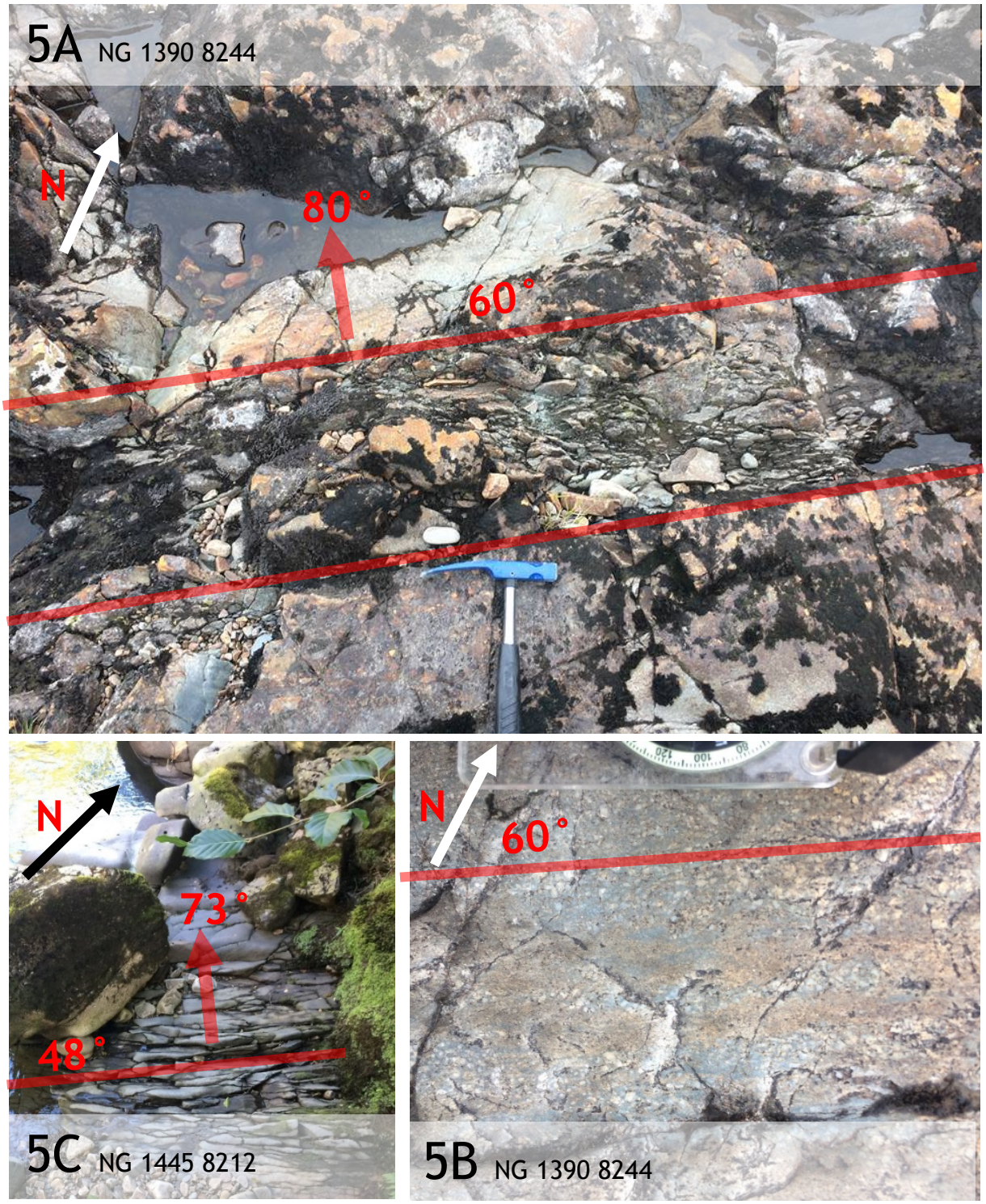

Figure 12: Shear zones found throughout the Glen Loy Complex. 5a) and 5b) show the intensely fracture nature of the diorite that identifies these zones as having been sheared. 5c) Primary magmatic fabric is lost. The hornblende crystals that defined the fabric a no longer present. Instead, granoblastic plagioclase define a faint tectonic fabric.

4.1.1.2 Petrography

The samples from Glen Loy and petrographic work are all of a medium to course grained diorite, consistent with the observations of the main lithology seen in the field (see *Figure 13*).

The samples from Glen Loy all exhibit secondary alteration assemblages associated with interaction with hydrothermal fluids. Phyllic and propylitic alteration assemblages dominate. Propylitic alteration is characterised by assemblages of secondary sericite, chlorite and epidote. Phyllic alteration assemblages consist of quartz, sericite and pyrite. Sericite is abundant, replacing k-feldspar and plagioclase. Mafic minerals (e.g. biotite) are replaced by secondary quartz. Fe oxides are common, with interstitial ilmenite and pyrite being most common.

Common accessory minerals included zircon and apatite, both of which are present in varying abundance throughout all samples collected. Zircon grains are at times large and euhedral – up to 2mm in length. A key textural feature of the samples are clumps/mats of biotite, which tend to be richer in zircon and apaitite inclusions. The mineral components of these aggregates to exhibit disequilibrium texture, and the crystal habit is typically anhedral. GL_LB_1 is the only sample to have an observable fabric, characterised by alignment of amphiboles and biotites (see *Figure 14*). This is consistent with the field observations - primary magmatic fabric was only observed in some sectors of the body.

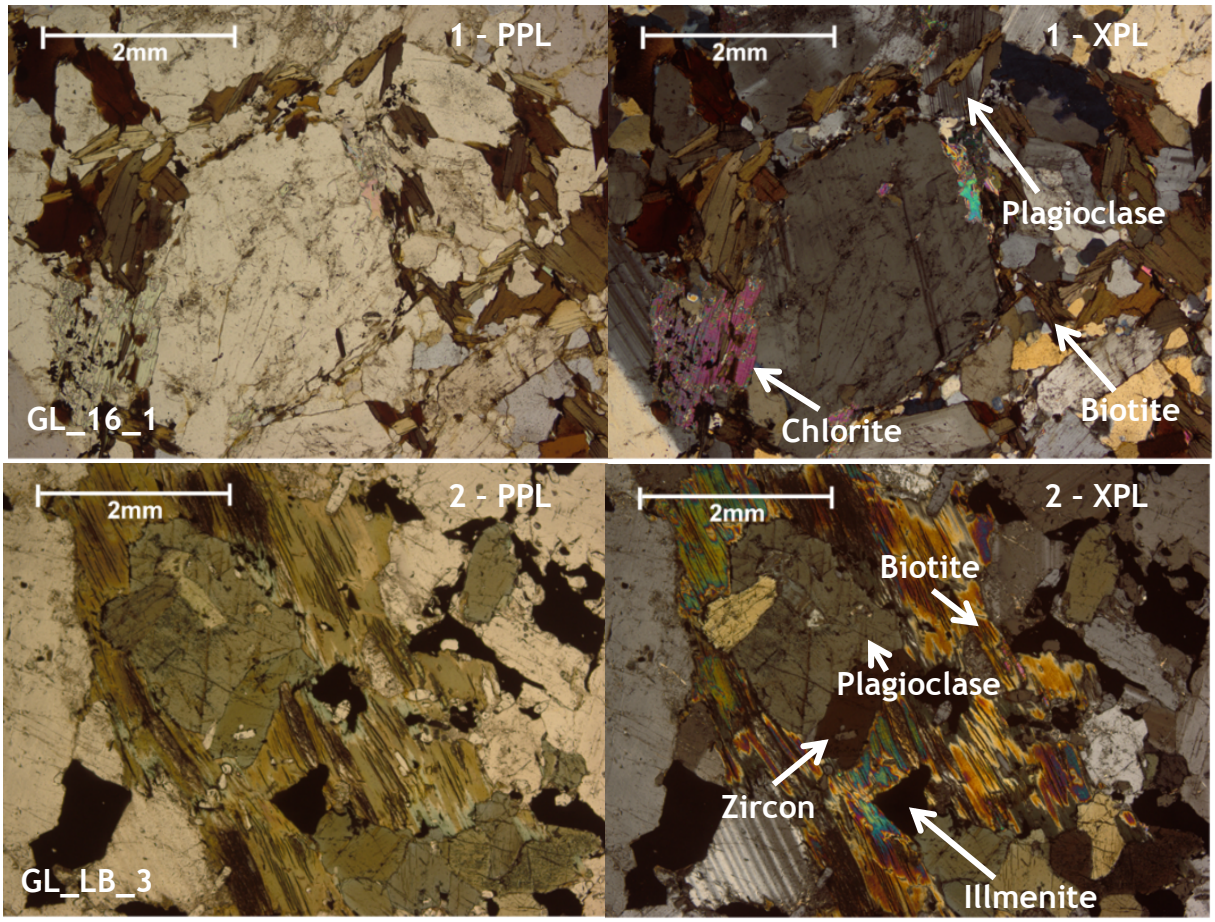

Figure 13: Labelled petrographic microscope images of thin sections from Glen Loy. GL-16-1: Numerous small accessory minerals can be seen in this sample (both zircon and apatite), commonly found within biotite grains. The feldspar grains show slight alteration to serecite. Fe-oxides are abundant, marking up around 10 – 15% of the assemblage. GL-LB-3: The groundmass consists of plagioclase, biotite and K –feldspar, with some secondary chlorite. Grains are generally >1mm in size. The main k-feldspar phenocryst is >2mm and shows only slight alteration to sericite. Chlorite appears to be replacing biotite. The chlorite crystal has itself been replaced by small opaque Fe – oxide grains of >0.1mm in size. These are the only oxides present in this sample.

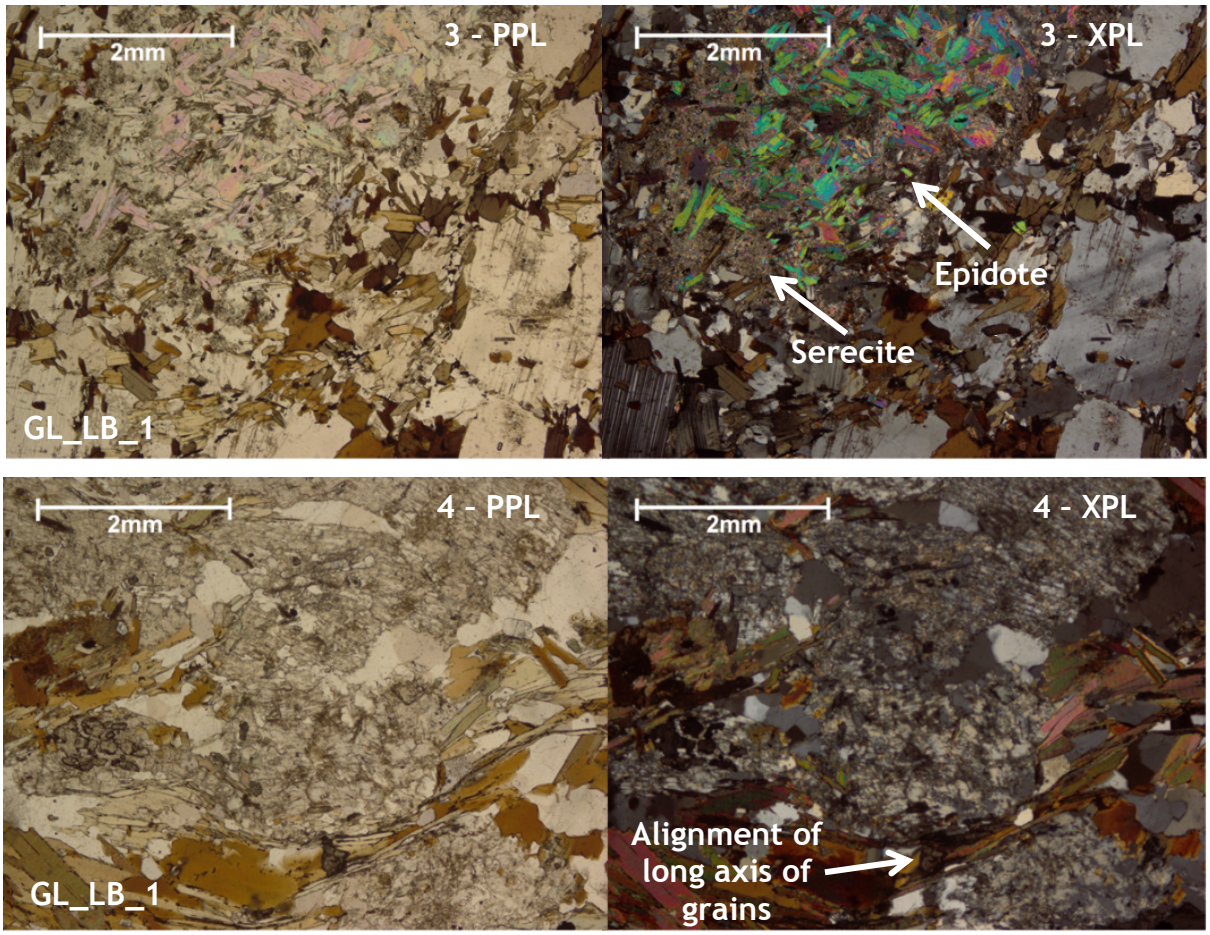

Figure 14: Labelled petrographic microscope images of thin sections from Glen Loy (both from GL_LB_1). The first set of images shows a matt like structure of grains containing accessory minerals sericite and epidote, alongside biotite. The grains in this clump are fine, typicallyless than 0.5mm along their long axis. The second image clearly shows alignement of grains of biotite and amphibole along their long axis. These minerals are extended round clumps of very fine (0.1mm) sericite.

4.2.1 Glen Scaddle

4.2.1.1 Field descriptions

The Glen Scaddle complex overs approximately 12km^2, and is located just north-east of Loch Linnhe, the geomorphological expression of the Great Glen Fault Zone (see supplementary item 2 and Figure 1). Like the Glen Loy Complex, it is intruded into the Loch Eil division of the Moine. A significant area of the Glen Scaddle pluton shows characteristics consistent with deformation (identified by the presence of a second 'tectonic' fabric/foliation interacting with the primary magmatic one). In some localities mylonitisation can be identified, indicating that high strain deformation occurred while the body was cooling. In undeformed sectors of the body, the lithology is similar to the hornblende diorite of Glen Loy.

4.2.1.1.1 Gabbro-Diorite

Undeformed sectors of the Glen Scaddle intrusion predominantly consists of a medium to course grained gabbro-diorite. At times the lithology is similar to that of Glen Loy i.e a hornblende diorite, with occasional well-defined primary magmatic fabric formed by the alignment of hornblende crystals. This primary magmatic fabric typically strikes at ~160° with an average dip of 61° (NE). Hornblende is not always present in other undeformed sectors of the body, where the mineralogy tends to be dominated by pyroxene and plagioclase. Centimetre scale rhythmic layering of zones of varying plagioclase content (40 – 70%) is a common feature of the lithology. Another common feature are sweats of tonalitic (plagioclase dominated) material of varying scale.

4.2.1.1.2 Meta - Gabbro

The deformed meta-gabbro is distinguished by its foliated nature. S – C fabrics are observable in these zones (where magmatic and tectonic fabrics are both visible). The magmatic fabric is as described above. The tectonic fabric is characterised by a separate set of similarly orientated grains, elongate along a different axis than the magmatic fabric. Tectonic fabrics were found to strike at ~130° and were steeply dipping (>80°) to the N/NW. Zones where the tectonic fabric is more intense tend to be at the south-eastern extent of the pluton. Zones of localised intense deformation and mylonitisation are observed in the river Scaddle, especially well exposed at NG 9967 6859. The mylonitised zones are less than

0.25m wide and are defined by a fine grain size and a loss of both magmatic and tectonic fabric. These are indicative of extensive high strain deformation while the body is still hot. In areas where S - C fabric is best developed the lithology can be classified as a gabbro –schist.

4.2.1.1.3 Felsic Intrusions

Several pegmatite intrusions, similar in character to those seen at Glen Loy, frequently crosscut the body, as do a network of medium-grained granitic veins. While some pegmatite bodies are of similar mineralogy to those at Glen Loy, others are significantly more plagioclase rich. The veins are predominantly quartz and plagioclase dominated. These felsic intrusions appear to have occurred at two different stages in the history of the complex. The quartz-plagioclase pegmatite intrusions are at times seen in the shear zones. The quartz veins crosscut all primary magmatic fabric and are randomly orientated, implying they are a later stage alteration feature introduced after deformation took place.

4.2.1.1.4 Contact with Country rock

The contact with the country rock was never directly observed. Small xenoliths of Moine psammites were common in the marginal zones of the pluton. Outcrops of Loch Eil psammite close to the boundary are often fractured and disassembled.

Table 14: Glen Scaddle complex lithologies.

Lithology	Mineralogy/characteristics	Modes
Gabbro - Diorite	Medium-grained (0.3 x 0.3cm). Primary magmatic fabric defined by the alignment of elongate hornblende grains. Avg. strike/dip: 160°/ 61°(NNW) (See Figure 15)	Plagioclase 25 - 50% Hornblende 0 - 30% Biotite 0 – 15% Pyroxene 10 – 40% Epidote 0 - 5% Chlorite 0 – 5%
Metagabbro	Coarse-grained (0.5 – 0.5cm). Primary magmatic fabric occasionally visible alongside tectonic fabric. Both are defined by the alignment of elongate grains (typically horneblende). Avg. strike/dip (tectonic): 131°/81° (NNW) Magmatic fabric as above. (See Figures 18)	Plagioclase 5 - 30% Hornblende 25 - 45% Biotite 5 – 15% Pyroxene 20 - 50% Epidote 0 - 5% Chlorite 0 – 5%
Granite pegmatite	Medium - course grained (0.3 – 0.5cm). Intrusions are up to 5 metres wide. No visible fabric, but occasionally sheared. (See Figure 16)	K- feldspar 25 - 50% Quartz 10 – 20% Plagioclase 5 – 50% Muscovite 0 – 15% Biotite 0 – 5%
Quartz veins	Medium-Coarse grained (0.3 – 0.5cm). No fabric observed. Veins range in thickness from decimetre scale to 10cm. Discordant both to primary and tectonic fabric. (See Figure 16)	Quartz 70 – 100% Plagioclase 0 – 30%

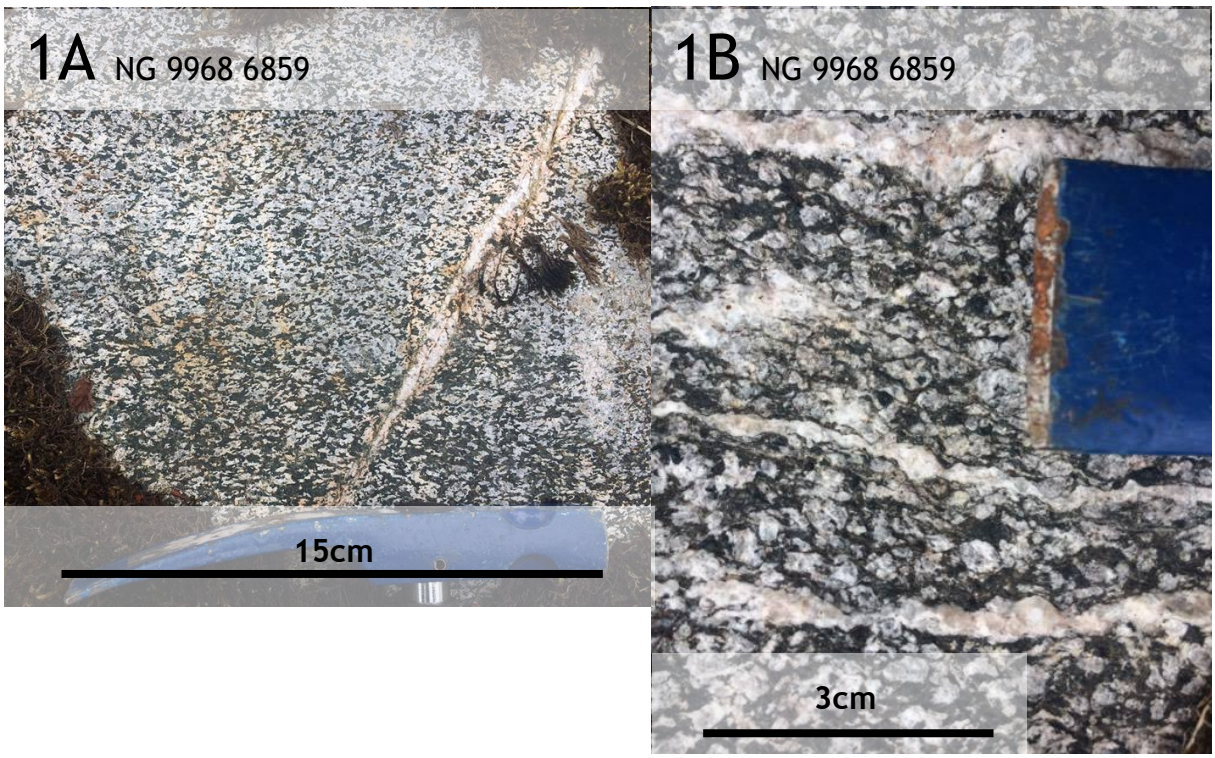

Figure 15: Diorite and Hornblende Gabbro. 1A) Rhythmic layering and primary magmatic fabric defined by alignment of long axis of hornblende, with discordant quartz vein. 1B) Primary magmatic fabric, with bands of plag rich material (interpreted as sweats of tonalitic material).

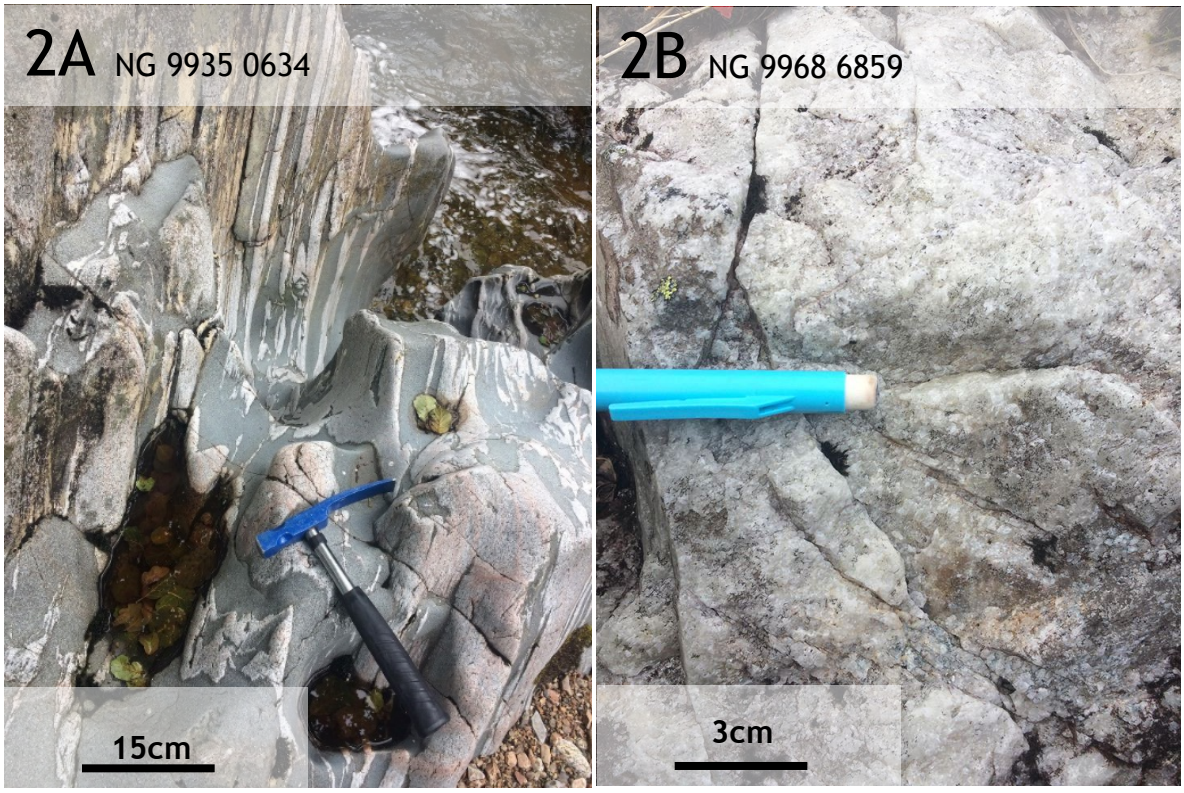

Figure 16: 2A) Zone of mylonitisation. Grain size is fine and both primary and tectonic fabric is lost. 2B) Plagioclase rich pegmatite.

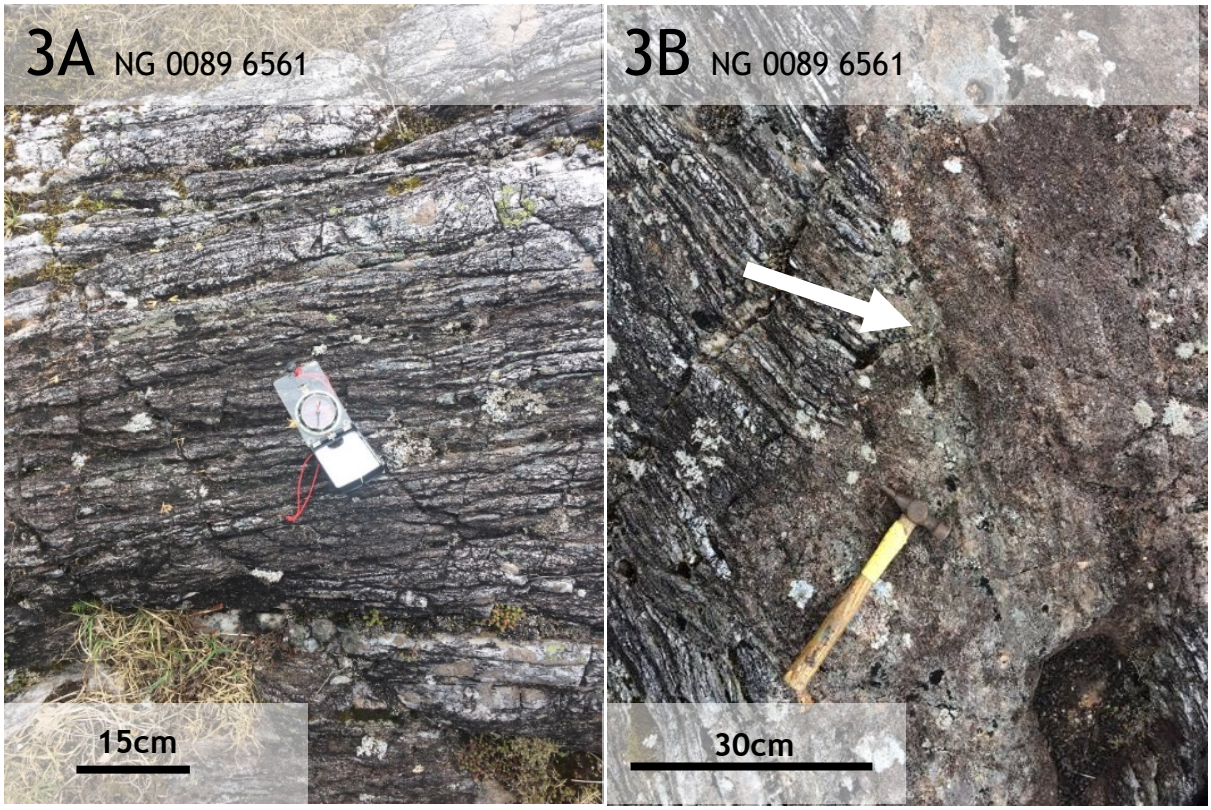

Figure 17: Shear zones. 3A) Foliated metagabbro in a 2m wide zone of intense shearing. 3B) Same shear zone as in 3A) with a raft of psammitic material.

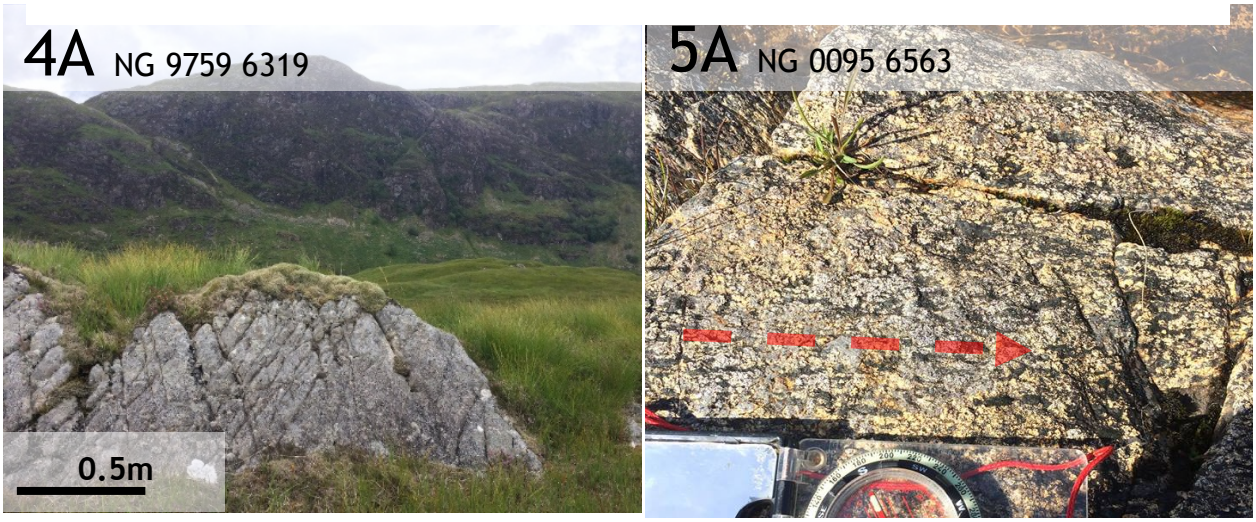

Figure 18: 4a) Two sets of fabric. 5A) Schistose metagabbro with clear foliation. Mafic minerals (hornblende and pyroxene) are aligned along the long axis of the grain (orientation highlighted with red arrow).

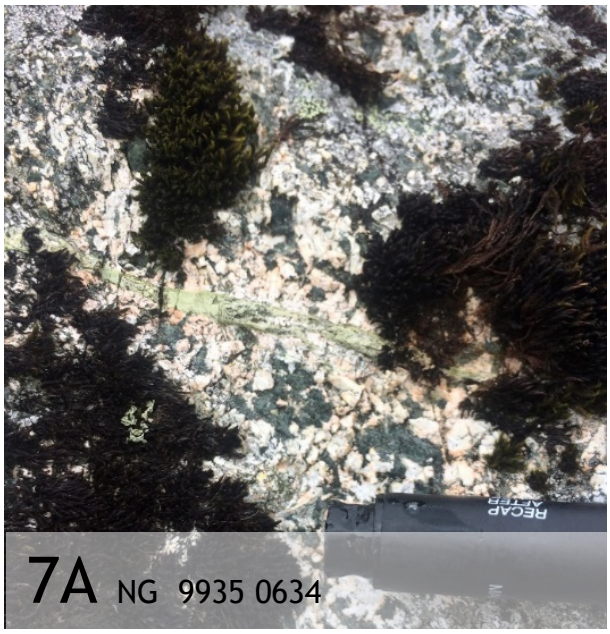

Figure 19: 6A) Epidote vein found in comparatively plagioclase rich zone of gabbro-diorite.

4.2.1.2 Petrography

The samples from Glen Scaddle show considerable variation in terms of degrees of alteration and deformation. In less altered or deformed samples, assemblages of plagioclase, K-feldspar, quartz, hornblende +/- biotite are in equilibrium. Feldspar grains are rarely fresh, with most showing sericite replacement. Secondary alteration assemblages associated with interaction with hydrothermal fluids are seen all samples, although the extent of alteration is variable. Propylitic alteration assemblages characterised by secondary sericite, chlorite and epidote are the most common feature of the altered specimens. Epidote and chlorite were mostly seen replacing hornblende and biotite. Myrmekitic texture (intergrowth of plagioclase and quartz) was occasionally seen, although this is commonly interpreted as a late magmatic feature. Feldspar is commonly highly altered and sericitized. None of the specimens collected showed any microfabrics indicative of the deformation and foliation type fabric observed in the field. Zircon apatite and titanite were present in significantly lower abundances as in Glen Loy (>0.1% of assemblage for each). Selected thin sections images are presented in Figures 20 and 21).

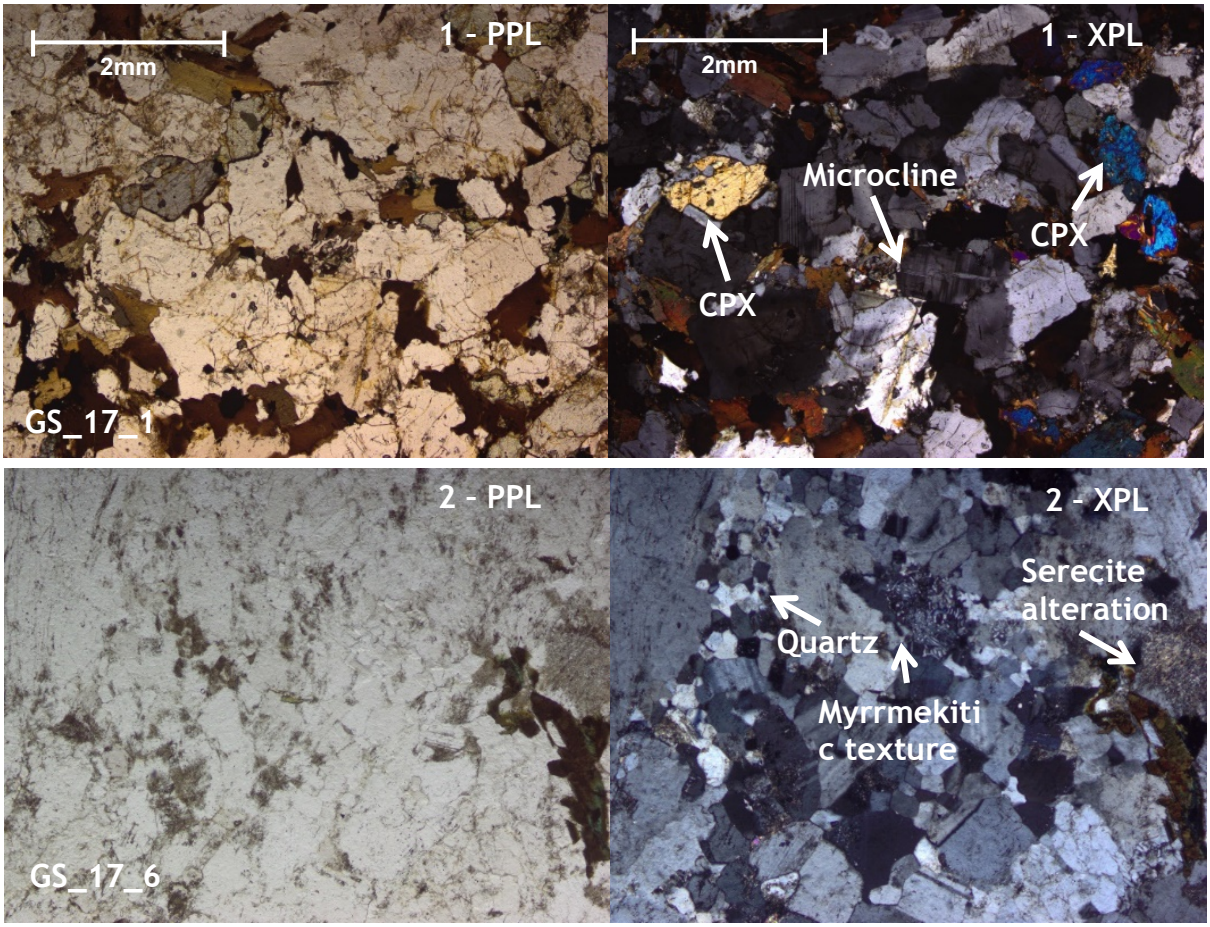

Figure 20: Relatively unaltered samples from Glen Scaddle. GS_17_1 shows a medium grained (1 – 2mm) groundmass of predominantly plagioclase, k- feldspar, horneblende and pyroxene grains. The mafic mineral content is around 40%. Microcline was identified by its cross hatched twinning. GS_17_6 is fine grained compared to other samples, and is also dominated by felsic minerals (plagioclase, k – feldspar and quartz). Myrrmekitic intergrowth of with quartz and feldspar was identified

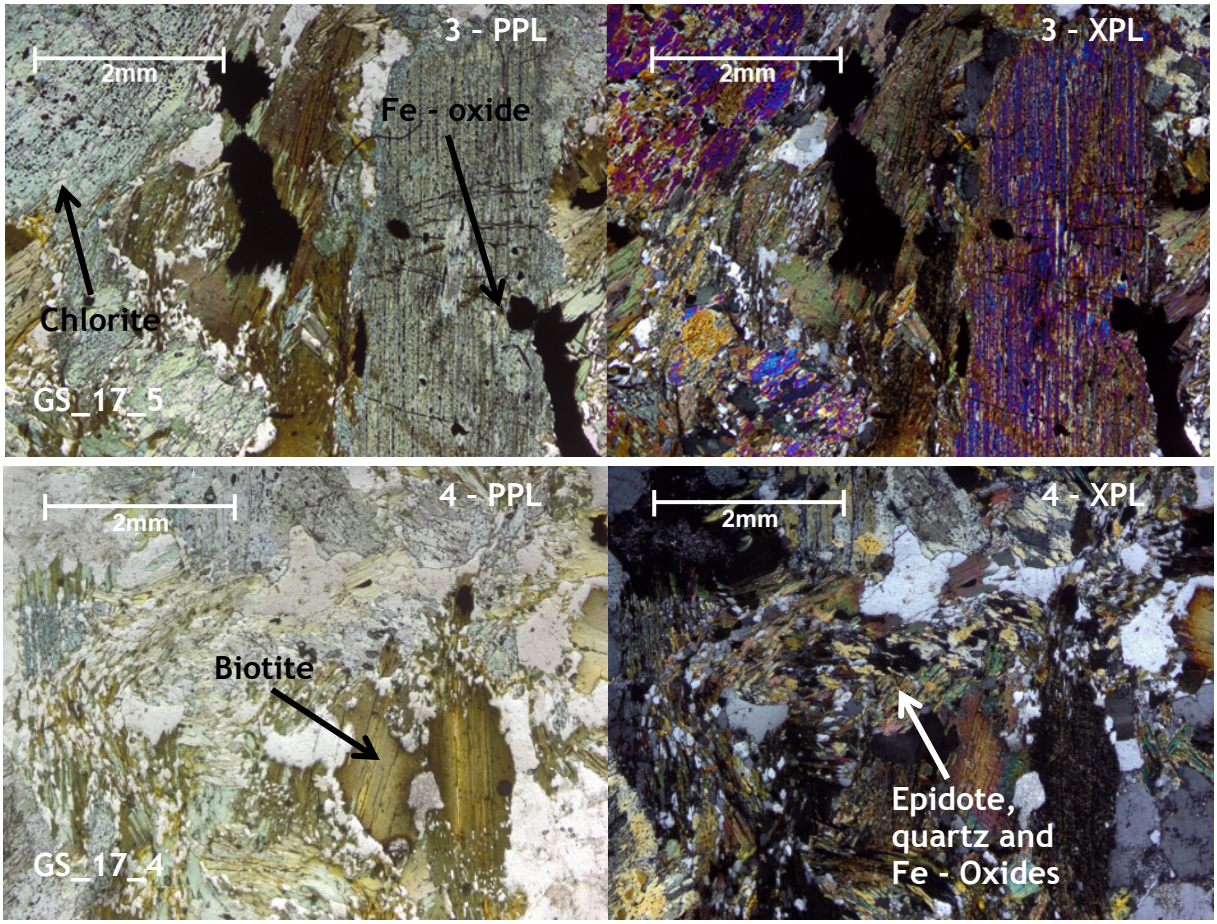

Figure 21: Altered metagabbro. GS-17-5 shows assemblages of chlorite, epidote, Fe-oxides. The pre-alteration/primary assemblage is not visible, with the exception of primary biotite. GS-17-4 is similar in its degree of alteration, with assemblages of secondary epidote, quartz and Fe-oxides.

4.3.1 Clunes

The samples from Clunes (see Figure 22) were compositionally homogenous relative to the other plutons. The mineralogy is dominated by plagioclase, quartz, biotite and hornblende. K-feldspar also present in varying abundances. Assemblages are dominated by felsic minerals (60%). Hornblende and biotite are often seen together. The samples are fine- to medium-grained (0.5 – 1mm), with a granular texture of interlocking grains. Sericite alteration of plagioclase grains is present in all samples, although to varying degrees. The samples are far less altered than other plutons, and secondary mineral assemblages of epidote and/or chlorite are not observed. Accessory minerals apatite, zircon and titanite are present in low concentrations (>0.1% of assemblage for each). There is no discernible fabric in any of the samples.

4.4.1 Cluanie

The samples from Cluanie are varied (see Figure 23 and 24). Generally, the mineral assemblage consists of plagioclase, k-feldspar, quartz, biotite and hornblende. Secondary alteration assemblages include epidote and sericite usually seen replacing feldspar grains of plagioclase and K-feldspar. Grain size is also variable, with some samples exhibiting a fine to mediums grains of 0.5 – 2mm, and others being coarsely crystalline with grains of over 4mm. Zircon, apatite and titanite are present in low abundances, although some large (0.5mm) zircon grains were identified. Some samples show a primary magmatic fabric defined by the preferred orientation of mafic minerals biotite and hornblende. Myrmekitic intergrowths of plagioclase and quartz are occasionally observed.

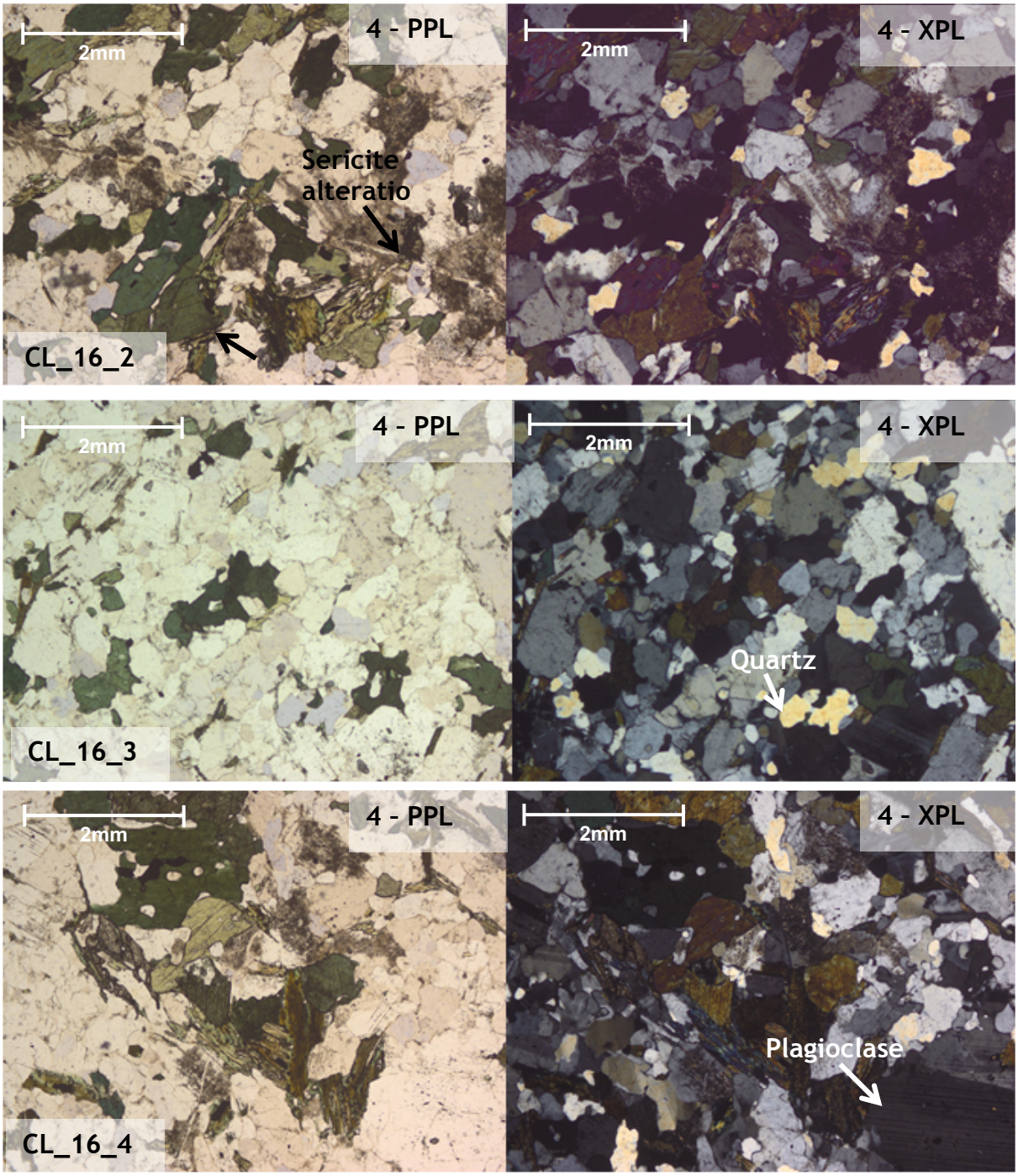

Figure 22: Samples from Clunes, all showing similar features. The groundmass consists of plagioclase, quartz, K-feldspar and amphibole with some minor biotite. Alteration of feldspar grains to sericite is apparent in CL_16_2, and less so in the other samples.

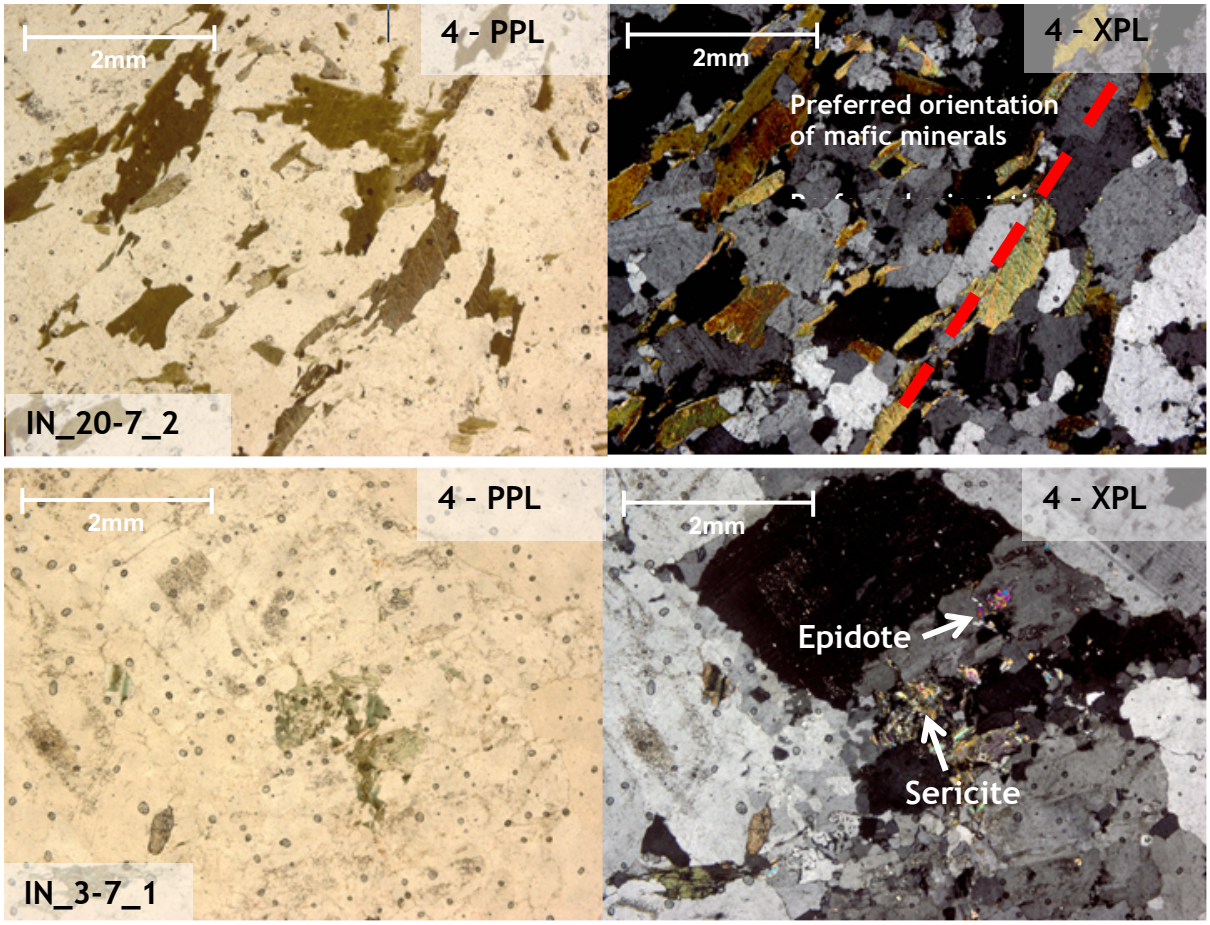

Figure 23: IN_20-7_2 shows a groundmass of predominantly medium grained (1-2mm) k-feldspar, plagioclase, amphibole and biotite. Biotite and amphibole are aligned along there long, defining a primary magmatic fabric. Grains are relatively unaltered, with only minor sericite on feldspar grain surfaces. IN_3-7_1 has a significantly more course grained groundmass with k-feldspar grains greater up to 4mm in size.

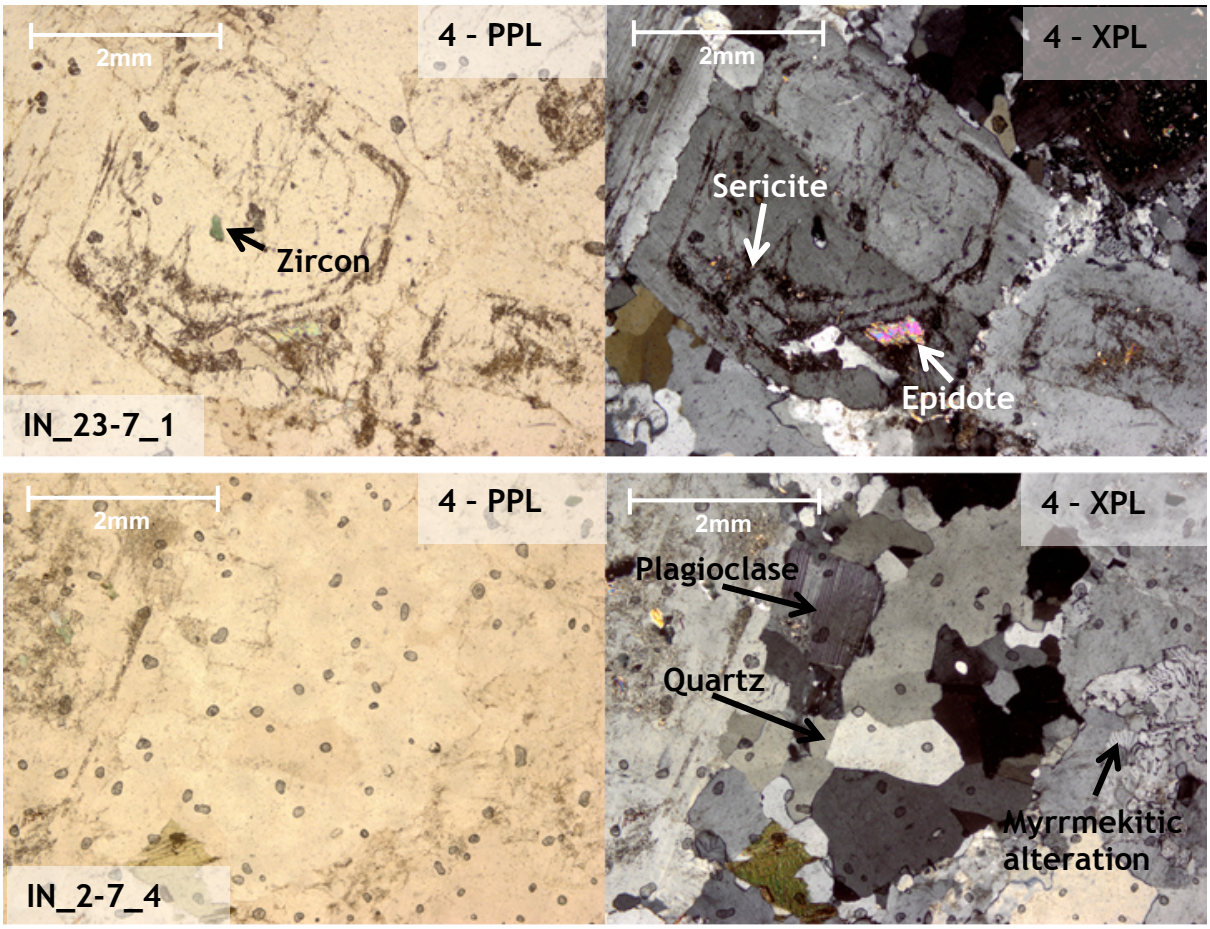

Figure 24: IN_23-7_1 shows a large (4mm), sector zoned phenocryst of K-feldspar with internal zoning defined by degrees of sericite and epidote alteration. IN_2-7_4 shows relatively fresh quartz and plagioclase grains. Myrrmekitic intergrowth of plagioclase and quartz is occasionally observed.

4.2 Mineral Chemistry

4.2.1 Plagioclase classification

The chemistry of plagioclase feldspar grains are presented, as calculated by EPMA analysis (see Table 15). Grains from Loy and Clunes show different compositions, in line with the contrasting degrees of evolution, as seen in the major element data. Labradorite, of which the samples at Glen Loy consist, is commonly associated with mafic lithologies (e.g. basalt and gabbro) and is commonly found alongside pyroxene and amphibole. Oligoclase, of which three of the grains from Clunes consist, is a high sodium feldspar, commonly found in more felsic rocks from granites – diorites. It is commonly found alongside orthoclase, quartz and epidote. The other samples from Clunes consist of andesine which typically occurs in intermediate rocks from diorite – syenite.

Table 15: Composition of plagioclase feldspar grains from Glen Loy and Clunes, as caculated by EPMA analysis. Subsequent classification was then carried out according to the Albite – Anorthite series (e.g. Winter, 2010).

SAMPLE	Na (Albite)	K (Orthoclase)	Ca (Anorthite)	Name	Formula
GL_Plg3	0.34621	0.00419	0.64960	Labradorite	$(Ca,Na)Al(Al,Si)Si_2O_8$
GL_Plg3	0.35058	0.00397	0.64546	Labradorite	$(Ca,Na)Al(Al,Si)Si_2O_8$
GL_Plg3	0.35032	0.00423	0.64545	Labradorite	$(Ca,Na)Al(Al,Si)Si_2O_8$
GL_Plag11	0.32456	0.00495	0.67048	Labradorite	$(Ca,Na)Al(Al,Si)Si_2O_8$
GL_Plag11	0.30674	0.00282	0.69044	Labradorite	$(Ca,Na)Al(Al,Si)Si_2O_8$
GL_Plag11	0.30061	0.00301	0.69638	Labradorite	$(Ca,Na)Al(Al,Si)Si_2O_8$
GL_Plag11	0.31266	0.00324	0.68410	Labradorite	$(Ca,Na)Al(Al,Si)Si_2O_8$
CL_feld	0.685375	0.015372	0.299252	Oligoclase	$Na,Ca)Al(Si,Al)Si_2O_8$
CL_feld	0.667869	0.018296	0.313836	Andesine	$(Na,Ca)Al(Si,Al)Si_2O_8$
CL_feld	0.66373	0.013825	0.322446	Andesine	$(Na,Ca)Al(Si,Al)Si_2O_8$
CL_feld6	0.725015	0.017785	0.2572	Oligoclase	$Na,Ca)Al(Si,Al)Si_2O_8$
CL_ feld 6	0.731963	0.025771	0.242266	Oligoclase	$(Na,Ca)Al(Si,Al)Si_2O_8$
CL_feld 6	0.678043	0.020838	0.301119	Andesine	$(Na,Ca)Al(Si,Al)Si_2O_8$

4.2.2 Geobarometry

The Al-in-hornblende geobarometer was applied to samples from Clunes that satisfied the requirements outlined by Stein and Dietl (2001). The major element composition of the amphibole grains analysed are presented in *Table 16*, while *Table 17* shows the results of the application of different calibrations of the geobarometer. When converting the resultant pressure values to depths, a pressure gradient of 3.7km/kbar is assumed (Neill and Stephens, 2009). Clunes appears to have been emplaced at a depth of 12 and 17km i.e. mid crustal depths. This is similar to the depth for the Cluanie pluton, as reported by Neill and Stephens (2009).

Table 16: Electron micro-probe analyses of amphibole grains in samples from Clunes.

SAMPLE ID (CL_)	SiO_2	TiO_2	Al_2O_3	Fe_2O_3	FeO	MnO	MgO	CaO	Na_2O	K_2O	H_2O*	Total
1	45.2	0.8	7.8	5.3	12.3	0.4	11.1	11.1	1.3	1.1	2.0	98.4
1	43.0	1.1	8.6	5.3	11.3	0.3	11.5	11.3	1.4	1.1	2.0	97.0
1b	45.1	0.8	8.2	6.3	10.8	0.3	11.6	11.1	1.4	1.0	2.0	98.6
1b	45.2	0.8	8.8	3.8	12.7	0.4	11.1	11.2	1.6	1.1	2.0	98.7
1b	43.8	1.1	9.2	6.8	10.7	0.4	11.3	11.0	1.7	1.1	2.0	99.1
2	45.4	1.1	8.4	4.7	11.7	0.4	11.6	11.2	1.3	1.1	2.0	98.8
2	45.3	1.4	8.0	5.2	10.5	0.5	12.4	11.5	1.3	0.8	2.0	98.9
2	44.9	1.0	8.7	3.0	13.6	0.6	10.7	11.4	1.3	1.1	2.0	98.4
4	46.1	1.2	9.5	3.3	13.1	0.3	11.8	11.9	1.5	1.2	2.1	101.9
4	45.8	1.2	9.7	2.5	14.6	0.4	11.0	11.8	1.7	1.1	2.1	102.0
4	45.3	1.3	9.5	4.5	12.5	0.2	11.1	11.5	1.2	1.0	2.0	100.2
5	46.4	0.7	8.9	5.6	11.6	0.3	11.8	11.7	1.2	0.9	2.1	101.2
5	44.0	0.9	9.4	5.4	11.6	0.4	11.3	11.6	1.3	1.1	2.0	99.2
5	44.5	1.2	9.9	5.4	12.0	0.3	11.0	11.4	1.4	1.1	2.0	100.2
5	45.8	0.8	8.6	4.3	12.4	0.4	11.7	11.7	1.4	1.1	2.0	100.2
5	45.7	0.8	9.3	3.1	13.3	0.3	11.1	11.3	1.6	1.1	2.0	99.4
5	44.1	1.0	10.0	1.7	14.8	0.3	10.5	11.7	1.8	1.2	2.0	99.0
6	46.2	0.8	9.2	2.1	13.8	0.4	11.2	11.8	1.2	1.1	2.0	99.8
6	45.0	1.3	9.1	5.4	10.9	0.4	11.8	11.3	1.5	1.0	2.0	99.7
6	44.8	1.1	9.1	6.4	11.0	0.3	11.6	11.4	1.3	1.1	2.0	100.1
8	46.2	0.9	8.7	4.6	11.6	0.3	12.2	11.7	1.4	1.0	2.0	100.6
8	46.7	1.0	9.2	3.7	12.4	0.4	11.8	11.7	1.5	0.9	2.1	101.3
8	46.2	1.1	9.0	4.7	11.9	0.2	11.8	11.7	1.2	1.0	2.1	100.8
8	46.1	1.0	8.5	4.6	12.1	0.5	11.6	11.5	1.3	1.0	2.0	100.3
8	46.3	1.0	8.9	3.3	13.2	0.2	11.4	11.7	1.2	1.0	2.0	100.3
9	45.1	1.4	9.9	1.4	15.0	0.4	10.5	11.7	1.5	1.2	2.0	100.0
9	44.9	1.1	9.0	3.9	12.3	0.3	11.7	11.7	1.5	1.0	2.0	99.5
9	45.7	0.9	8.3	3.1	14.0	0.6	11.1	11.9	1.4	0.9	2.0	99.9
11	45.3	1.4	9.5	3.3	13.4	0.4	10.9	11.7	1.1	1.1	2.0	100.2
11	45.6	1.1	9.2	2.3	14.2	0.4	11.2	11.8	1.5	1.1	2.0	100.4
11	45.6	1.1	9.1	0.7	15.4	0.2	11.1	12.0	1.7	0.9	2.0	99.7
12	44.9	1.1	8.8	3.8	12.7	0.4	11.6	11.9	1.3	1.2	2.0	99.7
12	44.2	1.3	9.0	4.9	11.8	0.3	11.3	11.4	1.4	0.9	2.0	98.6
12	44.6	0.9	8.7	5.2	12.1	0.5	11.0	11.5	1.2	1.1	2.0	98.7
1	46.9	1.0	8.3	2.7	13.9	0.4	11.3	11.6	1.3	1.0	2.0	100.4
1	45.6	1.2	9.4	3.1	13.1	0.3	11.4	11.6	1.5	1.1	2.0	100.5
1	46.0	0.9	8.9	3.1	13.2	0.4	11.4	11.8	1.3	1.0	2.0	100.1
1	44.6	1.1	9.7	3.5	13.4	0.3	11.0	11.7	1.5	1.2	2.0	100.1
1	45.0	1.1	9.6	3.9	12.9	0.3	11.2	11.6	1.5	1.2	2.0	100.3
1	45.2	1.2	9.4	3.0	13.4	0.3	11.4	11.7	1.5	1.2	2.0	100.3
1	45.5	1.0	9.4	2.6	13.8	0.3	11.1	11.8	1.3	1.1	2.0	100.0
1	44.5	1.1	9.7	4.1	12.8	0.3	11.0	11.5	1.5	1.2	2.0	99.8
1	45.2	1.2	9.4	3.7	13.1	0.4	11.1	11.5	1.5	1.2	2.0	100.3
1	45.3	1.3	9.4	3.6	12.7	0.3	11.6	11.7	1.5	1.2	2.0	100.5
1b	43.7	0.9	8.4	5.1	11.7	0.3	11.1	11.3	1.2	1.0	2.0	96.8

Table 17: Pressure calculated using the following geobarometers HZ: Hammarstrøm & Zen (1986), H: Hollister et al. (1987), JR: Johnson & Rutherford (1989), and S: Schmidt (1999).

SAMPLE	H&Z 86		H 87		J & R 89		S 92	
	P (Kbar)	D (km)	P (Kbar)	D (km)	P (Kbar)	D (km)	P (Kbar)	D (km)
1	3.0	***11.2***	3.0	***11.2***	2.4	***8.8***	3.6	***13.2***
1	3.9	***14.4***	4.0	***14.8***	3.1	***11.5***	4.4	***16.2***
1b	3.3	***12.4***	3.4	***12.5***	2.7	***9.8***	3.9	***14.3***
1b	3.9	***14.3***	4.0	***14.7***	3.1	***11.5***	4.4	***16.2***
1b	4.2	***15.7***	4.4	***16.2***	3.4	***12.6***	4.7	***17.4***
2	3.6	***13.1***	3.6	***13.4***	2.8	***10.4***	4.1	***15.0***
2	3.1	***11.5***	3.1	***11.6***	2.5	***9.1***	3.6	***13.5***
2	3.9	***14.4***	4.0	***14.9***	3.1	***11.5***	4.4	***16.3***
4	4.3	***15.9***	4.5	***16.5***	3.5	***12.8***	4.8	***17.7***
4	4.5	***16.6***	4.7	***17.3***	3.6	***13.4***	5.0	***18.3***
4	4.4	***16.3***	4.6	***16.9***	3.5	***13.1***	4.9	***18.0***
5	3.8	***14.0***	3.9	***14.3***	3.0	***11.2***	4.3	***15.8***
5	4.5	***16.5***	4.6	***17.1***	3.6	***13.3***	4.9	***18.2***
5	4.8	***17.6***	5.0	***18.4***	3.8	***14.2***	5.2	***19.2***
5	3.6	***13.4***	3.7	***13.6***	2.9	***10.6***	4.1	***15.2***
5	4.3	***15.9***	4.5	***16.5***	3.4	***12.8***	4.8	***17.6***
5	5.0	***18.4***	5.2	***19.3***	4.0	***14.9***	5.4	***20.0***
6	4.2	***15.5***	4.3	***16.0***	3.4	***12.4***	4.7	***17.3***
6	4.1	***15.0***	4.2	***15.5***	3.2	***12.0***	4.5	***16.8***
6	4.0	***14.9***	4.2	***15.4***	3.2	***11.9***	4.5	***16.7***
8	3.7	***13.6***	3.8	***13.9***	2.9	***10.8***	4.2	***15.4***
8	4.0	***14.8***	4.1	***15.3***	3.2	***11.8***	4.5	***16.6***
8	3.9	***14.5***	4.0	***14.9***	3.1	***11.5***	4.4	***16.3***
8	3.5	***13.0***	3.6	***13.2***	2.8	***10.3***	4.0	***14.9***
8	3.9	***14.3***	4.0	***14.7***	3.1	***11.4***	4.4	***16.1***
9	4.8	***17.8***	5.0	***18.6***	3.9	***14.3***	5.2	***19.4***
9	4.0	***14.9***	4.1	***15.3***	3.2	***11.9***	4.5	***16.7***
9	3.4	***12.7***	3.5	***12.9***	2.7	***10.1***	4.0	***14.6***
11	4.4	***16.4***	4.6	***17.0***	3.6	***13.2***	4.9	***18.1***
11	4.4	***16.4***	4.6	***17.0***	3.6	***13.2***	4.9	***18.1***
11	4.1	***15.1***	4.2	***15.6***	3.3	***12.1***	4.6	***16.9***
12	3.9	***14.4***	4.0	***14.8***	3.1	***11.5***	4.4	***16.2***
12	4.1	***15.1***	4.2	***15.6***	3.3	***12.1***	4.6	***16.9***
12	3.8	***14.1***	3.9	***14.5***	3.0	***11.3***	4.3	***16.0***
1	3.3	***12.2***	3.3	***12.3***	2.6	***9.7***	3.8	***14.1***
1	4.3	***16.0***	4.5	***16.5***	3.5	***12.8***	4.8	***17.7***
1	3.9	***14.4***	4.0	***14.8***	3.1	***11.5***	4.4	***16.2***
1	4.6	***17.1***	4.8	***17.8***	3.7	***13.8***	5.1	***18.7***
1	4.5	***16.8***	4.7	***17.4***	3.6	***13.5***	5.0	***18.5***
1	4.3	***16.0***	4.5	***16.6***	3.5	***12.8***	4.8	***17.7***
1	4.3	***16.0***	4.5	***16.6***	3.5	***12.8***	4.8	***17.7***
1	4.7	***17.3***	4.9	***18.0***	3.8	***13.9***	5.1	***18.9***
1	4.3	***16.0***	4.5	***16.6***	3.5	***12.9***	4.8	***17.7***
1	4.3	***15.8***	4.4	***16.4***	3.4	***12.7***	4.7	***17.5***
1b	3.8	***13.9***	3.8	***14.2***	3.0	***11.1***	4.2	***15.7***
Average	4.1	***15***	4.2	***15.5***	3.2	***12.0***	4.5	***16.8***
Std dev.	0.4	**1.7**	0.5	***1.9***	0.4	***1.4***	0.4	***1.6***

4.3 Geochemistry

Major and trace element chemistry is presented for the plutons Glen Loy, Glen Scaddle, Clunes, Cluanie and Loch Linnhe. Only one sample from Loch Linnhe was analysed. The major and trace element chemistry for Cluanie was collected by Dr Iain Neill. The data collected is presented in *Appendix X*.

4.3.1 Effect of Alteration on Elemental Chemistry

The degree of alteration of a sample must be considered in the discussion of major and trace element profiles. This is especially important for granite bodies as old as the Newer granites. Indeed, petrographic investigation of the samples showed an abundance of alteration assemblages and alteration products. Loss on ignition (LOI) values reflect the abundance of hydrous minerals, carbonates and hydrous silicates present in a sample. They are presented alongside major element data and were considered when making further comments on the data.

4.3.2 Major Element Chemistry - Total Alkali vs $Si0_2$ plot (TAS)

SiO_2 wt. % and NaO_2 wt. % + K_2O wt. % data was plotted on a Total Alkali vs Silica (TAS) diagram (*see Figure 25*). TAS diagrams are widely used in the classification of volcanic and plutonic suites – the chemical parameters SiO_2, NaO_2 and K_2O each play an important role in determining the normative mineralogy of rock. The TAS diagram is widely used in the classification and naming of igneous plutonic rocks. Field names are after Johannsen, 1937.

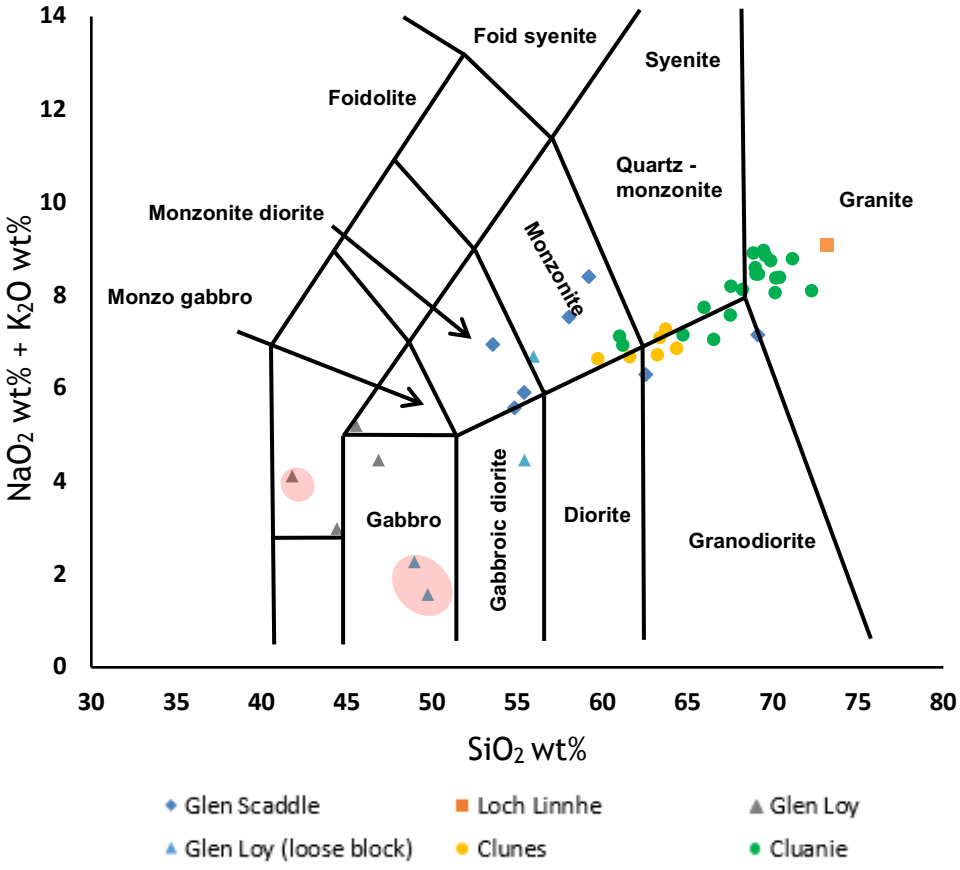

Figure 25: Total Alkali vs Silica plot. Total alkali: NaO_2 wt% + K_2O wt%. Classification of fields after Johannsen 1937. Red zones highlight the samples identified as cumulates.

4.3.2 Major Element Chemistry - Major Element Harker Diagrams

Major element Harker Diagrams (after Harker, 1990) plot wt. % SiO_2 against major oxides (see *Figure 26*). SiO_2 increases with magmatic evolution. Plotting oxide wt. % against a SiO_2 abisscus shows how said oxides concentration varies as a magma or magma series evolves. These plots are highly effective for identifying relationships controlled by magma chamber processes.

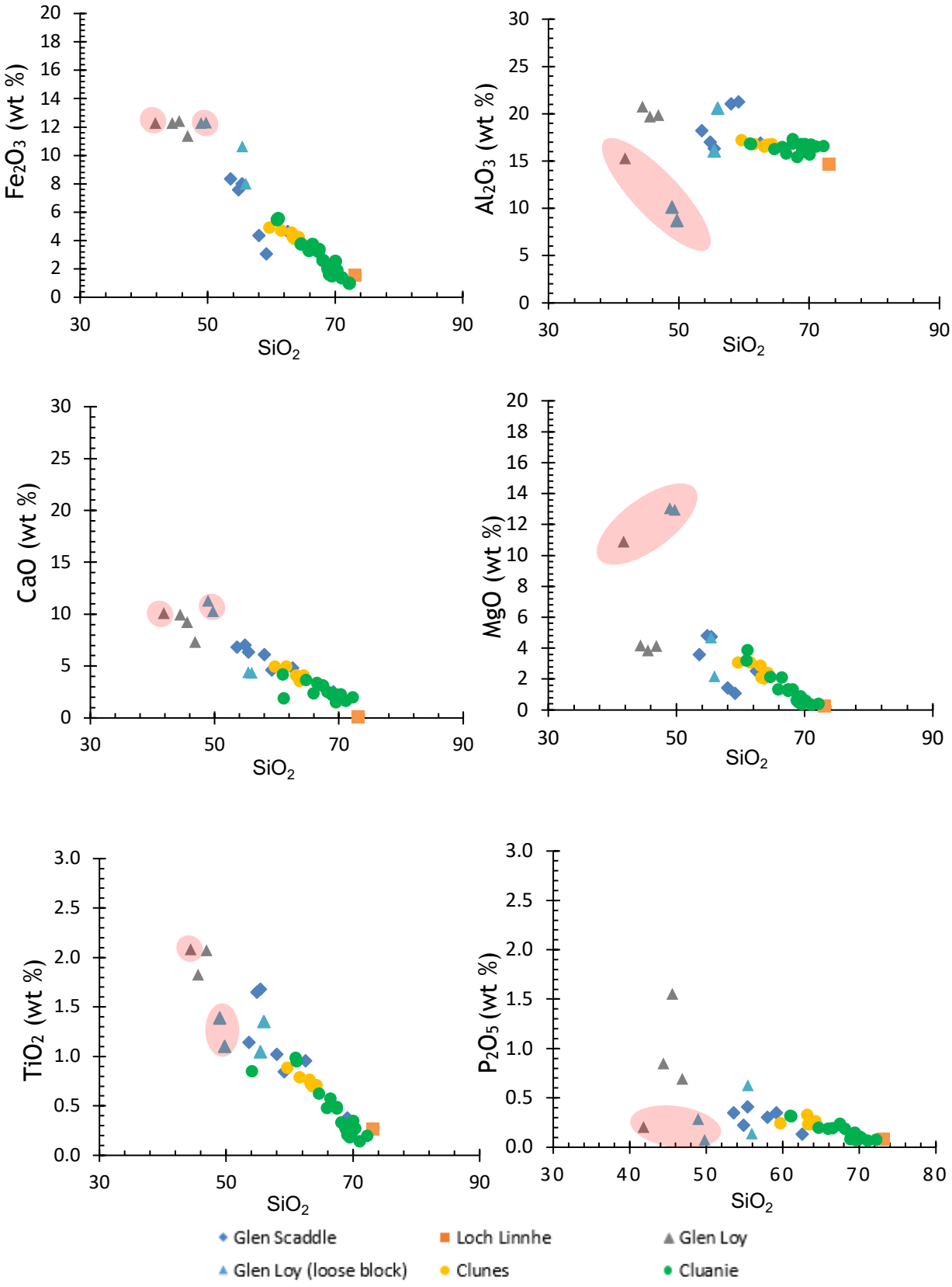

Figure 26: Major element Harker diagrams. Red zones highlight the samples identified as cumulates.

4.3.2.1 Glen Loy

The samples from Glen Loy show significant variability in both total alkali and SiO_2 content. SiO_2 content ranges from 42 wt. % to 56 wt. %. Total alkali content ranges from 2 wt. % - 7 wt. %. Two samples lie outwith what is otherwise an array of increasing total alkali content with evolution. These samples are identified as cumulates (GL_LB_2 and GL_LB_4). Classification is difficult as the samples plot across five different fields, all of which are at the ultra-mafic to mafic end of the SiO_2 axis (gabbro – gabbro–diorite).

Fe_2O_3 shows little change increasing SiO_2 content, with the exception of the two most evolved samples (GL_LB_3 and GL_LB_1), which have lower values. TiO2 and CaO contents decrease with increasing SiO_2 content. Al_2O_3, P_2O_5 and MgO contents do not show a linear relationship with increasing SiO_2 content. The samples previously identified as cumulate rocks (GL_16_2, GL_LB_2 and GL_LB_4) show a significant spike in MgO content and are relatively depleted in P_2O_5 and Al_2O_3.

4.3.2.2 Glen Scaddle

The samples from Glen Scaddle also show significant variability, more so in SiO_2 content than in total alkali content. SiO_2 content ranges from 52 wt. % to 62 wt. %, with one outlier of 70 wt. % (GS_17_7). Total alkali content ranges from 5 wt. % to 8 wt. %. Classification is difficult as the samples plot across many different fields.

Glen Scaddle samples show a consistently linear decrease in major element oxides with increasing SiO_2 content. There are two data points that are consistently slightly more enriched or depleted to be perfectly on trend (GS_17_5, GS_17_6). These points have slightly lower Fe_2O_3 and MgO, and slightly higher TiO_2 and Al_2O_3.

4.3.2.3 Clunes

The samples for Clunes do not show much variation with regards to SiO_2 content (59 - 64 wt. %) or total alkali content (6 - 7 wt. %). The samples all plot on or near Monzonite - Quartz monzonite - Diorite - Granodiorite boundary. Three samples plot within the granodiorite field.

The samples from Clunes all show linear decreases in major element oxides when plotted against SiO_2. The exception is Al_2O_3, which plots as flat trends (no variation in oxide compared to SiO_2).

4.3.2.4 Cluanie

The samples from Cluanie cover a broad range of SiO_2 values (61 - 72wt. %). Total alkalis increase with increasing SiO_2, covering a range from 6 - 8 wt. %. The samples plot across a range of categories: monzonite, quartz monzonite, granodiorite and granite. The majority lie within the granite field.

The samples from Cluanie all show linear decreases in major element oxides when plotted against SiO_2. The trends for P_2O_5 and Al_2O_3 plot more as flat trends (no variation in oxide compared to SiO_2).

4.3.2.5 Loch Linnhe

The sample from Loch Linnhe has 73 wt. % SiO_2 and a total alkali component is 9%, thus plotting within the granite field. The sample has very low values for all major element oxides, except Al_2O_3.

4.3.4 K – Na – Ca Ternary Diagram

Plotting potassium vs sodium vs calcium allows for classification as a TTG (Tonalite, trondhjemite, Granodiorite), or Island arc. This classification is used after Wareham et al. (1997). Since each parameter is normalized in order to sum 100%, values are relative rather than absolute (Winter 2001). The diagram is presented in *Figure 27*.

4.3.4.1 Glen Loy

The samples from Glen Loy plot close to the calcium apex, in an array that mirrors the calc-alkaline/island arc fractionation trend defined by Wareham et al. (1997). Only GL_LB_3 lies out with this trend, having a significantly higher K content.

4.3.4.2 Glen Scaddle

The samples from Glen Scaddle all plot roughly in the middle of the Na Ca axis with consistent, low – moderate K content. The majority of the samples plot within the island arc filed, with one sample (GS_17_6) plotting well within the TTG field, as defined by Wareham et al., (1997).

4.3.4.3 Clunes

The samples from Clunes plot roughly in the middle of the Na - Ca axis, forming an array projecting towards the Na apex. The samples all have low - moderate K contents, similar to Glen Scaddle.

4.3.4.4 Clunes

The samples from Cluanie plot close to the Na apex, forming an array that projects towards the Ca apex. Samples have low to moderate K contents, similar to Scaddle and Clunes. All samples plot within the TTG field, as defined by Wareham et al., (1997).

4.2.4.5 Loch Linnhe

The sample Loch Linnhe stands apart from the data from the other plutons. Loch Linnhe has negligible Ca content (0.05 wt. %), meaning it plots on the Na - K axis.

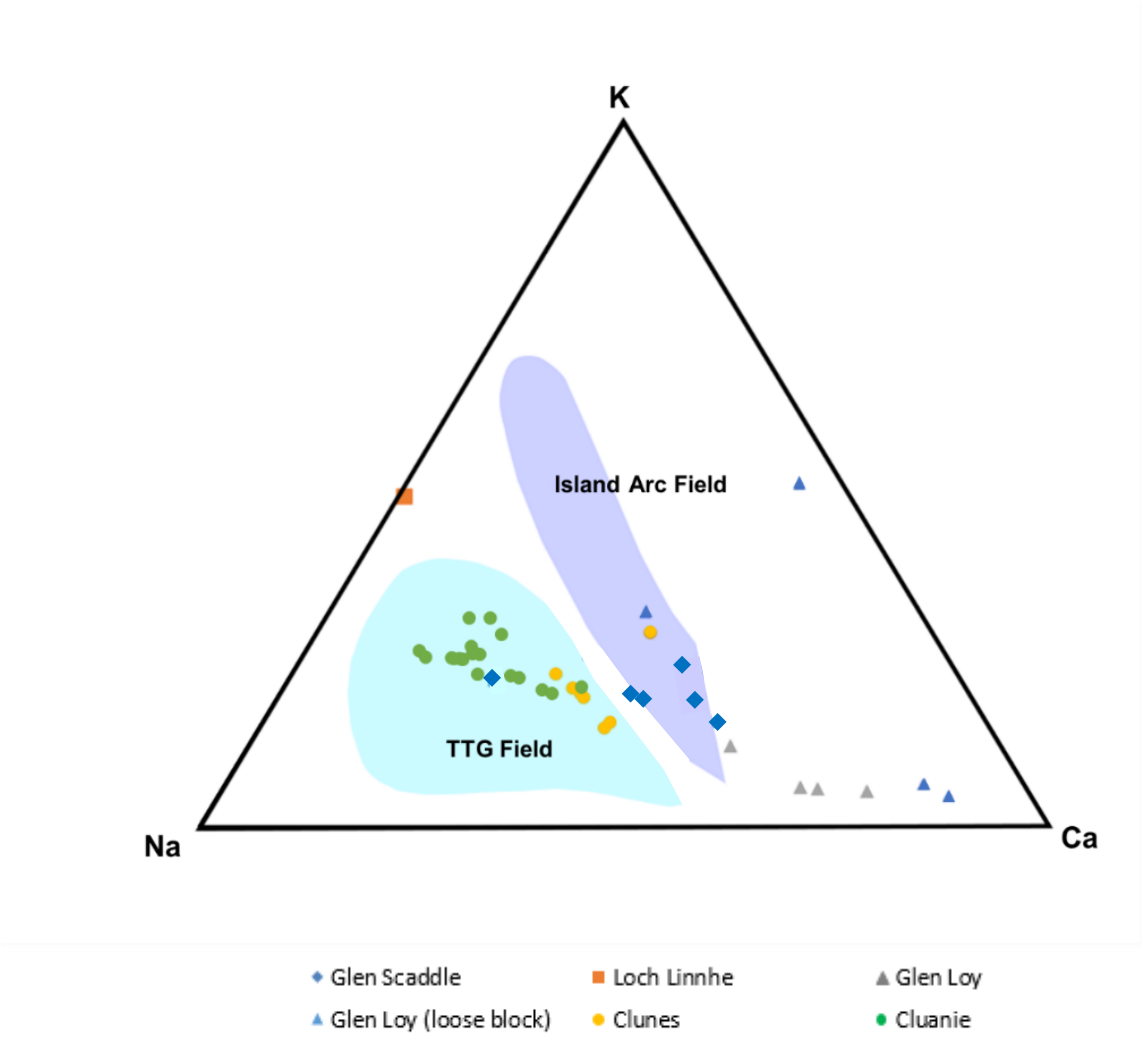

Figure 27: Na – K – Ca tertiary diagram with fields for TTG and Island arc classification after Wareham et al., (1997).

4.2.5 Trace element geochemistry – Bivariate plots

Ten trace element (ppm) vs SiO_2 (wt. %) bivariate plots are presented, allowing a more detailed investigation into the evolution of the plutonic suites (see *Figures 28 & 29)*. The trends seen in individual plutons are described in Table 24.

4.3.5.1 General Observations

Linear trends of decreasing trace element content with increasing SiO_2 content are seen in Eu, Dy, Yb and Cu. More complex trends are seen in the other elements.

Ni content is shows a loose convex upwards trend with increasing SiO_2 wt. %. The cumulate samples have significantly higher Ni ppm, as do three of the samples from Cluanie (IN/3-7/1, IN/20-7/4 and INC 6).

Values for Sr plot as a cluster rather than an array. The cumulate samples plot outwith this cluster (lower Sr ppm), as do three non-cumulate samples from Glen Loy (higher Sr ppm). The sample from Loch Linnhe has significantly lower Sr ppm.

La content plots as a convex upward trend with increasing SiO_2 wt. %. The cumulate samples also follow this trend. GL-LB-3 is the only sample that plots outwith this trend, with significantly high La ppm.

Cr ppm stays largely constant with increasing SiO_2 wt. %. Two of the samples identified as cumulates have significantly high Cr ppm (GL_LB_2, GL_LB_4).

Y and Zr do not show a linear trend with increasing SiO_2 wt. %. For both, a trend of linear decrease in visible, but there are numerous outlying data points.

Figure 28: Selected trace element vs. SiO_2 bivariate plots. Continued Overleaf.

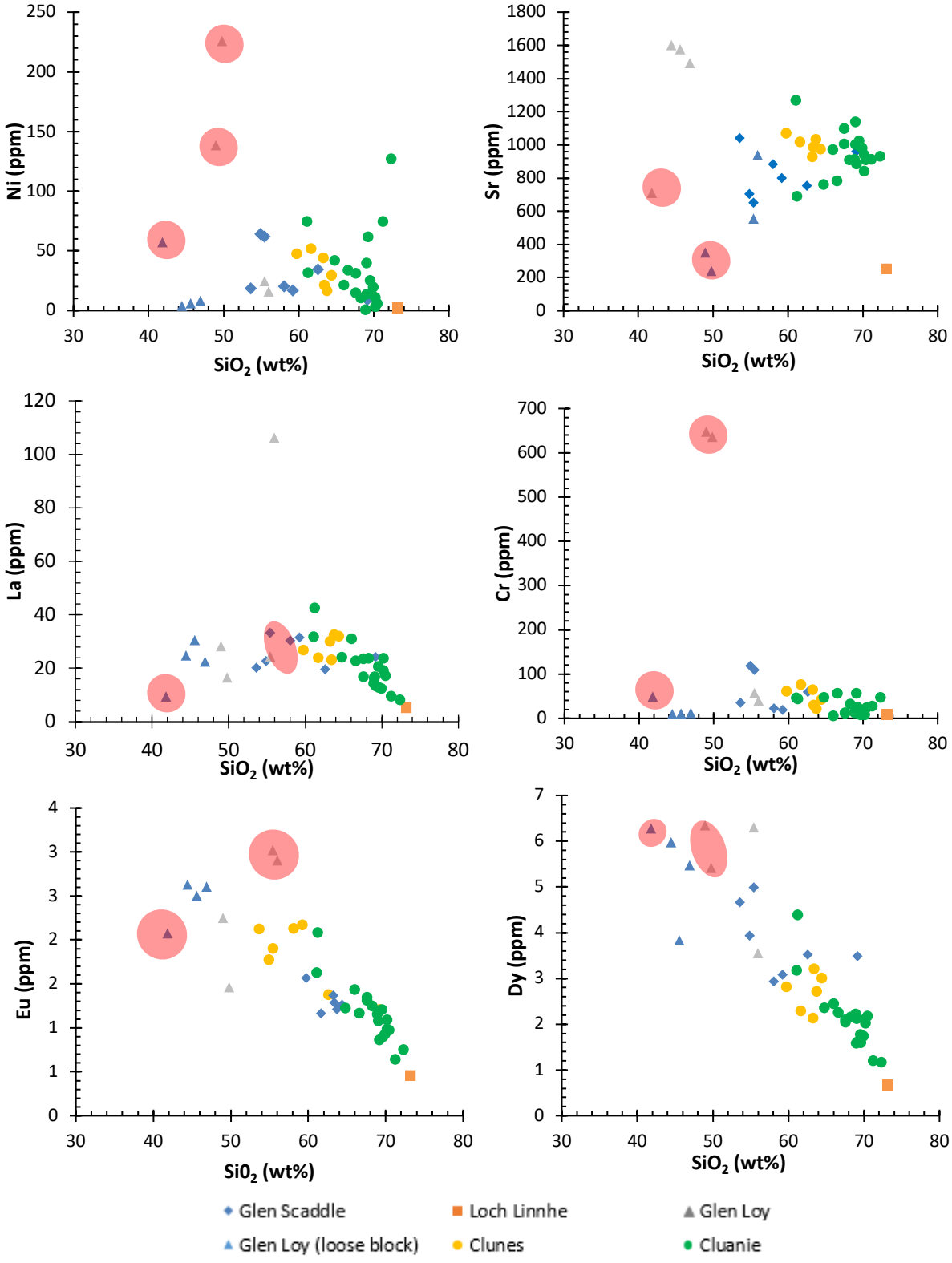

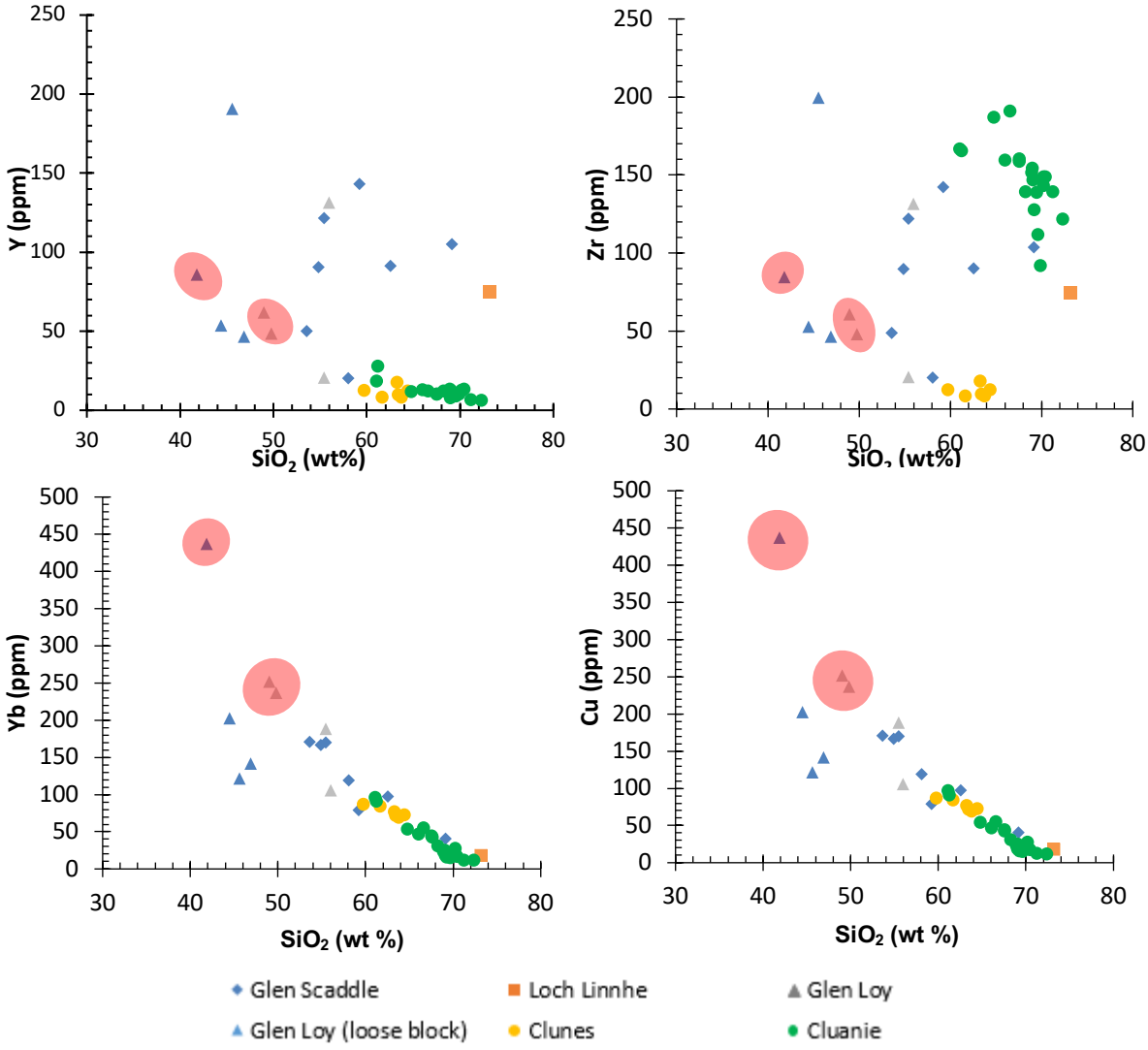

Figure 29: Selected trace element vs. SiO_2 bivariate plots.

	Glen Loy	Glen Scaddle	Clunes	Cluanie
Ni	No relationship with SiO_2 values. **GL_LB_2** and **GL_LB_4** have much higher values than the rest of the samples.	No relationship with SiO_2 values.	Values decrease with increasing SiO_2 content.	In general, Ni values decrease with increasing SiO_2. There are a number of outlying points with higher Ni values **(INC 2, IN/3-7/1, IN/20-7/4, INC 6).**
Sr	No relationship with SiO_2 values. **GL_LB_2**, **GL_LB_4** and **IN-GL-16-2** are outliers, having much lower values than the other the rest of the samples.	No relationship with SiO_2 values.	No relationship with SiO_2 values.	In general, La values increase with increasing SiO_2 content.
La	La values increase with increasing SiO_2 content. **GL_LB_3** has much higher values than the other samples.	No relationship with SiO_2 values.	No relationship with SiO_2 values.	La values decrease with increasing SiO_2 content.
Cr	No relationship with SiO_2 values. **GL_LB_2** and **GL_LB_4** have much higher values than other samples.	No relationship with SiO_2 values.	Values decrease with increasing SiO_2 values.	No relationship with SiO_2 values.
Eu	Values decrease with increasing SiO_2 values. **GL_LB_1** and **GL_LB_3** have high values in relation to this trend, while IN-GL-16-2 plots much lower.	No relationship with SiO_2 values.	No relationship with SiO_2 values. Samples plot in a tight cluster.	Eu values decrease with increasing SiO_2 content.
Dy	Values decrease with increasing SiO_2 values. **IN-GL-16-3** plots below this trend. **GL-LB-1** and **GL-LB-4** have high values in relation to this trend.	Values decrease with increasing SiO_2 values.	No relationship with SiO_2 values.	Dy values decrease with increasing SiO2 content.
Y	Values decrease with increasing SiO_2 values. **IN-GL-16-3** and **GL-LB-3** plot below this trend.	No relationship with SiO_2 values.	No relationship with SiO_2 values. Very low values.	Y values decrease very marginally with increasing SiO2 content.
Zr	Values decrease with increasing SiO_2 values. **IN-GL-16-3** and **GL-LB-3** plot below this trend.	No relationship with SiO_2 values.	No relationship with SiO_2 values. Very low values.	Zr values are high, and show steep decrease with increasing SiO_2 content.
V	Values decrease with increasing SiO_2 values. IN-GL-16-2 has significantly higher V content compared the other samples.	Values decrease with increasing SiO_2 values.	Values decrease with increasing SiO_2 content	V values decrease with increasing SiO_2 content.
Yb	No relationship with increasing SiO_2 values. GL-LB-3 has lower Yb content than the other samples.	Values decrease with increasing SiO_2 content	Values decrease with increasing SiO_2 content	Values decrease with increasing SiO_2 content
Cu	No relationship with increasing SiO_2 values. GL_LB_1 and GL_LB_2 both have significantly higher values than the other samples.	Values decrease with increasing SiO_2 content	Values decrease with increasing SiO_2 content	Values decrease with increasing SiO_2 content

Table 18: Observations from trace element Harker Diagrams (see Figures 27 and 28).

4.3.5.2 Trace Element Chemistry - Normalized Element Spider Diagrams

Chondrite normalized and primitive mantle normalized multi-element spider diagrams are presented for each of the plutons. Normalising values for chondrite normalized plots use values from Sun and McDonough, 1989. Normalising values for primitive mantle normalized plots also use values from Sun and McDonough, 1989.

4.3.5.1 Glen Loy

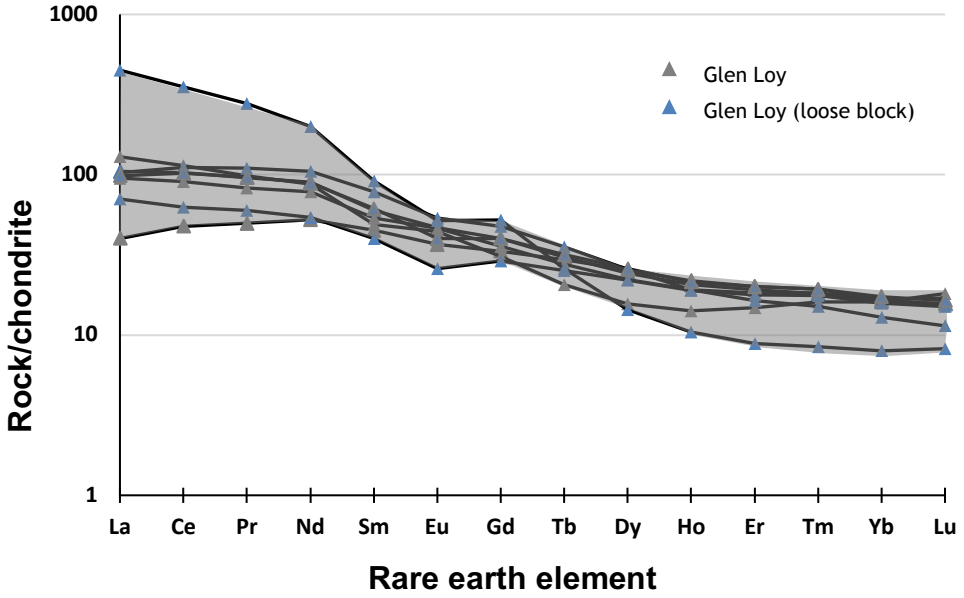

Figure 31: Chondrite normalized trace element for Glen Loy plot after Sun and McDonough, 1989.

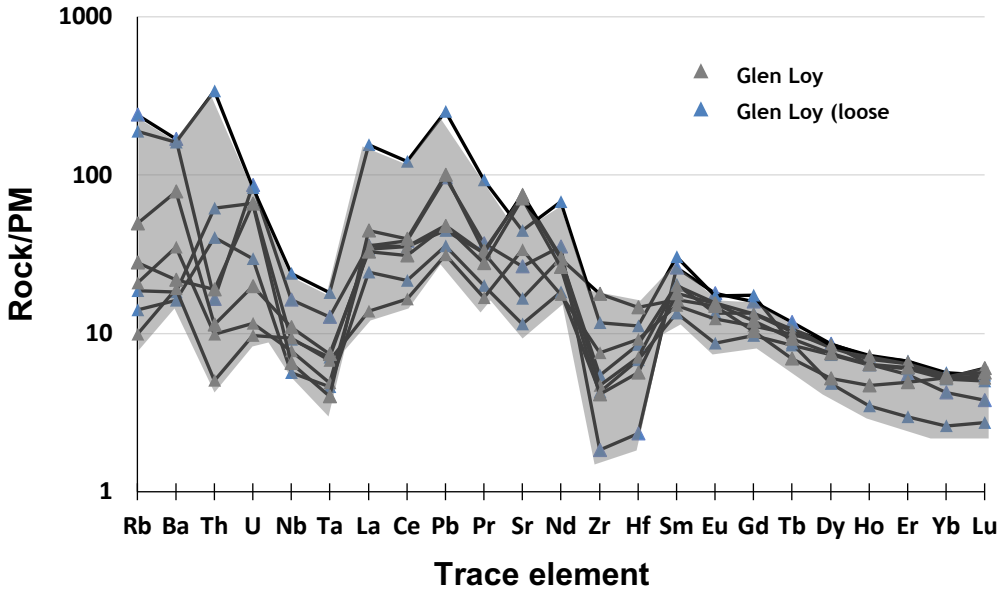

Figure 32: Primitive mantle normalized trace element for Glen Loy plot after Sun and McDonough, 1989.

Chondrite normalized trace element plot

The chondrite normalized multi-element spider diagrams from Glen Loy show relative enrichment in all elements (*see Figure 31*). All samples show broadly similar trends. LREEs (La - Gd) are enriched 50 - 100 times chondritic values. GL_LB_1 is more enriched - closer to 1000 times compared to chondritic values. HREEs (Tb – Lu) are enriched roughly by between 10 and 50 times chondritic values. GL_LB_1 is less enriched in HREEs at under 10 times chondritic value. The La - Yb ratio (represented by the gradient of the trend) is broadly consistent across the samples, with the exception of GL_LB_1, which has a steeper gradient. The samples form Glen Loy show very minor negative europium anomalies

Primative mantle normalized trace element plot

All samples from Glen Loy are enriched in incompatible elements compared to primitive mantle standards (*see Figure 32*). Beyond this, the samples are far from homogenous (i.e. the different samples have different chemistry).

GL_LB_1 and GL_LB_3 have significant enrichment in Rb and Ba (between 100 and 1000 times primitive mantle values). Both samples have higher Rb value than Ba. This trend is of Rb enrichment over Ba is also seen in IN_GL_16_3. All other samples show the opposite trend, with a spike seen in Ba.

The samples from Glen Loy also show complicated, decoupled trends for the Th and U. GL_LB_2, GL_LB_3 and GL_LB_5 all show a spike in Th (enriched by 50 – 500 times primitive mantle values). All samples show lower levels of enrichment in Nb and Ta (5 – 50 times primitive mantle values). GL_LB_1 and GL_LB_3 are comparatively more enriched. All samples all show a spike in Pb. GL_LB_1 shows significantly lower levels of enrichment Zr and Hf.

4.3.5.2 Glen Scaddle

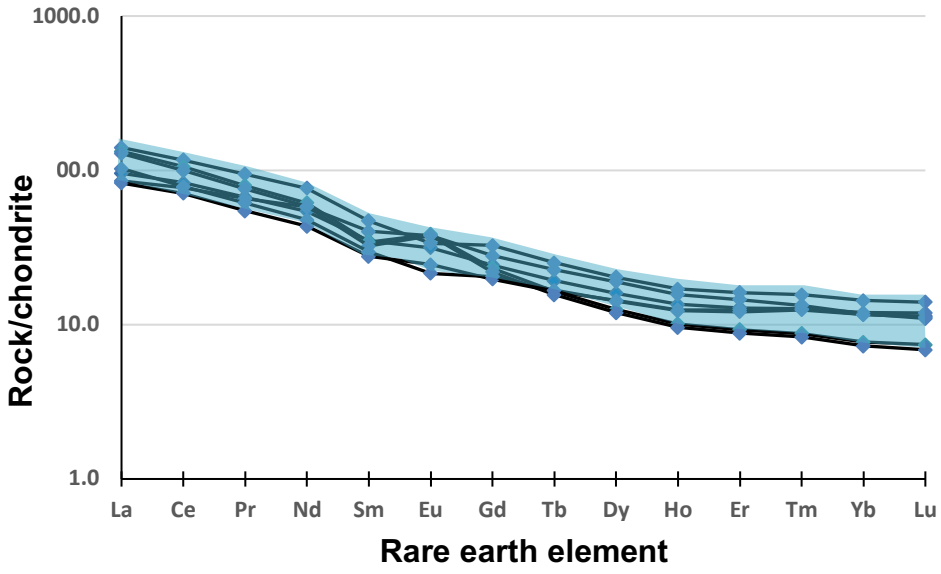

Figure 33: Chondrite normalized trace element plot for Glen Scaddle after Sun and McDonough, 1989.

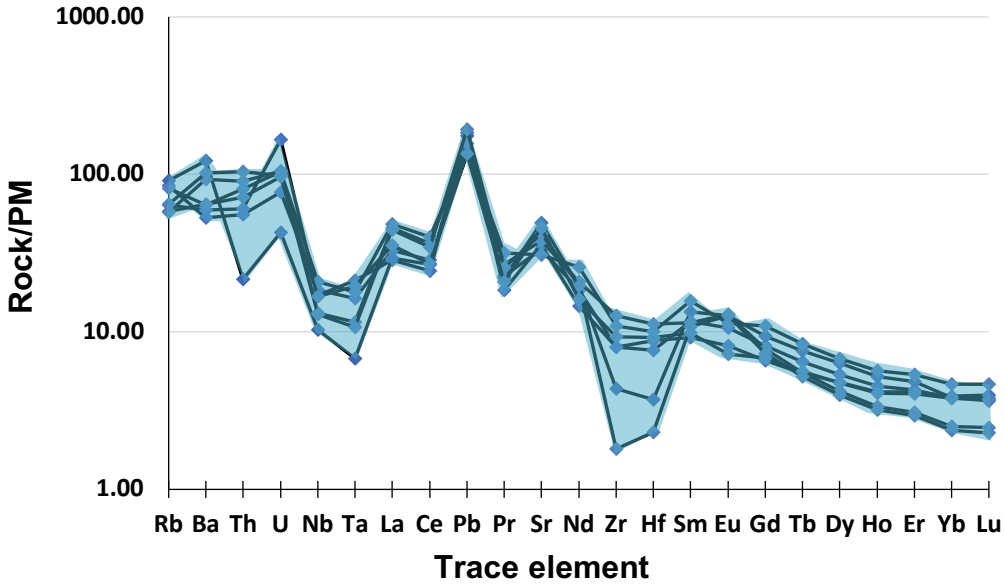

Figure 34: Primitive mantle normalized trace element plot for Glen Scaddle after Sun and McDonough, 1989.

Chondrite normalized trace element plot

The chondrite normalized multi-element spider diagrams from Glen Scaddle show relative enrichment in all elements (see *Figure 33*). All samples show broadly similar trends. LREEs (La - Gd) are enriched 50 - 100 times chondritic values. All samples show 100x enrichment in La, and around 50x enrichment in Gd. HREEs (Tb – Lu) are enriched around 10 times chondritic values. The La - Yb ratio (represented by the gradient of the trend) is broadly consistent across the samples. The samples form Glen Scaddle show only negligible Eu anomalies. GS_17_5 and GS_17_6 show slight positive anomalies.

Primative mantle normalized trace element plot

All samples from Glen Scaddle are enriched in incompatible elements compared to primitive mantle standards (see *Figure 34*). The samples are far more homogenous than the Glen Loy dataset (i.e. there is far less variation in chemistry between samples). Rb and Ba are enriched by around 100 times primitive mantle values in all samples. GS_17_3, GS_17_5, GS_17_6 and GS_17_7 show higher Ba than Rb, while GS_17_1, GS_17_2 and GS_17_4 show higher Rb and Ba. GS_17_3 is the only sample to show a lower level of enrichment in Th (closer 10 times primitive mantle values, as opposed to 100 times). The rest of the elements similar trends. GS_17_3 and GS_17_6 have significantly lower levels of enrichment in Zr and Hf. There is a consistent decrease in levels of enrichment from Sm to Lu.

4.3.5.4 Cluanie

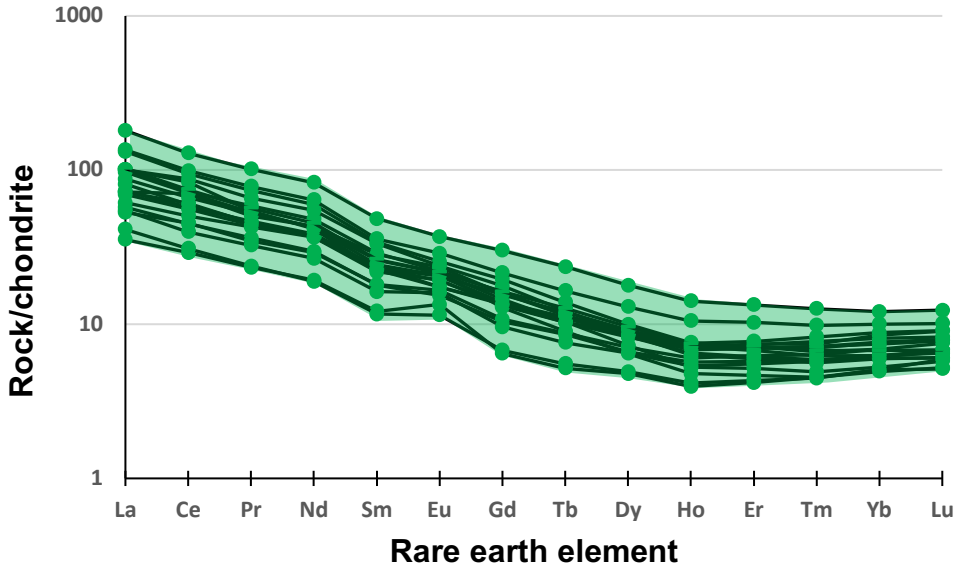

Figure 35: Chondrite normalized trace element plot for Cluanie after Sun and McDonough, 1989.

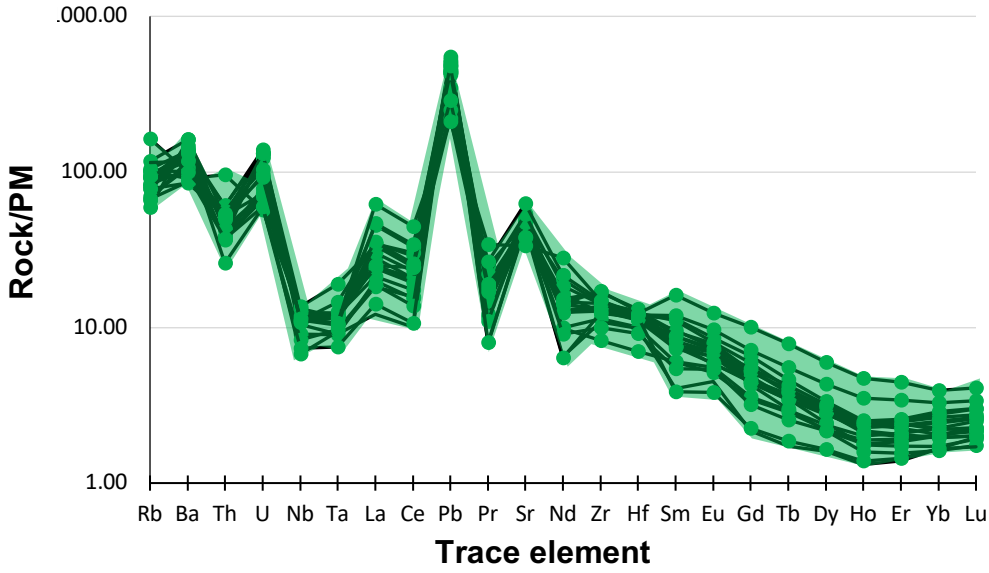

Figure 36: Primitive mantle normalized trace element plot for Cluanie after Sun and McDonough, 1989.

Chondrite normalized trace element plot

The chondrite normalized multi-element spider diagrams from Cluanie show relative enrichment in all elements (see *Figure 35*). All samples show broadly similar trends, while the levels of enrichment is varied consistently. LREEs (La - Gd) are enriched 50 - 150 times chondritic values. All samples show 50 - 100x enrichment in La, and around 10 - 50x enrichment in Gd. HREEs (Tb – Lu) are enriched around 10 – 50x times chondritic values. The La - Yb ratio (represented by the gradient of the trend) is broadly consistent across the samples. The samples form Cluanie show only negligible Eu anomalies.

Primitive mantle normalized trace element plot

All samples from Cluanie are enriched in all elements compared to primitive mantle standards (see *Figure 36*). The samples show very similar trends across the elements plotted, albeit with variable levels of enrichment. Rb and Ba are enriched by around 100 times primitive mantle values in all samples. Only INC_7 has higher Ba than Rb. All samples show lower levels of enrichment in Nb and Ta (10 times primitive mantle standards), and a significant spike in Pb (enriched by over 100 times primitive mantle standards). There is a consistent decrease in levels of enrichment from Zr to Lu.

4.3.5.5 Clunes

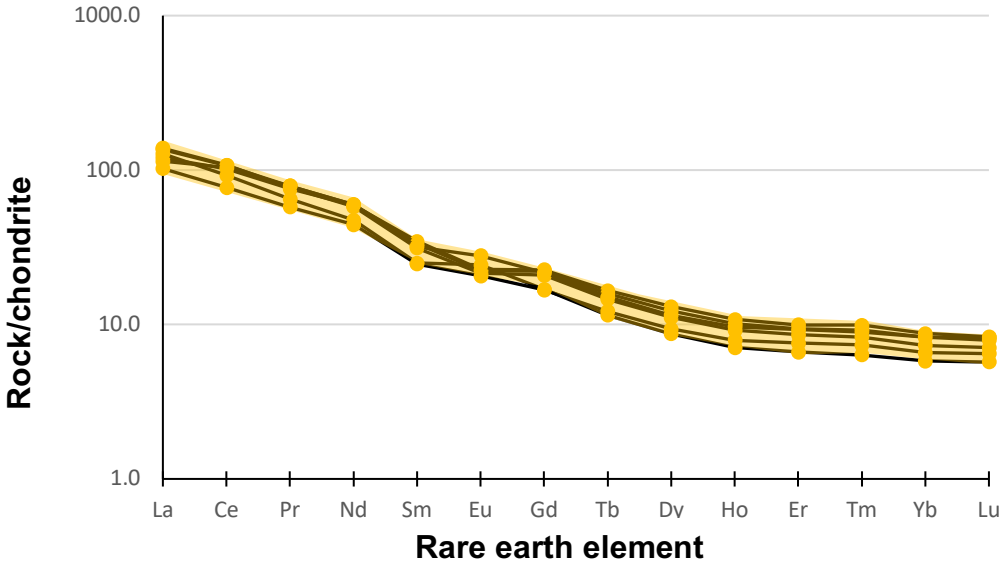

Figure 38: Chondrite normalized trace element plot for Clunes after Sun and McDonough, 1989.

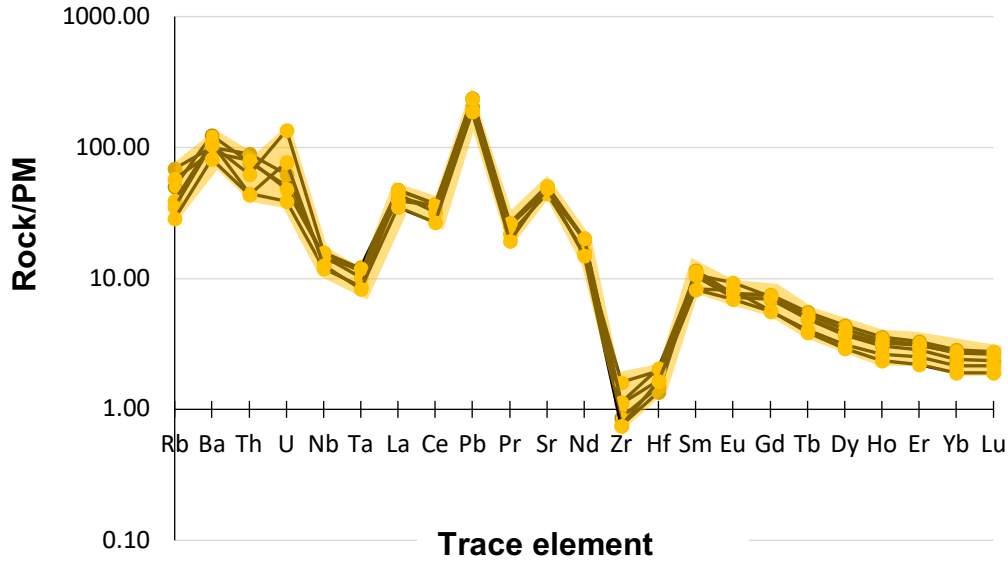

Figure 37: Primitive mantle normalized trace element plot for Clunes after Sun and McDonough, 1989.

Chondrite normalized trace element plot

The chondrite normalized multi-element spider diagrams from Clunes show relative enrichment in all elements (see *Figure 37*). All samples show broadly similar trends and levels of enrichment. LREEs (La - Gd) are enriched 50 – 100 times chondritic values. All samples show enrichment that is 100 times chondritic values for La, and around 10 - 50x enrichment in Gd. HREEs (Tb – Lu) are enriched around 10 – 50x times chondritic values. The La - Yb ratio (represented by the gradient of the trend) is broadly consistent across the samples. The samples form Clunes show no EU anomalies.

Primitive mantle normalized trace element plot

The samples from Clunes are enriched in most trace elements compared to primitive mantle standards, with the exception of Zr and Hf (see *Figure 38*). The different samples show largely homogenous trends, albeit with variable levels of enrichment. Rb and Ba are enriched by 50 - 100 times primitive mantle values in all samples. All samples show lower levels of enrichment in Nb and Ta (10 times primitive mantle standards), and a significant spike in Pb (enriched by over 100 times primitive mantle standards). Very low levels of enrichment, and in some case depletion, are observed of Zr and Hf. All samples subsequently show a spike in Sm (enriched 10 times primitive mantle standards), and a gradual decrease in enrichment to Lu, enriched by between 1- and 10-times primitive mantle standards.

4.3.5.6 Loch Linnhe

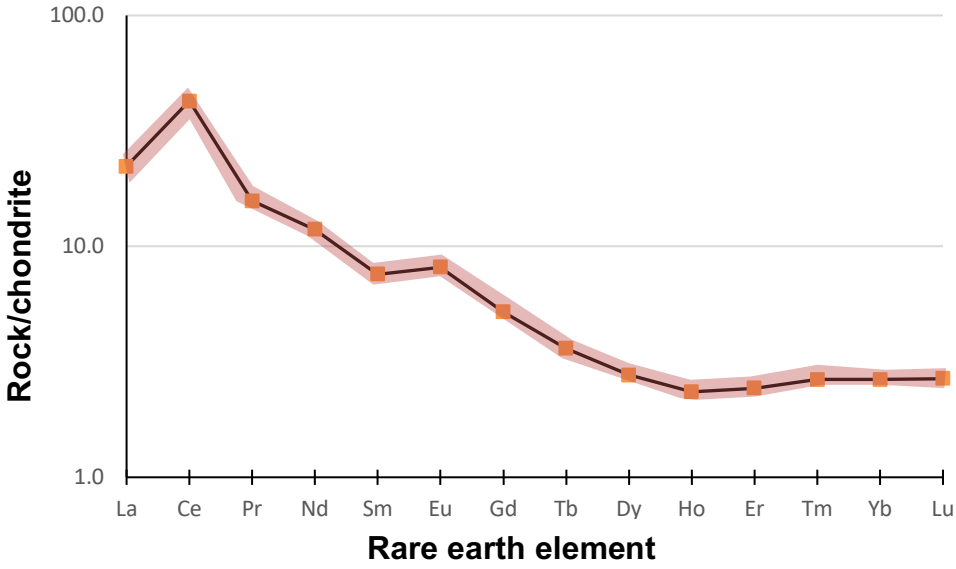

Figure 39: Primitive mantle normalized trace element plot for Loch Linnhe after Sun and McDonough, 1989.

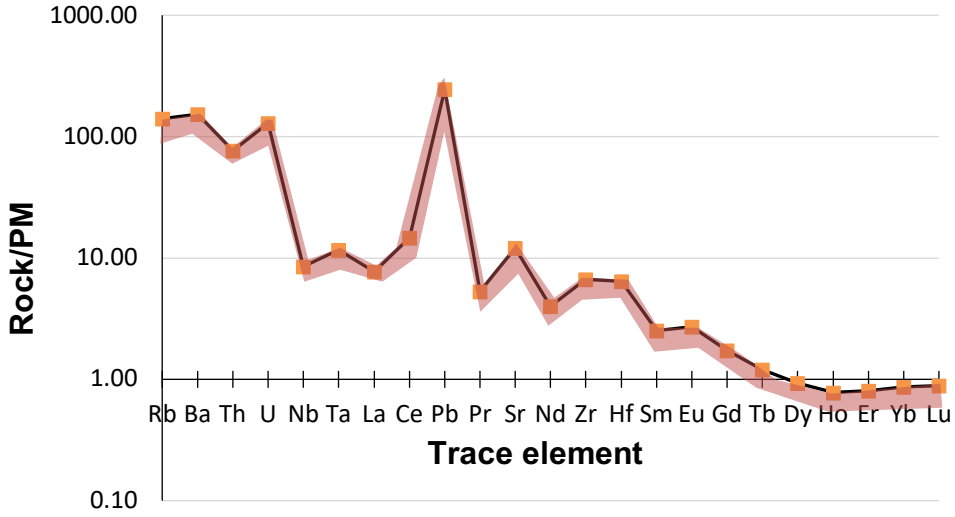

Figure 40: Chondrite normalized trace element plot for Loch Linnhe after Sun and McDonough, 1989.

Chondrite normalized trace element plot

The chondrite normalized multi-element spider diagram for Loch Linnhe shows relative enrichment in all elements. LREEs (La - Gd) are mostly enriched 10 – 100 times chondritic values (La – Nd). Sm – Gd are enriched by under 10 times chondritic values. HREEs (Gd – Lu) are enriched by under 10 times chondritic values. The La - Yb ratio is broadly similar to the other samples studied.

Primitive mantle normalized trace element plot

The sample from Loch Linnhe is enriched in most elements compared to primitive mantle standards, with the exception of Dy – Lu. Rb and Ba are enriched by around 100 times primitive mantle values, while Nb, Ta and La are enriched 10 times primitive mantle standards. The samples show similar trends across elements, including a significant spike in Pb. The lower levels of enrichment of Zr, Hf are less pronounced in all samples compared to Loy and Scaddle. There is a consistent decrease in levels of enrichment from Sm to Lu.

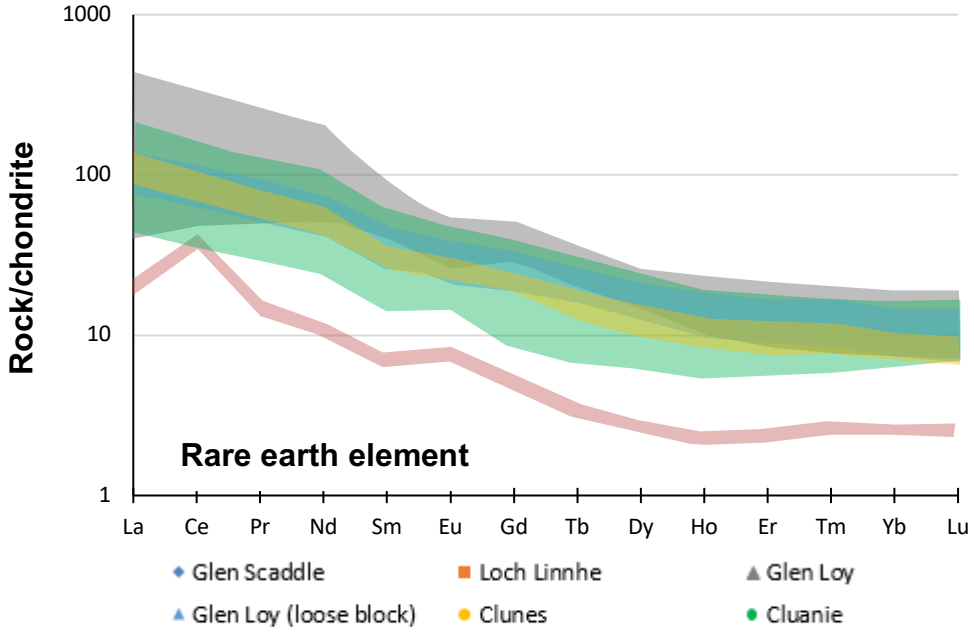

Figure 41: Combined chondrite normalized trace element plot after Sun and McDonough, 1989.

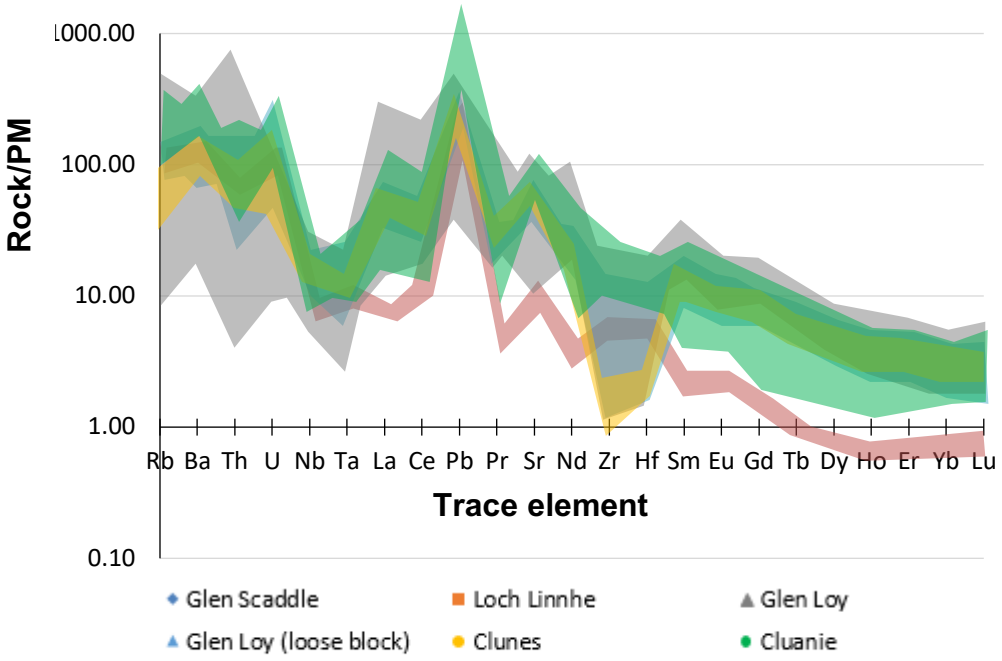

Figure 42: Combined chondrite normalized trace element plot after Sun and McDonough, 1989.

4.2.6.6 Comparisons between plutons

Chondrite normalized trace element plots

All plutons are enriched in all elements when normalized to chondritic values (See Figure 41). Glen Loy has the greatest compositional range within samples. This is particularly pronounced in the LREE (La - Gd) field of the plot, with the compositional range lessening for the HREE field (Gd – Lu). Samples from Glen Loy are the most enriched in LREEs. Glen Scaddle, Clunes and Cluanie all have broadly similar compositional profiles, although Cluanie does have a greater compositional range than Scaddle and Clunes. Loch Linnhe is comparatively less enriched in both LREEs and HREEs. Linnhe has a very slight positive Eu anomaly, which is mirrored by Cluanie. Scaddle and Loy both show slight positive Eu anomalies.

Primitive mantle normalized plots

With the exception of Clunes and Linnhe, the plutons are enriched in all elements when normalized to primitive mantle values (see Figure 42). Clunes shows marginal depletion in Zr, and Linnhe shows marginal depletion in elements Tb – Lu. Glen Loy has the greatest compositional range within samples, especially from Rb – U. Despite variability within the Glen Loy data set, the plutons all show high levels of enrichment in Rb and Ba, and negative spikes in HFSEs Nb and Ta. All plutons show a significant positive spike in Pb. Scaddle, Clunes and Loy show significant negative spikes in Zr and Hf not mirrored in Linnhe and Cluanie. Only Linnhe is enriched

4.2.6 Adakite classification

The fields for adakite classification presented in *Figures 43 - 46* are defined by Defant and Drummond (1990) in their pioneering work on the subject. The geochemical classifications shown generally relate to the fractionation of garnet and amphibole and the absence of plagioclase in the melt residue.

In *Figure 43* and *44*, Clunes plots within the adakite field. Several data points for Cluanie plot also within the adakite field based on their La/Yb values (*Figure 44)* but are too enriched in Y to classify as adakitic (*Figure 43*). These samples can be described as adakite like. One sample from Scaddle plots within the adakitic field for both Sr/Y and La/Yb contents, with the rest plotting in the calk alkaline field. Glen Loy and Loch Linnhe are calk alkaline.

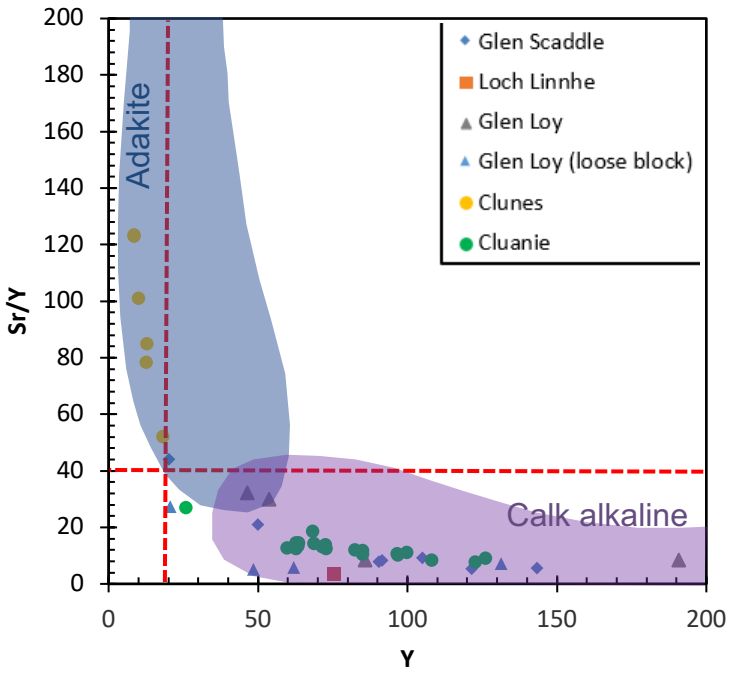

Figure 43: Sr/Y vs Y (pre-normalisation) with coloured zones taken from Martin, 1986 to define Adakite (blue) or Calk alkaline (purple) domains. The red dashed lines define the Adakite domains as defined by Defant and Drummond, 1990.

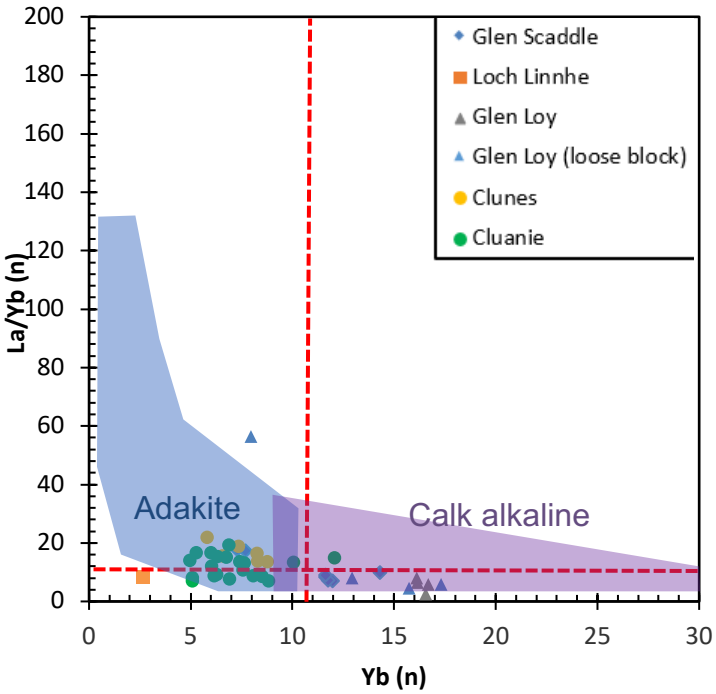

Figure 44 Chondrite normalised La/Yb vs Yb (normalisation values from Sun and Mcdonough, 1989). Coloured domains are taken from Martin, 1986, and define Adakite or Calk alkaline domains. The red dashed lines define the Adakite domains as defined by Defant and Drummond, 1990.

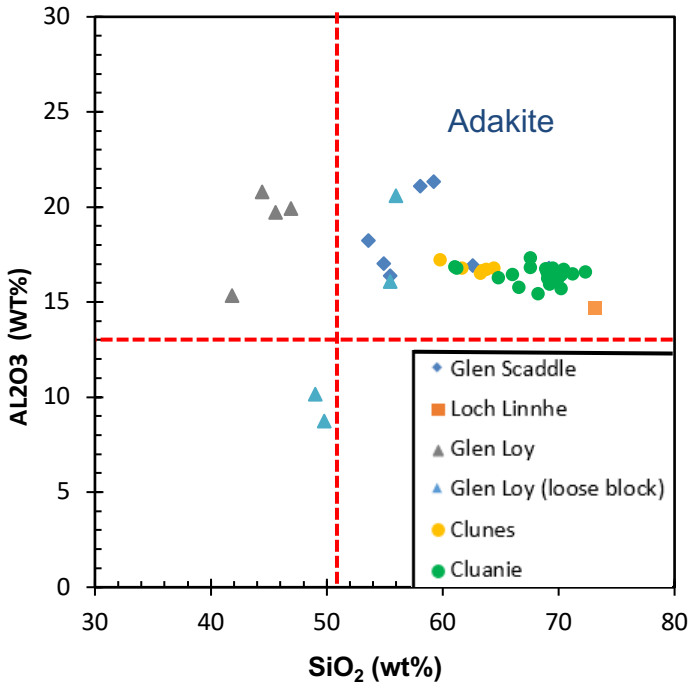

Figure 45: Al_2O_3 (wt %) vs SiO_2 (wt %), with the field for adakite classification as described by Defant and Drummond, 1990.

4.4 Geochronology

Data that lies within 2σ covaried uncertainty from the Concordia curve is presented for each pluton (i.e. data points that are <5% discordant). Grains from Glen Loy and Cluanie were run over two LA-ICPMS sessions, for which the mineral preparation and selection process and LA ICPMS set-up was identical. The data was reduction process was conducted separately, but the final crystallization age combined grains/ages from both analysis. Sample ID's are explained in section *3.4.6 - Grain Mounting*.

In order to identify different zircon populations and understand the spread of ages returned from analysis, a textural description was carried out for each of the zircon grain whose age was within 2σ covaried uncertainty of the Concordia. The morphology of each grain was described using the terminology in *Figure 46*. The zoning pattern was described using the terminology described in *Figure 47*. Where applicable, it is also stated whether the laser spot hit the core of the rim/overgrowth (OG) of the grain.

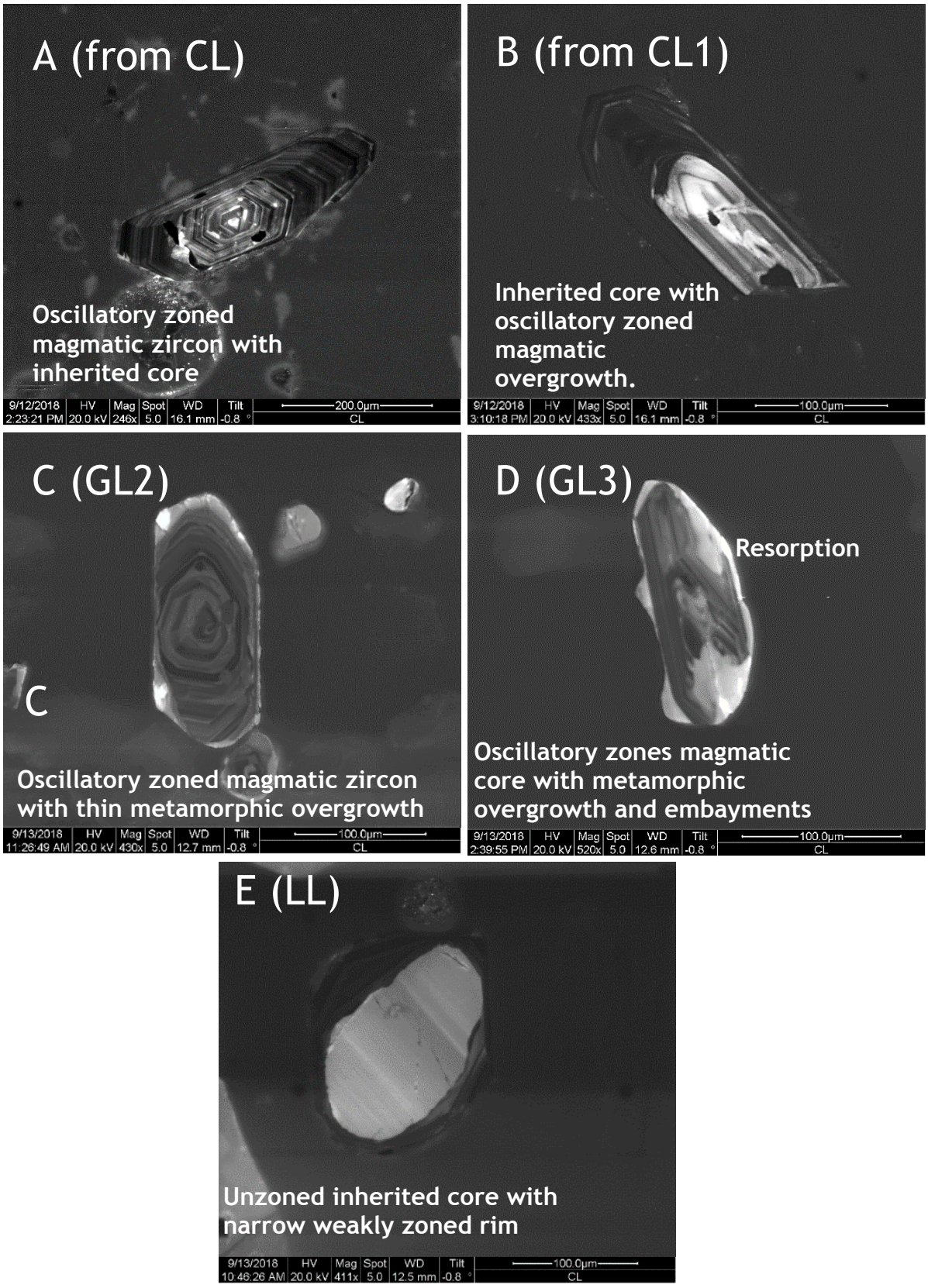

Figure 47: Cathodoluminescence images of zircon grains showing differing degrees of 'ideal' crystal morphology, with annotations highlighting different textural characteristics. A) is a euhedral grain, where ideal crystal morphology is apparent. B) is subhedral but is a fragment of a grain with seemingly ideal crystal morphology. It is referred to as Subhedral (broken). C) is Subhedral - ideal crystal morphology is discernible, but some aspects of morphology are altered. D) and E) are anhedral, ideal crystal morphology is not discernible, either because of resorption (D) or due to the grain being poorly developed (E).

4.4.1 Cluanie

CL1 contains 21 zircon grains. 94 spot analysis were carried out, 24 of which were within 2σ covaried uncertainty of the Concordia line for both D1 and D2 (see Equation 1). The data is presented in *Table 19*.

CL2 and CL3 were analysed in the same session. CL2 contains 20 grains. 112 spot analysis were carried out, 21 of which were within 2σ covaried uncertainty of the Concordia line for both D1 and D2. The data is presented in *Table 20*.

CL3 contains 18 grains. 56 spot analysis were carried out, 14 of which were within 2σ covaried uncertainty of the Concordia line for both D1 and D2. The data is presented in *Table 21*.

Table 19: Concordant data from U - Pb analysis of zircons from CL1. *D1 is the value given by [206Pb – 238U age/207Pb – 206Pb age)*100]. **D2 is the value given by [(206Pb-238Uage/207Pb-235U age]*100].

	Ratios					Ages				Concordance	
ID CL1	207Pb/235U	2σ	206Pb/238U	2σ	rho	207Pb/235U	2σ	206Pb/238U	2σ	D1*	D2**
1.1	0.552	0.011	0.071	0.000	0.16	446.7	7.3	439.6	2.5	95	98
1.2	0.545	0.014	0.070	0.001	0.15	441.7	8.6	438.8	3.3	101	99
1.3	0.546	0.011	0.070	0.001	0.31	440.9	6.9	438.1	3.1	98	99
3.1	3.160	0.065	0.250	0.002	0.31	1441	16	1440	11	100	100
3.2	3.202	0.077	0.252	0.002	0.18	1451	19	1446	11	100	100
3.5	0.543	0.018	0.069	0.001	0.16	438	11	430.8	3.5	97	98
4.5	3.691	0.073	0.277	0.004	0.58	1563	16	1575	21	102	101
5.1	3.329	0.091	0.252	0.003	0.22	1479	21	1449	14	95	98
5.2	3.331	0.075	0.256	0.003	0.32	1483	18	1469	13	98	99
8.4	4.178	0.097	0.293	0.003	0.30	1666	18	1655	14	99	99
8.5	3.888	0.073	0.280	0.003	0.02	1610	16	1589	14	98	99
11.2	3.200	0.100	0.251	0.003	0.00	1446	26	1445	16	100	100
12.2	0.552	0.015	0.071	0.001	0.16	444.2	9.6	441.5	3.2	101	99
13.1	4.135	0.076	0.296	0.002	0.10	1656	15	1669	12	102	101
13.2	4.159	0.070	0.295	0.002	0.00	1665	15	1667	11	101	100
14.1	0.534	0.015	0.069	0.001	0.13	432	10	431.3	3.5	100	100
14.3	0.554	0.013	0.071	0.001	0.31	445.9	8.4	441.9	3.2	97	99
17.2	4.104	0.095	0.296	0.004	0.48	1651	19	1670	19	103	101
17.3	4.009	0.076	0.287	0.002	0.19	1632	16	1627	12	100	100
17.4	4.069	0.099	0.288	0.004	0.42	1648	20	1629	20	98	99
18.1	0.541	0.015	0.070	0.001	0.09	439	11	433.8	3	98	99
18.3	0.532	0.015	0.069	0.001	0.10	432	10	430.9	3.7	104	100
18.4	0.545	0.017	0.069	0.001	0.11	438	11	432.1	3.7	97	99
19.2	0.564	0.014	0.073	0.001	0.02	454	9.8	451.5	3.6	100	99

Table 20: Concordant data from U - Pb analysis of zircons from CL 2. D* is the value given by [206Pb ‐ 238U age/207Pb ‐ 206Pb age)*100]. D is the value given by [(206Pb-238Uage/207Pb-235U age]*100].**

	Ratios					Ages				Concordance	
ID	**207Pb/235U**	**2σ**	**206Pb/238U**	**2σ**	**rho**	**207Pb/235U**	**2σ**	**206Pb/238U**	**2σ**	**D1***	**D2****
CL2											
4.2	0.565	0.013	0.073	0.001	0.25	454	8.5	451.2	3.2	101	99
4.4	0.661	0.022	0.081	0.001	0.03	512	14	504.9	4.6	97	99
6.5	0.718	0.018	0.087	0.001	0.19	548	11	540.4	4	95	99
6.6	0.868	0.023	0.102	0.001	0.31	630	12	624.1	6.8	96	99
10.2	0.593	0.016	0.076	0.001	0.12	470.7	9.9	470.1	4.5	98	100
13.2	4.239	0.064	0.300	0.002	0.53	1678	12	1691	12	101	101
15.1	0.556	0.018	0.072	0.001	0.35	447	12	448.8	4.3	102	100
16.3	1.507	0.054	0.157	0.003	0.57	926	21	937	16	105	101
16.6	0.564	0.018	0.072	0.001	0.06	452	12	449.8	3.5	103	100
16.7	0.551	0.011	0.071	0.001	0.19	445.4	6.9	443	3.1	99	99
17.3	0.534	0.009	0.069	0.000	0.19	433.3	6.1	430.1	2.8	99	99
22.2	0.589	0.012	0.075	0.001	0.29	469.9	7.9	464	3.8	95	99
26.1	0.576	0.012	0.073	0.001	0.32	461.2	8	455.6	3.2	98	99
26.6	4.030	0.160	0.296	0.004	0.19	1637	30	1671	21	105	102
26.7	4.010	0.130	0.290	0.004	0.03	1627	28	1643	20	103	101
26.8	3.880	0.140	0.283	0.004	0.15	1596	29	1606	19	102	101
27.1	3.893	0.072	0.286	0.002	0.08	1607	15	1620	12	102	101
27.2	4.081	0.075	0.296	0.003	0.32	1649	16	1668	13	104	101
28.3	2.092	0.032	0.191	0.001	0.28	1144	10	1125.1	6.9	97	98
29.1	1.806	0.024	0.178	0.001	0.22	1047.1	8.8	1052.9	7.2	103	101
29.3	1.620	0.059	0.165	0.003	0.71	973	22	985	18	104	101
2.3	0.565	0.013	0.073	0.001	0.25	459.1	8.3	456.6	3.3	102	99

Table 21: Concordant data from U - Pb analysis of zircons from CL 3. D* is the value given by [206Pb ‑ 238U age/207Pb ‑ 206Pb age)*100]. D is the value given by [(206Pb-238Uage/207Pb-235U age]*100].**

	Ratios					Ages				Concordance	
ID	207Pb/235U	2σ	206Pb/238U	2σ	rho	207Pb/235U	2σ	206Pb/238U	2σ	D1*	D2**
CL_3											
4.2	0.574	0.013	0.073	0.001	0.14	869	11	873	6.8	102	100
4.3	1.357	0.027	0.145	0.001	0.08	866	13	868.5	8.4	103	100
6.2	1.351	0.029	0.144	0.002	0.22	772	23	772	20	103	100
7.2	1.154	0.048	0.128	0.004	0.61	618	16	625	15	100	101
7.3	0.846	0.029	0.102	0.003	0.57	721	14	730.7	9.7	105	101
7.4	1.044	0.028	0.120	0.002	0.43	858	22	854	14	101	100
10.1	1.349	0.052	0.142	0.003	0.38	1319	21	1295	19	95	98
10.2	2.696	0.077	0.223	0.004	0.27	446	10	444.4	3.8	105	100
11.1	0.555	0.015	0.071	0.001	0.00	477	15	466.4	4.5	98	98
11.2	0.606	0.024	0.075	0.001	0.11	466	11	464.6	4.5	104	100
13.4	0.584	0.018	0.075	0.001	0.15	451.8	7.4	447.4	3.3	95	99
15.3	0.561	0.011	0.072	0.001	0.12	858	23	832	10	95	97
17.2	1.344	0.057	0.138	0.002	0.32	1299	14	1298	12	101	100

4.4.1.1 Concordia Plots

The associated Concordia plots for CL1 and CL2+3 are presented below (*see Figures 9 - 16*). For each dataset, all of the concordant datapoints are first presented with a Concordia curve that ranges from 0 – 2500 Ma. The individual clusters of ages are then plotted independently (termed Group A, B or C) in Concordia plots with narrowed age ranges. This allows greater clarity when interrogating the data. The youngest cluster of data points is interpreted to represent the crystallization age of the plutons. In the Concordia plots thought to display the crystallization age, the number of grains in the cluster is given (N), alongside the weighted mean 206Pb/238U age (with 2σ error), and the mean square weighted deviation (MSWD) of the weighted mean. The weighted mean and MSWD of each group of grains is calculated on Isoplot 3.7 using the 'mean age' function.

4.1.1.2 Cluanie 1

The data from CL1 (*see Figures 9 – 12*) shows three clusters of ages. These groups are marked in *Figure 9*, and labelled A – C (from youngest to oldest). Group A (*Figure 10*) is the youngest and most tightly clustered group of grains, from which a crystallisation is later calculated.

4.1.1.3 Cluanie 2 + 3

There is greater spread in the data from CL 2 and 3 (*See Figures 13 – 16*). Groups A, B and C from CL 1 are marked on Figure 13. Groups A and C from CL 1 are identifiable, although Group B is not. Instead there is a spread of 17 ages between groups A and C. Group A (*Figure 17*) is the youngest and most tightly clustered group of grains, from which a crystallisation is later calculated.

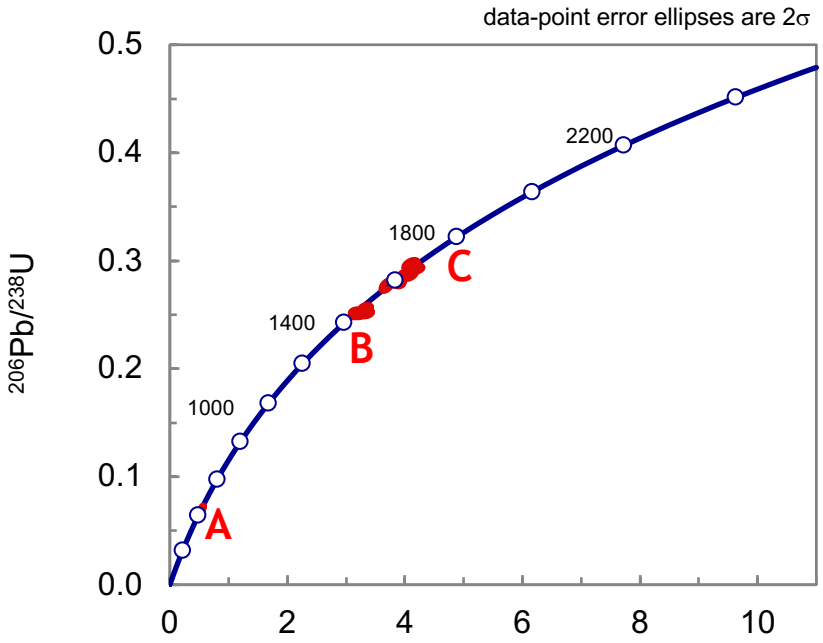

Figure 48: Concordia plot containing data for CL1 (data presented in Table 19). The plot shows all of thr data for CL1, from 0 – 2500Myra. Three distinct clusters of ages are noted, and labelled A, B and C.

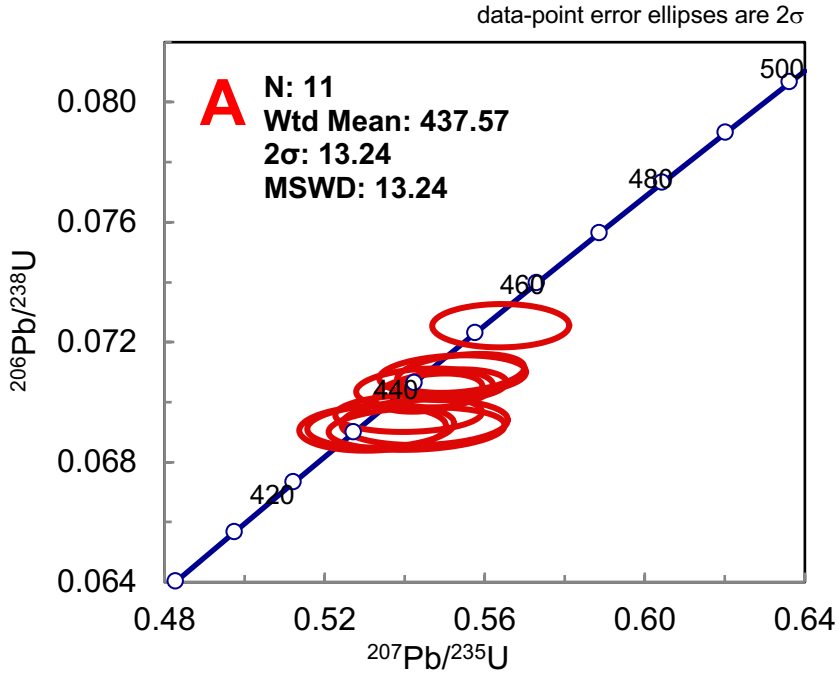

Figure 49: Concordia plot containing data for CL1 (data presented in Table 19). The plot shows the Concordia curve from 400 - 500Myra, group A is thus isolated. N: number of grains. Wtd mean: weighted mean of the data based on analytical errors. 2σ: 95% confidence error of mean. MSWD: Mean square weighted deviation of data based on analytical errors. Calculated on Isoplot 3.7.

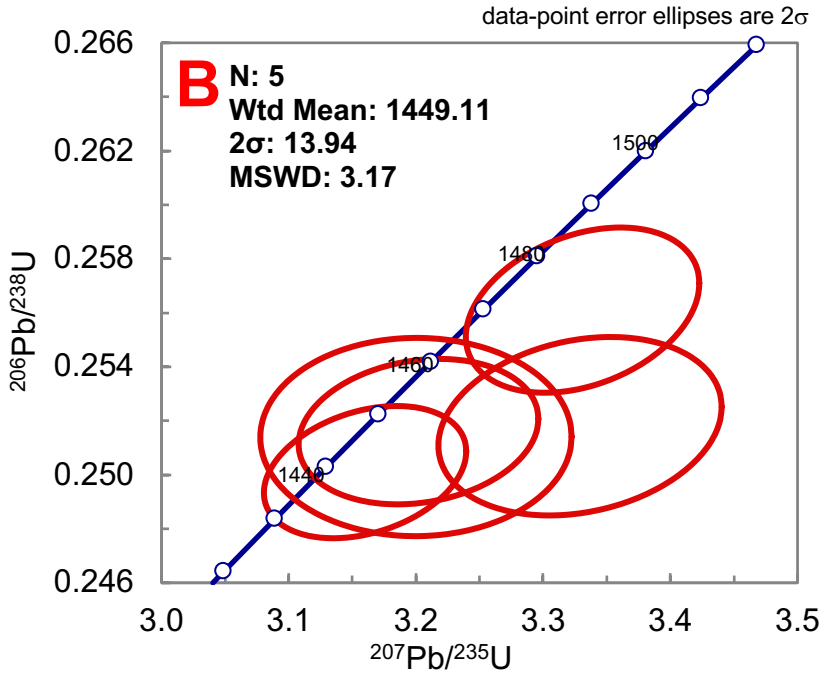

Figure 50: Concordia plot containing data for CL1 (data presented in Table 19). The plot shows the Concordia from 1420 - 1520Myra, group B is thus isolated. N: number of grains. Wtd mean: weighted mean of the data based on analytical errors. 2σ: 95% confidence error of mean. MSWD: Mean square weighted deviation of data based on analytical errors. Calculated on Isoplot 3.7.

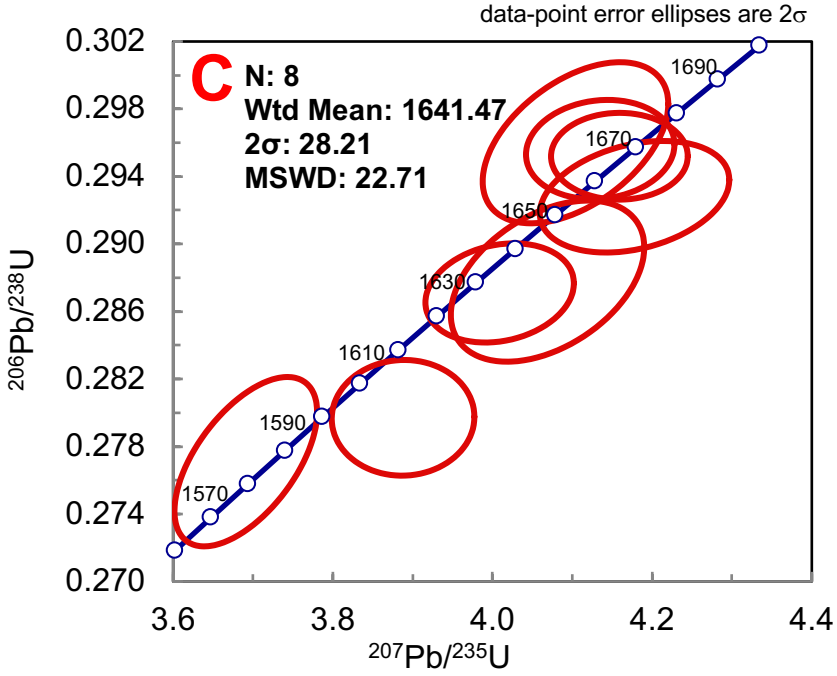

Figure 51: Concordia plot containing data for CL1 (data presented in Table 19). The plot shows the Concordia from 1420 - 1520Myra, group C is thus isolated. N: number of grains. Wtd mean: weighted mean of the data based on analytical errors. 2σ: 95% confidence error of mean. MSWD: Mean square weighted deviation of data based on analytical errors. Calculated on Isoplot 3.7.

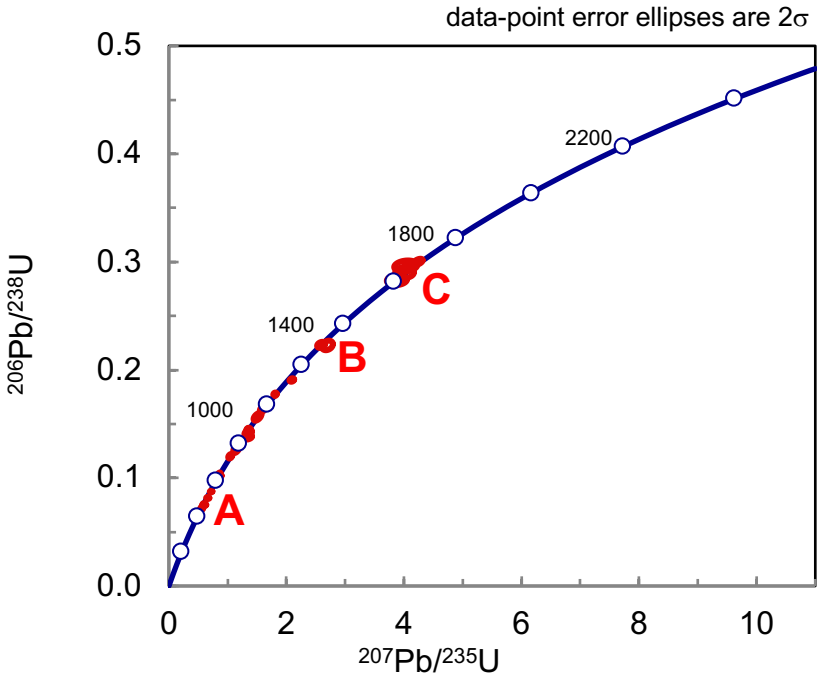

Figure 52: Concordia plot containing data for CL2 and CL3 (data presented in Table 20). The plot shows the Concordia from 0 – 2500Myra. Three distinct clusters of ages are noted, and labelled A, B and C.

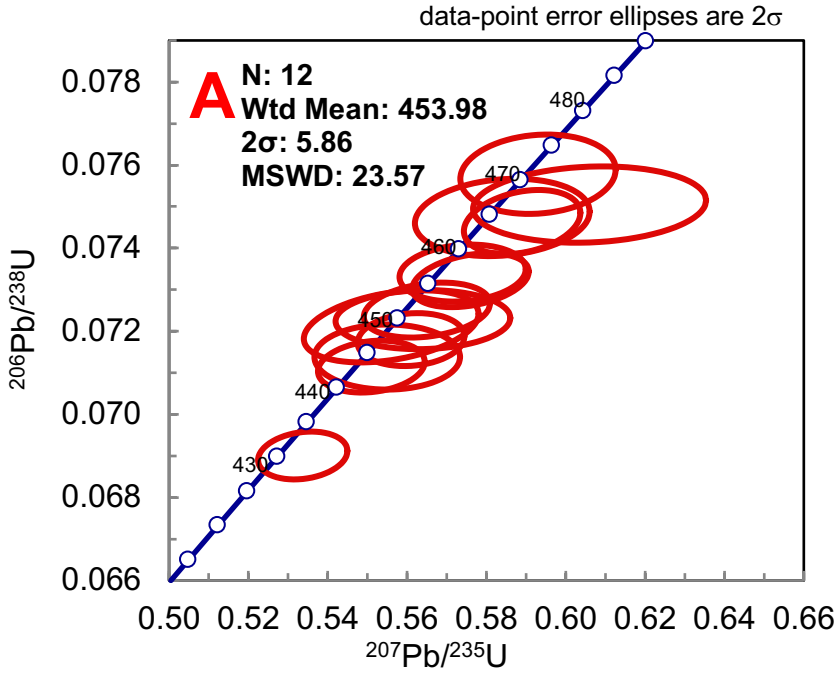

Figure 53: Concordia plot containing data CL2 & 3 (data presented in Table 20). The plot shows the Concordia from 400 – 500Myra, group A is thus isolated. N: number of grains. Wtd mean: weighted mean of the data based on analytical errors. 2σ: 95% confidence error of mean. MSWD: Mean square weighted deviation of data based on analytical errors. Calculated on Isoplot 3.7.

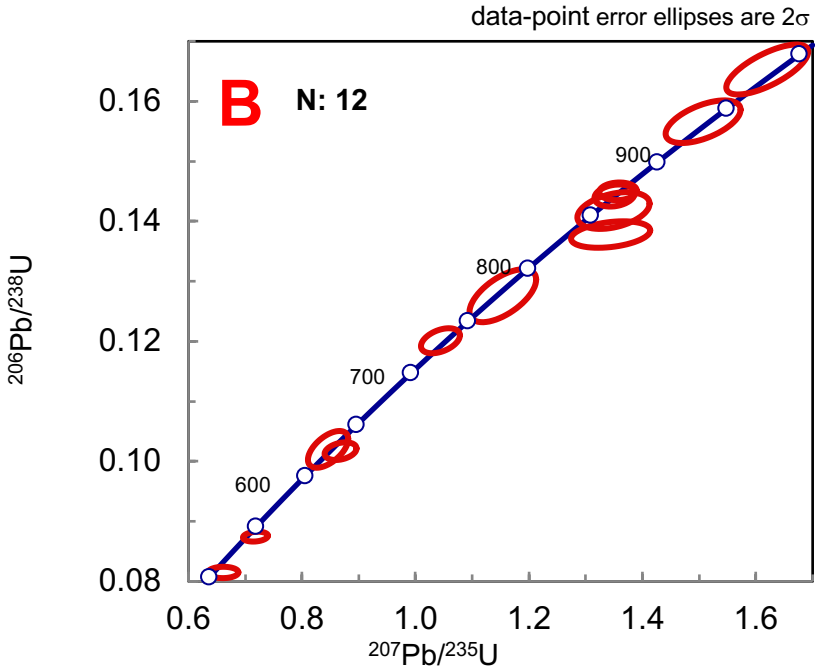

Figure 54: Concordia plot containing data CL2 and CL3 (data presented in Table 20). The plot shows the Concordia from 500 - 1000Myra, group B is thus isolated. Since the group B is diffuse, a weighted mean wasn't calculated.

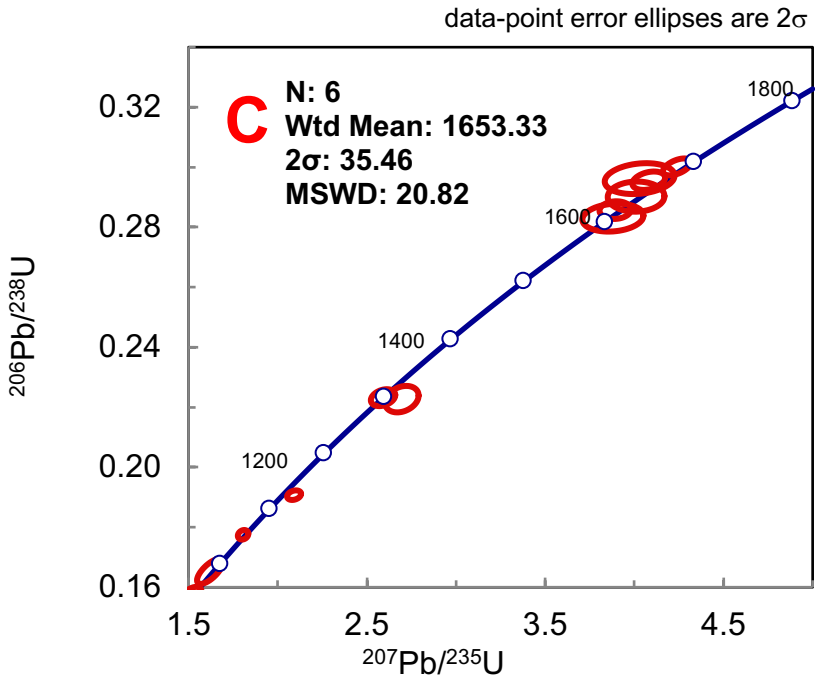

Figure 55: Concordia plot containing data from CL 2 and 3 (data presented in Table 20). The plot shows the Concordia from 1000 – 1800Myra. N: number of grains. Wtd mean: weighted mean of the data based on analytical errors. 2σ: 95% confidence error of mean. MSWD: Mean square weighted deviation of data based on analytical errors. Calculated on Isoplot 3.7.

4.1.1.2 Textural Descriptions

Textural descriptions of zircons was carried out in order to characterise different populations in accordance with ages U - Pb ages (*see Tables 22 - 24*).

	Ages				Zircon Texture		
ID	**207Pb/235U**	**2σ**	**206Pb/238U**	**2σ**	**Grain Shape**	**Zoning Pattern**	**Position of laser spot**
1.1	446.7	7.3	439.6	2.5	Euhedral	Faint oscillatory zoning on magmatic overgrowth. More prominent in core.	OG
1.2	441.7	8.6	438.8	3.3			OG
1.3	440.9	6.9	438.1	3.1			OG
3.1	1441	16	1440	11	Subhedral (broken)	Faint oscillatory zoning on magmatic overgrowth. More prominent in core.	Core
3.2	1451	19	1446	11			Core
3.5	438	11	430.8	3.5			OG
4.5	1563	16	1575	21	Euhedral	Faint oscillatory zoning on small magmatic overgrowth. Core is randomly zoned.	Core
5.1	1479	21	1449	14	Euhedral - Subhedral	Faint oscillatory zoning on small magmatic overgrowth. More prominent in core.	Core
5.2	1483	18	1469	13			Core
8.4	1666	18	1655	14	Subhedral	Faint oscillatory zoning on small magmatic overgrowth. Random zoning in core.	Core
8.5	1610	16	1589	14			Core
11.2	1446	26	1445	16		Oscillatory zoned magmatic overgrowth with prominent oscillatory and sector zoning in core.	Core
12.2	444.2	9.6	441.5	3.2	Subhedral (broken)	Faint oscillatory zoning on rim. More prominent in core.	Rim
13.1	1656	15	1669	12	Anhedral	Prominent oscillatory zoning throughout.	N/a
13.2	1665	15	1667	11			
14.1	432	10	431.3	3.5	Euhedral	Faint oscillatory throughout.	N/a
14.3	445.9	8.4	441.9	3.2			N/a
17.2	1651	19	1670	19	Subhedral (broken)	Faint oscillatory zoning on magmatic overgrowth. More prominent in core.	Core
17.3	1632	16	1627	12			Core
17.4	1648	20	1629	20			Core
18.1	439	11	433.8	3	Euhedral	Oscillatory zoning throughout.	N/a
18.3	432	10	430.9	3.7			
18.4	438	11	432.1	3.7			
19.2	454	9.8	451.5	3.6	Euhedral	Faint oscillatory zoning on overgrowth. More prominent in core.	OG

Table 22: Textural descriptions of concordant zircons from CL1. Ages are given as in Table 20.

	Ages				Zircon Texture		
ID	**207Pb/235U**	**2σ**	**206Pb/238U**	**2σ**	**Grain Shape**	**Zoning Pattern**	**Core/Rim***
4.2	454	8.5	451.2	3.2	Euhedral	Faint oscillatory zoning on magmatic overgrowth rim. More prominent in core.	OG
4.4	512	14	504.9	4.6			OG
6.5	548	11	540.4	4	Subhedral	Faint oscillatory zoning on magmatic overgrowth. Unboned core.	OG
6.6	630	12	624.1	6.8			OG
10.2	470.7	9.9	470.1	4.5	Euhedral	Oscillatory zoning throughout. No distinction between core and rim.	N/a
13.2	1678	12	1691	12	Anhedral	Faint oscillatory zoning on magmatic overgrowth. Prominent unzoned core.	Core
15.1	447	12	448.8	4.3	Anhedral/Broken	Faint oscillatory zoning throughout.	N/a
16.3	926	21	937	16	Euhedral	Faint oscillatory zoning throughout.	N/a
16.6	452	12	449.8	3.5			N/a
16.7	445.4	6.9	443	3.1			N/a
17.3	433.3	6.1	430.1	2.8	Subhedral (broken)	Faint oscillatory zoning but no distinction between core and rim.	N/a
22.2	469.9	7.9	464	3.8	Euhedral	Faint oscillatory zoning on magmatic overgrowth. Prominent unzoned core.	N/a
26.1	461.2	8	455.6	3.2	Subhedral	Faint oscillatory zoning on small magmatic overgrowth. More prominent in core.	OG
26b.6	1637	30	1671	21	Subhedral	Faint oscillatory zoning on small magmatic overgrowth. Large unzoned core.	Core
26b.7	1627	28	1643	20			Core
26b.8	1596	29	1606	19			Core
27.1	1607	15	1620	12	Subhedral	Faint oscillatory zoning on magmatic overgrowth. More prominent in core.	N/a
27.2	1649	16	1668	13			N/a
28.3	1144	10	1125.1	6.9	Euhedral	Faint oscillatory zoning throughout.	N/a
29.1	1047.1	8.8	1052.9	7.2	Subhedral/broken	Faint oscillatory zoning on overgrowth. More prominent random zoning in core.	Core
29.3	973	22	985	18			Core

Table 23: Textural descriptions of concordant zircons from CL2. Ages are given as before in Table 21.

	Ages				Zircon Texture		
ID	**207Pb/235U**	**2σ**	**206Pb/238U**	**2σ**	**Grain Shape**	**Zoning Pattern**	**Core/Rim***
2.3_1	459.1	8.3	456.6	3.3	Subhedral/broken	Faint oscillatory zoning but no distinction between overgrowth and core.	N/a
4.2_1	869	11	873	6.8	Subhedral	Oscillatory zoning throughout. Prominent metamorphic overgrowth.	N/a
4.3_1	866	13	868.5	8.4			N/a
6.2_1	772	23	772	20	Subhedral/broken	Faint oscillatory zoning on magmatic overgrowth. More prominent random zoning in core.	Core
7.2_1	618	16	625	15	Euhedral	Faint oscillatory zoning on large magmatic overgrowth. Small randomly zoned core	OG
7.3_1	721	14	730.7	9.7			OG
7.4_1	858	22	854	14			OG
10.1_1	1319	21	1295	19	Subhedral	Faint oscillatory zoning on magmatic overgrowth. More prominent random zoning in core.	Core
10.2_1	446	10	444.4	3.8			Rim
11.1_1	477	15	466.4	4.5	Subhedral/broken	Oscillatory zoning throughout. Core/overgrowth distinction difficult to discern.	N/a
11.2_1	466	11	464.6	4.5			N/a
13.4	451.8	7.4	447.4	3.3	Subhedral/broken	Oscillatory zoning throughout. Core/rim distinction difficult to discern.	N/a
15.3_1	858	23	832	10	Anhedral	Random zoning throughout.	N/a
17.2_1	1299	14	1298	12	Anhedral	Random zoning throughout	N/a

Table 24: Textural descriptions of concordant zircons from Cluanie 3. Ages are given as before in Table 22.

4.1.1.3 Establishing a crystallisation age

The youngest cluster of ages were carried forward to establish a crystallization age for the pluton (see Table 25 and 26). The grains selected from each sample (CL1, CL2 and CL3) showed similar textural characteristics, supporting classification as cogenetic. They are presented in *Figure 57*. The grains were all classified as euhedral or subhedral (broken), and ablation was carried out on oscillatory zoned areas of the crystal.

	Ages				Zircon Texture		
ID	**207Pb/235U**	**2σ**	**206Pb/238U**	**2σ**	**Grain Shape**	**Zoning Pattern**	**Core/Rim***
1.1	446.7	7.3	439.6	2.5	Euhedral	Faint oscillatory zoning on magmatic overgrowth. More prominent in core.	OG
1.2	441.7	8.6	438.8	3.3			OG
1.3	440.9	6.9	438.1	3.1			OG
3.5	438	11	430.8	3.5	Subhedral (broken)	Faint oscillatory zoning on magmatic overgrowth. More prominent in core	OG
12.2	444.2	9.6	441.5	3.2	Subhedral (broken)	Faint oscillatory zoning on rim. More prominent in core.	OG
14.1	432	10	431.3	3.5	Euhedral	Faint oscillatory zoning throughout.	OG
14.3	445.9	8.4	441.9	3.2			OG
18.1	439	11	433.8	3	Euhedral	Oscillatory zoning throughout	N/a
18.3	432	10	430.9	3.7			
18.4	438	11	432.1	3.7			
Wtd mean of 206/238 age.			**436.4682**				
2σ error of mean.			**3.149615**				
MSWD			**7.534364**				

Table 25: Grains used to establish crystallization age for CL1, including textural description as in table 3. Wtd mean: weighted mean of the data based on analytical errors. 2σ: 95% confidence error of mean. MSWD: Mean square weighted deviation of data based on analytical errors. CL images of grains are displayed in Figure 57.

	Ages				Zircon Texture		
ID	**207Pb /235U**	**2σ**	**206Pb/238U**	**2σ**	**Grain Shape**	**Zoning Pattern**	**Core/Rim ***
15.1	447	12	448.8	4.3	Subhedral (Broken)	No zoning or distinction between core and rim.	N/a
16.7	445.4	6.9	443	3.1	Euhedral	Faint oscillatory zoning on rim. Prominent unzoned core.	OG
17.3	433.3	6.1	430.1	2.8	Subhedral (broken)	Faint oscillatory zoning but no distinction between core and rim.	N/a
10.2	446	10	444.4	3.8	Subhedral	Faint oscillatory zoning on rim. More prominent random zoning in core.	OG
13.4	451.8	7.4	447.4	3.3	Subhedral (broken)	Oscillatory zoning throughout. Core/rim distinction difficult to discern.	N/a
Wtd mean of 206/238 age.			**441.1406**				
2σ error of mean.			**10.04971**				
MSWD			**23.41397**				

Table 26: Grains used to establish crystallization age for CL 2&3, including textural description as in table 3. Wtd mean: weighted mean of the data based on analytical errors. 2σ: 95% confidence error of mean. MSWD: Mean square weighted deviation of data based on analytical errors. CL images of grains are displayed in Figure 57.

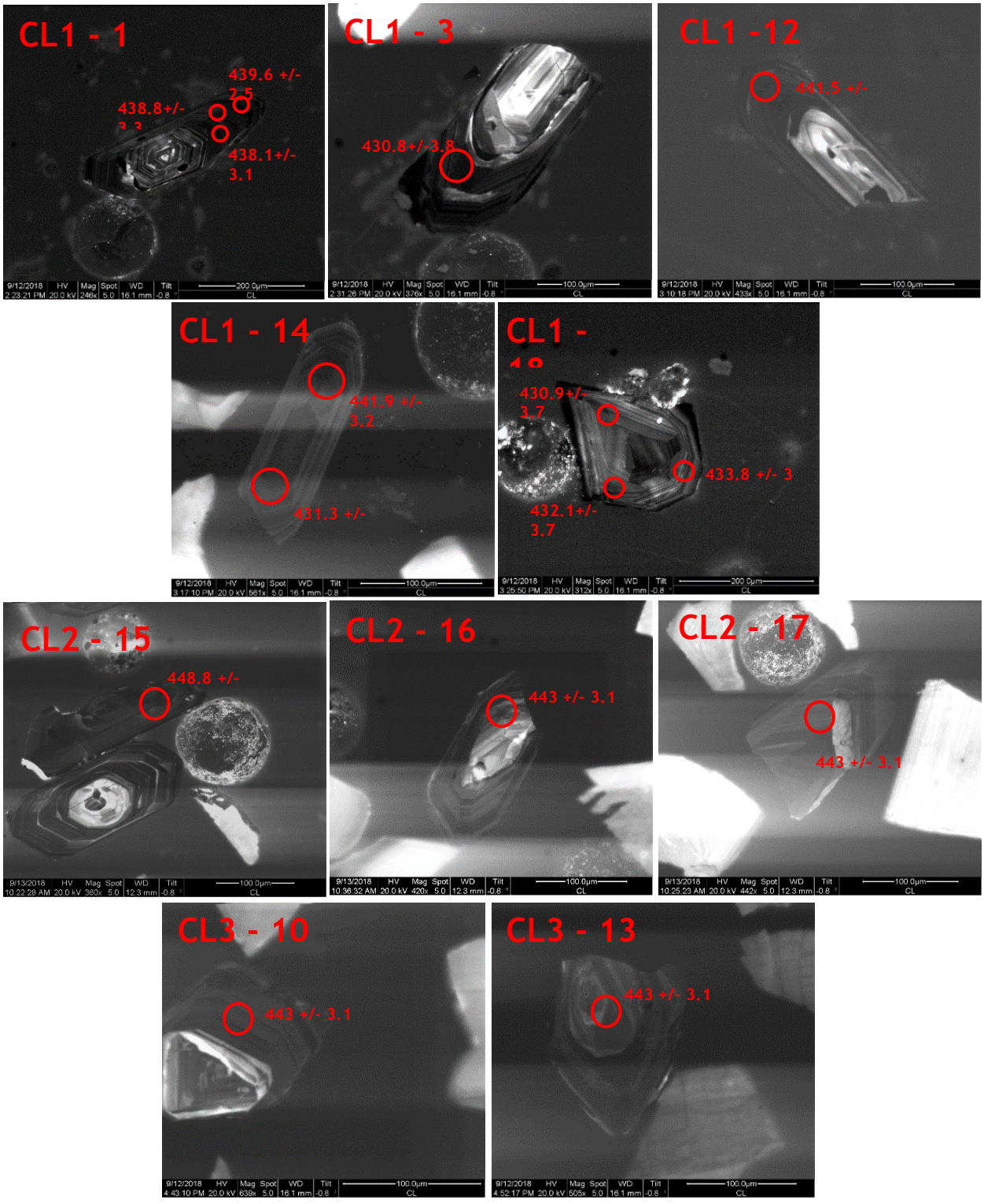

Figure 57: CL images of Cluanie zircon grains selected for establishing the crystallization age of the pluton. Grains from sample 1, 2 and 3 are presented with the sample ID in the top left corner (sample number – grain number). Ages are presented 206/238 (in Ma) with 2σ error. Red circles mark the position of the laser spot (scaled to size).

4.4.2 Glen Loy

GL1 and GL2 were run together. GL1 contains 18 grains, and GL2 contains 23 grains. Combined, 163 spot analysis were carried out, of which 24 were concordant. Concordant data is presented in Table 27.

GL3 contains 21 grains. 49 spot analysis were carried out, of which seven were concordant. Concordant data is presented in Table 28.

4.4.2.1 Concordia Plots

The associated Concordia plots for GL1+2 and GL3 are presented below (see Figures 58 – 62). Statistical interpretation of each group of grains was carried out on isoplot. The data from GL 1 + 2 shows two loose clusters of ages with some spread in between. These groups are marked in *Figure 58*, and labelled A and B (youngest to oldest). Group A (*Figure 59*) encompasses the majority of grains (N: 16), with ages that range between c. 430 and c. 460Ma. Data from GL3 is presented in Figures 63 – 65. Figure 63 shows one cluster of ages at c. 40Ma, with one grain at c. 460Ma and with one significantly older outlier (1692 Ma) (see Figure 65).

Table 27: Concordant data from U - Pb analysis of zircons from G1 and GL2. D* is the value given by [206Pb ‐ 238U age/207Pb ‐ 206Pb age)*100]. D is the value given by [(206Pb-238Uage/207Pb-235U age]*100].**

	Ratios					Ages				Concordance	
ID	207Pb/235U	2σ	206Pb/238U	2σ	rho	207Pb/235U	2σ	206Pb/238U	2σ	D1*	D2**
GL1											
1.6	4.159	0.058	0.290	0.002	0.465	1663	12	1638	11	97	98
3.1	0.563	0.025	0.071	0.001	0.084	449	16	442.6	5.5	102	99
4.3	0.559	0.026	0.071	0.001	0.014	446	17	439.4	5.7	101	99
5.3	0.576	0.019	0.073	0.001	0.243	458	12	455.5	4.7	100	99
6.1	2.985	0.091	0.241	0.005	0.850	1393	24	1391	26	100	100
6.5	0.544	0.018	0.069	0.001	0.066	437	12	430.2	3.9	98	98
9.2	4.287	0.066	0.292	0.003	0.503	1692	12	1650	12	95	98
12.3	0.549	0.016	0.070	0.001	0.121	442	11	438.3	4	101	99
15.1	0.597	0.039	0.074	0.001	0.228	466	25	456.8	6.5	102	98
15.4	4.266	0.078	0.299	0.003	0.509	1681	15	1687	17	101	100
17.2	0.573	0.018	0.073	0.001	0.074	458	12	456.5	4.2	104	100
18.4	0.571	0.024	0.073	0.001	0.061	453	15	453.3	6.1	101	100
18.6	1.692	0.031	0.170	0.002	0.247	1002	12	1009	8	102	101
GL2											
1.3	0.576	0.025	0.072	0.001	0.005	456	16	449.6	5.8	96	99
3.6	2.005	0.053	0.186	0.004	0.872	1109	19	1100	20	96	99
4.1	0.573	0.025	0.073	0.001	0.144	459	17	451.1	5.8	99	98
5.2	2.341	0.070	0.210	0.002	0.218	1218	23	1227	12	103	101
6.2	1.650	0.040	0.166	0.002	0.235	984	15	991.9	8.6	103	101
8.1	0.578	0.039	0.072	0.001	0.213	450	26	448.1	6.8	95	100
11.1	0.564	0.028	0.072	0.001	0.027	451	18	447.6	6.1	102	99
11.2	0.546	0.031	0.070	0.001	0.107	439	20	438.2	5.8	104	100
11.5	0.583	0.032	0.073	0.001	0.183	464	20	456.1	5.7	99	98
13.3	0.554	0.022	0.071	0.001	0.017	443	14	440	5	99	99
16.3	0.532	0.032	0.068	0.001	0.055	430	22	424.5	6.4	104	99

Table 28: Concordant data from U - Pb analysis of zircons from GL3. D* is the value given by [206Pb ‑ 238U age/207Pb ‑ 206Pb age)*100]. D is the value given by [(206Pb-238Uage/207Pb-235U age]*100].**

	Ratios					Ages				Concordance	
ID	207Pb/235U	2σ	206Pb/238U	2σ	rho	207Pb/235U	2σ	206Pb/238U	2σ	D1*	D2**
GL3											
4.2	4.324	0.082	0.293	0.004	0.365	1692	16	1657	18	95	98
8.2	0.541	0.016	0.068	0.001	0.222	437	11	426.1	4.5	95	98
11.2	0.532	0.027	0.069	0.001	0.210	430	17	427	6.6	104	99
15.1	0.551	0.027	0.069	0.001	0.003	440	17	432.5	5.9	101	98
17.1	0.544	0.020	0.069	0.001	0.111	437	13	427.8	4.9	98	98
20.2	0.578	0.021	0.074	0.001	0.089	462	14	460.8	7	101	100
21.3	0.530	0.024	0.068	0.001	0.029	428	16	424.2	5.9	100	99

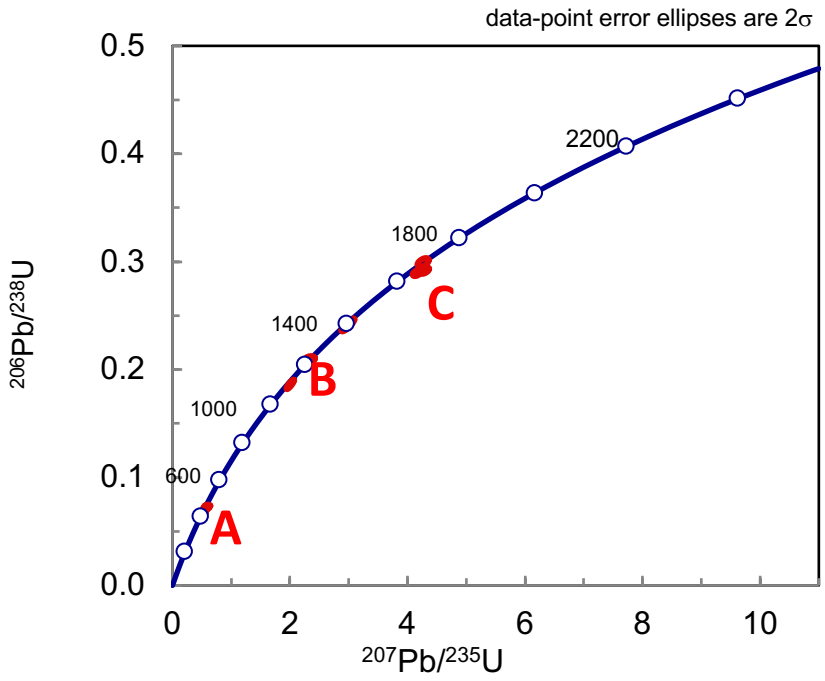

Figure 58: Concordia plot containing data GL 1 and 2. The plot shows the Concordia from 0 - 2500Myra (data presented in Table 27).

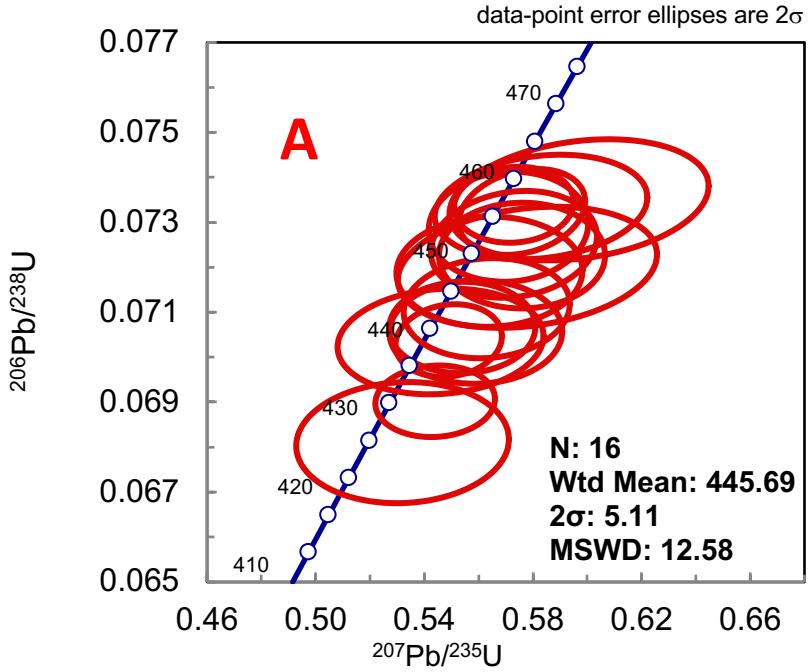

Figure 59: Concordia plot containing data GL 1 and 2 (data presented in Table 27). The plot shows the Concordia from 400 - 500Myra, group A is thus isolated. N: number of grains. Wtd mean: weighted mean of the data based on analytical errors. 2σ: 95% confidence error of mean. MSWD: Mean square weighted deviation of data based on analytical errors.

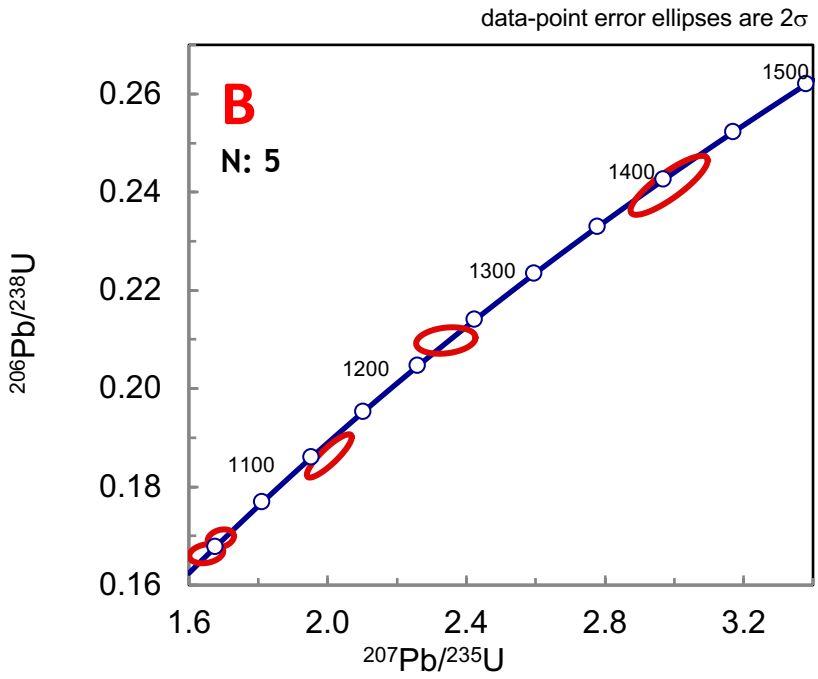

Figure 60: Concordia plot containing data GL 1 and 2 (data presented in Table 27). The plot shows the Concordia from 1000 - 1500Myra Since group B is diffuse, no weighted mean was calculated.

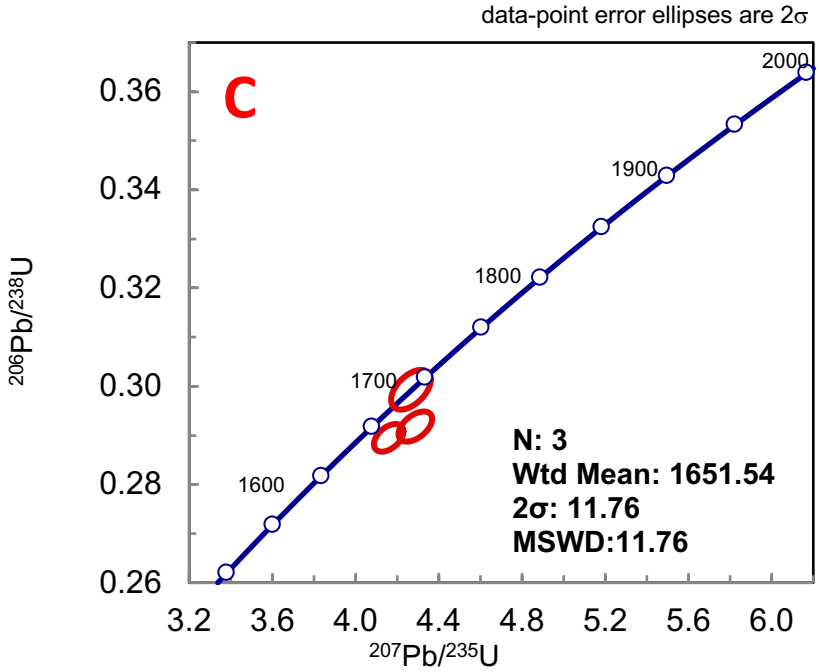

Figure 61: Concordia plot containing data GL 1 and 2 (data presented in Table 27). The plot shows the Concordia from 1500 – 2000 Myra. N: number of grains. Wtd mean: weighted mean of the data based on analytical errors. 2σ: 95% confidence error of mean. MSWD: Mean square weighted deviation of data based on analytical errors.

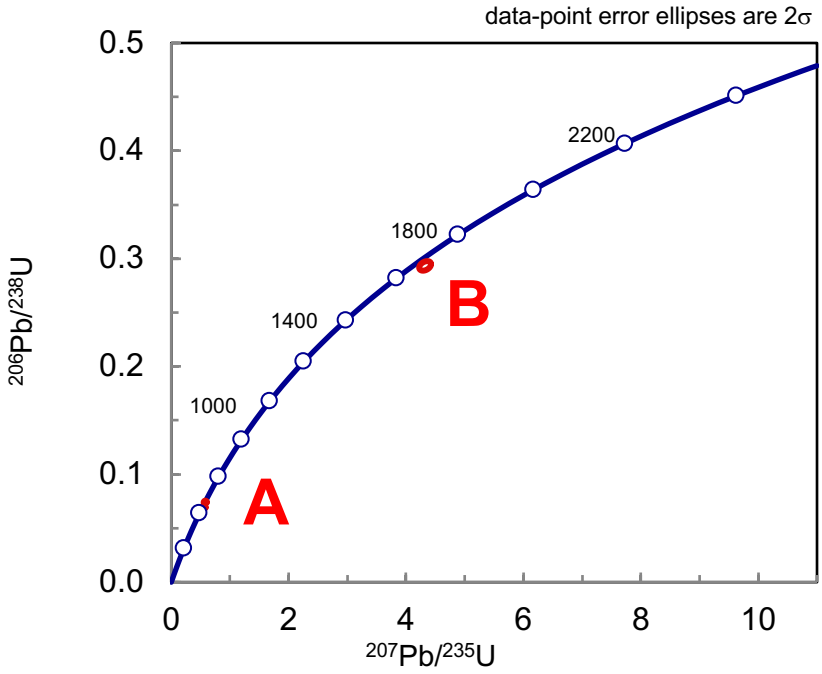

Figure 63: Concordia plot containing data GL 3. The plot shows the Concordia from 0 – 2400 Myra (data presented in Table 28).

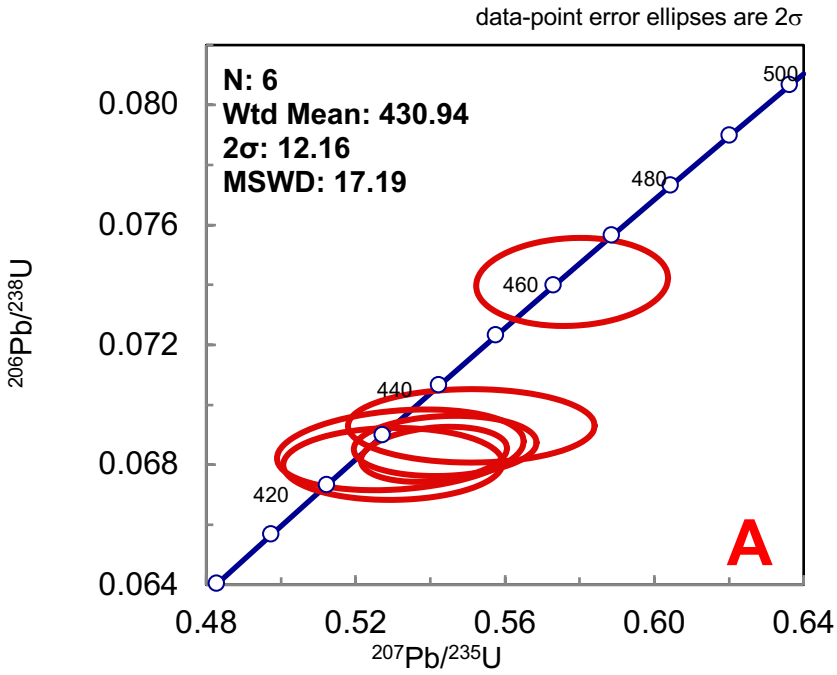

Figure 64: Concordia plot containing data GL 3 (data presented in Table 28). The plot shows the Concordia from 400 - 500Myra. N: number of grains. Wtd mean: weighted mean of the data based on analytical errors. 2σ: 95% confidence error of mean. MSWD: Mean square weighted deviation of data based on analytical errors.

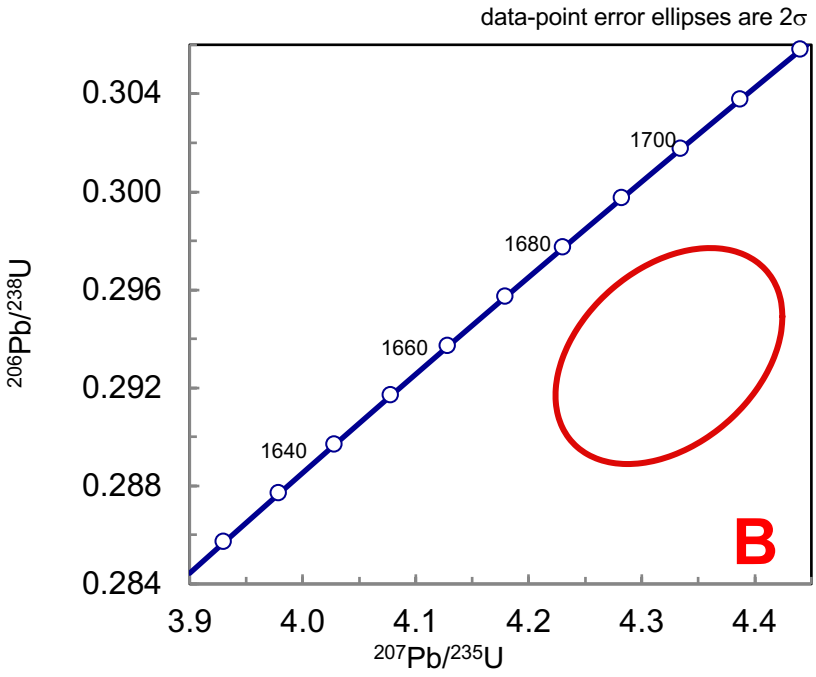

Figure 65: Concordia plot containing data from GL 3 (data presented in Table 28). The plot shows the Concordia from 1620 – 1720 Myr.

4.4.2.2 Textural Descriptions

Textural descriptions of the concordant zircon grains was carried out in order to characterise different populations in accordance with U - Pb ages. The textural descriptions are given in *Tables 29 - 31*.

The grains selected showed similar textural characteristics that supporting classification as cogenetic. They are different to the Cluanie grains in numerous ways, in general showing less ideal crystal morphology. The majority of the grains have bright luminescent rims and embayments. These were avoided when selecting targets, and in general most of the analysis were carried out on oscillatory zoned sectors of grains. Three of the grains analysed were very small (~50µ x 50µ). In general, these small grains returned the youngest ages.

Table 29: Textural descriptions of concordant zircons from GL 2. Ages are given as before in Table 20.

	Ages				Zircon Texture		
ID	**207Pb/235U**	**2σ**	**206Pb/238U**	**2σ**	**Grain Shape**	**Zoning Pattern**	**Core/Rim***
1.6	1663	12	1638	11	Subhedral/ broken	Oscillatory zoning throughout. Thin brighter zone surrounds the grain.	Core
3.1	449	16	442.6	5.5	Subhedral	Oscillatory zoning throughout. Thin brighter zone surrounds the grain.	Outermost part of core
4.3	446	17	439.4	5.7	Subhedral	Very faint zoning on innermost part of the grain. Thin brighter zone surrounds the grain.	Core
5.3	458	12	455.5	4.7	Euhedral	Very small grain. Zoning is difficult to discern.	n/a
6.1	1393	24	1391	26	Euhedral	Oscillatory zoning throughout. Thin bright zone surrounds the grain.	Core
6b.5	437	12	430.2	3.9	Euhedral	Very small grain. Zoning is difficult to discern.	n/a
9.2	1692	12	1650	12	Subhedral	Faint zoning in innermost part of grain. Thin brighter zone surrounds the grain.	Core
12.3	442	11	438.3	4	Subhedral/ broken	Faint zoning in innermost part of grain. Thin brighter zone surrounds the grain.	Core
15.1	466	25	456.8	6.5	Subhedral/ broken	Faint zoning in innermost part of grain. Thin brighter zone surrounds the grain.	Core
15b.4	1681	15	1687	17	Euhedral/ subhedral	Oscillatory zoning throughout.	Core
17.2	458	12	456.5	4.2	Subhedral/ broken	Oscillatory zoning throughout. Thin brighter zone surrounds the grain.	Core
18.4	453	15	453.3	6.1	Subhedral	Faint zoning throughout.	Core
18b.6	1002	12	1009	8	Subhedral	Oscillatory zoning throughout. Thin brighter zone surrounds the grain.	Core

Table 30: Textural descriptions of concordant zircons from GL 3. Ages are given as before in Table 20.

	Ages				Zircon Texture		
ID	**207Pb/235U**	**2σ**	**206Pb/238U**	**2σ**	**Grain Shape**	**Zoning Pattern**	**Core/Rim***
1.3	456	16	449.6	5.8	Subhedral/broken	Faint zoning throughout grain. Thin brighter zone surrounds the grain.	Core
3.6	1109	19	1100	20	Subhedral	Faint zoning throughout grain. Thin brighter zone surrounds the grain.	Core
4.1	459	17	451.1	5.8	Subhedral/broken	Zoning occurs in bands along the long length of the grain.	N/a
5.2	1218	23	1227	12	Euhedral/subhedral	Oscillatory zoning throughout. Thin brighter zone surrounds the grain.	Core
6.2	984	15	991.9	8.6	Euhedral/Subhedral	Oscillatory zoning throughout. Thin brighter zone surrounds the grain.	Core
8.1	450	26	448.1	6.8	Subhedral	Faint horizontal zones along the long axis of the grain.	Core
11.1	451	18	447.6	6.1	Euhedral/subhedral	No discernible zoning	Core
11.2	439	20	438.2	5.8			Core
11b.5	464	20	456.1	5.7	Euhedral/subhedral	Thin brighter zone surrounds the grain.	Core
13.3	443	14	440	5	Euhedral		Core
16.3	430	22	424.5	6.4	Euhedral	Very small grain. Zoning is difficult to discern.	N/a

Table 31: Textural descriptions of concordant zircons from GL 3. Ages are given as before in Table 21.

	Ages				Zircon Texture		
ID	**207/235**	**2σ**	**206/238**	**2σ**	**Grain Shape**	**Zoning Pattern**	**Core/Rim***
4.2	1692	16	1657	18	Subhedral	Oscillatory zoning throughout. No apparent magmatic overgrowths. Thin brighter rim surrounds the grain.	Core
8.2	437	11	426.1	4.5	Subhedral - anhedral	Prominent brighter rim surrounds grain. No oscillatory magmatic zoning present.	Core
11.2	430	17	427	6.6	Euhedral	Patchy oscillatory zoning in core of grain, prominent brighter zone surrounds grain.	Core
15.1	440	17	432.5	5.9	Subhedral – Anhedral	Prominent brighter rim surrounds grain. Oscillatory present in core.	Core
17.1	437	13	427.8	4.9	Subhedral (broken)	Oscillatory zoning throughout. Thin brighter rim surrounds the grain.	Core
20.2	462	14	460.8	7	Subhedral (broken)	Oscillatory zoning throughout. Thin brighter rim surrounds the grain.	Core
21.3	428	16	424.2	5.9	Subhedral (broken)	Patchy oscillatory zoning in core of grain, prominent brighter zone surrounds grain.	Core

4.4.2.3 Establishing a crystallisation age

The youngest prominent group of ages were carried forward to establish a crystallization age for the pluton. The crystallization ages are presented in *Table 32* and *Table 33*. The grains are presented in *Figure 66*.

Table 32: Grains used to establish crystallization age for GL 1 and 2, including textural description as in Table 26. Wtd mean: weighted mean of the data based on analytical errors. 2σ: 95% confidence error of mean. MSWD: Mean square weighted deviation of data based on analytical errors. CL images of grains are displayed in Figure 24.

	Ages				Zircon Texture		
ID	**207/235**	**2σ**	**206/238**	**2σ**	**Grain Shape**	**Zoning Pattern**	**Core/Rim***
3.1	449	16	442.6	5.5	Subhedral	Oscillatory zoning throughout. Thin brighter zone surrounds the grain.	Outermost part of core
3.1	449	16	442.6	5.5	Subhedral	Oscillatory zoning throughout. Thin brighter zone surrounds the grain.	Outermost part of core
4.3	446	17	439.4	5.7	Subhedral	Very faint zoning on innermost part of the grain. Thin brighter zone surrounds the grain.	Core
6b.5	437	12	430.2	3.9	Euhedral	Very small grain. Zoning is difficult to discern.	n/a
12.3	442	11	438.3	4	Subhedral/ broken	Faint zoning in innermost part of grain. Thin brighter zone surrounds the grain.	Core
11.2_1	439	20	438.2	5.8	Euhedral/ subhedral	No discernible zoning	Core
13.3_1	443	14	440	5	Subhedral	Very faint zoning on innermost part of the grain. Thin brighter zone surrounds the grain.	Core
Wtd mean of 206/238 age.	436.4682						
2σ error of mean.	3.149615						
MSWD	7.534364						

Table 33 Grains used to establish crystallization age for GL3, including textural description as in Table 27. Wtd mean: weighted mean of the data based on analytical errors. 2σ: 95% confidence error of mean. MSWD: Mean square weighted deviation of data based on analytical errors. CL images of grains are displayed in Figure 24.

	Ages				Zircon Texture		
ID	**207/235**	**2σ**	**206/238**	**2σ**	**Grain Shape**	**Zoning Pattern**	**Core/Rim***
8.2	437	11	426.1	4.5	Subhedral - anhedral	Prominent brighter rim surrounds grain. No oscillatory magmatic zoning present.	Core
11.2	430	17	427	6.6	Euhedral	Patchy oscillatory zoning in core of grain, prominent brighter zone surrounds grain.	Core
15.1	440	17	432.5	5.9	Subhedral – Anhedral	Prominent brighter rim surrounds grain. Oscillatory present in core.	Core
17.1	437	13	427.8	4.9	Subhedral (broken)	Oscillatory zoning throughout. Thin brighter rim surrounds the grain.	Core
21.3	428	16	424.2	5.9	Subhedral (broken)	Patchy oscillatory zoning in core of grain, prominent brighter zone surrounds grain.	Core
11.2	430	17	427	6.6	Euhedral	Patchy oscillatory zoning in core of grain, prominent brighter zone surrounds grain.	Core
Wtd mean of 206/238 age.			427.3875				
2σ error of mean.			2.415123				
MSWD			1.135135				

Figure 66: CL images of Glen Loy zircon grains selected for establishing the crystallization age of the pluton. Ages are presented 206/238 (in Ma) with 2σ error. Red circles mark the position of the laser spot (scaled to size).

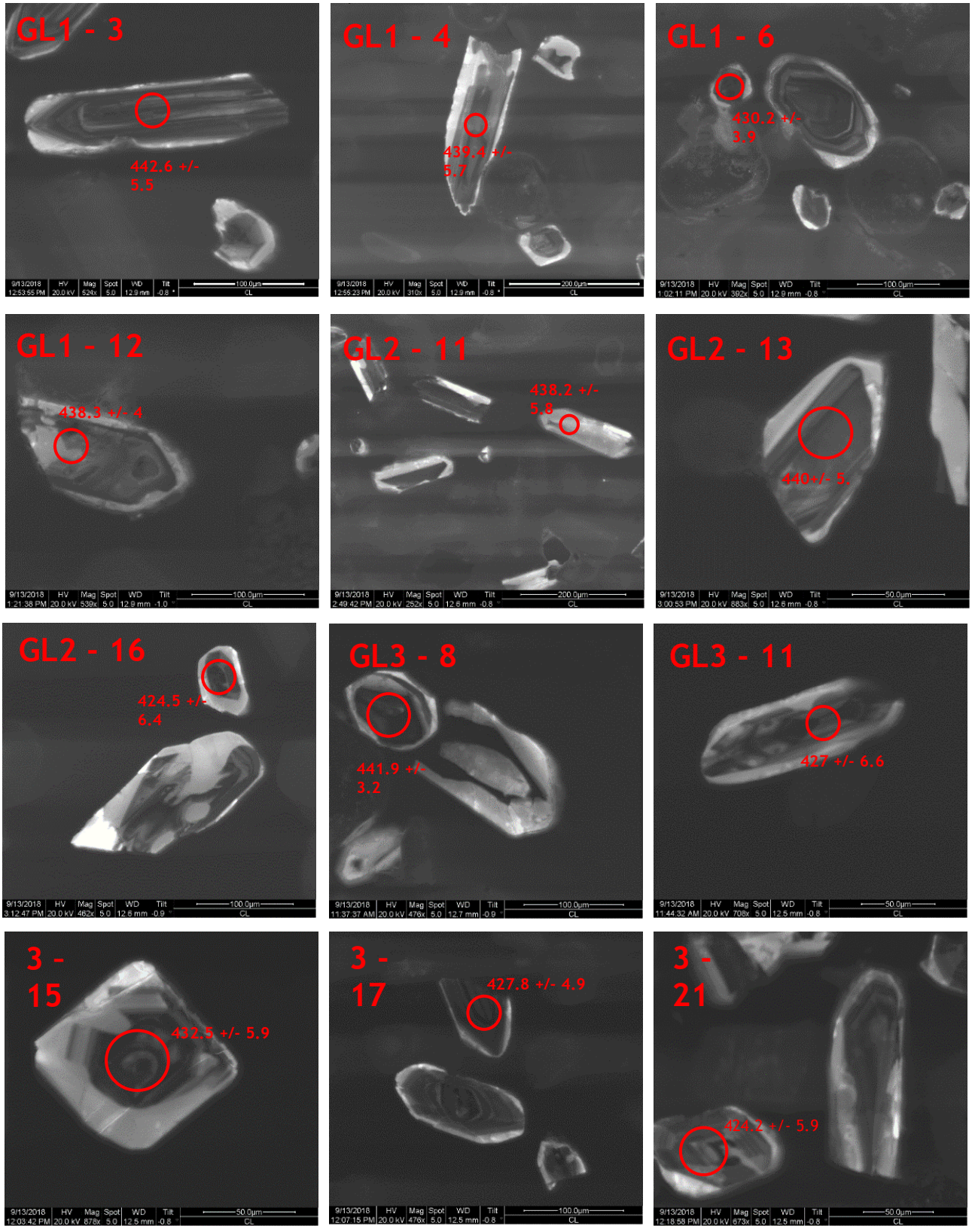

4.4.3 Loch Linnhe

One sample from Loch Linnhe was analysed. The sample contained 27 grains. 48 analysis were carried out, 17 of which were concordant. The concordant data is displayed in *Table 34*.

Table 34: Concordant data from U - Pb analysis of zircons from Loch Linnhe. D* is the value given by [206Pb ‑ 238U age/207Pb ‑ 206Pb age)*100]. D is the value given by [(206Pb-238Uage/207Pb-235U age]*100].**

	Ratios					Ages				Concordance	
ID	207Pb/235U	2σ	206Pb/238U	2σ	rho	207Pb/235U	2σ	206Pb/238U	2σ	D1*	D2**
1.1	3.310	0.120	0.250	0.007	0.77	1465	30	1432	36	96	98
2.2	0.534	0.020	0.068	0.001	0.07	430	13	422.4	4.1	99	98
3.2	4.018	0.095	0.282	0.003	0.13	1632	19	1601	17	97	98
4.2	4.039	0.097	0.287	0.004	0.46	1633	19	1627	18	101	100
8.1	2.919	0.066	0.240	0.002	0.22	1384	19	1384	13	102	100
9.1	0.587	0.019	0.074	0.001	0.33	467	12	459.5	6	96	98
9.2	0.547	0.012	0.071	0.001	0.25	442.3	7.7	441.3	4.9	102	100
10.2	3.188	0.068	0.247	0.004	0.20	1452	16	1421	20	95	98
12.1	0.550	0.019	0.070	0.001	0.03	442	12	437.8	5	96	99
15.1	3.110	0.120	0.242	0.004	0.36	1424	30	1396	19	97	98
16.2	12.900	0.160	0.505	0.004	0.38	2671	12	2635	18	98	99
18.1	0.570	0.015	0.072	0.001	0.42	455.9	9.7	450.5	5	95	99
20.1	0.580	0.011	0.074	0.000	0.07	463.4	7.2	462.4	2.9	100	100
20.2	0.974	0.072	0.109	0.005	0.85	668	35	663	30	99	99
24.1	0.538	0.011	0.070	0.001	0.30	435.9	7.5	438.5	7.2	98	101
24.1	0.714	0.037	0.090	0.003	0.52	545	19	553	19	105	101
26.1	12.560	0.170	0.510	0.006	0.42	2647	12	2657	26	100	100

4.4.3.1 Concordia Plots

The associated Concordia plots for LL1 are presented below (see Figures 67 - 71). Statistical interpretation of each group of grains was carried out on Isoplot

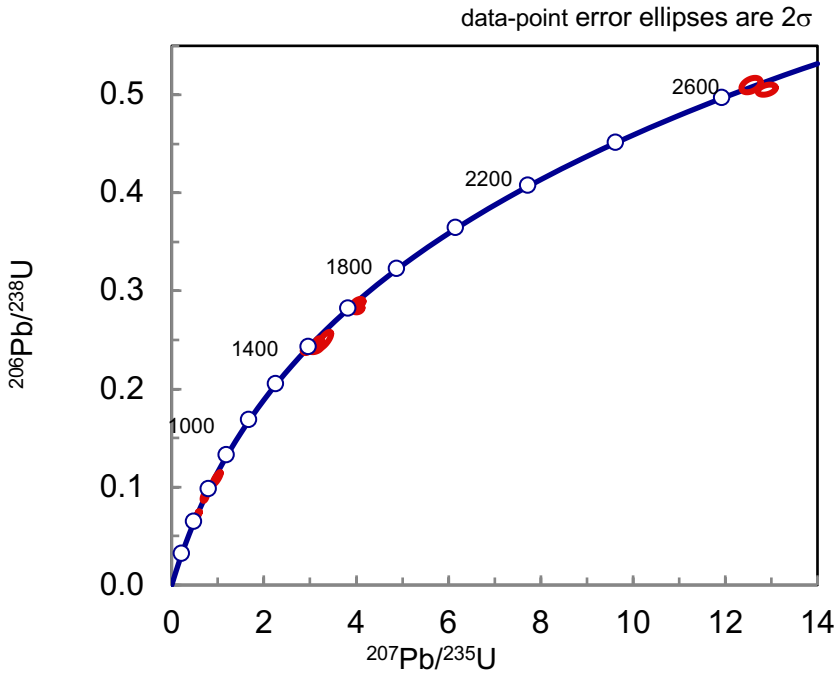

Figure 67: Concordia plot for LL1 containing data from Table 34. The plot shows the Concordia from 0 – 2700Myra.

3.7.

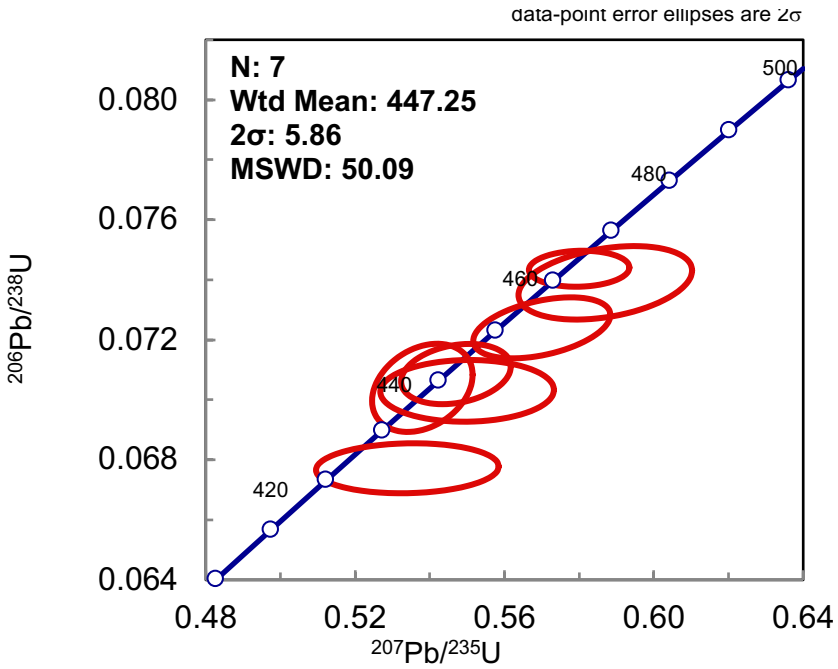

Figure 68: Concordia plot for LL1 containing data from Table 34. The plot shows the Concordia from 400Myra – 500Myra.

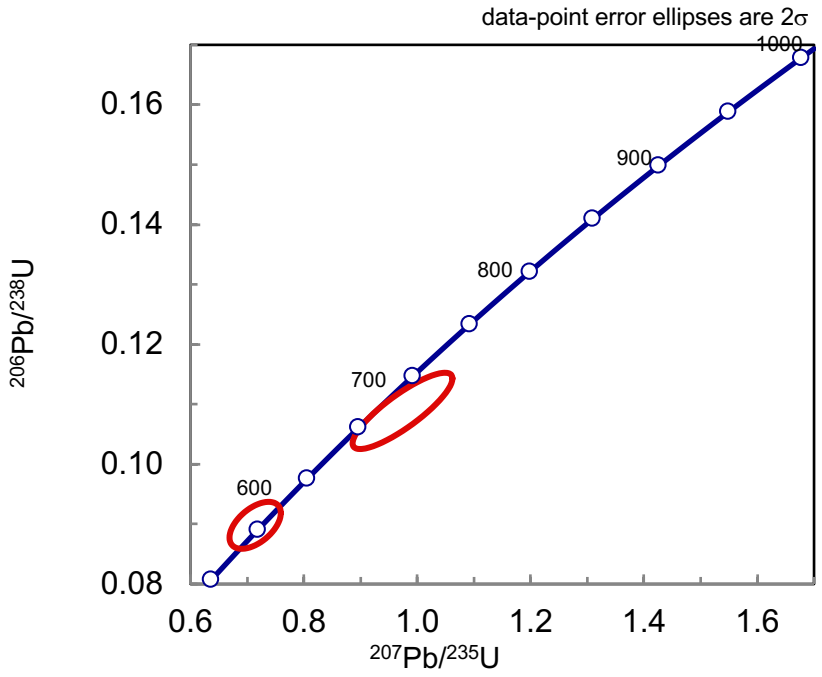

Figure 69: Concordia plot for LL1 containing data from Table 34. The plot shows the Concordia from 500Myra – 1000Myra.

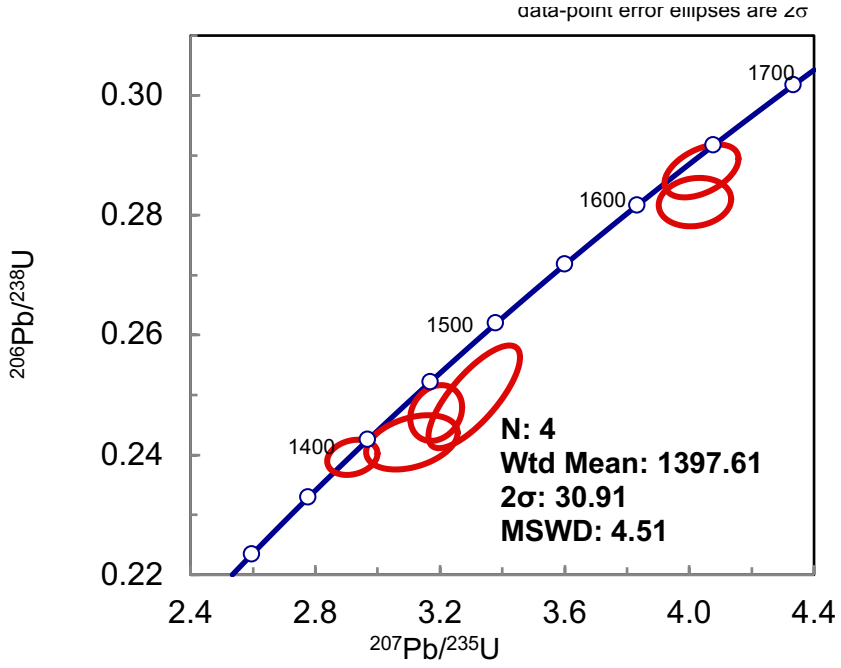

Figure 70: Concordia plot for LL1 containing data from Table 34. The plot shows the Concordia from 1300 – 1700Myra.

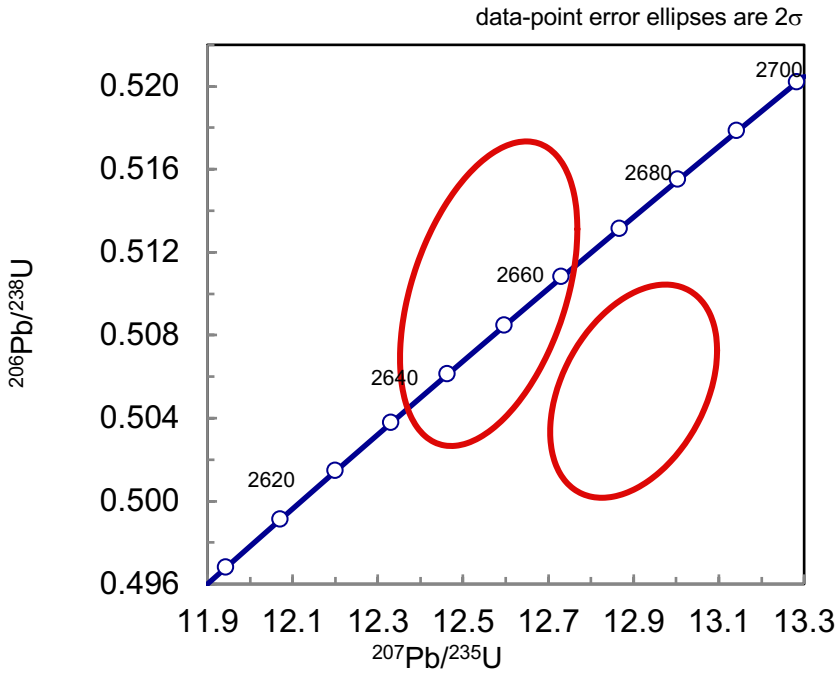

Figure 71: Concordia plot for LL1 containing data from Table 34. The plot shows the Concordia from 2600 – 2700Ma.

4.4.3.2 Textural Descriptions

Textural descriptions of zircons was carried out in order to characterise different populations in accordance with ages U - Pb ages (see Table 35).

Table 35: Textural descriptions of concordant zircons from Cluanie sample 1. Ages are given as before in Table 30.

	Ages				Zircon Texture		
ID	**207/235**	**2σ**	**206/238**	**2σ**	**Grain Shape**	**Zoning Pattern**	**Core/Rim***
1.1	1465	30	1432	36	Subhedral	Oscillatory zoning on rim. Brighter, more prominent core.	Core
2.2	430	13	422.4	4.1	Euhedral	Oscillatory zoning throughout.	N/a
3.2	1632	19	1601	17	Subhedral/broken	Random zoning throughout	N/a
4.2	1633	19	1627	18	Euhedral	Oscillatory zoning on rim. Brighter, more prominent core.	Core
8.1	1384	19	1384	13	Euhedral	Oscillatory zoning on rim. Brighter, more prominent core.	Core
9.1	467	12	459.5	6	Euhedral	Oscillatory zoning throughout.	N/a
9.2	442.3	7.7	441.3	4.9			N/a
10.2	1452	16	1421	20	Euhedral	Large prominent core. Faint oscillatory zoning on rim	Core
12.1	442	12	437.8	5	Euhedral	Oscillatory zoning throughout,	N/a
15.1	1424	30	1396	19	Euhedral	Oscillatory zoning on rim. Random zoning in core	Core
16.2	2671	12	2635	18	Euhedral	Oscillatory zoning on rim. Brighter, more prominent core.	
18.1	455.9	9.7	450.5	5	Subhedral/broken	Oscillatory zoning throughout.	N/a
20.1	463.4	7.2	462.4	2.9	Euhedral	Oscillatory zoning on rim. Brighter, more prominent core.	
20.2	668	35	663	30			
24.1	435.9	7.5	438.5	7.2	Subhedral/broken	Oscillatory zoning throughout.	Rim
24.1_1	545	19	553	19			Core
26.1	2647	12	2657	26	Euhedral		

4.4.3.3 Establishing a crystallisation age

The youngest group of ages was carried forward to establish a crystallization age for the pluton (see Table 36). The grains selected show similar textural characteristics that supported classification as cogenetic. The grains were all classified as euhedral or subhedral (broken), and ablation was carried out on oscillatory zoned sectors of the crystals. The grains are presented in Figure 72.

Table 36: Grains used to establish crystallization age for GL3, including textural description as in Table 10. Wtd mean: weighted mean of the data based on analytical errors. 2σ: 95% confidence error of mean. MSWD: Mean square weighted deviation of data based on analytical errors. CL images of grains are displayed in Figure 72.

	Ages				Zircon Texture		
ID	**207Pb/235U**	**2σ**	**206Pb/238U**	**2σ**	**Grain Shape**	**Zoning Pattern**	**Core/Rim***
9.2	442.3	7.7	441.3	4.9	Euhedral	Oscillatory zoning throughout.	N/a
12.1	442	12	437.8	5	Euhedral	Oscillatory zoning throughout.	N/a
24.1	435.9	7.5	438.5	7.2	Subhedral (broken)	Oscillatory zoning throughout.	Rim
Wtd mean of 206/238 age.					439.44		
2σ error of mean.					3.15		
MSWD					0.54		

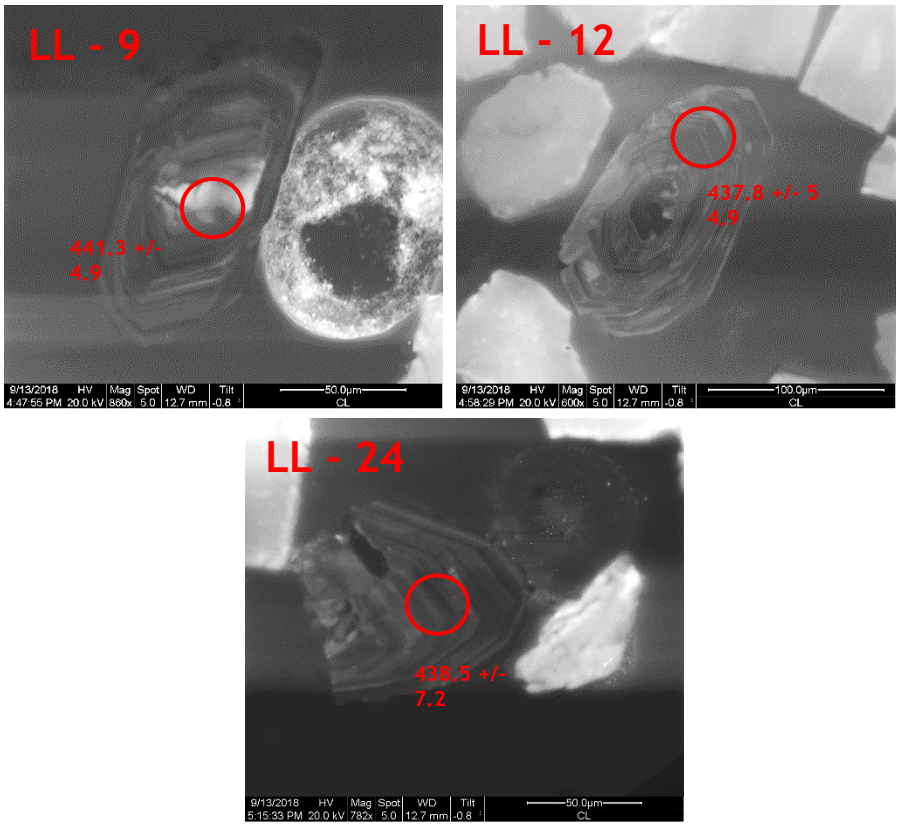

Figure 72: CL images of Loch Linnhe zircon grains selected for establishing the crystallization age of the pluton. Ages are presented 206/238 (in Ma) with 2σ error. Red circles mark the position of the laser spot (scaled to size).

5 Discussion

The implications of the new geochronological and geochemical data are discussed, where appropriate considering petrologic and field observations and mineral chemistry data. Critical reflection on some presently accepted ideas in Scottish Caledonian discourse is undertaken, in light of both the new data gathered and the identification of some inconsistencies in the existing literature. Some potential alternative hypotheses are then explored. A summary of data gathered in this work is presented in Table 37 alongside previously published in the literature (building on Table the information in Table 3).

The U – Pb isotope data from Cluanie, Loy and Linnhe is discussed first. Potential provenance of the older inherited zircon grains is explored and interpretation of the spread of ages upwards of final crystallization is attempted. The wider geological significance of the data is then explored, followed by a discussion of how to reconcile the newly acquired isochrons with the currently accepted timeline of geologic events for the final stages of Baltica Laurentia collision.

The major and trace elemental data from Loy, Scaddle, Cluanie and Clunes is then discussed. First order interpretations based on each plutons individual geochemical characteristics are presented, followed by a comparison to other Scandian age intrusive suites in the NHT. Fractional crystallization models are presented for each pluton. A discussion of the source of melting is then undertaken, followed by an exploration of what the implications of the geochemical data means for the timeline of Baltica Laurentia collision. Finally, implications of the characterisation of Clunes and Cluanie as adakitic allows for comments to be made on the petrogenetic controls on the development of the adakitic signature.

	Geochronology	Geochemistry	Key Structural Observations
Glen Scaddle	U-Pb zircon: 426 +/- 3 Ma (Strachan and Evans, 2008) A 'Structural' age for Scaddle is suggested to be between D2 and D3 stages of regional Loch Eil (Moine) deformation. (Strachan and Evans, 2008)	***Major and trace element profiles acquired. Key features include:*** **- 54 – 69 wt. % SiO_2** **- LREE's and HREE's both relatively enriched, LREE's more so than HREE's.** **- Trace elements: High Ba - Sr, low Nb – Ta and Zr -Hf.** **- Low Sr/Y and La/Yb ratios.**	The pluton occupies major D3 fold (Glen Scaddle synform). Emplaced prior to D2 stage and deformed by D3 stage of regional deformation. Margins of the pluton are broadly parallel to the regional composites for D2 (Strachan and Evans, 2008). **Evidence of significant deformation of body while cooling. Suggests emplacement occurs concurrent or just prior to D3 deformation of the Loch Eil group (this work).**
Clunes	U-Pb zircon: 428 +/- 2Ma Stewart et al. (2001)	***Major and trace element profiles acquired. Key features include:*** **- 59 – 64 wt. % SiO_2** **- LREE's and HREE's both relatively enriched, LREE's more so than HREE's.** **- Trace elements: Depleted Zr - Hf and Nb – Ta, all other trace elements are enriched (high Ba – Sr).** **- High Sr/Y and La/Yb ratios (samples plot as adakitic)**	No reported evidence for regional scale deformation structures associated with D2 or D3 events. Fabrics are magmatic, reflecting processes that occurred during cooling (Stewart et al. 2001).
Cluanie	U-Pb zircon: 417 Ma (Pidgeon and Aftalion, 1978) Rb – Sr: 425 +/- 4 Ma (Powell 1983). **U-Pb zircon: 437 +/- 3 (This work)**	***Major and trace element profiles acquired (considered alongside previously published data). Key features include:*** **- 61 – 72 wt. % SiO_2** **- Trace elements: High Ba – Sr, low Nb – Ta.** **- LREE's and HREE's both relatively enriched, LREE's more so than HREE's.** **- Mixed Sr/Y ratios and La/Yb ratios (some samples plot as adakitic).**	No reported evidence for regional scale deformation structures associated with D2 or D3 events.
Glen Loy	**U-Pb zircon: 433 +/- 3 (This work)**	***Major and trace element profiles acquired. Key features include:*** **- 44 – 56 wt.% SiO_2 (non-cumulate samples)** **- Trace elements plots show differing degrees of enrichment in almost all elements, including Ba -Sr and Nb – Ta.** **- LREE's and HREE's both relatively enriched, LREE's more so than HREE's.** **- Low Sr/Y and La/Yb ratios.**	**No reported evidence for regional scale deformation structures associated with D2 or D3 events, but there is a suggestion that the body has been folded (Johnstone and Mykura, 1989).** **Several small shear zones were mapped throughout the body. No evidence for significant deformation of the melt as it cooled (as in Scaddle) suggesting body had cooled by the time D3 deformation of the Loch Eil Group occurred. Magmatic fabric occasionally well developed and independent of regional tectonic regimes. (This work)**
Loch Linnhe	**U-Pb zircon: 439 +/- 3 (This work)**	***Only one sample was analysed.*** **- 73 wt% SiO_2** **- LREE's significantly more enriched than HREE's.** **- Trace elements: High Ba – Sr, low Nb – Ta.** **- Low La/Y and Sr/Y ratios**	N/A

Table 37: Summary of the results from this body of work presented alongside that in the published literature (building on Table 3). Results from this work are in bold.

5.1 Interpretation of the new geochronology data

The final crystallization/emplacement for Cluanie, Glen Scaddle and Loch Linnhe, as established by U-Pb zircon dating, are detailed in Table 37. The analysis of the standard materials (Plesovice and Nist10 show good precision and accuracy, allowing confidence that the results can be reflective of the crystallization and/or metamorphic overgrowth ages of the grains and emplacement ages of the plutons (See Appendix D). The textural study carried out to eliminate data points acquired from metamict grains or inherited rims was also deemed successful.

5.1.2 Provenance of inherited grains

Grains with ages that significantly pre-date final crystallization/emplacement are assumed to be inherited. The concept of zircon inheritance is widely accepted (Bea et al. 2007; Paterson et al. 1992; Pidgeon and Aftalion, 1978; and references therein). Inherited grains are incorporated into the magma during partial melting or crustal transport/storage. Inherited zircons survive when the temperature, water content or Zr content of the melt is not high enough to dissolve an entire xenocryst/grain (Bea et al. 2007). Xenocrysts are grains which are entirely foreign to the magmatic system (e.g. grains incorporated wall rock of a magma chamber), while antecrysts crystalized from a progenator magma (a parent magma, or a less evolved version of the current magma) (Jackson et al., 2018). Both xenocrysts and antecrysts often host new zircon growth, derived from the surrounding magma (Paterson et al. 1992). There is an abundance of grains with older cores and younger magmatic overgrowths and the samples for Cluanie, Loy and Linnhe (i.e. grains that can be characterised as xeno/ante crysts). The array of data from each pluton are presented in *Figures 73 – 75*.

5.1.2.1 Cluanie

The spread of only concordant data from each analysis from Cluanie are presented. *Figure 73* shows a clear majority of grains with ages within range of the final crystallization age established (437 +/- 3.4 Ma). There are several individual grains that lie between this crystallization age and c. 600 Ma. The majority of these grains lie within 30Ma upwards of the final crystallization age established (11 grains lie between 447 and 477Ma. There is clear spike at c. 1450Ma, and another a significant cluster at c. 1600 – c. 1700 Ma. There are several individual grains with ages that lie in the range of c. 700 – c. 1200 Ma.

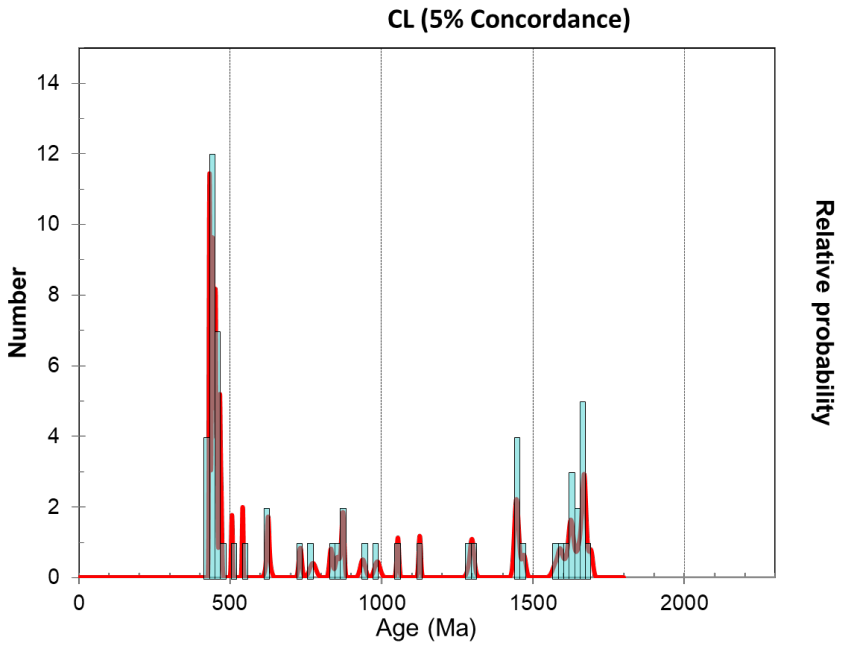

Figure 73: Probability density plot for 5% concordant data from Cluanie (samples 1 - 3 combined). Produced using Isoplot 3.7 (http://www.bgc.org/isoplot_etc/isoplot.html).

5.1.2.2 Glen Loy

The spread of concordant data from each analysis from Glen Loy are presented. Figure 74 shows a majority of grains with ages within close range of the final crystallization age established (434 +/- 3.3 Ma). There is a significant cluster at c. 1600 – c. 1700 Ma, and several individual grains between c. 700 and c. 1400 Ma.

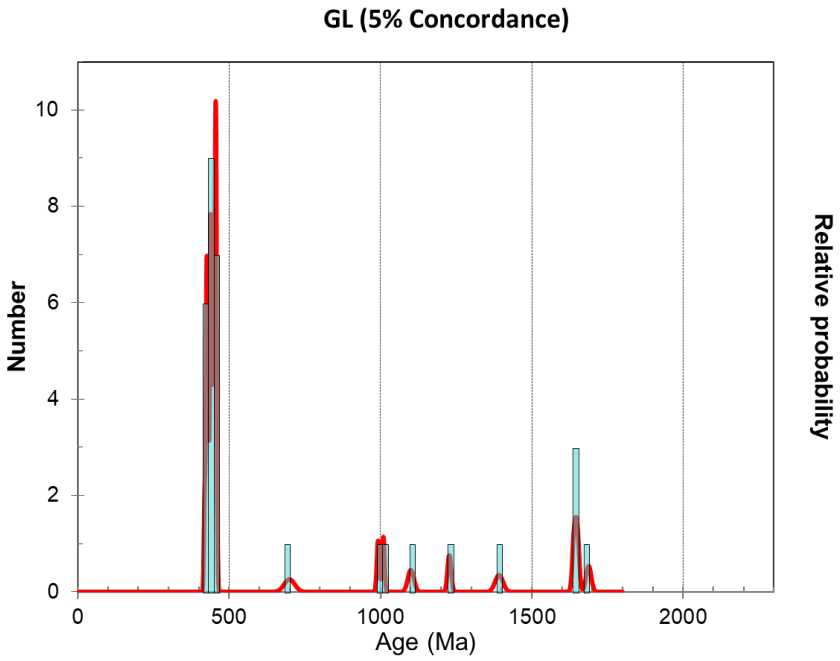

Figure 74: Probability density plot for 5% concordant data from Glen Loy (samples 1 – 3 combined). Produced using Isoplot 3.7 (http://www.bgc.org/isoplot_etc/isoplot.html).

5.1.2.3 Loch Linnhe

In the concordant dataset for Loch Linnhe, the majority of grains lie close to the final crystallization age of the body (439.4 +/- 3.1 Ma) (see Figure 75). There are two grains between this crystallization age and 700 Ma. There are clusters of grains at c. 1600 Ma and c. 1400 Ma, and two grains of Archean age (c. 2600 Ma).

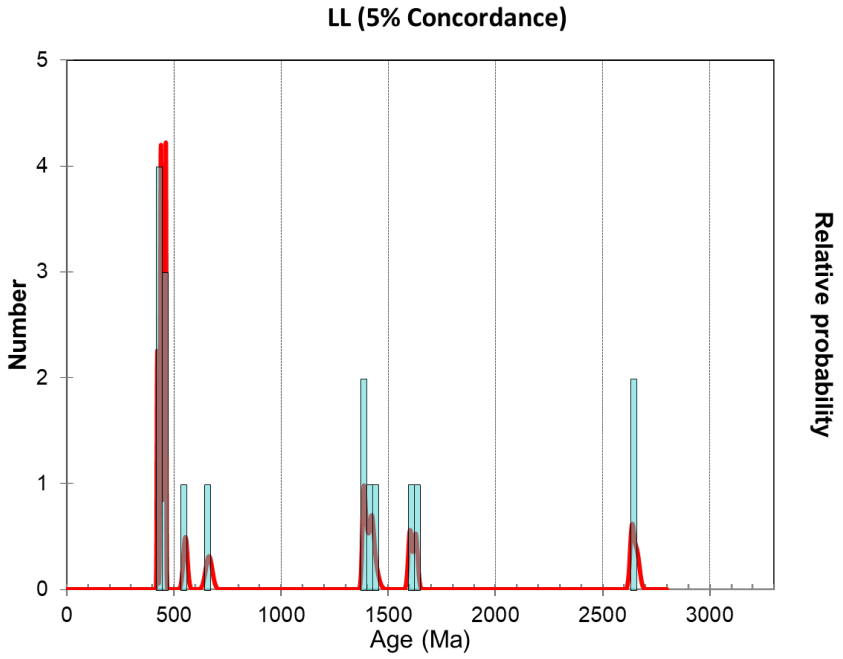

Figure 75: Probability density plot for 5% concordant data from Loch Linnhe (samples 1 – 3 combined). Produced using Isoplot 3.7 (http://www.bgc.org/isoplot_etc/isoplot.html).

5.1.2.4 Interpreting the spread of U-Pb data

The spread of data presented and described above is largely consistent with the bodies being emplaced within the Loch Eil division of the Moine Supergroup. Zircon grains from the Loch Eil group of the Moine are reported to range in age from c. 947 – 1889 Ma (Friend et al. 2003 and; references therein). The inherited grains whose ages lie within this range can be assumed to be sourced from the Loch Eil division of the Moine during emplacement, but prior to final crystallization of the bodies (Bea et al., 2007; Paterson et al., 1992; Bird et al., 2019).

The provenance of grains within this age range can be further linked to a series of orogenic events experienced on the margin of Laurentia, where the Moine sediments were deposited (Friend et al., 2003). Grains of c. 1800 – 1600 Ma are thought to have been derived from the Labradorean - Gothian provinces exposed within Laurentia (Friend et al., 2003). Grains of c. 1100 Ma are thought to be associated with Grenvillian orogeny (Bird et al., 2018; Cawood et al., 2007; Kirkland et al., 2008).

The provenance of the c. 700 – c. 900Ma grains can be linked to tectono-thermal episodes recorded by the Moine. The Knoydartian orogeny (~830 – 730 Ma) is associated with the emplacement of igneous bodies and pegmatites around Knoydart and Morar, and extensional tectonics are thought to be associated with formation of the West Highland Granite Gneiss at 870 Ma (Millar, 1990; Tanner and Evans, 2013; Fowler et al., 2013). Prominent members of this latter group include outcrops at Fort Augustus and Glen Doe, the latter just east of Cluanie (Millar, 1999).

Grains of c. 600 – 540 Ma age could be associated with a spate of magmatic activity within the Moine and Dalradian metasedimentary sequences (e.g. the Ben Vuirich granite of Perthshire (Tanner et al., 2006) and Carn Chuinneag granites of Easter Ross), emplaced associated with accelerated rift thinning of the lithosphere occurring at this time (Dewey et al., 2015).

There are two grains of Archean age found in the sample from Loch Linnhe. The grains are 2635+/- 18 Ma and 2657+/- 26 Ma. Grains of this age are rare within the Moine, comprising only 8 % of the dataset examined by Friend et al. (2003). These

ages can be assumed to be associated with the basement to the Moine Supergroup; basement inliers are common throughout the Moine, although not all are dated (Friend et al., 2008; Mendum et al., 2010). The basement is exposed at one location along the GGFZ, at Rosemarkie and Cromarty, which explains the presence of the inherited Archean zircons found in the Linnhe granite (Mendum et al. 2010).

5.1.3 Protracted age range seen in zircon ages

The U – Pb isotope datasets for Cluanie, Glen Loy and Loch Linnhe show broadly similar characteristics. The main peak, identified as representing crystallization age, is c. 433 – 441 Ma for each of the plutons. Each dataset also shows a spread of data upwards in age from the main peak of interpreted as representing final crystallization. This spread of concordant and seemingly magmatic zircons upwards of final crystallization is a difficult to reconcile with the model of coeval crystallization of grains in magma chambers post-emplacement.

One possible scenario to explain the spread of ages is to invoke crystallisation in the 'deep crystal hot zone' (DCHZ) (e.g. Annen et al. 2006; Wang et al. 2017 and references therein). The concept of the DCHZ is used to explain the occurrence of mantle derived intermediate and silicic melts in collisional and post-collisional tectonic settings. The DCHZ develops when mafic magmas are injected in the lower crust, acting as a heat and fluid source to help drive crustal melting (Annen et al. 2006). The mafic sills are mantle melts, melting initiated by subduction or mantle advection associated with break-off (Annen et al., 2005). The sills are successively emplaced at the mantle-crust interface which behaves as a rheological trap. When enough heat has been advected by the mafic magma, melts are sustained or generated by a) incomplete crystallisation of the mafic magma, b) partial melting of existing crust and c) re-melting of formerly emplaced mafic intrusions (Annen et al. 2006; Wang et al. 2017).

Assimilation and fractional crystallization processes (AFC) and melting, assimilation, storage and homogenization (MASH) occur in what has been termed the DCHZ (Annen et al, 2006). Thus, zircon crystallization can occur over an extended period, relating to the duration of magmatism and elevated thermal input to the crust. This leads to a spread in zircon ages – the older grains classified as antecrysts since the magma has evolved away from melt from which they crytsalised (Jackson et al., 2018). During this period, partial assimilation of the crust/wall rock occurs, leading to inheritance of xenolithic zircon grains in addition to a range of antecryst. Indeed, Oliver et al. (2008) invoke interaction of Scandian age melts with the DCHZ, using residence in the lower crust to explain the geochemical characteristics of the Newer granites.

Such a phenomenon is reported by Miles et al. (2018) with regards to the Devonian granites of Northern England, emplaced during the Acadian orogeny. They report a spectrum of U-Pb zircon ages for the Shap granite (from c. 428 – 403 Ma) citing a long magmatic history with an extended residence in the mid crustal mush zone as the source of the protracted age range (Miles et al., 2018). They propose that the early zircon ages date crystallization in a mid - crustal mush reservoir (now preserved at 10k depth as a component of the North Pennine and Lake District batholith). Steep strike skip faults intersecting the reservoir are then thought to have piped the near solidus crystal rich mush into the middle/upper crust where it continued to cool (Miles et al., 2018). Miles et al. (2018) infer similar emplacement methods for Caledonian plutons in Donegal (Hutton, 1982) and the Grampian terrane (Jacques & Reavy, 1992).

The range of ages seen in the Cluanie, Loy and Linnhe datasets exceeds that reported by Miles et al. of 15 Ma. For Cluanie, a total of 11 grains are in the 40 Ma age range from the final crystallization age of 437 – 477 Ma. The existence of a batholith/mush zone of the extent discussed by Miles et al. (2018) to have lasted c. 40 Ma seems untenable -the lifespan of a deep crustal hot zone is limited by how long it can remain above solidus (Jackson et al., 2018).

This is modelled by Jackson et al., 2018 who, while investigating the processes of cold storage (of melts) and magma remobilization, confirm that antecryst ages could span the duration of a magma reservoirs lifespan, through periods of cold storage and rejuvenation via new magma injection. They suggest using zircon grain chemistry to classify grains as antecrysts.

In the Cluanie and Glen Loy, the upper age of inherited grains limit coincides with the onset of Grampian orogenic events, estimated at c. 478 (Dewey et al., 2005). There is presently no Grampian age intrusive bodies in the NHT, but the presence of pegmatites dated at c. 450Ma (as reported by Cawood et al., (2015) stand as evidence for melt existing beneath the NHT during this time. These datasets provide further evidence for melt generation at this time. It is therefore viable that some of the grains closer to this upper limit are Grampian age grains existing in ‘cold storage’ in a Grampian age magma reservoir that is rejuvenated by the Scandian age melt. Crystal chemistry would be required to confirm this.

Indeed, the U –Th ratios, commonly used as an indicator of the magmatic or metamorphic nature of a zircon, indicate all grains in the Glen Loy and Claunie datasets are magmatic in origin. This further implies melt generation took place beneath the NHT during the Grampian orogeny. U/Th ratios of <0.5 indicate metamorphic reworking of a grain, or that the grain grew during pro-grade metamorphism (Chen et al., 2010. the values for Cluanie and Loy being consistently above this value (see Table 38). It is however peculiar that the Grampian age grains show no signs of metamorphic reworking associated with experiencing so called Scandian orogenic events.

Table 38: Maximum, minimum and mean U – Th ratios for the datasets. Ratios >0.5 indicate a magmatic origin for a zircon grain, while ratios <0.5 indicate a metamorphic orogin.

	Max U/Th ratio	Min U/Th ratio	Mean U/Th ratio
Cl 1	12.33 +/- 2.2	0.549 +/- 0.0085	4.60
Cl 2 & 3	22.66 +/- 0.51	0.731 +/- 0.0049	5.67
Gl 2	40.9 +/- 1.6	0.546 +/- 0.0085	2.80
Gl 1 & 3	9.726 +/- 0.065	0.6733 +/- 0.0047	1.74

5.1.4 Wider implications of new age data: debating the 'two-stage' model for Baltica Laurentia closure

The newly acquired U – Pb ages are added to the table of dated Newer granite intrusions (*see Table 40 and Figure 76*). Considered alongside the previously published Newer granite data, the U – Pb zircon isochrons acquired in this work can provide new insights into the timing of final Baltica - Laurentia Collison, and the generally accepted 'two-stage' model for the orogeny (i.e. meaning Grampian and Scandian, not including the Acadian). Said generally accepted model is outlined below, followed by a critical review of how recently acquired data (both from this study and from recently published literature) has affected our understanding of the temporal framework for Caledonian orogenic events. By association, the timing of events geologic events associated with the orogeny, such as first movement on the GGFZ, are also considered.

Previous frameworks for orogenic events associated with Iapetus ocean closure invoked two main phases intermediate phases before final Iapetus closure (the Acadian event); the Mid-Ordovician Grampian phase (478 – 460 Ma; Dewey, 2005; Chew et al., 2010) and Silurian Scandian phase (435 – 425 Ma; Atherton and Ghani, 2002, Neilson, 2009; Rogers and Dunning, 1991). The Mid-Ordovician Grampian event is discussed in detail in Dewey, 2005. The timeline of events is summarized in Table 39.

Defining a timeline for Scandian orogenic events has proven more problematic, with particular difficulties arising from reconciling the timeline with the ages of the Newer Granites of the NHT. Following the Grampian 'Arc accretion' style collision, Iapetus crust continued to be subducted beneath the Laurentian Foreland. Subduction ceased following the sinistrally oblique continental collision of Baltica (in the east) and Avalonia (in the South) with the Laurentian margin (Kinny et al., 2003; Soper et al., 1992). Exactly when this final collision was experienced in Scotland is still disputed (Dewey et al., 2015), but has traditionally been dated at c. 435 – 425 Ma using structural proxies and metamorphic mineral assemblages from the NHT (Kinny et al. 2003; Bird et al. 2013; Freeman et al. 1998; Dallmeyer et al. 2001). Said proxies include the 435 - 425 Ma Rb/Sr, K/Ar and 49Ar/30Ar mica ages from Moine Mylonites and schists at Knocken and

Dundonnel (Freeman et al., 1998), dating of D2 isoclinal folding in the western Moine units (Dallmeyer et al., 2001), and the formation of the Northern Highland steep belt (Strachan et al., 2002).

Mantle derived magmatism associated within the c. 435 – 425 Ma Scandian event is reported to have occurred in the NHT from c. 435 – 390 Ma, with a maximum at 410 Ma (Table 44) (Fowler et al., 2008). A popular hypothesis for explaining this spate of mantle-derived magmatism is the occurrence of a slab break-off event (Atherton and Ghani, 2002; Fowler et al., 2008). The association of the NHT granites with lamprophyric, minette type magmas, and appinites, hypothesised to have been sourced in a metasomatized lithospheric mantle, stands as evidence that the Newer Granites were not produced by the recycling of old continental crust and rather relate to an episode of mantle melting (Fowler et al., 2018).

A more detailed summary of the Scandian phase of the orogeny and the issues that have arisen in the demarking of its timeline can be found in found in Sections 2.2.2; 2.3.2 and 2.3.3.

Table 39: Summary of timeline of Grampian orogenic events as reported by Dewey (2004).

GRAMPIAN OROGENIC TIMELINE	
478 MA	Initial 'soft touch' between oceanic arc and Laurentian rifted margin.
475 467 MA	Arc/ophiolite obduction (e.g. Shetland, Ballantrae and Newfoundland), transpressional collision and crustal thickening occur.
467 MA	Subduction polarity flip from toward to away from the continent follows a slab break off event.
467 - 464.5 MA	Extensional collapse of the Grampian orogenic belt
455 MA	Renewed shortening as northerly-directed subduction of the Iapetus ocean crust is established (onset of subdution of the Southern uplands accretionary prism).

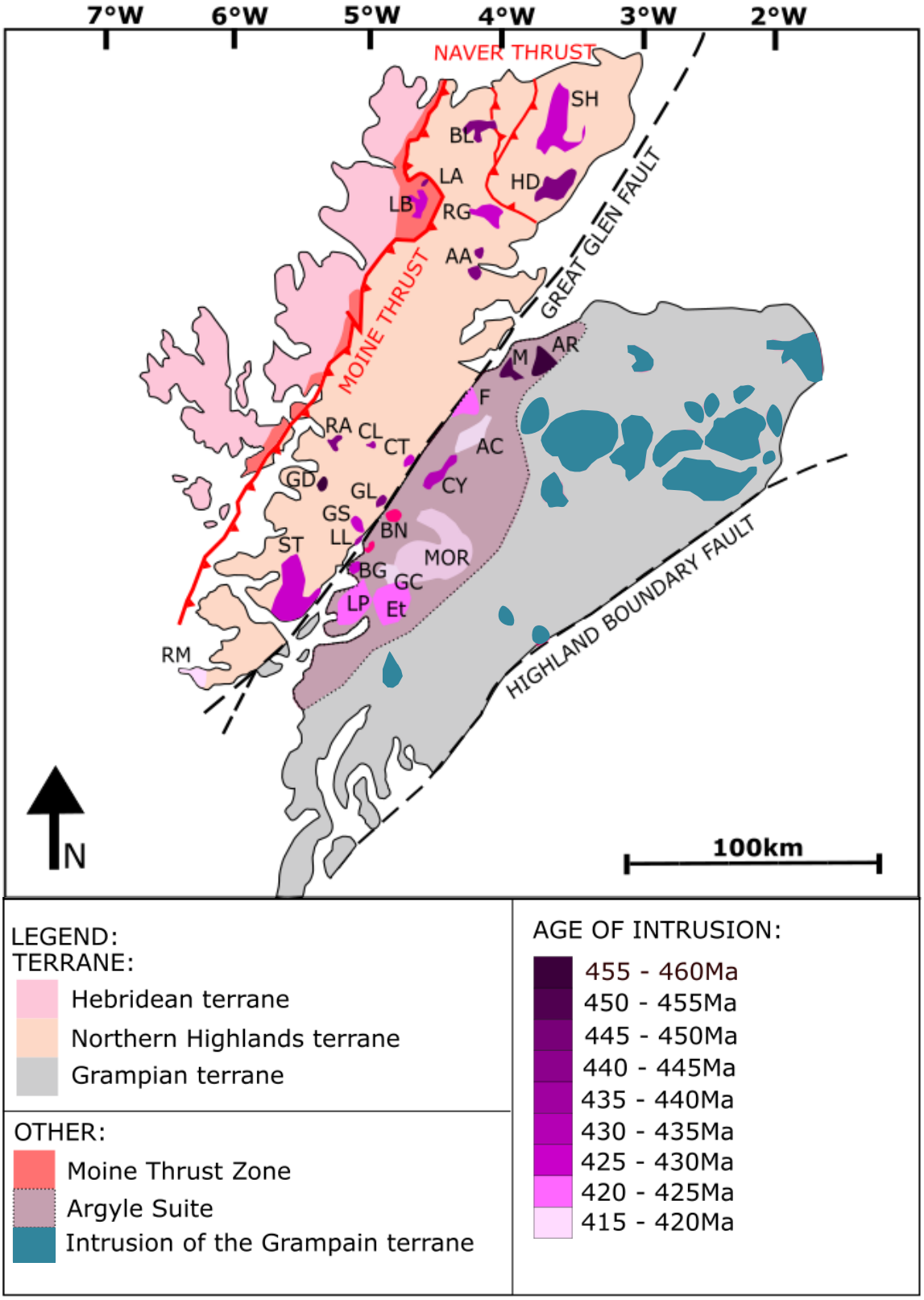

Figure 76: Map of the Hebridean, NHT and grampian terrane with dated Newer granite intrusions and Caledonian structures. Pluton data in Table 40.

Pluton Name/Location	Abbreviation	Method	Age (Ma)	Error (2σ)	Reference
NHT					
Glen Dessary Syenite	GD	U – Pb zircon	456	5	Goodenough et al. 2011
Loch Linnhe	LL	U – Pb Zircon	439	3	This work
Cluanie Intrusion	CL	U – Pb Zircon	438	3	This work
Glen Loy complex	GL	U – Pb Zircon	434	5	This work
Loch Borrolan Syenite	LB	U – Pb Zircon	430	4	Millar et al. 2008
Strathnaver Granite	SN	U – Pb Zircon	429	11	Kinny et al. 2003
Clunes Tonlaite	C	U – Pb Zircon	428	2	Stewart et al. 2001
Glen Scaddle Intrusion	GS	U – Pb Zircon	426	3	Strachan and Evans, 2008
Ben Loyal Granite	BL	U – Pb Zircon	426	9	Halliday et al. 1987
Strath-Halliday Granite	SH	U – Pb Monzanite	426		Kocks and Strachan, 2006
Rogart Igneous Complex	RI	U – Pb Zircon	425	1.5	Kocks et al. 2014
Strontian granodiorite	ST	U – Pb Zircon	425	3	Rogers and Dunning 1991
Ratagain Granite	R	U – Pb Badellyite	425	3	Rogers and Dunning 1991
Vagastie Bridge Granite	VB	U – Pb Zircon	424	8	Kinny et al. 2003
Kilbreck Bridge Granite	KB	U – Pb Zircon	420	6	Kinny et al. 2003
Ross of Mull Granite	RM	U – Pb Zircon	418	5	Oliver et al. 2008
Strontian Granite	ST	U – Pb Zircon	418	1	Paterson et al. 1993
ARGYLL SUITE					
Moy	M	U – Pb Zircon	452	3	Oliver et al. 2008
Ardclach	ARD	U – Pb Zircon	477	11	Oliver et al. 2008
Foyers	F	U – Pb Zircon	424	4	Oliver et al. 2008
Corrieyairack		Rb/Sr	434		Clayburn, 1981
Allt Crom	AC	Rb/Sr	405	-	Oliver et al. 2008
Strath Ossian	SO	Rb/Sr	405	9	Clayburn, 1981
Moor of Rannoch	MOR	K/Ar Bi; Rb/Sr	408	18	Clayburn, 1981
Ballachulish		*U – Pb Zircon*	427	1	Fraser et al. 2005
Etive	Et	U-Pb zircon	423	2	Oliver et al. 2008

Table 40: Magmatism recorded in the NHT and Grampian terrane (limited to the Argyle Suite) associated with the Scandian Orogeny

5.1.4.1 Recent insights into the timeline of Baltica – Laurentia collision

New isotope work on metamorphic mineral assemblages from within the Moine Nappe by Bird et al. (2013), and U – Pb dating of pegmatites and their hosts gneisses by Cawood et al. (2015) have prompted a rethink of the currently accepted timeline for Caledonian orogenic events, especially with regards to a) the 'Grampian – Scandian' two stage model, or b) the timing at which these events occurred.

Bird et al. (2013) present new Lu – Hf and Sm – Nd isotope data from prograde garnets in metamorphic assemblages from the Moine Supergroup. The Moine Nappe isochrons strongly imply a more complex metamorphic history for the Caledonian metamorphic belt the current two-phase orogeny involving Grampian metamorphism at ~475-467 Ma, followed by a Scandian phase around ~435-425 Ma (in addition to the pre-Caledonian metamorphic events recorded by the Moine sediments (Strachan et al., 2010)). The ages acquired range from 458.7+/-4.5Ma to 443.1+/-5.3 Ma, indicating prograde metamorphism and shortening was occurring during this time period in the nappe. The nappe itself was long considered to represent the Moine metasediments initially experiencing Grampian events associated with arc collision before being thrust over the Laurentian foreland during Baltica-Laurentia (Scandian) collision. The latter event is said to have resulted in the development of the D2 metamorphic fabric seen throughout the NHT (Holdsworth et al. 2007; and references therein). Previous work on dating the Scandian event included the study of syntectonic mineral assemblages in the thrust zone (Freeman et al., 1998; Dallmeyer et al., 2001) and syntectonic migmatites of central Sutherland (Kinny et al., 2003). These studies produced ages of c. 435 – 425 Ma. The results of Bird et al. (2013) push the occurrence of prograde metamorphism ~450 Ma, which is clearly neither Grampian nor Scandian in the traditional sense.

The plate-tectonic model proposed by Bird et al. (2013) invokes a further collision event, this time between a microcontinental fragment and the Laurentian continental margin at c. 460-440 Ma, creating a short-lived orogenic event similar in style to the Grampian orogeny (c. 460 – 470 Ma). The Grampian event is thought to have been short-lived (Dewey and Ryan 1990; Soper et al. 1999) and it should be noted that the prograde nature of the garnets (evidenced by Lu enrichment in

their cores) also rules out slow Grampian cooling as the mechanism for their formation (Bird et al., 2013).

U-Pb zircon data from the Glenelg pegmatite and U - Pb monzonite data form the gneissic host to the Carn gorm pegmatite presented by Cawood et al. (2015), stands as further evidence for a tectono-thermal episode experienced by the Moine successions at c. 450 Ma. Cawood et al. (2015) state that their data, combined with those of Bird et al. (2013), confirms that high-grade metamorphism and pegmatite formation occurred in the Morar group of the Moine at 458 – 446 Ma. Cawood et al. (2015) concludes that the Moine Supergroup of the NHT was affected by an additional phase of metamorphism, on top of that produced by the Grampian and Scandian collisions. Like Bird et al. (2013) they cite the collision of a micro-continental arc system, drawing on evidence of such events occurring at this time along strike in both Newfoundland (the Popelogan - Victoria arc collision; Van Stall et al. 2009) and Scandinavia (Corfu et al., 2003).

However, confirming the occurrence of Bird et al. (2013) and Cawood et al. (2015)'s ~450 Ma collision would require the identification of a continental sliver, much like the un-exposed arc proposed to underlie the Midland Valley Terrane associated with the Grampian Orogeny (Armstrong and Owen, 2001). Such a continental sliver is yet to be identified in Scotland. However, it is possible that evidence of such a structure has since been erased by movement on the GGFZ. The mantle peridotite seen at Glen Urquart (Neill, I., unpublished data 2018) is an important consideration in this hypothesis, since the identification of oceanic basement of appropriate age would stand as evidence for the occurrence of this accretion event. However it is difficult to reconcile the magmatic record in the NHT with a second arc accretion and subsequent return to subduction - evidence for mantle-derived magmatism (which would indicate a return to subduction) from this time exists only as the Glen Dessary syenite (~448 Ma; Goodenough et al., 2011). A possible explanation for this apparent lack of magmatism is the poor preservation potential of arc rocks resulting in their removal via erosion and weathering. This eventuality is difficult to substantiate, but the poor preservation potential of arc rocks is well reported (Bluck 2000; 2013). It could be that the intrusion at Glen Dessary represents the eventual resurgence of subduction related

magmatism following collision, while other intrusions of this age have long since been eroded from the landscape.

In the absence of firm field evidence for an accretion event magmatism and given the lack of firm evidence in the magmatic record, alternative explanations for the presence of prograde metamorphism at c. 450 Ma can also be entertained.

The possibility of a period of flat slab subduction during Baltica Laurentia collision was discussed by Dewey et al. (2015), referred to as an event termed the 'Mayoian'. Flat slab subduction is understood to be a result of changing subduction dynamics, and is phenomenon proposed to have occurred in numerous other subduction zones globally (Verdel et al., 2011). Flat slab subduction results in a compressional tectonic regime, for which there is evidence for in the NHT, the Dalradian of the Grampian terrane, Country Mayo in Ireland and the Appalachians of Newfoundland (Dewey, 2005; Chew and Strachan 2013). Importantly, flat slab subduction will exclude the mantle wedge as a melt source, resulting in limited mantle derived magmatism. This is compatible with the limited magmatic activity between the Grampian and Scandian events as they are currently understood. However, the mantle-derived Glen Dessary body would require explanation (Goodenough et al., 2011).

Another alternative is that the evidence currently presented in favour of a distinct Scandian event is in some way mistaken. For example, could the Scandian collision have begun some 20 Ma earlier than previously thought, as evidenced by the prograde metamorphic minerals reported by Bird et al. (2013) and Cawood et al. (2015)? In this scenario, thrust movement and migmatite development around c. 435-425 Ma represents the termination of collision, and the maximum extent of crustal heating (and the timing of slab breakoff) rather than the Baltica – Laurenita collision 'event'. This is explored further in the following section.

5.1.4.2 Significance of age data gathered in this study

The U – Pb zircon data collected from Cluanie, Glen Loy and Loch Linnhe does not fit particularly well with the previously outlined tectonic models for the 'Scandian orogeny' with Baltica - Laurentia collision occurring at c. 435 – 425 Ma (e.g. Kinny et al., 2003; Oliver et al., 2008; Freeman et al., 1998; Dallmeyer et al., 2001).

For a start, the emplacement of mantle derived Glen Loy at 433.6 +/- 3.3 Ma is not compatible with the collision and peak crustal thickening that traditionally accepted to be occurring at this time (see *Section 6.2.5 for geochemical classification of Glen Loy*). Indeed, a mantle source is strongly implied for many of the NHT intrusions emplaced between c. 435 and 425 Ma (see *Table 45)* (Fowler et al., 2008, this work).

In orogenic environments, a mantle derived signature will occur due to a) melting of the mantle wedge during subduction, or b) melting of the SCLM initiated by increased asthenospheric flow induced by slab break-off. It is less likely for mantle derived mafic magmatism to occur during peak collision, crustal thickening and regional metamorphism (Song et al., 2016). This is reflected in studies of the nature of magmatism in the Turkish-Iranian plateau and the Himalayan orogeny (Mo et al., 2008), and is linked to the presence of a substantially thickened continental crust. The presence of continental crust thickened by compressional tectonics can inhibit mantle derived magmatism by a) increasing the depth at which mantle melting may occur, b) restricting the rise magmas through the crust, and c) would restrict crustal melting until the radiogenic heating sufficiently caught up (Mo et al., 2008; England and Thompson, 1984).

As stated previously, there are numerous seemingly mantle-derived intrusions that lie within the age range previously given for Scandian collision, peak crustal thickening and regional metamorphism at c. 435 – 425 Ma (e.g. Kinny et al., 2003; Oliver et al., 2008; Freeman et al., 1998; Dallmeyer et al., 2001). Table 41 details the major intrusions of the NHT intruded between c. 435Ma and c. 425 Ma. Intrusions that are thought to be mantle derived are marked. The Assynt minor intrusion suite (Goodenough et al., 2004) is omitted from the table as it details major intrusion, but the mantle derived nature of the suite is worth highlighting.

While the suite is currently undated it is generally assumed that emplacement is associated with movement on the Moine thrust (Goodenough et al., 2004).

Given this contradiction, it is solicited to consider that c. 435 – 425 Ma may record the maximum heating of the crust and of deformation (as demarked by the metamorphic assemblages and deformation structures of Kinny et al., 2003, Freeman et al., 1998 and Dallmeyer et al., 2001), but not peak crustal thickening associated with Baltica - Laurentia collision. If Baltica - Laurentia collision and crustal thickening occurred earlier than c. 435 Ma, then it may be considered that the c. 450 Ma age recorded by the prograde garnets of the moine Nappe and the Carn Gorm pegmatites mark its onset. As previously stated, without the identification of substantial field evidence, it is impossible to confirm the arc-collision hypothesis proposed by Bird et al. (2013) and Cawood et al. (2015). Thus, it may instead be considered that the regional metamorphic event recorded by both authors represents the 'Scandian event', occurring c. 20Ma earlier than traditionally hypothesized. This idea was addressed briefly by Dewey et al. (2015), who stated that 'the Glen Dessary Pluton (447±2.9 Ma) pre-dates the formation of the early Scandian steep belt and therefore 'sets a lower limit to Scandian deformation'.

This hypothesis will be explored in the following sections, with close consideration of the magmatic record. The emplacement ages and geochemical profiles acquired in this study will be used to constrain the occurance of certain geodynamic regimes, and test how they fit with the potential c. 450 collision.

Table 41: Intrusions of the NHT reported to have been intruded during Scandian collision, shortening and peak crustal thickening. Those marked * are known to contain significant mafic facies which indicate mantle melting taking place at these times.

Pluton Name/Location	Method	Age (Ma)	Error (2 σ)	Reference
Glen Loy complex*	U – Pb Zircon	434	5	This work
Loch Borrolan Syenite	U – Pb Zircon	429.2	0.5	Van Breeman et al. 1979
Strathnaver Granite	U – Pb Zircon	429		Kinny et al. 2003
Clunes Tonalite	U – Pb Zircon	428	2	Stewart et al. 2001
Glen Scaddle Intrusion*	U – Pb Zircon	426	3	Strachan and Evans, 2008
Ben Loyal Granite*	U – Pb Zircon	426	9	Halliday et al. 1987
Strath-Halliday Granite	U – Pb Monzanite	426		Kocks and Strachan, 2006
Rogart Igneous Complex*	U – Pb Zircon	425	1.5	Kocks et al. 2014
Strontian granodiorite *	U – Pb Zircon	425	3	Rogers and Dunning 1991
Ratagain Granite *	U – Pb Badellyite	425	3	Rogers and Dunning 1991

5.1.4.3 Implications of the new age data to the timing of first movement of the GGFZ

The age of structures associated with Scandian events must be examined in order to test the hypothesis detailed in the previous section. One such structure is the GGFZ. Movement on the GGFZ is currently dated using U-Pb zircon dating of syn-tectonic intrusions (Strachan and Evans, 2008).

The concept of magma emplacement being controlled by post-orogenic regional strike-slip faulting is widely accepted both globally, and in the context of the Caledonides (Kocks et al., 2013; Soper and Hutton, 1984; Groom and Hall, 1974; Pankhurst and Sutherland, 1982). So-called syn-tectonic bodies are a common feature of orogenic belts and provide a key method of constraining the displacement history of associated faults. An understanding of the displacement history of fault zones is a key detail in the development of regional models for orogenesis, since it indicates the point at which the crust relaxes around the termination of collision (Hutton and McEarlean, 1991; Holdsworth et al., 2006). There are numerous Caledonian igneous complexes that are classified as syn-tectonic: namely the Scaddle Intrusion, the Clunes tonalite, the Rogart Igneous complex, and the Strontian Granite (Strachan and Evans, 2008; Stewart et al., 2001; Kocks et al., 2014 and Rogers and Dunning, 1991, respectively).

The current model for GGFZ first movement is that Scandian crustal thickening (peaking at c. 430 Ma) was followed by a period crustal relaxation which initiated the development of orogen-parallel faults (Kinny et al. 2003; Oliver et al., 2008). These NE-SW trending transpressional faults and shear zones cut through the crust and upper mantle and are intrinsically linked to granite genesis and emplacement (Jacques and Reavy, 1994; Atherton and Ghani, 2002).

The Glen Scaddle body, dated by Strachan and Evans, (2005), has a crystallization age of c. 426 +/- 3 Ma. A similar age (425+/- 1 Ma) was acquired by Kocks et al. (2014) for the Rogart Igneous complex, emplaced along the Loch Shin line (an anti - riedel shear to the GGFZ). The crystallization age for the Clunes tonalite is given as 427.9 +/-1.9 MA (Stewart et al. 2001). The strontian granite is dated at 425 +/- 3 Ma (Rogers and Dunning, 1991). Thus, the onset of displacement along the GGFZ is thus currently given at c. 428 Ma (Stewart et al, 2001).

The U-Pb data acquired for Loch Linnhe, Glen Loy and Cluanie suggests this model may need revision. The emplacement ages acquired all pre-date this estimate for GGFZ first movement, and yet each body shows features of being syn-tectonic with either the GGFZ (Loy and Linnhe), or an associated strike slip fault (Cluanie lies at the intersection between the GGFZ parallel Strathglass fault and other minor northern – SE trending faults) (Neill and Stephens, 2009).

Neill and Stephens (2009) report that emplacement of the Cluanie pluton was controlled by dextral movement on the Strathglass Fault (adjacent to the pluton), which would in turn have been initiated by sinistral movement on the GGFZ. The mechanism behind emplacement involves a 'releasing bend' in the Strathglass fault creating an area of dilation into which the magma was injected. Thus, according to the model of Neil and Stephens (2009), the GGFZ must have been active at the time of Cluanies emplacement.

The intrusion at Glen Loy is found in an almost identical structural setting as the Clunes and Scaddle intrusions, both of which have been deemed to have been emplaced in association with fault movement (Stewart et al., 2001 and Strachan and Evans, 2008, respectively). Emplacement associated with GGFZ movement is also consistent with the field evidence collected at Glen Loy.

Steeply inclined parallel fabrics are cited as a key feature of bodies emplaced associated with trasnpressional zones of strike - slip faults systems (Hutton and Reavy, 1992; Moyen et al., 2003). The development of intra-intrusion syn-magmatic shear zones is also cited by Moyen et al., 2003 as an indication of a body being emplaced associated with major strike – slip fault zones (or shear zones). Further, in their study of the South Indian Closepet granite, Moyen et al., 2003 describe these intra-intrusion shear zones being exploited or invaded by late granite pegmatites.

Steeply inclined parallel fabrics and shear zones both trending nearly parallel to GGFZ can both be observed in the intrusion at Glen Loy. Since there is no increase in the intensity of the fabric at the margins of the pluton it can be assumed that magma buoyancy forces are not responsible for the development of this fabric (Stewart et al., 2001). The fabric at Loy is largely similar to that at Scaddle, which

is already deemed syn-tectonic by Strachan and Evans (2008). Scaddle, however, also has zones of mylonitisation, indicative of high strain while the melt was cooling. No mylonite was observed at Glen Loy, but several more small shear zones were observed, again running roughly parallel to the main magmatic fabric and the GGFZ. The above field evidence is largely in accoradance with that desbribed by Moyen et al., 2003 for the syn-tectonical Closepet granite of South India.

The Linnhe granites geographic positioning at the heart of the GGFZ strongly implies emplacement was linked to the development of the fault zone, but further fieldwork is underway in order to evaluate this relationship.

With the U - Pb zircon ages reported for Cluanie, Loy and Linnhe all predating the currently reported age for GGFZ movement (428 Ma; Strachan and Evans, 2008), it must be considered that first movement along this major crustal structure was earlier than previously thought. Again, this calls into question the currently accepted timeline for Scandian Orogenic events. Strike slip faulting on the scale of the GGFZ is highly unlikely before to have occurred prior to the cessation of major crustal thickening (Stewart and Strachan, 1999; Underhill and Brodie, 1993).

This considered, the new crystallization ages acquired imply first movement on the GGFZ was not at c. 428 Ma, as previously reported by Stewart et al. (2001). The new data invokes first movement may have been up to 10 - 15 Ma earlier, as demarked by the emplacement of the Loch Linnhe intrusion (441 +/- 3). However, it is noted that further fieldwork is required to identify the phases of deformation affecting the Linnhe intrusion and its nearby neighbour, the Scaddle Pluton before substantive claims can be made. The geochronological data does strongly imply that the GGFZ was active for the emplacement of Cluanie and Glen Loy plutons, at 437 +/- 3 Ma and 433 +/- Ma respectively. The fault zone continued to act as a channel for melt, facilitating the emplacement many younger Caledonian igneous bodies (e.g. Stontian, Ratagain a Clunes), with movement continuing until more recent times (Rogers et al. 1989; Andrews et al. 1990; Underhill & Brodie 1993; Roberts & Holdsworth, 1999).

Again, the geochronological data appears to favour the hypothesis that Scandian collision and crustal thickening took place sometime before the currently proposed time of c. 435-425 M. Further, the data favours the proposals of Bird et al. (2013) and Cawood et al. (2015) for a collisional event at c. 450 Ma, although it again solicits considering that this event may not represent the collision of a micro-continental fragment, and perhaps the onset of Baltica – Laurentia collision (Bird et al. 2013; Cawood et al. 2015).

It is important, however, to recognise further steps towards proving one or other of these hypotheses. Additional structural data is required from Loch Linnhe to confirm its kinematic relationship with the fault zone. The Linnhe granite is currently being investigated as being an 'exotic' sliver of material sourced from the Grampian terrane. As such, its emplacement age may not mark the onset of GGFZ movement, but instead demarks the point after which first movement took.

It is also necessary at this stage to acknowledge Rb – Sr age acquired by Powel, (1983). As discussed previously (Section 2.5.2), after applying the correction for Rb – Sr ages suggested by Miles et al. (2016), the crystallization age for Cluanie works out at 433+/-4 Ma. Not only is this within error of the age required in this work, it is also in line with age required for Glen Loy. Accepting the crystallisation age for Cluanie as 433 +/-4Ma would alter slightly the line of enquiry presented in this work, in that it wouldn't necessarily require the timing of 'Scandian' (Baltica - Laurentia) collision to be reconsidered. Briefly, this scenario could entail c. 438 dating melt generation, and associated with subduction, and emplacement taking place at 433 Ma. The line of enquiry presented here is based on the ages acquired in this body of work. It is necessary that further enquiry is done to consider the geodynamic model implied by the ages presented by Powel 1983.

Figure 77 presents a schematic summary of the geochronology data gatherered in this study presented alongside the timeline associated geodynamic events as discussed in this work. Other NHT intrusions are also included in the figure. The ages for these (and associated references) are as presented in Table 40. The following key points can be drawn from the figure and from the geochronology data more broadly:

- Inherited xenocrysts are present in the datasets from Glen Loy, Cluanie and Loch Linnhe. The ages are consistent with their emplacement within the Loch Eil division of the Moine Supergroup. The two archean age grains in the dataset from Loch Linnhe are interpreted as being derived from the basement to the Moine, most probably from inliers at Rosemarkie or Cromarty, which lie along strike on the GGFZ.

- The data sets for the zircons from Cluanie and Glen Loy contain a range of antecryst ages from the period associated with the Grampian orogeny. This is interpreted as evidence of assimilation of Grampian age zircons, which crystallised in a deep crustal hot zone and remained in cold storage until their incorporation and reactivation in ‘Scandian’ age melts.

- The ages acquired for Cluanie, Glen Loy and Loch Linnhe predate current estimates for GGFZ first movement. Given that the bodies can justifiably be considered syn-tectonic, the timing of GGFZ should then be reconsidered (given as c. 441Ma in this work in line with the age acquired from the intrusion at Loch Linnhe).

- The data gathered in this study favours the onset of Scandian collision taking place earlier than current estimates of c. 430Ma, since GGFZ movement and granite emplacement is unlike to have occurred prior or during peak metamorphism associated with the collision.

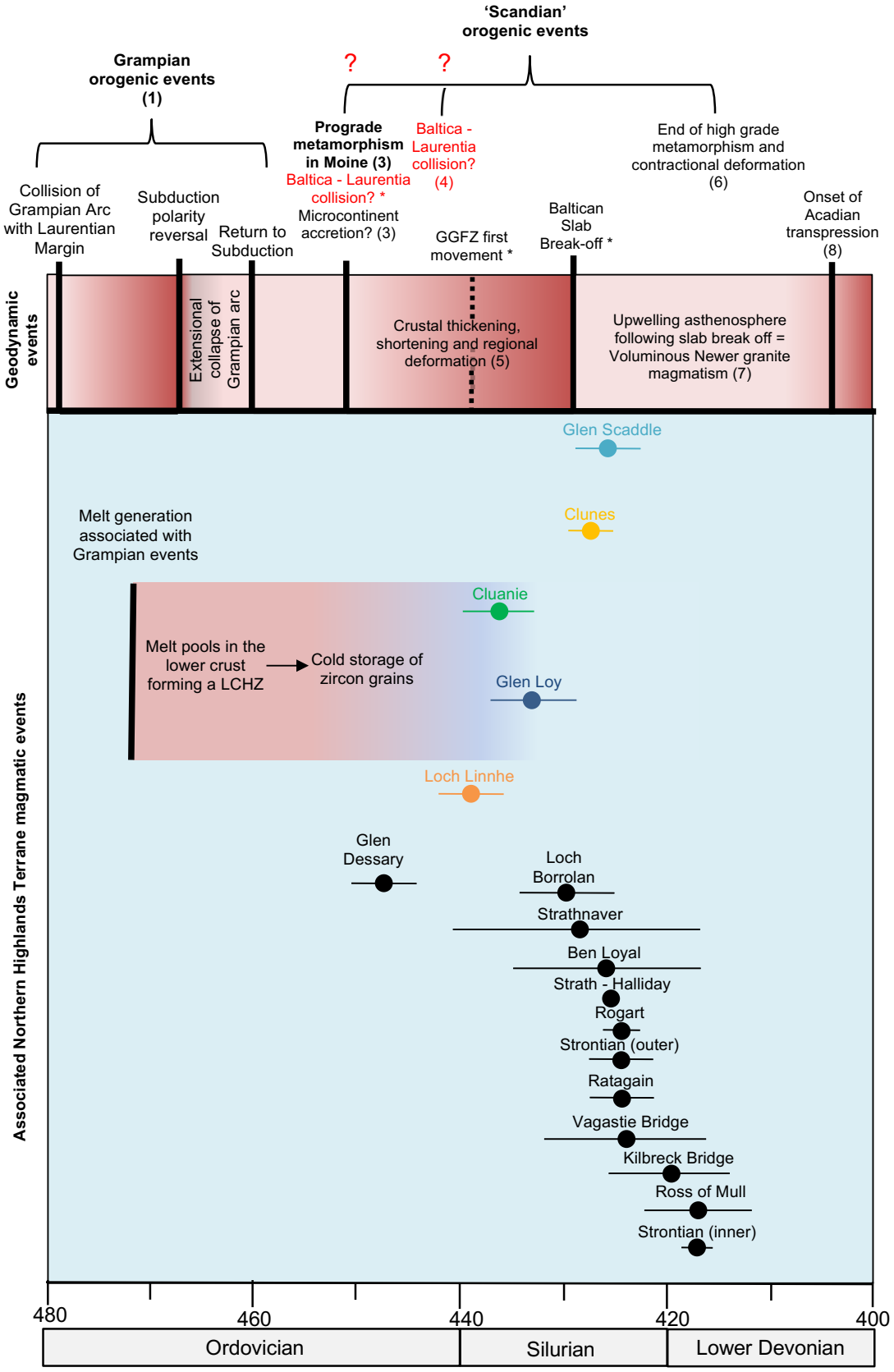

Figure 77: Timeline of events is as discussed in this work. schematic timeline of Caledonian orogenic events. References are numbered as follows: (1) Dewey, 2005, (2) Jackson et al., 2018, (3) Bird et al., 2015, (4) Freeman et al., 1998, (5) Chew and Strachan, 2013, (6) Mako et al., 2019 (7) Stewart et al., 2008 (8) Mendum (2012). *Marks hypotheses presented in this work. The ages of the NHT intrusions not studied directly in the work (in black) are as in Table 40.

5.2 Interpretation of the new geochemical data

First order interpretations of the geochemical profiles of the plutons studied are followed by comments comparing the data to the Caledonian plutonism across the NHT, as reported by Fowler et al. (2008). Trace element fractional crystallisation models are presented for Glen Loy, Scaddle, Clunes and Cluanie, confirming that the systems can evolve through the fractionation and accumulation of a given mineral assemblage. The meaning of the geochemical data with regards magma genesis and evolution is then discussed. Interpretations based on the petrogenetic history of Loch Linnhe are avoided, with the single sample being insufficient for any robust interpretation.

Finally, a tectonic model for emplacement is synthesized, taking into account the interpretation of the geochronological data presented previously. The classification of the Clunes and Cluanie intrusions as adakitic is then discussed and considered in the context of this tectonic model, allowing some conclusions to be reached regarding adakite genesis globally.

5.2.1 Interpretation of major element data

The geochemical characteristics of Loy, Scaddle Clunes and Cluanie are similar to other plutonic suites of the NHT, as summarized in Fowler et al. (2008), and references therein. Fowler explores the occurrence of high Ba - Sr granites, appinites/diorites and syenites in the NHT (as well as the Argyll suite just south of the GGFZ), using elemental geochemistry and isotopic work to establish a source and evolutionary history for the magmas.

5.2.1.1 Major element control on magma evolution: Total alkali vs. Silica plot

Figure 78 shows a Total alkali vs. Silica plot populated with the data from this study, alongside data from other NHT suites (Fowler et al. 2008).

The plot emphasises the considerable variability of major elements and SiO_2 compositions in the NHT plutons. Glen Loy is the most mafic of the plutons studied (SiO_2 wt. %: 41 - 55), followed by Scaddle (SiO_2 wt. %: 53 - 69), Clunes (59 - 64 wt. %), Cluanie (SiO_2 wt. %: 61 - 72) and Loch Linnhe (SiO_2 wt. %: 73). The plot demonstrates the coherence of the plutons in this study to Fowlers NHT suites. Loy and Scaddle plot close to the samples characterized as mafic appinites and diorites, with the samples from Cluanie, Loch Linnhe, and most of those from Clunes plotting alongside the granites (data from Fowler et al., 2008). However, a direct evolutionary relationship between the plutons is not supported by the geochronological data (from this study or otherwise). This is highlighted by the emplacement age of Cluanie - the most evolved suite studied, predating that of Loy - the least evolved. The apparent relationship between the plutons can therefore be explained by invoking similar melt sources and differing degrees of similar evolutionary processes.

5.2.1.2 Major element control on magma evolution: Major element Harker Diagrams

The comparative major element Harker diagrams further demonstrate the coherence of the plutons studied here to the NHT data of Fowler et al. (2008) (see *Figure 79*). Similar to the TAS plot in *Figure 78*, Glen Loy and Scaddle largely plot amongst the appinites/diorites, while the Clunes, Cluanie and Loch Linnhe plot alongside the granites. This is not entirely true for MgO and Al_2O_3, where only the Glen Loy samples identified as cumulates are in line with the appinites/diorites of Fowler et al. (2008), suggesting that mineral accumulation concentrated MgO rich minerals (e.g. olivine, pyroxene and amphibole), and not Al_2O rich minerals (feldspars). The decrease seen in Fe_2O_3, CaO, and TiO2 wt. % with increasing SiO_2 wt. % is consistent with the progressive removal of mafic minerals (biotite, clinopyroxene and amphibole) from a mafic parent magma.

An inflection point at ~55% wt. % SiO_2 is seen in the trends for MgO, P_2O_5, Fe_2O_3, and Al2O3. For MgO, P_20_5 and Fe_2O_3, ~55% wt.% SiO_2 this marks to point where the decline in wt.% becomes less severe, and is also the point at which Al_2O_3 wt.% begins to drop off. This is indicative on the onset of feldspar fractionation.

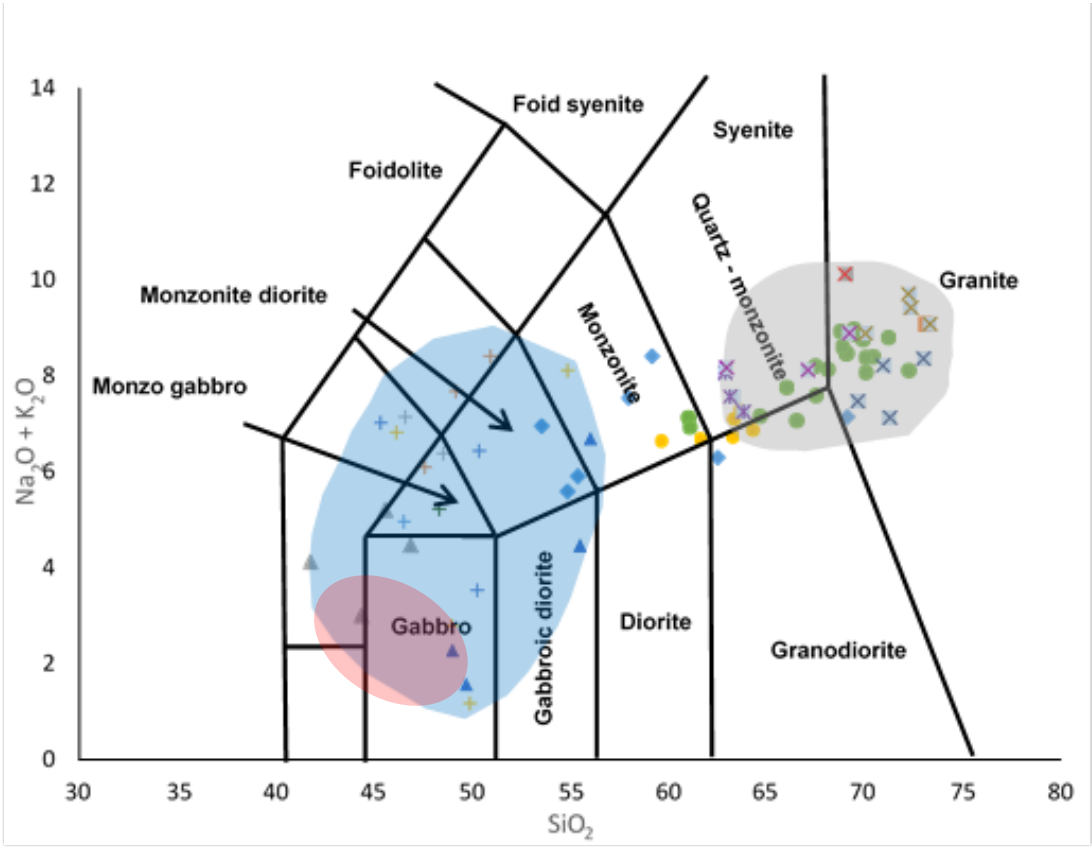

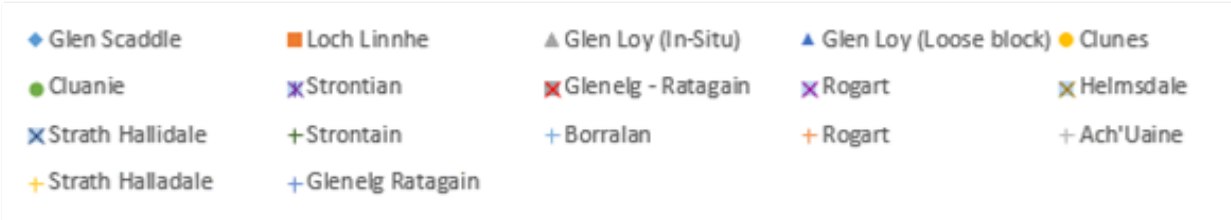

Figure 78: Total alkali vs Silica plot with fields defined by Johannsen, 1937. Data from this study is plotted alongside data for NW highland granites (X) and appinites and diorites (+), as reported by Fowler et al., (2008). Blue coloured overlay defines the mafic appinite and diorite field, while the grey overlay defines the granite field. The red domain highlight samples idenitified to be cumulates.

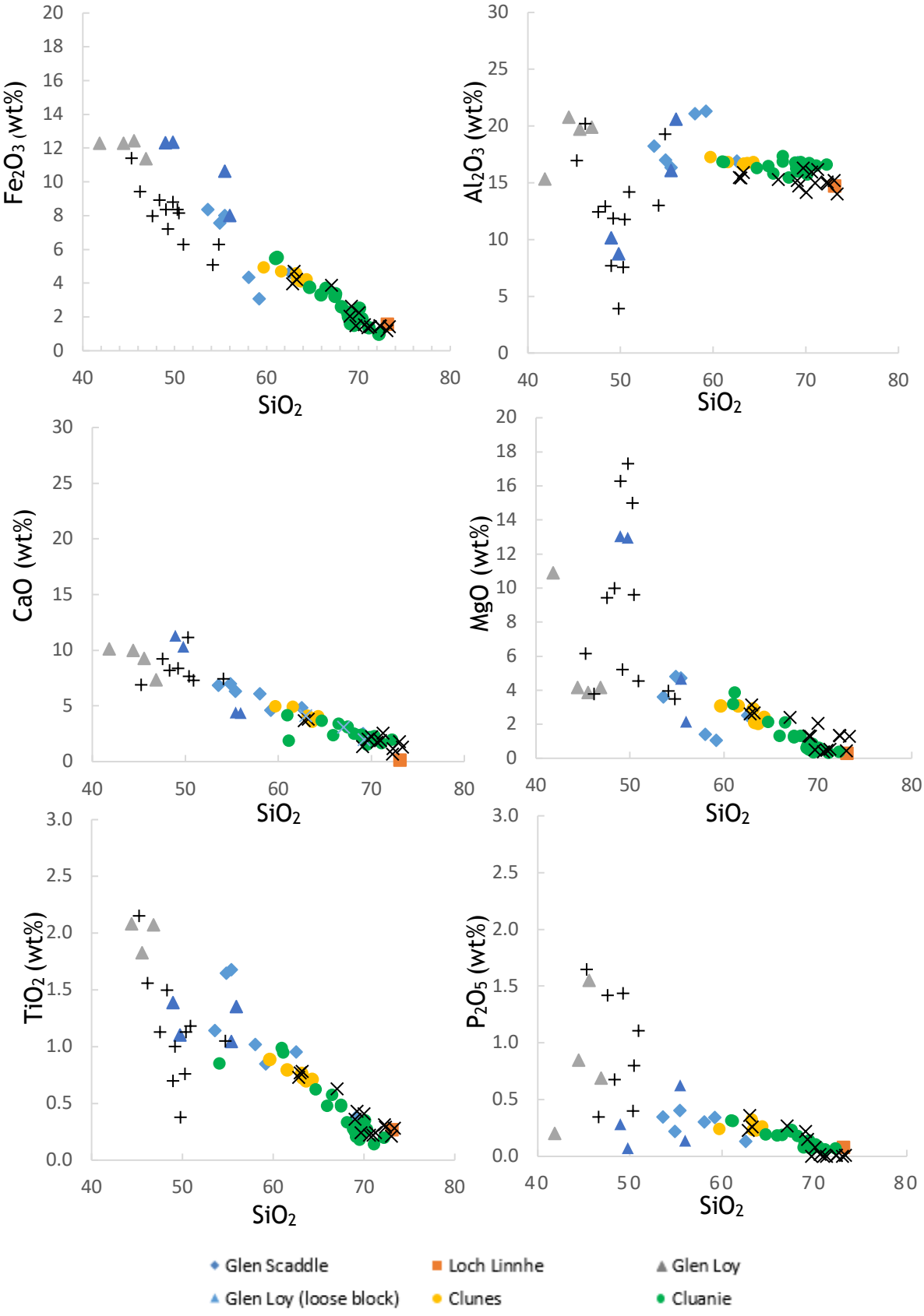

Figure 79: Major element Harker diagrams. Data from this study is plotted alongside data for NW highland granites (X) and appinites and diorites (+), as reported by Fowler et al. (2008).

5.2.2 Interpretations of REE data

Figures 80 - 83 are chondrite normalised REE plots with data from this study plotted alongside data from the appinites/diorites and granites from Fowler et al., 2008.

The plots show general coherence in trends between plutons (the exception being Loch Linnhe), with moderate La – Lu gradients, enriched LREE's (La – Gd) and moderately depleted HREEs (Tb – Lu).

LREEs are generally enriched over 100x chondritic values, implying involvement with the LREE enriched continental crust (Winter, 2014). Eu anomalies are rarely present, and are negligible when they are, with the exception of Glen Loy, and the most evolved samples from Clunes, suggesting feldspar fractionation is limited. Alternatively, the Eu anomaly could have been stifled by amphibole cofractionation, which produces a positive Eu anomaly (Winter, 2014). Such positive anomaly is observed in the samples from Glen Scaddle.

The general decrease in the degree of enrichment of elements from the SiO_2 poor to SiO_2 rich samples is suggestive the removal of abundant REE-rich accessory phases such as titanite, apatite, zircon and allanite (Winter, 2014). The moderately enriched HREE patterns suggests a garnet free source, implying magma genesis did not occur at significant depth (garnet fractionation occurs at depths of over 100km) (Winter, 2014).

The coherence seen in the REE plots indicates some degree of relationship between Loy, Scaddle, Clunes and Cluanie. Similar to the major element data Loy and Scaddle bear closer REE resemblance to appinites and diorite of Fowler et al., 2008, while Clunes and Cluanie are similar the granites.

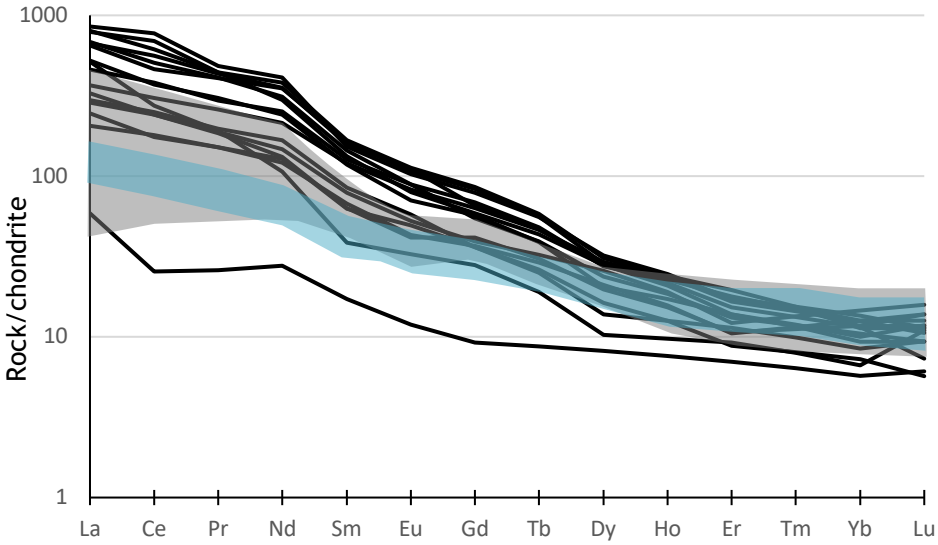

Figure 80: Chondrite normalized trace element plot after Sun and McDonough, 1989. The black lines represent the NW highlands granites identified by Fowler et al. (2008). Grey coloured overlay represents spread of data from Glen Loy. Blue coloured overlay represents spread of data from Glen Scaddle

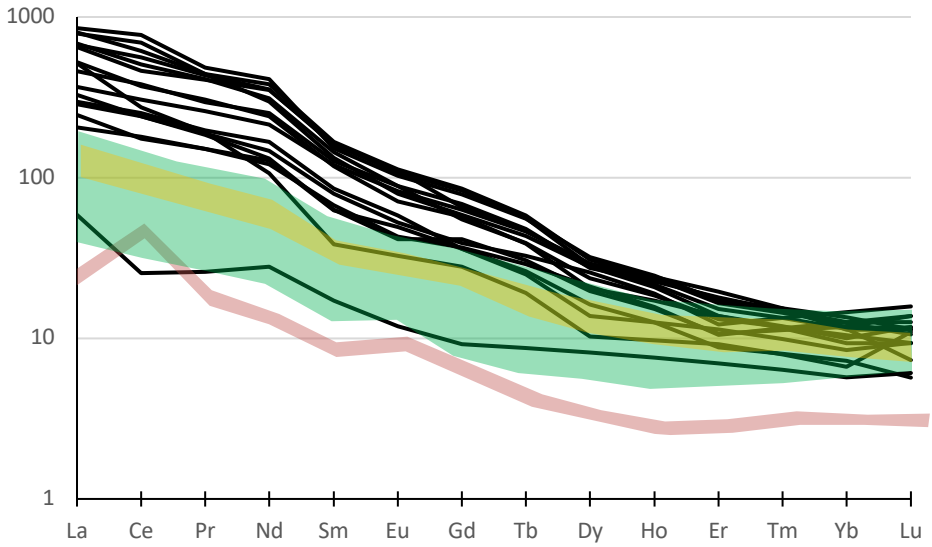

Figure 81: Chondrite normalized trace element plot after Sun and McDonough, 1989. The black lines represent the NW highlands granites identified by Fowler et al. (2008). Green coloured overlay represents spread of data from Cluanie, the yellowing representing the data from Clunes and the orange the data from Loch Linnhe.

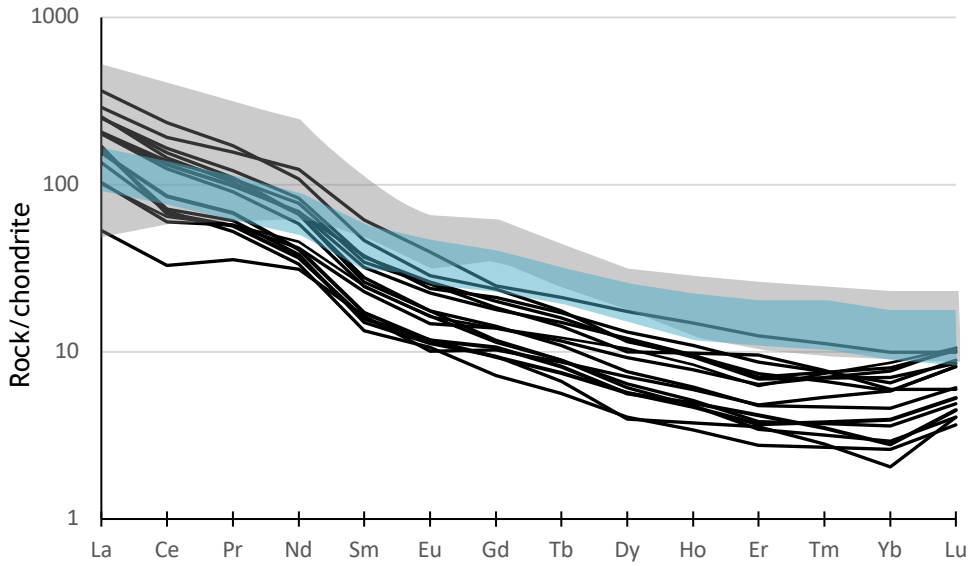

Figure 82: Chondrite normalized trace element plot after Sun and McDonough, 1989. The black lines represent the NW highlands granites identified by Fowler et al. (2008). Grey coloured overlay represents spread of data from Glen Loy. Blue coloured overlay represents spread of data from Glen Scaddle.

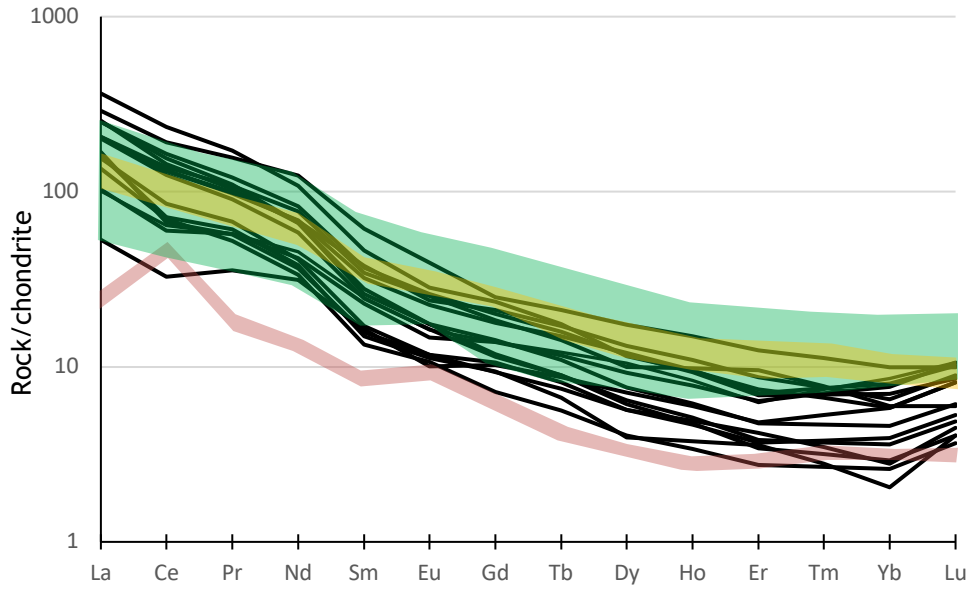

Figure 83: Chondrite normalized trace element plot after Sun and McDonough, 1989. The black lines represent the NW highlands granites identified by Fowler et al. (2008). Green coloured overlay represents spread of data from Cluanie. Yellow coloured overlay represents spread of data from Clunes, and orange from Loch Linnhe.

5.2.3 Interpretations of trace element data

The primitive mantle normalised multi-element diagrams for the plutons (see *Figures 32, 34, 36 and 38*) show a steep left - right slope, indicating a general enrichment in the incompatible elements. Nb-Ta troughs are seen in all plutons – a signature of subduction related magmatism (Winter, 2014).

The concentration of highly incompatible elements Zr-Hf is variable both between plutons and individual samples. Values are very low – depleted in Clunes. Similar troughs, albeit not as dramatic, are seen in some samples from Scaddle and Loy. Values are enriched 10x primitive mantle standards in Cluanie, and the majority of samples from Glen Loy and Scaddle. Zr and Hf are generally used as measures of the level of enrichment of the melt source, or the degree of liquid evolution (Winter, 2014). It is thus peculiar to see such variation in samples with characteristic that otherwise imply a similar source. The variability of Zr and Hf is difficult to explain, especially considering more evolved rocks such as Clunes tend to be more enriched in Zr and Hf relative to mafic lithologies (Zr-Hf decoupling is rare) (Winter, 2014). Furthermore, the remobilisation of Zr and Hf by metasomatism and granite related hydrothermal process is generally limited (Alderton et al., 1980; Forum of European geological surveys, 1998).

Ba – Sr are consistently high in Scaddle, Clunes and Cluanie. Values are lower and more variable in Glen Loy. The origin of the high Ba-Sr signature is thought to be associated with sedimentary contributions associated with the subduction of Iapetus crust (Fowler et al., 2008; Blundy and Dalton, 2000; Andersson et al., 2016). Pelagic sediments are Ba and Sr rich. High levels of Ba are a result of hydrothermal interactions or biogenic barite (Blundy and Dalton, 2000). High Sr quantities are found in marine carbonates. Marine sediments are also typically LREE enriched (Blundy and Dalton, 2000; Andersson et al., 2016). Thus, the LREE enriched, high Ba – Sr nature of these bodies, and many other plutons in the NHT, may be attributed to the elemental contribution of subducted marine sediment to the SCLM and mantle wedge. Fowler et al. (2008) supports this, hypothesizing that the source for plutonism in the NHT highlands is a sediment contaminated mantle. Similar conclusions are reached by Andersson et al. (2016), who study the high Ba-Sr plutons of Fennoscandia. They conclude that the high Ba Sr and LREE enriched

nature of the plutons is associated with mantle carbonates, and carbonate dominated metasomatism derived from the subducted metasediments. Variability of the Ba – Sr content seen in Glen Loy can be attributed to weathering, and particularly the breakdown of Sr rich plagioclase to sericite. Sr is easily mobilised during weathering, consistent with the degree of weathering indicated by the LOI values (Alderton et al., 1980; Forum of European geological surveys, 1998).

5.2.3.1 Ni and Cr content

Concentrations of elements Ni and Cr are commonly used as a proxy for the level of involvement of the mantle in the generation of a melt. Indeed, Ni and Cr contents are a key feature used by Condie et al. (2005) in the classification of the Patagonian TTG's and adakites, and in the ultimate determination of their petrogenetic source (mantle wedge vs. lower crust; See *section 2.6.1*) High values (Cr>80ppm and Ni > 50ppm; Condie et al., 2005) are markers of involvement with the mantle wedge, or mantle involvement generally. Ni and Cr ppm vs SiO_2 wt. % are plotted in *Figure 84,* alongside data from the appinites/diorites and granites from Fowler et al. (2008).

The appinites/diorites have consistently higher Ni and Cr contents than Loy and Scaddle, the exception being the samples identified as cumulates. The fact that the Glen Loy cumulates are significantly enriched Ni and Cr accounts for the low values in the other samples, suggesting the Ni and Cr enriched minerals are primarily concentrated in the cumulate material. The high Ni and Cr content of the Glen Loy cumulates is a strong indication extensive interation with the mantle during melt genesis and transport.

When plotted alongside the data from Fowler et al. (2008), the data from Cluanie and Clunes plot in line with the NHT granites. The higher Ni content in some of the Cluanie samples may indicate the melt spent a greater time in contact with SCLM or mantle wedge material.

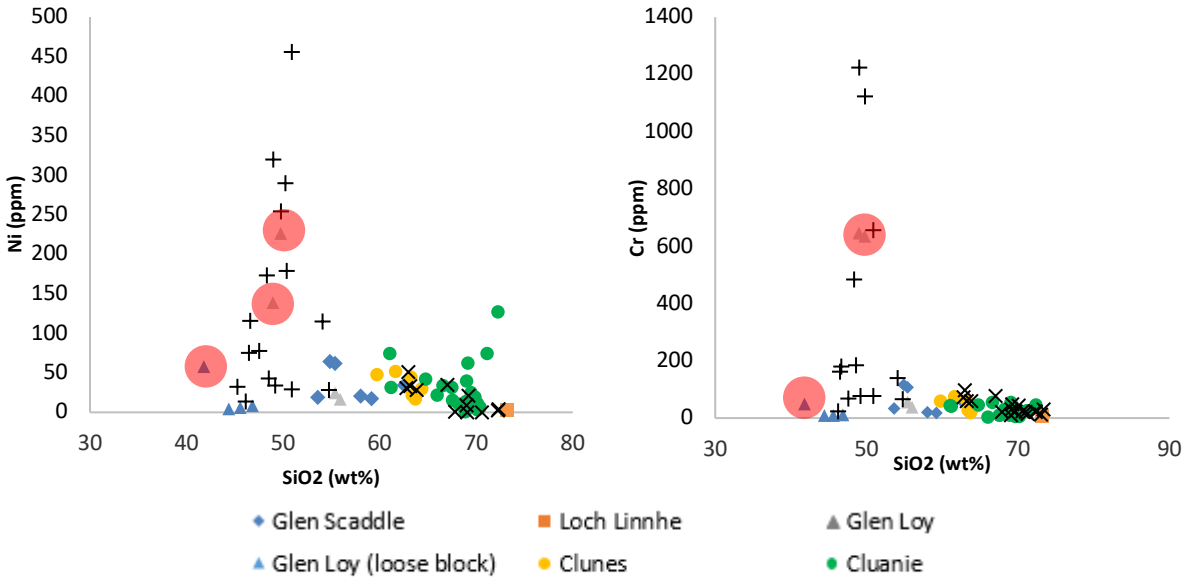

Figure 84: Ni and Cr (ppm) vs SiO_2 (wt%). Data from Glen Loy, Glen Scaddle, Clunes, Cluanie and Loch Linnhe are plotted alongside the appinites and and diorites (+) and granites (x) of the NHT. Glen Loy cumulate samples are highlighted in red.

5.2.4 Modelling fractional crystallization of the Loy, Scaddle, Clunes and Cluanie intrusions

Fractional crystallization models were constructed for Glen Loy, Scaddle, Clunes, and Cluanie (see Figures 85 – 88). The models are constructed using the equation for Rayleigh fractionation, modeling up to 20% fractionation of a given assemblage. The Rayleigh fractionation equation is given in Equation 2:

$$(c1/c0) = (F^{(D-1)})$$

c1: Final composition (most evolved, non-cumulate sample)

c0: Starting composition (least evolved, non-cumulate sample)

F: Fraction remaining

D: Distribution coefficient

Equation 2: Rayleigh fractionation equation (Winter, 2014)

The bulk partition coefficients used to calculate the distribution coefficients are presented in Appendix F. Coefficients were kept constant between models. Fractional crystallization models assume fractionation has taken place in a stationary magma chamber at a constant pressure (Winter, 2014).

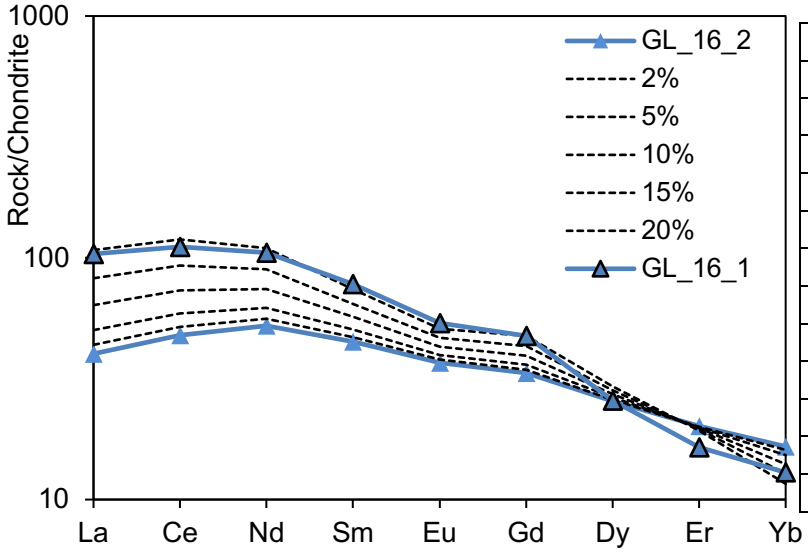

Amphibole	-0.20000
Titanite	0.00500
Apatite	0.00100
Zircon	0.01400
Allanite	-0.00140
Biotite	0.10000
Ilmenite	0.01000
Quartz	0.30000
Plagioclase	-0.50000
Orthoclase	0.40000
Clinopyroxene	0.50000
Orthopyroxene	0.37140
Sum	1.00000

Figure 85: Fractional crystallization model for Glen Loy, with suggested fractionating assemblage presented in the table to the right.

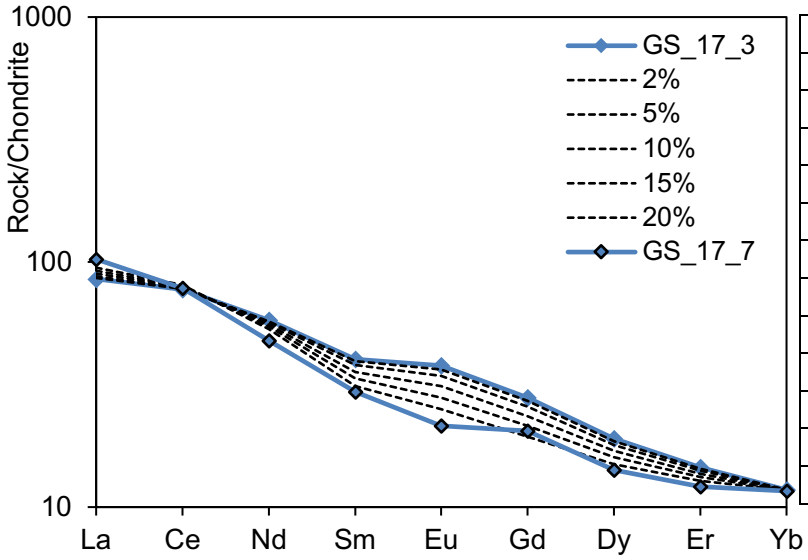

Amphibole	0.40000
Titanite	0.05000
Apatite	0.00236
Zircon	-0.00200
Allanite	-0.00035
Biotite	0.15000
Ilmenite	-0.00001
Quartz	-0.20000
Plagioclase	0.40000
Orthoclase	0.10000
Clinopyroxene	0.05000
Orthopyroxene	0.05000
Sum	1.00000

Figure 86: Fractional crystallization model for GlenScaddle, with suggested fractionating assemblage presented in the table to the right.

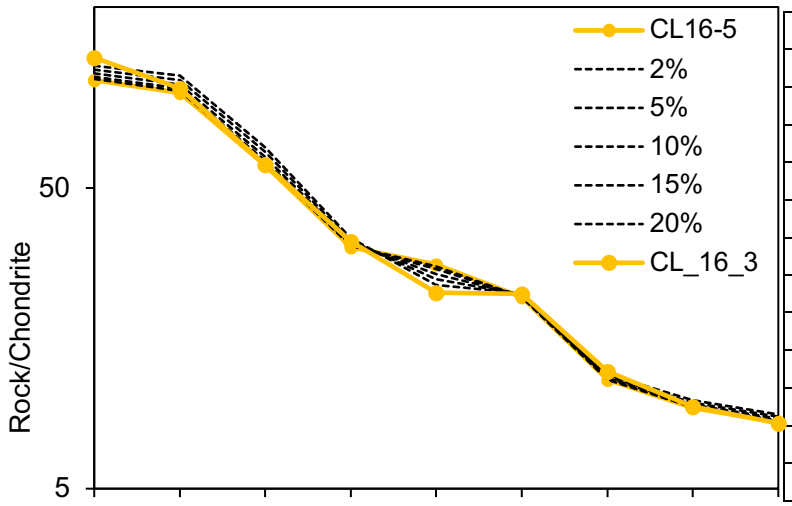

Amphibole	0.10000
Titanite	0.00500
Apatite	0.00600
Zircon	0.00100
Allanite	-0.00027
Biotite	0.17000
Ilmenite	0.00100
Quartz	-0.10000
Plagioclase	0.31727
Orthoclase	0.70000
Clinopyroxene	-0.10000
Orthopyroxene	-0.10000
Sum	1.00000

Figure 87: Fractional crystallization model for Clunes, with suggested fractionating assemblage presented in the table to the right.

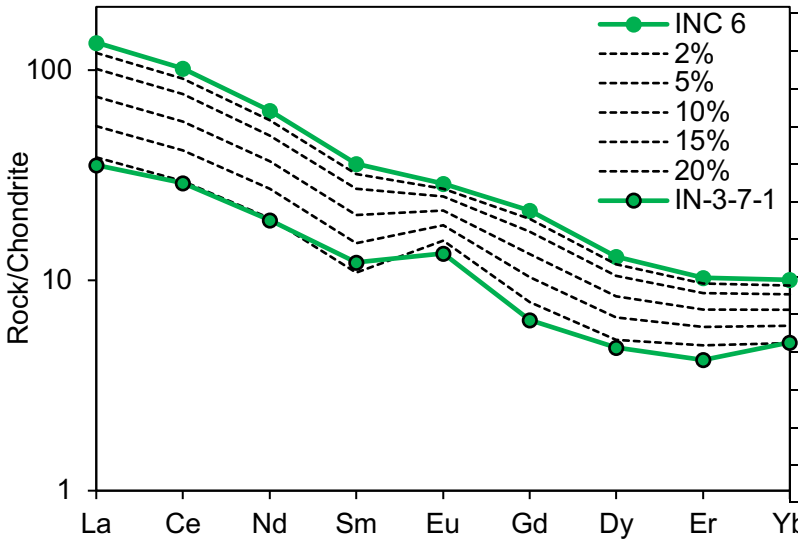

Amphibole	0.80000
Titanite	0.00250
Apatite	0.06000
Zircon	0.00500
Allanite	0.00150
Biotite	0.20000
Ilmenite	0.00100
Quartz	-0.20000
Plagioclase	0.33000
Orthoclase	-0.05000
Clinopyroxene	-0.1
Orthopyroxene	-0.05
Sum	1.00000

Figure 88: Fractional crystallization model for Clunes, with suggested fractionating assemblage presented in the table to the right.

The fractional crystallization models constructed for Glen Loy, Scaddle, Clunes and Cluanie show that it is possible for each pluton to have evolved primarily by mineral fractional, albeit of varying assemblages.

Plagioclase and amphibole accumulation appear to be a necessary feature of Glen Loy's evolution, consistent with the plagioclase and amphibole dominated cumulate samples identified in the petrographic study. Amphibole fractionation is an important feature of the evolution of Scaddle, producing the fractionated MREE and HREE's and slightly concave upwards trend. Feldspar (plagioclase and orthoclase) fractionation is an important control of the evolution of Clunes. However, the geochemical range seen in the samples set is small, meaning assumptions based on the model are limited. Amphibole fractionation dominates the fractionating assemblage of Cluanie.

A small degree of crustal assimilation does appear to be required in addition to crystal fractionation for Loy, Scaddle and Cluanie. This requirement is supported by the $^{143}Nd/^{144}Nd$ and $^{87}Sr/^{86}Sr$ isotope work carried out by Fowler et al. (2008) (see Figure 89).

As there is no whole rock isotope or large-scale zircon study for Clunes, there is no clear answer as to whether it requires crustal input during its petrogenesis. Limited degrees of crustal assimilation are also implied by the number of inherited zircon grains found in the study of the Loy and Cluanie plutons in this study, and the metasedimentary xenoliths and rafts observed in the field (this work; Neill and Stephens, 2009). The ages of the inherited zircon grains are largely consistent with grains found in the Loch Eil group of the Moine, the contaminant identified in the isotopic work by Fowler et al. (2008).

In keeping with the conclusions reached by Fowler et al. (2008), and based on the fractional crystallization models constructed, it can be invoked that the plutons evolved primarily by fractional crystallisation, with a limited degree of crustal assimilation. Based on the disparity of U-Pb emplacement ages, it can be assumed that discrete batches of melt evolved independently, their fractionation pathways depending on the crystalizing assemblage and the nature and degree of contamination from the Moine country rock, resulting in the variable geochemical signatures seen.

5.2.5 Establishing a source of melt for the Loy, Scaddle, Clunes and Cluanie intrusions

Given the geochemical profiles and mafic mineral assemblages observed both through field and petrographic work, it is invoked that a mantle source was tapped for both Loy and Scaddle. Clunes and Cluanie are significantly more evolved and are not obviously mantle derived. The absence of mafic phases seen in the field also suggested a non-mantle source. (Neill and Stephens, 2009; Stewart et al., 2001). However, their general coherence with the REE trends seen in Loy, Scaddle, and with the granites of the NHT (as reported by Fowler et al. 2008) indicates otherwise. Further, the data isotope data from Folwer et al., (2008) confidently invokves a mantle source for Cluanie, similar to the other NHT granites (the CPMA).

5.2.5.1 Glen Loy and Glen Scaddle

With the mafic enclaves and mineral assemblages seen in the field (see *Figure 50*, 51 and 57), combined with their low – moderate silica contents (See *Table 29*), Loy and Scaddle can be confidently invoked as being derived from a mantle source. Given their coherence with the data of Fowler et al. (2008) for the appinites/diorites of the NHT, it follows that Loy and Scaddle tapped a similar source – hypothesized by Fowler et al. (2008) to be in the subduction modified mantle. Fowler et al. (2008) term this source region the Caledonian Parental Magma Array (or CPMA). The CPMA shows variable degrees of isotopic enrichment, with the oxygen isotope and high Ba-Sr signature suggesting some influence from subducted pelagic sediments.

Without further isotope data from Loy and Scaddle, it is not possible to outright confirm their association with the CPMA. However, the field evidence of mafic enclaves and mineral assemblages, combined with REE and trace element trends strongly indicative mantle source, mean this can be confidently ascertained.

5.2.5.2 Clunes and Cluanie

The evolved nature Cluanie and Clunes and lack of mafic facies observed in the field both indicate that the intrusions may not be mantle derived. However, the REE and trace element coherence with the other mantle derived Newer granite plutons of a similar ages complicates matters. Further, the isotope data presented for Cluanie by Fowler et al. (2008) strongly implies a mantle source, similar to the other NHT granites.

In this regard, it could be the case that the absence of mafic lithologies at both Clunes and Cluanie was overstated. For Clunes, issues of limited exposure, sampling bias, and level of erosion down to deeper levels within the pluton could be responsible. At Cluanie, Neill and Stephens (2009) observed some mafic clots, at the time considered to be restitic rather than evidence for involvement of mafic magmas during petrogenesis. Less evolved microdiorite dykes (~61-67 wt.% SiO_2: See Table 31) at Cluanie are at the low end of the scale for crustally-derived melts but are also only found in sharp cross-cutting contact with the Cluanie pluton. The high SiO_2 contents (see *Table 30*) could be a result of extended evolution via fractional crystallization and minor crustal assimilation (Fowler et al., 2008).

The Sr - Nd and oxygen isotopic signature of Cluanie, as reported by Fowler et al. (2008) supports this line of evidence (see Figure 89). The isotope data presented for Cluanie is interpreted to imply derivation from a depleted mantle source (εNd of between 2.6 and 3.2 and ^{87}Sr ^{86}Sr between 0.7047 and 0.7052 can be interpreted as a clear mantle signature). Fowler et al. (2008) therefore invoke a similar source to the rest of the NHT plutons – the CPMA. More specifically, Cluanie is one of the two the most isotopically depleted NHT melts (alongside Glen Dessary). These are hypothesized to have been derived from a subduction-modified arc source or lithospheric mantle, potentially with some involvement of the asthenospheric mantle (Fowler et al., 2008).

There is currently no isotope data available for Clunes, which limits the extent to which a source can be established.

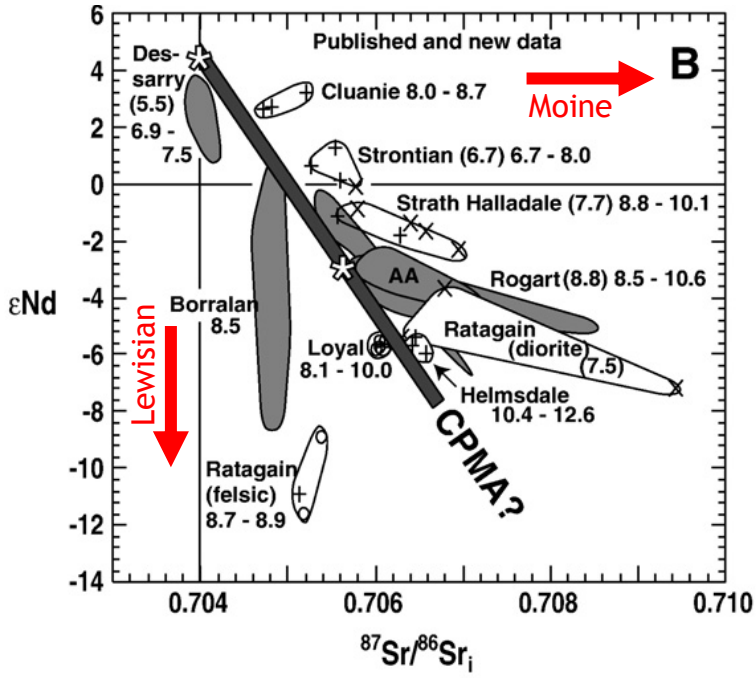

Figure 89: From Fowler et al., 2008. Nd–Sr–O isotope data for the Northern Highland high Ba–Sr suite. The CPMA is a hypothetical Caledonian Parental Magma Array, and is plotted by Fowler et al (2008) at the approximate intersection of fields for the individual plutons. Cluanie plots close to the CPMA, implying this is a viable source of melt. Red vectors indicate increasing contamination from different sourcers (Lewisian and Moine). Cluanie can be seen to follow the vector for Moine contamination and has the highest ENd value alongside Glen Dessary, indicating little contamination form the Lewisian.

Given the apparent lack of mafic facies resported at Clunes (Sterwart et al., 2001), it is worth considering that Clunes and/or Cluanie may be petrogenetically distinct from the rest of the NHT plutons. An alternative hypothesis for their genesis is melting of a lower crustal garnet amphibolite underplate, as is described by Chung et al. (2003) in Southern Tibet.

In this scenario, the mantle derived isotopic signature of Cluanie presented by Fowler et al. (2008) is explained by the isotopic similarity of the mantle and lower crust beneath the NHT (an artefact on numerous mantle additions being added to the lower crust during the Grampian Orogeny). While there is little no evidence of Grampian age plutonism in the NHT, the abundance of Grampian age zircons in the Cluanie dataset stand as evidence that melting did occur in beneath the NHT as this time (see *Section 6.1.3)*.

Melting of a mafic underplate is modelled to have occurred in Tibet, where remelting of an eclogitic – garnet amphibolite underplate formed by prior calk-alkaline magmatism produced a suite of rocks that show strong geochemical similarities to adakites (Chung et al., 2003).

The major and trace element profiles described by Chung et al. (2003) are broadly similar to those seen in Clunes and Cluanie. For the Tibetan suite, SiO_2 ranges from 53 – 73 wt.%, while Al_2O_3 values range from 15 – 19% wt% (SiO_2 and Al_2O_3 being the key major element oxides for adakite classification). The samples from Clunes and Claunie all fall within these ranges.

Melting of a mafic underplate would be expected to produce high Sr/Y and La/Yb signatures, since garnet and amphibole are likely present as residual phases at lower crustal depths (the stability of garnet and amphibole as fractionating phases over plagioclase is a major control of Sr and Y content). Indeed, Chung et al. (2003) reports the melts produced from the south Tibetan mafic underplates to have high Sr/Y and La/Yb ratios.

While Clunes and Cluanie have high La/Yb ratios, there is a clear decoupling seen in Sr/Y ratios. The Sr/Y ratio for the samples from Clunes range from 55 – 125; while the ratios for the Cluanie samples are much lower at 15 – 30. As can be seen in Figures 90 and 91, this results in Cluanie plotting within the calk – alkaline field

and Clunes plotting within adakite field (fields as used by Chung et al. (2003) as defined by Defant and Drummond (1990)).

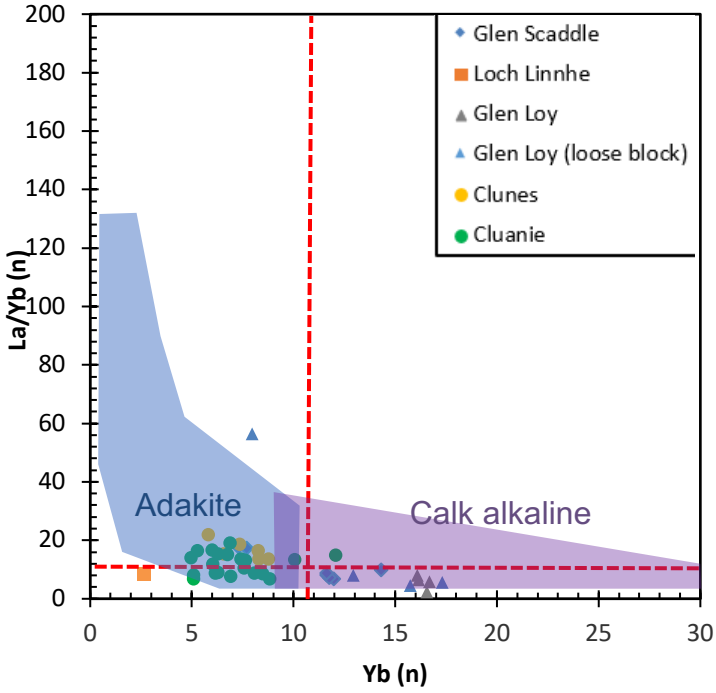

Figure 91: Sr/Y vs Y (pre-normalisation) with coloured zones taken from Martin, 1986 to define Adakite (blue) or Calk alkaline (purple) domains. The red dashed lines define the Adakite domains as defined by Defant and Drummond, 1990.

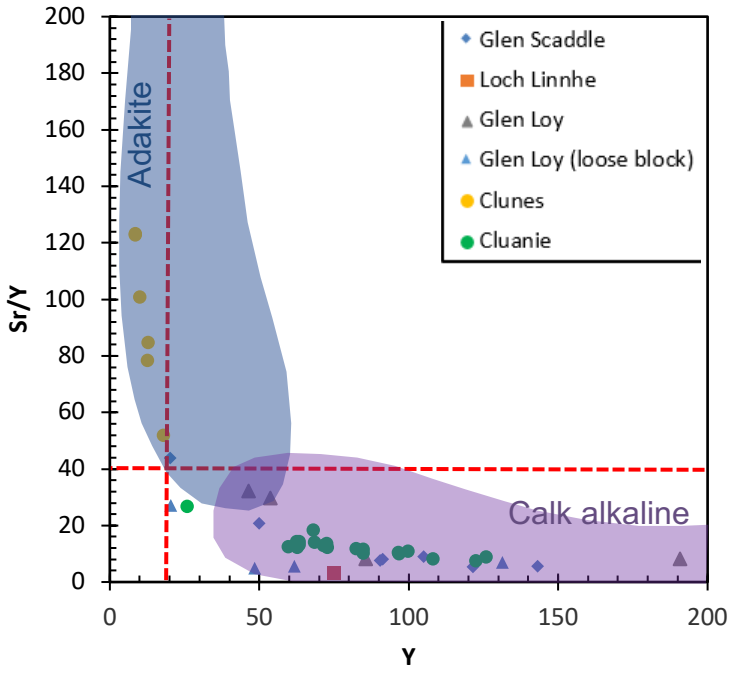

Figure 90: Chondrite normalised La/Yb vs Yb (normalisation values from Sun and Mcdonough, 1989). Coloured domains are taken from Martin, 1986, and define Adakite or Calk alkaline domains. The red dashed lines define the Adakite domains as defined by Defant and Drummond, 1990.

Ni and Cr content are also an important consideration when establishing the melt source tapped by an intrusion. High values are a proxy for degree of involvement with the mantle wedge (Cr > 80ppm; Ni > 50ppm). With the exception of one sample, the samples from Clunes all have lower concentrations of Ni and Cr (CL-16-5 has 52ppm Ni, but only 76ppm Cr). Such values do not indicate mantle or mantle wedge involvement in the genesis of Clunes. The samples from Cluanie tell a far less straightforward story, with values for both Ni and Cr varying dramatically. Ni content ranges from 2.3 – 130.7ppm, and Cr content ranges from 5.2 – 57.2. This complex trend is largely at odds with the rest of the data from Cluenie and may be an artefact of mineral fractionation or accumulation.

The geochemical profile for Clunes is largely similar to that described by Chung et al. (2003) for the lower crustal underplate melts of southern Tibet, compatible with the lack of mafic facies reported in the intrusion by Stewart et al. (2001) and the low Ni and Cr content of the samples. Without further isotope work it is not possible to be entirely prescriptive about a source, but it is viable that Clunes may be formed by melting of the mafic lower crust.

Cluanie does not seem to fit with the model, given its low La/Y ratio. The data gathered in this study neither precludes nor confirms the conlusions of Fowler et al. (2008) – that Cluanie is formed from melting of the CPMA.

As demonstrated above, it is difficult to be prescriptive about the sources of melt for the plutons at Scaddle, Loy and Clunes without isotopic analysis. However, while further isotopic work from Loy, Scaddle and Clunes would be useful to help determine the level of crustal involvement in their evolution, it would not be able to out right confirm a source of the magmatism (as previously stated, a mafic underplate the beneath the NHT can be expected to be isotopically similar to the mantle). Thus, the discussion of a source of melt for the plutons remains largely speculative.

5.2.6 Tectonic implications of new geochemical data

In the context of the NHT Newer granite intrusions, melt generation is intrinsically linked in some way to the north-directed subduction of Iapetus oceanic lithosphere during the Baltica and Laurentia collision (e.g. Soper et al., 1992). This is reflected in the geochemical profiles of the plutons studied, with the typical markers of subduction related magmatism being present (e.g. Nb, Ta troughs when normalised to primitive mantle standards). It is generally accepted that subduction had ceased when the emplacement of the majority of NHT granites occurred – traditionally accepted models involve collision beginning at 435Ma and lasting until 425Ma (Soper 1982). This is largely incompatible with the intrusion of mantle derived melts of this age (e.g. Loy and Scaddle).

With more recent models involving collision beginning as early as c. 450M now being explored (as outlined in *Section 6.1.4*), what can the geochemical profiles of these bodies reveal about the timing of certain of certain orogenic events?

5.2.6.1 Slab break off as a mechanism behind mantle melting

The slab break-off model is often used to explain the temporal expression of magmatism associated with the Baltica – Laurentia collision, especially with regards to the pulse of magmatism occurring seemingly after subduction had ceased (Atherton and Ghani, 2002). Atherton and Ghani draw on models of Davies and von Blanckenburg (1995), who used a slab break off model to explain seemingly syncollisional magmatism postdating subduction in the Tertiary Alps.

An extended period of mantle derived, calk-alkaline appinitic and granitic magmatism; extensive strike slip faulting; and rapid uplift leading to granite unroofing, are all features of the British Caledonian landscape that are also detailed by Davies and von Blanckenburg as being essential indicators of slab break-off (Fowler et al. 2008; Atherton and Ghani, 2002; Mendum and Noble, 2010, respectively).

What Atherton and Ghani's discussion does not fully address is the timeline over which slab break-off occurred in the British Caledonides. The appinites and granites associates with the Scandian phase of the orogeny are detailed to have been emplaced from c. 435 – c. 390 Ma, with an apparent maxima at c. 410 – 400 Ma (Atherton and Ghani, 2002; Oliver et al., 2008). These intrusions are assumed to have been emplaced through the entire process of subduction, collision and break off (Atherton and Ghani, 2002; Oliver et al., 2008).

Modelling of slab-break off, and the timelines over which it takes place, was carried out by van Hunen and Allen (2011), specifically with regards to the Paleogene Arabia-Eurasia collision and the development of the Turkish Iranian plateau. Van Hunen and Allen use 2-D and 3-D models to investigate the dynamics of break-off following the attempted subduction of continental crust. Their modelling focuses on the timescales that orogenic belts and subduction zones evolve.

They conclude that the delay time expected between initial collision and final slab break off during the orogenic cycle depends largely on the strength and age of the oceanic plate being subducted. Young, weak slabs can be expected to

rupture just 10 Myr after collision, while older stronger slabs are modelled to tear after around 20 Myr.

Parallels between the Caledonian orogeny and the Arabian – Eurasia collision zone are numerous. In one regard, the age of the subducting oceanic crust is largely similar, being around c. 200Ma for both Iapetus and Neo-Tethyan oceanic lithosphere (Stone, 2012; Van Hunen and Allen, 2011, respectively). Thus, the conclusion that Neo-Tethyan oceanic lithosphere took c. 25 Myr to rupture might be used as an analogue for Scandian collisional events. This comparison is naturally limited by the lack of information on important variables such as the angle the slab was being subducted, the occurrence of discontinuities (e.g. transform faults), and whether collision was head on or oblique. Regardless, magmatism following break-off is expected to be expressed immediately after the event, and is modelled to last until extension following break-off is complete (Gerya et al. 2004). In Scotland, this point is marked by the cessation of Newer Granite magmatism, around 390 Ma.

A 25 Ma delay from initial collision and prograde metamorphism to final slab break-off is not obviously compatible with the initial Scandian collision occurring at c. 435 Ma (Kinny et al. 2003; Bird et al. 2013; Freeman et al. 1998; Dallmeyer et al. 2001). As the collision proceeds and during the formation of metamorphic belts, it is considered unlikely for mantle derived magmas to be emplaced (Song et al., 2015). Without active subduction, there is no mechanism for generating melts in the mantle wedge, and compressional tectonics will hinder the ascent of melt through the crust.

As stated in *Section 6.1.4.3*, Mantle-derived magmatism is present in the NHT in several localities. A tectonic model for Scandian collision must therefore consider the temporal distribution of mantle derived magmatism in the NHT and allow for an interval of up to tens of millions of years from initial collision and the development of the Scandian steep belt, to slab break-off. The possibility that this record of magmatism is skewed by preservation bias (specifically the poor preservation potential of arc rocks) is addressed by Miles et al., 2016. While difficult to substantiate, it is a worthy consideration when discussing the timing and volume of ‘Scandian’ magmatism.

5.2.6.2 The timing of Scandian collision

In line with the model proposed previously (*see Section 6.1.4*), it is viable to suggest that initial Scandian collision of Baltica – Laurentian continent occurred at c. 450 Ma, with regional metamorphism and considerable shortening lasting until c. 443 Ma (Bird et al. 2012; Cawood et al. 2013). Thereafter, shortening ceased and a period of slab rollback and extension may have occurred, facilitating the onset of subduction related magmatism. It is possible that the older mafic - felsic bodies at Cluanie, Loy and Glen Dessary may fall into this category, produced via melting of the subduction modified mantle wedge (Glen Loy) and perhaps the lower crust (Cluanie) (Fowler et al., 2008; Neill and Stephens, 2009).

Slab break-off is typically expressed by a significant upsurge in magmatic activity. It therefore seems most likely to have occurred beneath the NHT sometime between c. 433 Ma – c. 428 Ma, as evidenced by number of plutons of this age or slightly younger (including Clunes and Glen Scaddle) (see Table 44). The magmatic gap of five Myr from 433Ma – 428Ma is similar to that reported in the TIP (Lechmann et al., 2018). This is followed by an extended period of break-off magmatism, sourced from the SCLM, as hypothesized by Fowler et al. (2008). The total length of break-off related magmatic activity in the northern Highlands seems to be somewhat less than 20 Myr, based on ~418 Ma ages for parts of the Strontian pluton and the Ross of Mull granite (Oliver et al. 2008; Paterson et al. 1993). The reason for this protracted magmatic episode may be due to break-off occurring diachronously towards the SW in line with the oblique nature of the collision.

5.2.7.3 The meaning of the Clunes adakitic signature: implications for the Caledonian tectonic model

In accordance with the criteria outlined by Defant and Drummond (1990), Clunes can be classified as an adakite. Cluanie fulfils the criteria for adakite-like, despite its somewhat lower Sr/Y ratios. Many of the NHT Caledonian granitoids may also be termed 'adakite-like' based on their enriched LREEs and depleted HREE and Y contents (Fowler et al., 2008).

The fact the Clunes fulfils the geochemical parameters for adakite classification, and that Cluanie can be termed 'adakite-like', is an important consideration in the discussion of their genesis and evolution - the adakitic geochemical fingerprint can only be formed in a limited number of scenarios (as detailed in *Section 2.6.1*).

The melting or evolution of basalt in the garnet amphibolite stability field is a pervasive factor in all scenarios. The absence of plagioclase as either a residual or fractionating phase is another conditional factor. The importance of garnet, amphibole and plagioclase in the formation of the adakite signature hinges on their preferred elemental chemical composition: Y is highly compatible in amphibole and garnet, and Sr in plagioclase. Thus, fractionating or melting in the garnet and amphibole stability field in the absence of plagioclase results in Y depletion and Sr enrichment.

The complex scenarios detailed in *Section 2.6.1* must be unravelled by careful investigation both of the geochemistry of the proposed adakitic magmas (including identification of their source and subsequent history of assimilation and fractional crystallisation) and of their contemporary tectonic setting.

In this respect, slab melting seems an unlikely source for the adakitic nature of the Clunes and the 'adakite-like' nature of Cluanie. The original specification for young, hot crust is not satisfied: Iapetus oceanic crust is proposed to have been c 250 Myr old when it was subducted beneath the Laurentian margin (Stone, 2012 and references therein). Further, slab melting of any scale would be expected to produce a greater volume of adakitic melts, not a few isolated bodies (as discussed by Fowler et al. 2008). Slab melting, especially in a flat slab scenario (as proposed by Dewey et al., 2005) where a limited mantle wedge would be present, would

also fail to explain the presence of associated coeval mafic suites of non-adakitic nature (e.g. Loy and the appinites and diorites described by Fowler et al., 2008).

It is possible that melting of a lower crustal mafic underplate of older subduction related melts (likely garnet – amphibole – CPX) could have remelted to form Clunes and/or Cluanie. The occurrence of lower crustal melting would be significantly more likely post-slab break off, as the detachment of the slab initiates voluminous melting, providing a significant source of heat to the lower crust by advection. The limited magmatism prior to the proposed slab break-off event thus makes Cluanie an unlikely candidate for slab melting, as a significant heat source is lacking. This is consistent with the decoupling of the Sr/y ratio values between Clunes and Cluanie. The high Sr/Y values at Clunes are far more conducive to a source from remelting a mafic lower crust those of Cluanie.

The third petrogenetic pathway described above is also a viable source for the adakitic/adakite-like nature of Clunes and Cluanie respectively. The occurrence of normal-arc and adakitic or adakite-like samples within close spatial and temporal proximity bears resemblance to the normal-arc and adakitic rocks of the Balkan – Carpathian arc (Kolb et al., 2012). Kolb et al (2012) was successful in identifying two distinct fractionation and assimilation paths – with the adakitic rocks experiencing high pressure amphibole fractionation in the lower crust, followed by ascent and plagioclase fractionation in the upper crust. The normal arc magmas evolved only through upper crustal fractionation pathways.

As stated previously, given the geochemical data, and in accordance with the work by Fowler et al., 2008, it is apparent that Cluanie evolved by fractional crystallization with minor crustal assimilation. Clunes is more difficult to comment on given the REE and trace element similarity of the samples. The REE plot for Clunes and Cluanie suggests garnet is not a major fractionating phase; HREE depletion is only moderate (as stated previously, the fractionation between LREEs and HREES is an artefact of relative LREE enrichment). Thus, high pressure fractionation of amphibole in the lower crust is a viable method for producing the adakitic signature. Cluanie stands as potential evidence for said fractionation pathway, with the data forming array projecting into the adakitic zone.

5.2.7.4 Towards a model

A possible model for the geochemical profiles of Loy, Scaddle, Clunes and Cluanie which takes into account the adakitic nature of Clunes and the adakite-like nature of Cluanie while also adhering to the conclusions reached in previous sections is presented below and summarised in Figure 92.

Baltica – Laurentia collision occurs at ~ 450 Ma (see *section 6.1.4.1*). Glen Loy and Cluanie are generated after collision and crustal shortening had ceased, during a period of slab rollback and extension. Mantle wedge melting provides a feed for Cluanie, whose evolved nature and 'adakite-like' signature results from a period stalling in the lower crustal hot zone, where it fractionates extensively at a depth where amphibole and garnet are stable, while also incorporating some Grampian age material (hence the protracted age range seen in the U-Pb zircon dataset). Glen Loy is also sourced from the mantle wedge, and evolves by fractional crystallization, while remaining comparatively mafic. This model is supported by the isotopic evidence from Fowler et al., 2018 – the isotopic signature indicating a source in the enriched CPMA would be maintained during these processes.

Continued slab roll back and extension initiates crustal scale strike slip faulting, including along Great Glen Fault Zone (GGFZ). Cluanie and Glen Loy are channelled to the surface associated with early movement of the Great Glen Fault Zone, also perhaps responsible for the emplacement of Linnhe – although further geochemical and structural work is required to investigate the source of melt for this intrusion.

Slab break off occurs at c. 433 – 428Ma, alluded to by the magmatic gap observed across the NHT terrane (similar to that seen in the Turkish Iranian plateau; Lechmann et al., 2018). Melting of the subduction modified lithospheric mantle following this break-off event is widespread. This voluminous pulse of magmatism produces melt for Glen Scaddle, which undergoes similar processes experienced by Cluanie, experiencing fractional crystallization at the base of the lower crust in the garnet and amphibole stability field. The additional heat source from melting and mantle convection produced by slab break-off initiates re-melting mafic lower crust/Grampian age underplate, with additional mantle derived

components. This results in the strongly adakitic signature of Clunes, while being slightly less evolved than Cluanie.

It is also necessary at this stage to acknowledge Rb – Sr age acquired by Powel, (1983). As discussed previously (Section 2.5.2), after applying the correction for Rb – Sr ages suggested by Miles et al. (2016), the crystallization age for Cluanie works out at 433+/-4 Ma. Not only is this within error of the age required in this work, it is also in line with age required for Glen Loy. Accepting the crystallisation age for Cluanie as 433 +/-4Ma would alter slightly the line of enquiry presented in this work, in that it wouldn't necessarily require the timing of 'Scandian' (Baltica - Laurentia) collision to be reconsidered. Briefly, this scenario could entail c. 438 dating melt generation, and associated with subduction, and emplacement taking place at 433 Ma. The line of enquiry presented here is based on the ages acquired in this body of work. It is necessary that further enquiry is done to consider the geodynamic model implied by the ages presented by Powel 1983.

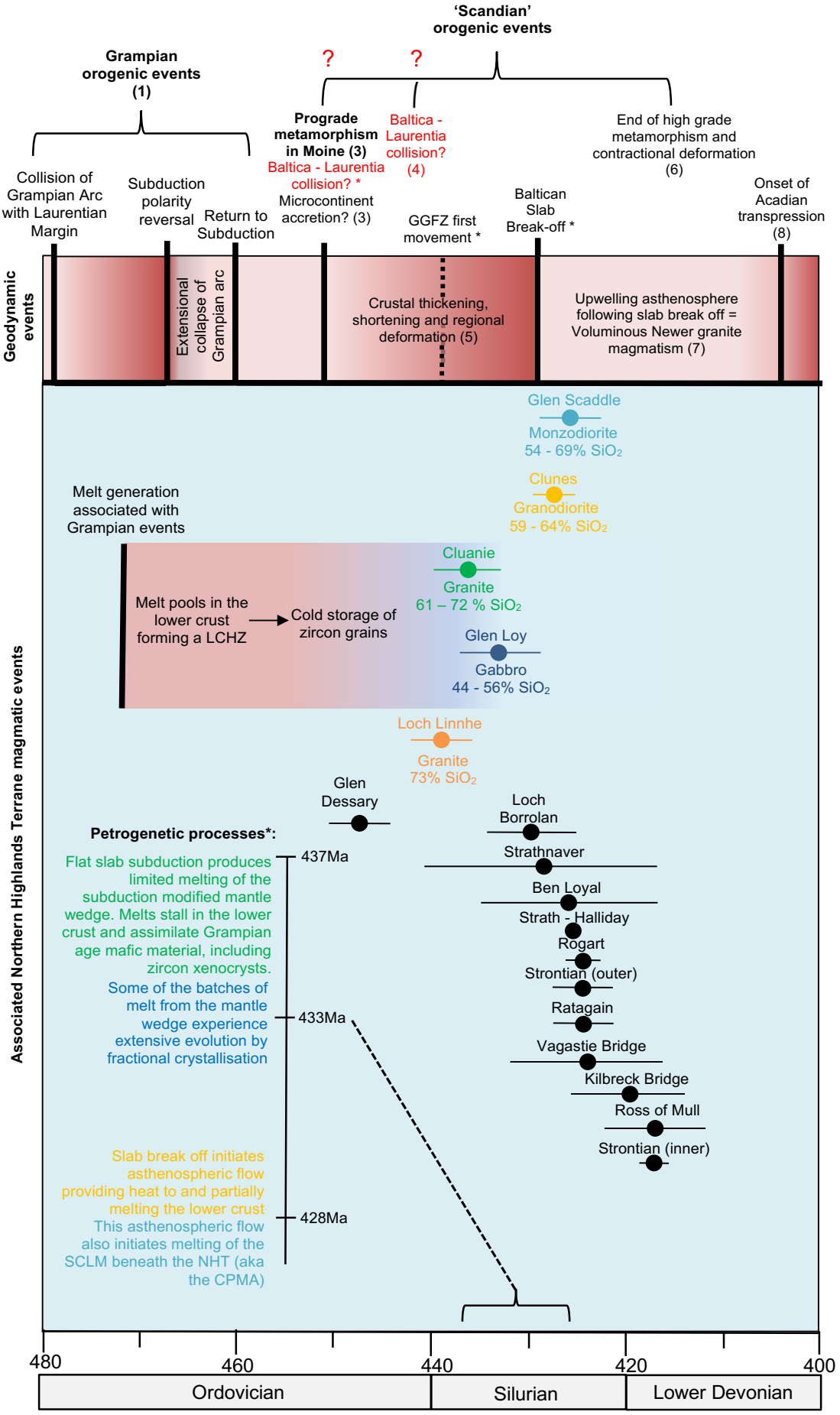

Figure 92: Timeline of events is as discussed in this work. schematic timeline of Caledonian orogenic events. References are numbered as follows: (1) Dewey, 2005, (2) Jackson et al., 2018, (3) Bird et al., 2015, (4) Freeman et al., 1998, (5) Chew and Strachan, 2013, (6) Mako et al., 2019 (7) Stewart et al., 2008 (8) Mendum (2012). *Marks hypotheses presented in this work. The ages of the NHT intrusions not studied directly in the work (in black) are as in Table 40.

6. Conclusions

This project set out to use U – Pb single grain zircon geochronology, bulk rock geochemistry field observations, petrogenetic work and EPMA investigation of crystal chemistry to address the following **aims** and *objectives*.

- **Determine crystallization ages for the Glen Loy, Cluanie and Loch Linnhe intrusions of the NHT** *(U-Pb zircon dating via La-ICPMS).*

- **Establish the source of melt, evolutionary pathway and emplacement method for the intrusion at Glen Loy, Glen Scaddle, Clunes and Cluanie** *(through interpretation of major and trace elemental datasets acquired via XRF and ICP MS respectively).*

- **Explore the previous geochemical classification of the Clunes and Cluanie intrusion as TTG-like or adakitic, and further unravel the implications of these classifications with regards to the model for their genesis and evolution** *(through modelling specific aspects of genesis, ascent and evolution using major and trace element data).*

- **Assess the coherence of the newly acquired data to the currently accepted timeline of the geodynamic events associated with final Baltica – Laurentia (Scandian) collision.** *This will involve a discussion of the implications of recent literature invoking the need to revise the timeline (e.g. Bird et al., 2013; Cawood et al., 2015).*

Crystallization ages of 437.9 +/- 3.3 Ma, 434.6 +/- 3.9 Ma and 439.4+/- 3.14 Ma were returned from the plutons at Cluanie, Loy and Linnhe respectively (errors given as 2σ). Inherited grains from each dataset reflect provenance from the Moine (Loch Eil division) sediments into which they were emplaced (from crystallization age up to c. 1700 Ma). A spread of ages upwards of the final crystallization age seen in the datasets for Loy and Cluanie (from crystallization age up to c. 477 Ma), interpreted as an indication of an extended residence in a lower crustal hot zone, and the incorporation of antrcryts from previous batches of melt.

Glen Loy, Scaddle and possibly Cluanie are sourced from the lithospheric mantle beneath the Scottish Caledonides. Loy and Cluanie are emplaced prior to the break-off of the Baltican slab beneath Laurentia and are thus sourced from a subduction modified mantle wedge. Scaddle is produced from voluminous melting

of the lithospheric mantle initiated by slab break-off (c. 433 – 428 Ma). Clunes' origin is less equivocal. Its adakitic nature may, like Cluanie, be produced by extensive fractional crystallization of a mantle derived magma in the lower crust. However, it is also conceivable that Clunes is produced by melting of a mafic lower crustal underplate, triggered by the additional heat provided by the widespread melting associated with Baltican slab break – off.

The newly acquired U-Pb zircon isochrons highlight issues with timeline of orogenic events and Newer granite magmatism associated with the so-called Scandian orogeny. Such issues are previously raised by Bird et al. (2013), Cawood et al. (2015) and Dewey, (2005) and are summarised below.

- The definitive mantle derived nature of Loy and Scaddle is inconsistent with emplacement during a period of peak crustal thickening, as is inferred in the currently upheld model of Oliver et al. (2008), Atherton and Ghani. (2002).

- Crystallization ages from Glen Loy, Claunie and Loch Linnhe, predate early GGFZ movement as it is currently understood. This is not compatible, since the GGFZ appears to be an important mechanism controlling the emplacement of the bodies.

A rethinking of the model for the Scandian phase of the orogeny is proposed, at all times acknowledging the requirement for further work. This model is outlined in Table 42.

Table 42: Proposed geodynamic model for the Scandian phase of the Caledonian orogeny

450Ma: Baltica Laurentia (Scandian) collision	Scandian collision takes place not at c. 430Ma as previously hypothesized (Oliver et al., 2008; Atherton and Ghani, 2002 and references therein), but at c. 450Ma, supported by evidence of shortening and metamorphism presented by Bird et al., 2013 and Cawood et al., 2015.
441Ma: First movement of the GGFZ.	First movement of the Great Glen Fault takes place any time after c. 441, demarked by the emplacement of the Linnhe Granite. Continued movement on the fault zone and accommodation via low strain zones during Scandian upright folding is the mode of emplacement for many more Newer granites, including Scaddle and Clunes.
437Ma: Emplacement of the Cluanie pluton	Melt associated with extension and post collisional thickening and a return to flat slab subduction produces limited melting of the subduction modified mantle wedge. The batch of melt that forms Cluanie stalls in the lower crustal hot zone, where it incorporates Grampian age mafic material, including numerous zircon xenocrysts.
433Ma: Emplacement of the Glen Loy Pluton	Melting of the mantle wedge continues to produce occasional batches of melt, including Glen Loy, which experiences extensive evolution by fractional crystallization. Some residence in the deep crustal hot zone results in the inheritance Grampian age zircon grains.
Slab break off: 433 – 428Ma.	A 5 Myr gap in magmatic activity indicates the timing of slab roll back followed by the detatchement of the Baltican slab beneath Laurentia.
Emplacement of Glen Scaddle **c. 428Ma**	Voluminous melting associated with slab break of is manifested in widespread Newer granite magmatism. Melting of the SCLM is initiated by mantle flow following break off and produces many mantle derived melts seen throughout the NHT. The timing of Scaddle's emplacement coincides with large-scale Scandian reworking, as evidenced by the synmagmatic high-strain features seen in the Scaddle body. Scaddle evolves primarily by fractional crystallization of an assemblage which eventually leads to a near adakitic character.
Emplacement of Clunes. **c. 428Ma.**	This pulse of melting generated by asthenospheric flow associated with slab break-off provides heat to the lower crust, which may itself have been formed of a mafic underplate formed during previous magmatic episodes (e.g. Grampian age melting). Thus, partial melting produces a melt with an adakitic character.

Further Work

Further field mapping and structural investigation of the Loch Linnhe Granite should be carried out to establish its relationship with the GGFZ. Confirming its kinematics may elucidate further details of GGFZ first movement, which would in turn be greatly beneficial for the investigation of Baltica – Laurentia collision. The possibility that the Loch Linnhe Granite represents a slice of 'exotic' material displaced by fault movement may be investigated by a further zircon provenance study and geochemical work. This line of enquiry would also require the identification of a source body in the Grampian terrane. The Abriachan granite is be investigated in this regard. These lines of enquiry are currently being investigated in collaboration with Iain Neil, Eddie Dempsey, Anna Bird and Rob Strachan.

Further detailed structural mapping of the other plutons (Loy, Scaddle, Clunes and Cluanie) coud also reveal more information their relationship to the deformation history of the region, a critical element of dating the emplacement of intrusions that was not fully explored in this work due to time financial constraints.

The older U-Pb zircon ages acquired in this study (in spite of data quality and zircon choice) do open questions on whether the LA – ICPMS analyses are providing the 'true ages'. A project to re-date a pluton with an already excellent CA-ID-TIMS constraint via LA-ICPMS (Strontian) is currently underway.

Further investigation into the factors controlling the formation and non – formation of Cu and Au deposits could be carried out using the analogue of the Scottish Caledonides. The geodynamic setting is largely similar to the TIP, where economically significant deposits of Cu and Au are being prospected for, and yet the Newer granite bodies are completely barren. Understanding the factors controlling the formation and non-formation of ore deposits could be significant for mineral prospecting efforts globally.

Appendices

Appendix A: Thin section preparation

Rock Cutting

For the preparation of thin sections, chips of dimensions 3cm by 2cm were cut using the CS10 Cut-Off saw. The chips were coated in resin to ensure the specimen was cohesive. The resin was prepared by mixing 3ml of epo-heat resin and 1.2ml of hardener. The chips were left in the furnace overnight to set.

Polishing

The resin coated chips were polished using aluminium oxide powder and water. 30 micron powder was used first to; remove damage left by the saw; remove all resin; and achieve a flat surface in on the sample. 20μm powder was used to remove the scratches left by the 30 micron powder. 12μm powder was used until a uniform reflection and shine could be seen over the sample surface.

Mounting

The chips were mounted polished glass dimension 3cm by 2cm using Buehler Epo-thin 2 resin (3ml) and hardener (1.2ml). The mixture was stirred carefully to avoid the incorporation of bubbles and dabbed onto the surface of the rock chip. The glass slide lowered carefully into place on top (the frosted side in contact with the chip). The samples was placed under a weighted spring press for 8 hours.

Cutting

A Logitech trim saw with vacuum chuck was used to cut mounted chips down to a thickness of approximately 1mm. 3 slides were mounted into the vacuum chuck and steadily passed across the blade. The chips were ground down to 50μm using the grinding device of the Logitech trim saw.

Grinding and Polishing

The chips were returned to the aluminium oxide powder and water mixture to take them down to a thickness of 30μm. This was initially done using the 20μm powder. The 12μm powder was used once the section as approaching the desired thickness. The section was checked at regular intervals to prevent over polishing. This was judged by eye with the Michel Levy birefringence/interference colour chart.

Once the sections were the correct thickness, they were ground briefly on the silicon carbide abrasive papers of grit size P1200, P2400, P4000. The papers were wet and the sections ground over them steadily in a figure of 8 motion. The samples were checked regularly with the reflected light microscope. These papers were used to reduce imperfections introduced by the previous step of grinding. Once no further improvements were observed, the next grit size was used.

Polishing was carried out in order to remove scratches and imperfections introduced by the grinding. The sample is mounted onto a Kemet 300 series polishing device with a pad wetted with 1μm alumina powder and water. The mounts were polished until mineral faces were clear and unscratched.

Appendix B: Glen Loy and Glen Scaddle field measurements

Table 43: Field measurements from Glen Loy.

	Pegmatite	
Location	Width (Cross sectional expression)	Orientation*
1126 8209	4	55
1145 8156	3.3	51
1190 8332	3	65
1271 8189	5	61
1334 8100	4	69
1335 8302 (1)	5	70
1335 8302 (2)	5.5	20
1355 8274	4	87
1356 8282	4.5	55
1368 8295	4.5	30
1377 8256	2.5	41
1385 8249	2	24
1392 8250	3.5	77
1393 8242	3	82
1392 8264	3.2	45
1428 824	5.5	28
1432 8266	3	49
1451 8265	3.3	66
1451 8208	2.7	72
1455 8262	3.3	82
1455 8210	4.1	71
1458 8196	3.5	59
1462 8270	2.8	79
1469 8189	3	68
	Shear Zone	
Location	**Width (Cross sectional expression)**	**Strike / Dip of fabric**
1124 8210	0.75	51 / 80- 90
1445 8209	0.5	30 / 65
1162 8340	1	15 / 77
1353 8283	1	57 / 75
1390 8250	0.5	60 / 80
1391 8248	0.5	48 / 80 - 90
1445 8212	0.75	48 / 73
	Magmatic fabric	
Location	**Strike**	**Dip**
1272 8138	12	62 (NW)
1310 8282	2	60 (NW)
1355 8215 (1)	2	66 (NW)
1355 8215 (2)	5	82 (NW)
1377 8256 (1)	65	65 (NW)
1377 8256 (2)	63	62 (NW)
1377 8256 (3)	60	71 (NW)
1377 8256 (4)	62	74 (NW)
1445 8209	30	70 (NW)

Table 44: Field measurements from Glen Scaddle.

	Pegmatite	
Location	**Width (Cross sectional expression)**	**Orientation***
9670 6840	>5	171
9700 6842	>5	165
9755 6805	>5	72
9755 6800	>5	125
9753 6772	>5	69
9820 6831	>5	137
9835 6780	>5	161
9834 6765	>5	117
9834 6761	>5	135
9833 6755	>5	137
9831 6753	>5	131
9850 6833	>5	140
9851 6797	>5	151
9852 6781	>5	74
9853 6775	>5	101
9858 6761	>5	146
9860 6759	>5	72
9862 6752	>5	98
9870 6748	>5	103
9900 6800	>5	102
9900 6795	>5	159
9911 6755	>5	39
9932 6750	>5	45
9954 6850	>5	171
9960 6860	>5	161
9971 6862	>5	133
0090 6999	>5	91
0072 6767	>5	71

	Tectonic fabric	
Location	**Strike**	**Dip**
9935 0634	129	82
9885 6830	132	80
0095 6563	130	83
0089 6561	125	85
	Magmatic fabric	
Location	**Strike**	**Dip**
9759 6319	162	52
	150	62
	162	52
9975 6860	155	72
	160	62
9885 6830	168	69
9810 6811	195	65
	168	56

Appendix C: Major and trace element data

Glen Loy	SiO_2	Al_2O_3	Fe_2O_3	FeO	MgO	CaO	Na_2O	K_2O	TiO_2	MnO	P_2O_5	LOI	Total
IN-GL-16-1	44.43	20.78	12.29	11.06	4.16	9.96	3.37	0.651	2.084	0.100	0.850	**1.32**	98.96
IN-GL-16-2*	**41.82**	**15.32**	**12.28**	**11.05**	**10.88**	**10.10**	**2.43**	**0.566**	**3.488**	**0.121**	**0.202**	**1.76**	**100.31**
IN-GL-16-3	45.57	19.71	12.45	11.21	3.86	9.24	3.47	0.645	1.828	0.129	1.553	**1.85**	99.85
IN-GL-16-4	46.87	19.91	11.39	10.25	4.15	7.30	3.94	1.264	2.075	0.116	0.691	**2.14**	99.38
Glen Loy (LB)	**SiO_2**	**Al_2O_3**	**Fe_2O_3**	**FeO**	**MgO**	**CaO**	**Na_2O**	**K_2O**	**TiO_2**	**MnO**	**P_2O_5**	**LOI**	**Total**
GL-LB-1	55.43	16.07	10.65	9.58	4.68	4.40	0.46	4.001	1.045	0.156	0.627	**1.86**	99.32
GL-LB-2*	**49.78**	**8.73**	**12.35**	**11.11**	**12.94**	**10.30**	**1.12**	**0.448**	**1.103**	**0.193**	**0.074**	**2.28**	**99.49**
GL-LB-3	55.97	20.58	8.03	7.22	2.16	4.36	3.62	3.072	1.353	0.056	0.141	**0.15**	100.00
GL-LB-4*	**48.96**	**10.13**	**12.31**	**11.08**	**13.05**	**11.29**	**1.56**	**0.706**	**1.388**	**0.194**	**0.283**	**0.12**	**99.33**
Glen Scaddle	**SiO_2**	**Al_2O_3**	**Fe_2O_3**	**FeO**	**MgO**	**CaO**	**Na_2O**	**K_2O**	**TiO_2**	**MnO**	**P_2O_5**	**LOI**	**Total**
GS17-2	62.55	16.90	4.64	4.17	2.53	4.80	4.51	1.778	0.954	0.069	0.133	**0.71**	99.52
GS17-3	53.59	18.23	8.35	7.52	3.59	6.82	4.24	2.706	1.141	0.081	0.349	**0.42**	99.94
GS17-4	55.43	16.35	8.02	7.22	4.73	6.31	3.95	1.959	1.679	0.120	0.407	**0.99**	99.95
GS17-5	59.20	21.30	3.09	2.78	1.06	4.60	5.49	2.917	0.848	0.042	0.345	**1.06**	99.90
GS17-6	58.04	21.07	4.36	3.92	1.41	6.07	5.41	2.133	1.021	0.052	0.303	**0.04**	99.79
GS17-7	69.13	16.78	2.13	1.92	0.78	2.48	5.32	1.827	0.380	0.023	0.097	**0.84**	99.84
Clunes	**SiO_2**	**Al_2O_3**	**Fe_2O_3**	**FeO**	**MgO**	**CaO**	**Na_2O**	**K_2O**	**TiO_2**	**MnO**	**P_2O_5**	**LOI**	**Total**
CL-16-1	63.35	16.65	4.25	3.83	2.08	3.95	5.14	1.957	0.721	0.068	0.238	**0.92**	99.51
CL-16-2	63.70	16.71	4.11	3.70	2.01	3.54	5.17	2.121	0.695	0.062	0.231	**1.16**	99.69
CL-16-3	64.34	16.78	4.23	3.81	2.37	4.04	5.01	1.856	0.709	0.066	0.227	**0.05**	100.05
CL-16-4	63.20	16.51	4.57	4.11	2.86	4.07	4.95	1.780	0.762	0.069	0.261	**1.02**	99.85
CL-16-5	59.70	17.21	4.92	4.43	3.06	4.92	5.12	1.529	0.881	0.081	0.327	**2.10**	99.84
CL-16-6	61.61	16.79	4.69	4.22	3.04	4.90	5.24	1.443	0.791	0.073	0.241	**1.02**	99.57
Loch Linnhe	**SiO_2**	**Al_2O_3**	**Fe_2O_3**	**FeO**	**MgO**	**CaO**	**Na_2O**	**K_2O**	**TiO_2**	**MnO**	**P_2O_5**	**LOI**	**Total**
LL17-1	73.16	14.68	1.56	1.40	0.26	0.07	5.04	4.042	0.263	0.017	0.079	**0.67**	99.99

Table 45: Major element compositions and LOI values for Glen Loy, Glen Scaddle, Clunes and Cluanie. Samples marked * are identified as cumulate

Table 46: Major element compositions and LOI values for Cluanie.

Cluanie	SiO_2	Al_2O_3	Fe_2O_3	FeO	MgO	CaO	Na_2O	K_2O	TiO_2	MnO	P_2O_5	LOI	Total
IN/20-7/2	69.00	16.23	1.96	1.77	0.53	2.39	6.06	2.41	0.25	0.05	0.09	**0.17**	100.77
INC 1	70.39	16.73	1.87	1.68	0.51	2.26	6.00	2.40	0.27	0.05	0.09	**0.21**	102.24
INC 2	69.15	15.96	1.58	1.42	0.47	2.16	6.18	2.29	0.20	0.04	0.09	**0.50**	99.56
INC 4	68.85	16.77	2.26	2.03	0.61	2.34	5.88	3.05	0.28	0.06	0.08	**0.40**	102.20
INC 8	70.15	16.41	1.92	1.73	0.50	2.15	5.93	2.45	0.25	0.05	0.09	**0.09**	101.63
INC 9	69.85	16.14	1.93	1.74	0.46	2.17	6.39	2.37	0.22	0.05	0.07	**0.22**	101.40
IN9-7/3	69.45	16.79	2.14	1.92	0.84	2.08	6.57	2.40	0.30	0.05	0.14	**0.47**	102.70
IN/21-7/4	68.96	16.59	1.99	1.79	0.75	2.18	6.28	2.32	0.27	0.05	0.11	**0.17**	101.30
IN/21-7/3	68.19	15.44	2.58	2.32	1.31	2.47	5.50	2.63	0.33	0.06	0.18	**0.23**	101.01
IN/3-7/5	70.14	15.70	2.51	2.26	0.60	1.79	5.40	2.67	0.35	0.05	0.10	**0.26**	101.56
IN/3-7/1	72.27	16.57	0.97	0.87	0.36	1.93	5.94	2.17	0.19	0.03	0.07	**0.13**	101.37
INC 10	69.57	16.49	1.50	1.35	0.33	1.48	6.51	2.36	0.18	0.03	0.07	**0.18**	99.87
IN/20-7/4	71.15	16.50	1.34	1.20	0.30	1.62	6.52	2.28	0.14	0.03	0.06	**0.15**	101.14
IN/3-7/4	67.51	16.83	3.21	2.89	1.23	3.03	5.56	2.03	0.47	0.06	0.22	**0.39**	103.04
IN/27-6/2	65.96	16.45	3.30	2.97	1.30	2.34	5.78	1.97	0.48	0.06	0.19	**0.67**	100.79
IN/24-7/1	67.52	17.32	3.36	3.02	1.30	3.09	6.02	2.18	0.49	0.06	0.23	**0.32**	104.58
INC 3	66.52	15.79	3.68	3.31	2.09	3.35	5.24	1.82	0.57	0.05	0.19	**1.46**	102.63
INC 5	64.73	16.27	3.72	3.35	2.12	3.63	5.33	1.83	0.62	0.05	0.19	**1.18**	101.84
INC 6	61.01	16.85	5.45	4.90	3.17	4.14	5.12	2.01	0.99	0.09	0.31	**0.71**	104.03
INC 7	61.18	16.79	5.50	4.95	3.84	1.85	4.97	1.96	0.95	0.09	0.31	**2.22**	102.40

Table 47: Concentrations of high field strength elements, large ion lithophile elements, and transition metals. Samples marked * are identified as cumulates.

ID.	Glen Loy													
	Sr	Ba	Rb	K	Zr	Hf	Ta	Nb	U	Pb	Th	Ni	Cr	Cu
IN-GL-16-1	1601.70	246	13.16	5451	52.48	2.18	0.20	5.54	0.24	3.42	0.84	4.22	9.64	22.82
IN-GL-16-2*	**712.71**	**133**	**6.28**	**4928**	**84.48**	**2.84**	**0.28**	**6.67**	**0.20**	**2.23**	**0.43**	**57.51**	**48.93**	**24.07**
IN-GL-16-3	1578.88	152	17.86	5540	199.42	4.53	0.16	4.64	1.39	7.13	1.62	6.34	10.89	34.95
IN-GL-16-4	1494.77	549	31.38	10500	46.17	1.74	0.30	7.79	0.42	3.37	0.97	8.42	11.03	10.79
GL-LB-1	558.05	1184	152.42	32373	20.56	0.72	0.52	11.60	1.82	6.85	1.40	24.93	57.28	210.17
GL-LB-2*	**242.86**	**113**	**8.91**	**3941**	**47.76**	**2.11**	**0.19**	**4.01**	**0.62**	**2.53**	**3.43**	**226.03**	**634.99**	**119.56**
GL-LB-3	940.52	1123	119.59	25040	131.28	3.43	0.74	17.06	1.75	17.84	28.95	16.24	39.53	33.85
GL-LB-4*	**351.82**	**127**	**11.84**	**5923**	**60.80**	**2.63**	**0.29**	**6.54**	**1.39**	**3.17**	**5.25**	**138.67**	**647.48**	**7.06**
	Glen Scaddle													
GS 17-1	704.45	372	53.81	13644	89.65	2.37	0.67	13.17	1.62	9.58	4.71	64.19	118.06	0.00
GS 17-2	755.36	416	40.52	14580	89.89	2.71	0.87	12.13	3.49	13.11	5.15	34.69	59.37	37.27
GS 17-3	1041.83	852	58.15	22216	48.81	1.15	0.28	7.35	0.90	12.44	1.83	18.64	34.71	110.28
GS 17-4	653.18	447	51.72	16224	121.72	3.10	0.73	14.88	2.18	9.88	6.87	62.08	108.84	5.86
GS 17-5	801.26	650	36.72	23217	142.34	3.48	0.47	9.39	2.20	11.15	7.66	16.95	18.52	7.61
GS 17-6	886.64	711	41.04	17456	20.23	0.71	0.44	9.21	2.08	13.77	8.85	20.65	21.43	10.84
GS 17-7	962.89	450	37.04	14980	103.75	2.85	0.80	11.95	2.02	9.58	6.07	9.52	12.41	30.93
	Clunes													
CL16-1	990.46	863	31.81	15988	9.72	0.46	0.47	10.63	1.07	16.88	6.53	22.00	29.69	41.35
CL16-2	1036.81	696	43.96	17664	8.43	0.42	0.50	9.80	1.30	14.54	7.61	17.21	21.46	2.79
CL16-3	978.65	635	36.66	14996	12.37	0.51	0.42	10.57	1.01	13.67	6.78	30.14	43.08	2.64
CL16-4	933.10	752	25.05	14792	18.03	0.61	0.36	8.50	0.82	13.32	3.79	44.51	64.40	3.64
CL16-5	1075.29	733	22.28	12623	12.67	0.64	0.49	11.20	2.83	16.75	5.31	48.15	61.12	0.91
CL16-6	1022.58	573	18.16	11935	8.41	0.51	0.34	9.00	1.63	13.29	3.71	52.39	76.03	0.00
	Loch Linnhe													
LL 17-1	254.89	1063	88.74	32714	74.42	1.98	0.48	6.07	2.71	17.39	6.54	2.81	8.52	1.62

Table 48: Rare earth element compositions for Glen Loy, Glen Scaddle, Clunes and Loch Linnhe. Samples marked * are identified as cumulates.

Glen Loy	La	Ce	Pr	Nd	Sm	Eu	Gd	Tb	Dy	Ho	Er	Tm	Yb	Lu
IN-GL-16-1	24.86	63.02	8.89	41.20	8.88	2.63	7.95	1.10	5.98	1.12	3.08	0.45	2.60	0.39
IN-GL-16-2*	**9.48**	**29.24**	**4.62**	**23.92**	**6.66**	**2.07**	**6.65**	**1.07**	**6.29**	**1.19**	**3.22**	**0.48**	**2.67**	**0.38**
IN-GL-16-3	30.66	70.21	9.14	40.06	7.24	2.50	6.14	0.75	3.83	0.77	2.36	0.40	2.59	0.45
IN-GL-16-4	22.58	55.31	7.67	35.64	7.94	2.61	7.14	1.00	5.48	1.05	2.93	0.45	2.69	0.42
Glen Loy (LB)	**La**	**Ce**	**Pr**	**Nd**	**Sm**	**Eu**	**Gd**	**Tb**	**Dy**	**Ho**	**Er**	**Tm**	**Yb**	**Lu**
GL-LB-1	24.52	68.05	10.24	47.94	11.56	3.02	9.47	1.27	6.31	1.04	2.63	0.37	2.08	0.28
GL-LB-2*	**16.71**	**38.29**	**5.56**	**24.69**	**5.94**	**1.46**	**5.77**	**0.91**	**5.42**	**1.04**	**2.86**	**0.43**	**2.54**	**0.37**
GL-LB-3	106.36	217.55	25.77	91.55	13.53	2.90	10.37	0.94	3.55	0.57	1.42	0.21	1.28	0.20
GL-LB-4*	**23.34**	**62.65**	**8.93**	**40.59**	**9.09**	**2.25**	**7.98**	**1.14**	**6.36**	**1.17**	**3.20**	**0.48**	**2.79**	**0.40**
Glen Scaddle	**La**	**Ce**	**Pr**	**Nd**	**Sm**	**Eu**	**Gd**	**Tb**	**Dy**	**Ho**	**Er**	**Tm**	**Yb**	**Lu**
GS 17-1	22.70	50.83	6.22	24.86	5.17	1.78	4.84	0.70	3.94	0.74	2.06	0.31	1.88	0.28
GS 17-2	19.61	43.50	5.08	19.80	4.10	1.38	3.93	0.59	3.52	0.68	2.00	0.31	1.93	0.29
GS 17-3	20.23	47.50	6.09	26.39	5.95	2.12	5.58	0.82	4.67	0.86	2.32	0.33	1.89	0.27
GS 17-4	33.32	71.38	8.76	35.09	6.96	1.90	6.50	0.91	4.99	0.93	2.58	0.39	2.30	0.34
GS 17-5	31.52	64.55	7.38	28.09	5.08	2.17	4.62	0.59	3.09	0.55	1.48	0.22	1.24	0.18
GS 17-6	30.48	61.19	7.05	26.67	4.78	2.13	4.36	0.56	2.94	0.52	1.41	0.21	1.17	0.17
GS 17-7	24.36	48.01	5.72	21.79	4.38	1.21	4.08	0.60	3.49	0.67	1.94	0.31	1.87	0.28
Clunes	**La**	**Ce**	**Pr**	**Nd**	**Sm**	**Eu**	**Gd**	**Tb**	**Dy**	**Ho**	**Er**	**Tm**	**Yb**	**Lu**
CL16-1	28.41	62.70	7.02	26.93	5.11	1.29	4.50	0.60	3.22	0.59	1.59	0.24	1.41	0.20
CL16-2	32.78	65.87	7.14	26.44	4.62	1.21	4.15	0.53	2.73	0.50	1.37	0.21	1.18	0.17
CL16-3	32.17	65.67	7.31	27.36	4.93	1.26	4.42	0.57	3.01	0.55	1.50	0.23	1.33	0.19
CL16-4	30.20	56.72	6.01	21.66	3.70	1.37	3.37	0.42	2.14	0.39	1.06	0.16	0.94	0.14
CL16-5	27.06	63.63	7.33	27.27	4.71	1.57	4.31	0.54	2.83	0.53	1.48	0.22	1.34	0.20
CL16-6	24.20	47.30	5.34	20.23	3.65	1.16	3.33	0.44	2.30	0.43	1.21	0.18	1.06	0.16
Linnhe	**La**	**Ce**	**Pr**	**Nd**	**Sm**	**Eu**	**Gd**	**Tb**	**Dy**	**Ho**	**Er**	**Tm**	**Yb**	**Lu**
LL 17-1	5.27	26.14	1.46	5.42	1.12	0.46	1.03	0.13	0.68	0.13	0.39	0.07	0.43	0.07

Table 49: Rare earth element chemistry for Cluanie.

Cluanie														
	La	**Ce**	**Pr**	**Nd**	**Sm**	**Eu**	**Gd**	**Tb**	**Dy**	**Ho**	**Er**	**Tm**	**Yb**	**Lu**
IN/20-7/2	17.03	37.19	4.19	16.87	3.44	1.08	2.66	0.39	2.13	0.39	1.18	0.19	1.30	0.20
INC 1	17.30	35.25	4.31	17.66	3.50	0.98	2.72	0.39	2.19	0.39	1.19	0.18	1.37	0.22
INC 2	13.61	27.41	3.36	13.54	2.66	0.86	2.06	0.31	1.63	0.31	0.92	0.14	1.01	0.17
INC 4	14.58	31.01	3.96	16.73	3.43	1.16	2.77	0.40	2.24	0.41	1.24	0.20	1.42	0.22
INC 8	19.22	36.70	4.23	16.86	3.23	1.09	2.62	0.37	2.03	0.38	1.12	0.17	1.22	0.19
INC 9	12.59	27.86	3.21	13.37	2.67	0.93	2.14	0.32	1.75	0.33	1.01	0.16	1.11	0.19
IN9-7/3	20.76	40.61	4.83	19.63	3.86	1.21	2.88	0.37	1.79	0.29	0.83	0.12	0.85	0.14
IN/21-7/4	16.48	34.17	4.08	16.94	3.37	1.20	2.56	0.32	1.59	0.26	0.75	0.11	0.80	0.13
IN/21-7/3	23.91	44.59	5.46	22.04	4.26	1.25	3.21	0.41	2.17	0.39	1.12	0.18	1.19	0.19
IN/3-7/5	23.92	51.08	5.03	19.00	3.33	0.98	2.67	0.37	2.13	0.37	1.12	0.18	1.23	0.20
IN/3-7/1	8.38	17.87	2.16	8.82	1.80	0.76	1.29	0.19	1.18	0.22	0.67	0.11	0.82	0.13
INC 10	12.93	24.34	3.01	12.22	2.41	0.90	1.91	0.27	1.60	0.29	0.89	0.14	0.99	0.16
IN/20-7/4	9.76	18.98	2.22	8.68	1.72	0.64	1.35	0.20	1.21	0.23	0.69	0.11	0.82	0.15
IN/3-7/4	17.09	43.05	4.68	19.68	4.19	1.32	3.16	0.41	2.06	0.36	0.98	0.15	0.97	0.15
IN/27-6/2	31.26	58.26	6.84	27.40	5.04	1.44	3.90	0.50	2.46	0.41	1.15	0.16	1.11	0.16
IN/24-7/1	23.78	53.52	6.10	25.05	4.92	1.35	3.52	0.44	2.11	0.35	0.96	0.14	0.97	0.15
INC 3	23.00	43.55	4.97	19.34	3.61	1.17	3.09	0.43	2.26	0.39	1.08	0.15	1.01	0.16
INC 5	24.28	45.72	5.25	20.65	3.90	1.22	3.24	0.46	2.36	0.41	1.15	0.17	1.09	0.17
INC 6	32.07	60.66	7.27	29.29	5.29	1.63	4.28	0.60	3.19	0.57	1.65	0.24	1.62	0.25
INC 7	42.82	78.86	9.43	38.01	7.16	2.09	6.01	0.85	4.40	0.77	2.14	0.31	1.94	0.30

Table 50: Concentrations of high field strength elements, large ion lithophile elements, and transition metals (Cluanie).

	Sr	Ba	Rb	K	Zr	Hf	Ta	Nb	U	Pb	Th	Ni	Cr	Cu
IN/20-7/2	1072.9	961.2	59.2	3.70	151.2	3.45	0.47	7.93	1.50	39.01	3.70	41.2	57.2	9.2
INC 1	949.7	703.4	64.3	3.27	152.1	3.59	0.48	9.47	1.63	30.60	3.27	5.2	24.8	10.6
INC 2	903.6	710.4	53.2	3.27	131.0	3.10	0.37	6.44	2.74	30.91	3.27	22.0	25.0	13.3
INC 4	940.9	1129.3	74.4	3.56	156.4	3.71	0.49	8.01	2.64	35.42	3.56	2.3	12.7	14.9
INC 8	991.9	949.2	66.4	3.10	151.0	3.44	0.47	8.60	1.52	32.42	3.10	2.7	8.1	13.3
INC 9	1013.9	860.6	62.0	3.18	93.1	2.16	0.39	4.82	1.39	33.63	3.18	18.5	13.4	13.1
IN9-7/3	1045.6	1123.6	37.6	4.43	142.0	3.54	0.50	7.96	1.52	29.91	4.43	18.2	12.1	13.3
IN/21-7/4	1133.7	1022.6	51.7	3.64	157.8	3.96	0.51	8.88	1.46	37.30	3.64	11.2	17.9	14.2
IN/21-7/3	944.9	980.6	58.4	5.14	142.7	3.60	0.43	8.25	2.90	36.11	5.14	15.5	32.9	14.4
IN/3-7/5	834.3	631.9	64.6	8.12	147.6	3.52	0.47	8.92	1.20	31.74	8.12	2.8	9.5	17.0
IN/3-7/1	959.4	817.6	73.2	4.39	128.5	3.06	0.37	7.48	2.33	33.14	4.39	130.7	47.2	11.8
INC 10	1009.7	944.4	52.1	2.21	118.8	2.83	0.40	5.92	1.24	31.82	2.21	10.2	8.3	6.4
IN/20-7/4	917.5	668.7	58.3	3.15	142.4	3.64	0.31	5.27	1.25	34.53	3.15	72.4	27.8	7.1
IN/3-7/4	1000.5	822.9	41.7	4.41	167.0	3.92	0.52	7.73	2.77	24.68	4.41	32.7	12.0	19.0
IN/27-6/2	994.0	919.6	49.5	5.16	159.8	3.70	0.49	7.68	2.75	30.65	5.16	11.5	5.2	17.1
IN/24-7/1	1125.5	747.4	44.1	4.67	149.0	3.82	0.48	8.42	2.59	34.05	4.67	17.0	12.6	20.9
INC 3	800.6	594.6	49.7	4.45	194.6	3.93	0.78	9.69	2.76	15.73	4.45	38.7	56.7	23.0
INC 5	803.5	606.9	42.5	4.74	194.0	4.04	0.60	7.88	2.18	17.68	4.74	43.7	47.9	26.6
INC 6	1319.0	820.5	59.9	4.21	170.5	3.71	0.43	7.96	2.02	20.44	4.21	72.2	45.8	25.0
INC 7	708.3	696.5	103.6	4.59	170.0	3.79	0.43	8.12	1.95	15.01	4.59	34.6	44.1	24.4

Appendix D: LA – ICPMS Standards

Probability density plots are presented for the two reference materials used for each pluton (NIST 610 and Plesovice). Independent runs on samples from each pluton are presented separately.

The plots presented indicate the effectiveness of the operating conditions of the LA-ICPMS, as there is consistency in the 206/238 ages given for both NIST610 and Plesovice. The Plesovice age provided in the literature is given at 337.13 ± 0.37Ma (Slama et al., 2008)

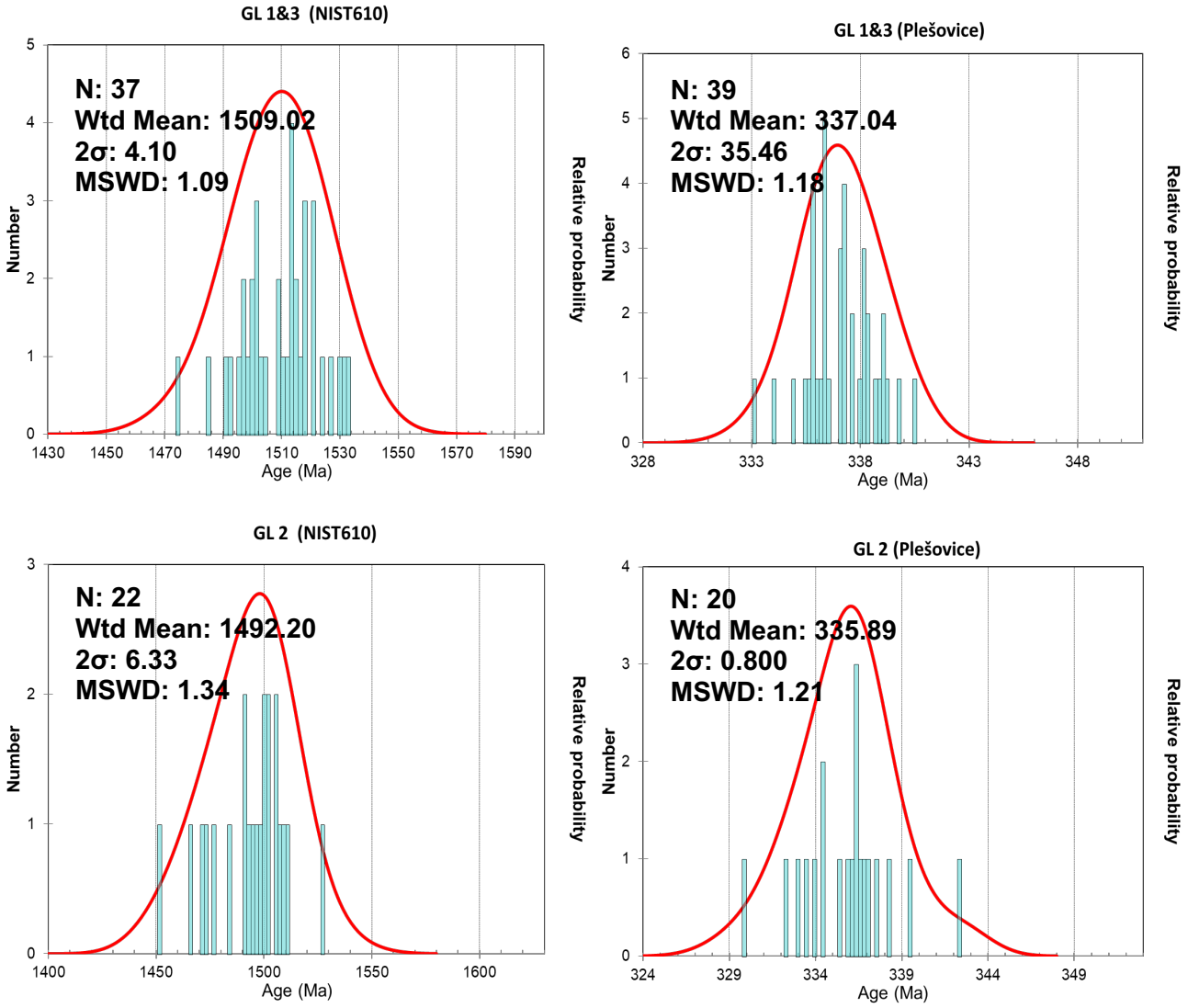

Figure 94: The ages (in Ma) of the reference materials NIST 610 and Plesovice are plotted in probability-density plots. The two runs for Glen Loy are plotted separately. The 206/238 age was used for the plot, which was constructed using the excel add-in Isoplot 3.7 (http://www.bgc.org/isoplot_etc/isoplot.html).

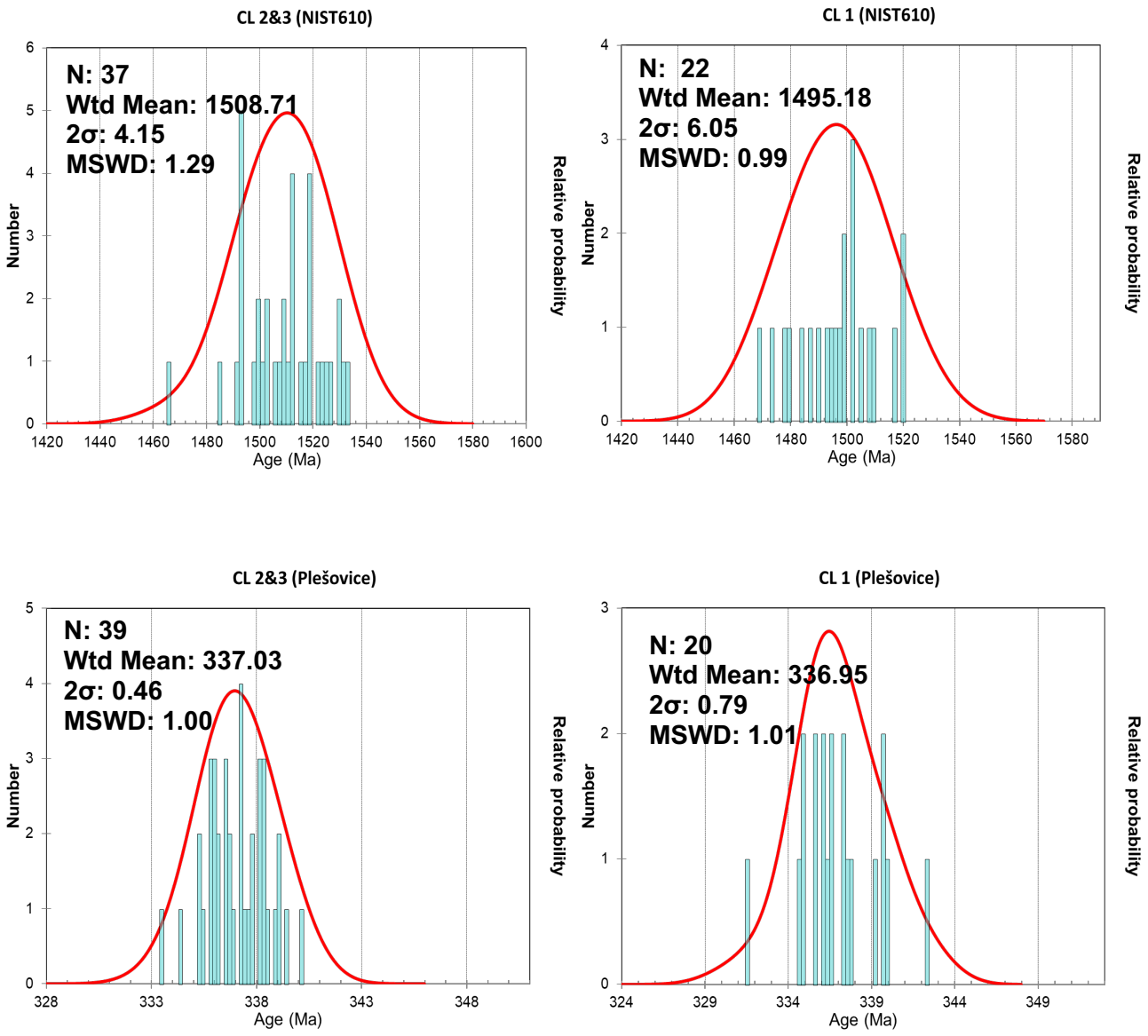

Figure 95: The ages (in Ma) of the reference materials NIST 610 and Plesovice are plotted in probability-density plots. The two runs for Cluanie are plotted separately. The 206/238 age was used for the plot, which was constructed using the excel add-in Isoplot 3.7 (http://www.bgc.org/isoplot_etc/isoplot.html)

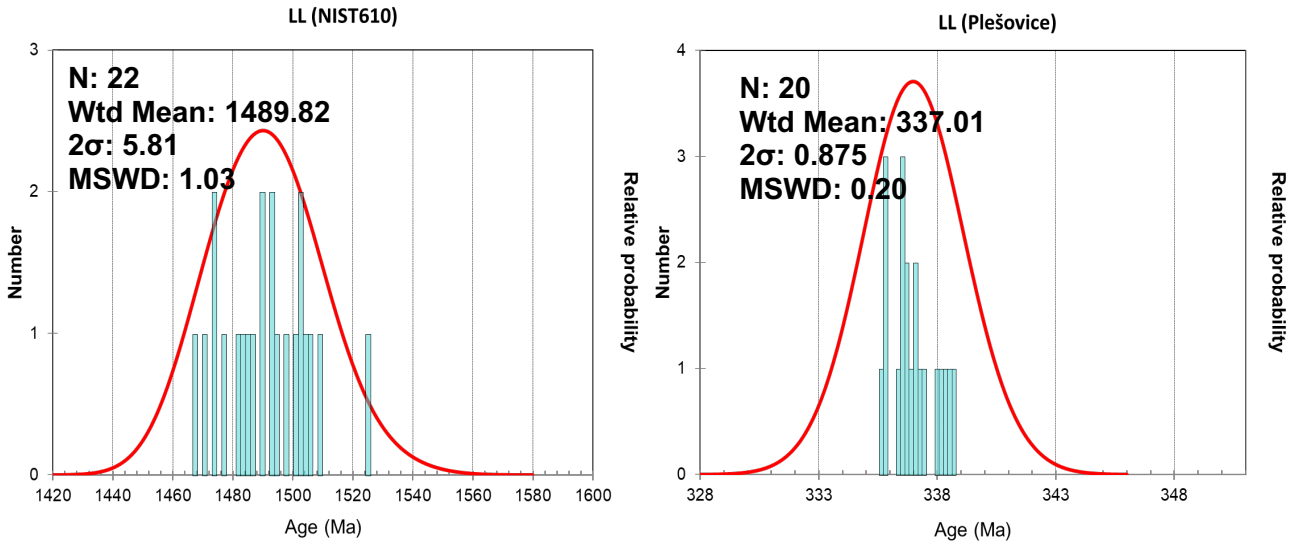

Figure 96: The ages (in Ma) of the reference materials NIST 610 and Plesovice are plotted in probability-density plots. The 206/238 age was used for the plot, which was constructed using the excel add-in Isoplot 3.7 (http://www.bgc.org/isoplot_etc/isoplot.html).

Table 51: Summary of the ages of Plesovice and Nist (with 2σ uncertainty values) and MSWD's. The age for Plesovice quotes in the literature is 337.13 ± 0.37 Ma (Slama et al., 2008)

	Glen Loy		Cluanie		Loch Linnhe	Average
	GL1 & 3	GL 2	CL 1	CL 2 & 3	LL1	
Nist 610	1509.02 +/- 4.10 MSWD: 1.09	1492.20 +/- 6.33 MSWD: 1.34	1495.18 +/- 6.05 MSWD: 0.99	1508.71 +/- 4.15 MSWD: 1.29	1489.82 +/- 5.81 MSWD: 1.03	1502.07 +/- 11.4 MSWD: 13.60
Plesovice	337.04 +/- 0.45 MSWD: 1.18	335.89 +/- 0.800 MSWD: 1.21	336.95 +/- 0.79 MSWD: 1.01	337.03 +/- 0.46 MSWD: 1.00	337.01 +/- 0.875 MSWD: 0.20	336.89 +/- 0.26 MSWD: 1.79

Appendix E: Assessing the effectiveness of the discordance filter

Percentage discordance of the zircon U-Pb ages was the primary method for filtering the datasets. Discordance was quantified via Equation 1. This is seen as a robust and reproducible first step in discriminating data prior to any direct interpretation (Spencer et al. 2016). Without applying a discordance filter, the ability to acquire ages for individual geologic events is severely limited (Spencer et al. 2016).

Regardless, Spencer et al. 2016 also stress the importance of considering the entire dataset without a filter, stating that a correctly applied discordance filter should not significantly alter the position of age peaks. Comparing the position of age peaks between filtered and unfiltered can be used to measure the effectiveness of the discordance filter.

Probability - density plots for each unfiltered dataset are presented, alongside the same plots for the dataset with a 2σ covaried uncertainty filter. The data from Glen Loy and Cluanie have at this stage been combined, in moving towards establishing a single crystallization age for each pluton.

Given the aim of this study was to establish a precise crystallization age for the plutons, and that the discordance filter used did not significantly alter the position of age peaks, it can be deemed an effective method for reducing the dataset prior to interpretation.

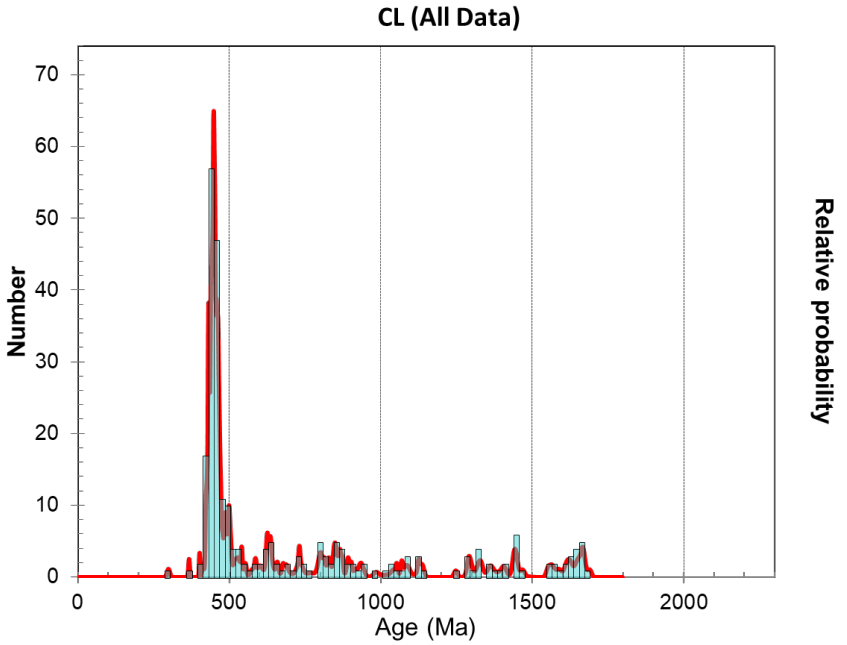

Figure 98: Probability density plot for the unfiltered CL data (CL1, CL2 and CL3). Created in Isoplot 3.7.

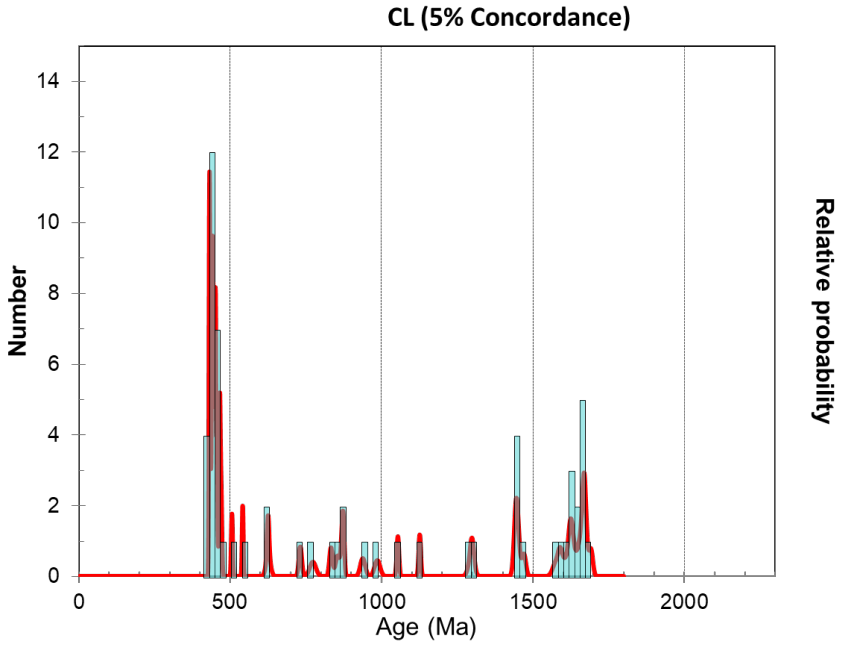

Figure 99: Probability density plot for the CL data with >5% discordance removed. Created in Isoplot 3.7.

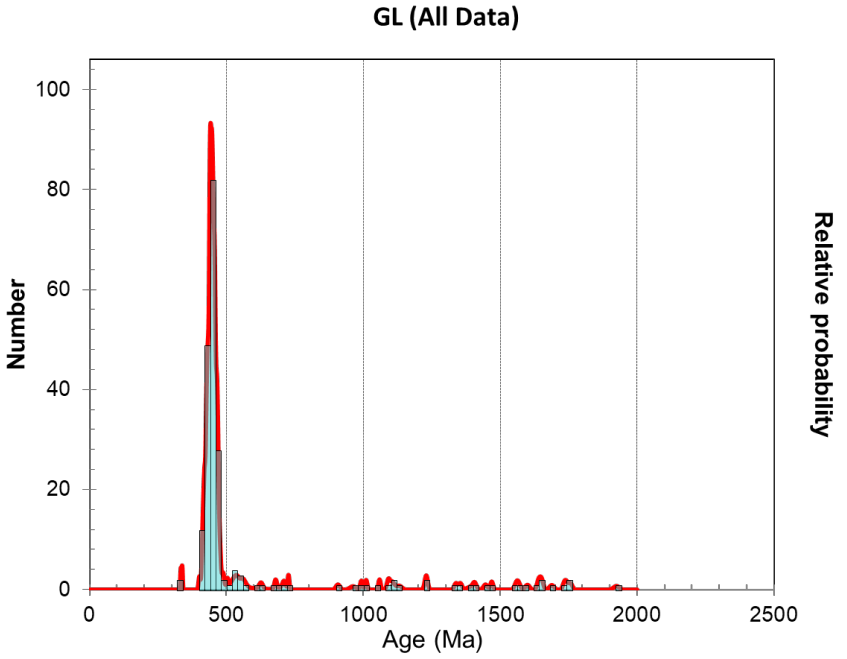

Figure 100: Probability density plot for the unfiltered GL data (GL1, GL2 and GL3). Created in Isoplot 3.7.

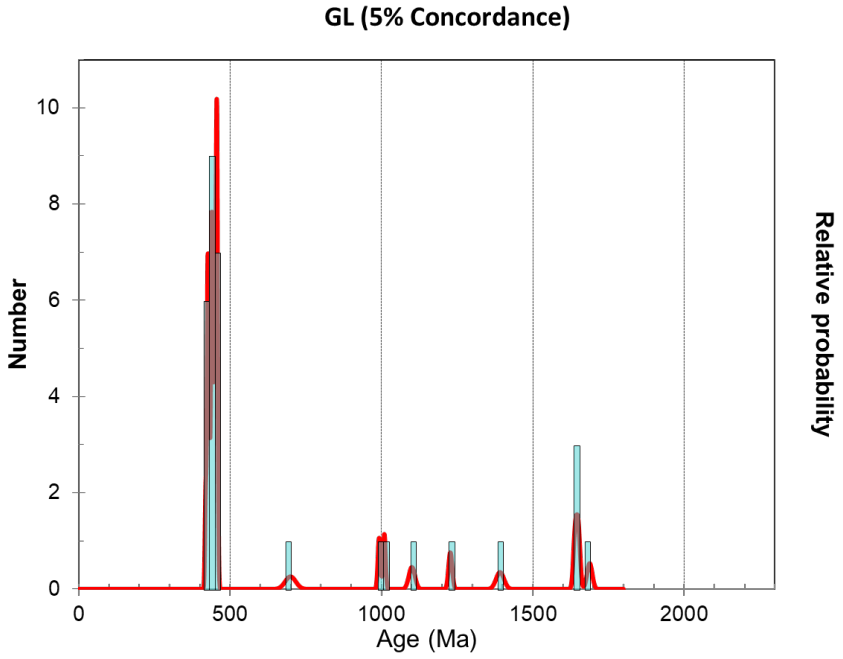

Figure 101: Probability density plot for the GL data with >5% discordance removed. Created in Isoplot 3.7.

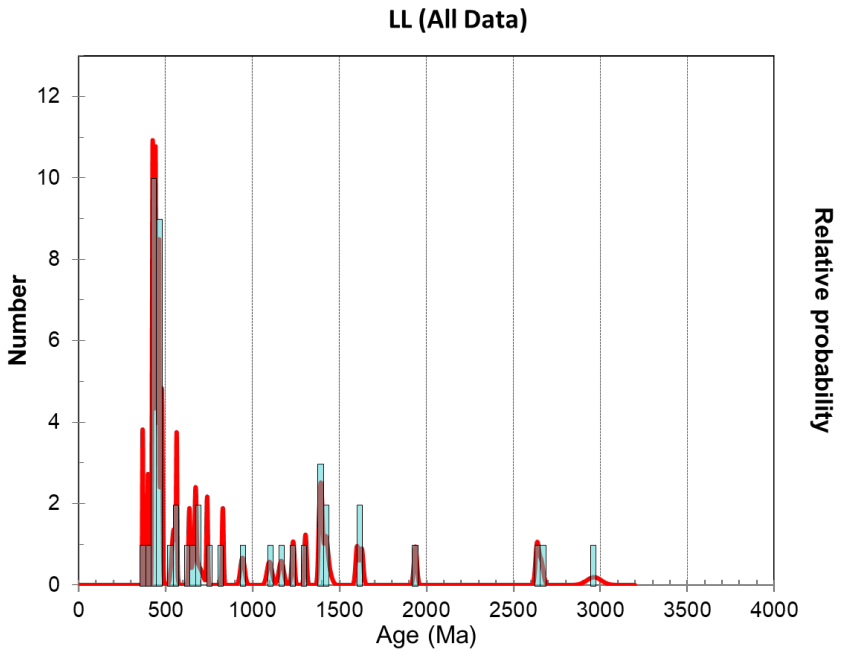

Figure 102: Probability density plot for the unfiltered LL data. Created in Isoplot 3.7.

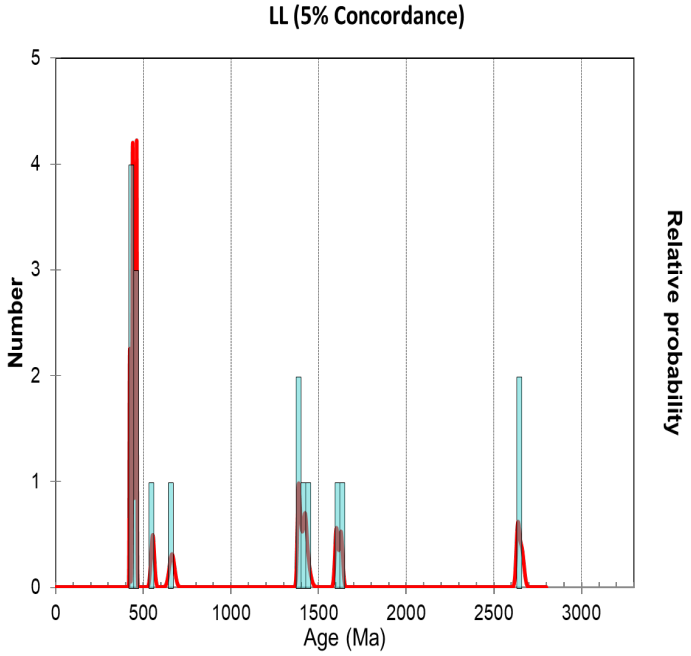

Figure 103: Probability density plot for LL the with >5% discordance removed. Created in Isoplot 3.7.

Glen Loy:

In the unfiltered data, the main peak consists of over 80 grains of 440 - 460Ma. Around 50 grains at 420 - 440Ma.

With the discordance filter, the main peak is at 420 - 440Ma with 9 grains. 7 grains plot 440 - 460Ma. The trend is largely uniform between the 2 plots, with the spread of ages upwards form the main peaks being eliminated by the concordance filter. There are a significant number of grains eliminated from 500 – 2000 Myr. Peaks remain at 700 Ma (1 grain), 1000Ma (2 grains), 1100Ma, 1600 - 1700Ma.

Cluanie:

A Significant amount of grains plot between 400 - 500Ma. The position of the main peak is in similar position for both the filtered and unfiltered data (44-450Ma), and the trend is largely uniform between the two plots. In the unfiltered data, there is spread of ages upwards from the main cluster at 440 – 450 crystallization age - with 500 – 1700Ma being populated. Some peaks in this range are preserved by the discordance. 700 Myr – 1000 Myr is populated with several peaks, another at 1300Ma 1450Ma and 1000Ma – 1200a.

Loch Linnhe:

Main peak at 440 - 450Ma. In the unfiltered data, peaks are preserved at 1400 - 1500Ma, 1600 - 1700Ma, 2600Ma. The trend is largely uniform between the two plots, with the spread of ages upwards form the main peaks being eliminated by the concordance filter.

Appendix F: Partition coefficients for trace elements in fractionating minerals as used in the fractional crystallization models

Table 52: Partition coefficients for trace elements in fractionating minerals as used in the fractional crystallization models

Mineral	Partition coefficient for Trace element									Reference
	La	**Ce**	**Nd**	**Sm**	**Eu**	**Gd**	**Dy**	**Er**	**Yb**	
Amphibole	0.37	0.73	1.20	2.01	1.33	2.30	2.68	2.47	2.1	Klein et al. 1997
Titanite	6.43	11.10	18.60	21.40	20.40	18.30	12.30	8.32	4.51	Tiopolo et al. 2002
Apatite (Dacite)	28.20	37.40	61.20	98.50	17.10	95.60	91.00	41.6	27.6	Fujimaki, 1986
Zircon	4.18	4.31	4.29	4.94	3.31	6.59	47.40	99.8	191	Rollinson, 1993
Allanite	2827.00	2494.00	1840.00	977.00	100.00	200.00	150.00	65	37	Mahood & Hildreth, 1983
Biotite	5.71	4.36	2.56	2.12	2.02	2.00	1.72	1.5	1.473	Mahood & Hildreth, 1983
Ilmenite	1.22	1.64	2.267	2.83	1.01	2.00	2.63	2	1.467	Mahood & Hildreth, 1983
Quartz	0.00	0.00	0.00	0.00	0.00	0.00	0.00	0.00	0.00	Mahood & Hildreth,, 1983
Plagioclase	0.30	0.24	0.17	0.13	2.11	0.90	0.09	0.084	0.077	Mahood & Hildreth, 1983
Orthoclase	0.08	0.04	0.025	0.02	1.13	0.01	0.01	0.006	0.012	Mahood & Hildreth, 1983
Clinopyroxene	0.054	0.098	0.21	0.26	0.31	0.3	0.33	0.3	0.28	McKenzie and O'Nions, 1991
Orthopyroxene	0.0080	0.0016	0.0056	0.0150	0.0300	0.0340	0.0770	0.1200	0.22	Green et al. 2000

Bibliography

Alderton, D. H., & Pearce, J. (1980). Rare Earth mobility during granite alteration: Evidence from southwest England. *Earth and Planterary Sceince Letters*, 149 – 165.

Allen, M., Armstrong, H. A., Arabia-Eurasia collision and the forcing of Mid Cenozoic global cooling. *Palaeogeography Palaeoclimatology Palaeoecology,* 52 – 58.

Andersson, U., Eklund, O., Fröjdö, S., & Konopelko, D. (2006). 1.8 Ga magmatism in the Fennoscandian Shield; lateral variations in subcontinental mantle enrichment. *Lithos*, 110 - 136 .

Andrews, I. L. (1990). *United Kingdom Offshore Regional Report: The Geology of the Moray Firth* . London: HMSO for British Geological Survey.

Annen, C, Blundy, J. D, & Sparks, R. S. J. (2005). The Genesis of Intermediate and Silicic Magmas in Deep Crustal Hot Zones. *Journal of Petrology* , 505 - 539.

Annen, C, Blundy, J. D., & Sparks, R. S. J. (2008). The source of granitic melt in Deep Hot Zones. *Transactinos of the Royal Society of Edinburgh* , 297 - 309.

Appleby, S. K (2007). The origin and evolution of granites: an in-situ study of zircons from Scottish Caledonian intrusions. Unpublished doctoral dissertation, University of Edinburgh.

Armstrong, H. A., & Owen A. W. (2001). Terrane evolution of the paratectonic Caledonides of northern Britain. *Journal of the Geologial Society,* 475 - 486.

Atherton, M.P., & Ghani, A.A. (2002). Slab breakoff: A model for Caledonian, Late Granite syn-collisional magmatism in the orthotectonic (metamorphic) zone of Scotland and Donegal, Ireland. *Lithos* , 65 - 85 .

Atherton, M. P., & Petford, N. (1993). Generation of sodium-rich magmas from newly underplated basaltic crust. *Nature*, 144 - 146.

Bea, F., Montero, P., Lodeiro, G., & Talavera, C. (2007). Zircon Inheritance Reveals Exceptionally Fast Crustal Magma Generation Processes in Central Iberia during the Cambro-Ordovician. *Journal of Petrology*, 2327 - 2339.

Bird, A., Cutts, K., Strachan, R., Thirlwall, M. F., & Hand, M. (2018). First evidence of Renlandian (c. 950–940 Ma) orogeny in mainland Scotland: Implications for the status of the Moine Supergroup and circum-North Atlantic correlations. *Precambrian Research*, 283 - 294.

Bird, A., Thirlwall, M.F., Strachan, R., & Manning, C. J. (2013). Lu–Hf and Sm–Nd dating of metamorphic garnet: evidence for multiple. *Journal of the Geological Society* , 301 - 317.

Blanckenburg, F. V., & Davies, J. H. (1995). Slab breakoff: A model for syncollisional magmatism. *Tectonics*, 120 - 131.

Bluck, B. J (2013) ; Geotectonic evolution of Midland Scotland from Cambrian to Silurian: a review. *Scottish Journal of Geology* 49 (2). 105–116

Bluck, B.J. (2001). Caledonian events in Scotland. Transactions of the Royal Society of Edinburgh, Earth Sciences, 91, 375–404

Breemen, O.V., Aftalion, M., Pankhurst, & Richardson. (1979). Age of the Glen Dessary Syenite, Inverness-shire: diachronous Palaeozoic metamorphism Across the Great Glen. *Scottish Journal of Geology*, 49 - 62.

Calmus, T., Robles, A., Maury, R., Bellon, H., Benoit, M., Cotten, J., Michaud, F. (2003). Spatial and temporal evolution of basalts and magnesian andesites

(‘‘bajaites’’) from Baja California, Mexico: the role of slab melts. *Lithos*, 77 - 105 .

Carty, J. P., Connelly, J. N., Hudson, N. F. C. & Gale, J. F. W. (2012). Constraints on the timing of deformation, magmatism and metamorphism in the Dalradian of NE Scotland. *Scottish Journal of Geology,* 103-117.

Castillo, P. (2006). An overview of Adakite Petrogenesis . *Chinese Science Bulletin*, 257 - 268 .

Cawood, P. A., & Buchan, C. (2007). Linking accretionary orogenesis with supercontinent assembly. *Earth Science Reviews*, 3-4.

Cawood, P. A., Strachan, R. A., Merle, R. E., Millar, I. L., Loewy, S. L., Dalziel, I. W., Connelly, J. N. (2015). Neoproterozoic to early Paleozoic extensional and compressional history of East Laurentian margin sequences: The Moine Supergroup, Scottish Caledonides. *GSA Bulletin*, 349 - 371.

Cawood, P. A., Wang. Y, Xu. Y, & Zhao, G. (2013). Locating South China in Rodinia and Gondwana: A fragment of greater India lithosphere. *Geology*, 903 - 906.

Crowley, Q. G., & Strachan, R. A. (2015). U–Pb zircon constraints on obduction initiation of the Unst Ophiolite: an oceanic core complex in the Scottish Caledonides? Journal of the Geological Society, 279 - 282.

Chew, D.M., Daly, J.S., Magna, T., Page, L.M., Kirkland, C.L.,Whitehouse, M.J. & Lam, R. (2010). Timing of ophiolite obduction in the Grampian orogen. *Geological Society of America Bulletin*, 1787–1799.

Chew, D. C. & Strachan, R. A. (2013). ‘The Laurentian Caledonides of Scotland and Ireland’ from Corfu, F., Gasser, D. & Chew, D. M. (eds), ‘New perspectives on the Caledonides of Scandinavia and Related areas’. Geological Society, London, Special Publications 390.

Chiaradia, M., Ulianov, A., Kouzmanov, K., & Beate, B. (2012). Why large porphyry Cu deposits like high Sr/Y magmas? *Nature Sceintific Reports* .

Chung, S., Liu, D., Ji, J., Chu, M., & Lee, H. (2003). Adakites from continental collision zones: melting of thickened lower crust beneath southern Tibet. *Geology*, 1021 - 1024.

Chung, S.-L., Chu, M.-F., Zhang, Y., Xie, Y., Lo, C.-H., Lee. T.-Y., Lan, C.-Y., Li, Z, Zhang, Q, Wang, Y (2005). Tibetan tectonic evolution inferred from spatial and temporal variations in post collisional magmatism, *Earth Science Reviews,* 173 – 196

Clayburn, C. (1981). Age and petrogenetic studies of some magnetic and metamorphic rocks in the Grampian highlands. *University of Oxford Ph.D Thesis*.

Condie, K.C. (2004), ‘TTG’s and Adakites: are they both slab melts?’ Lithos, 80, 33 - 44

Corfu, F., Ravna, E. J. K., & Kullerud, K. (2003). A Late Ordovician U–Pb age for the Tromsø Nappe eclogites,. *Contributions to Mineral Petrology* , 502 - 513 .

Dallemeyer. R. D., Strachan. R. A., Rogers, G., & Watt G. R. (2001). Dating deformation and cooling in the Caledonian thrust nappens of north Sutherland, Scotland: Insights from 40Ar/ 39Ar and Rb-Sr chronology. *Journal of the Geological Society* , 501 - 521.

Defant, M. J. & Drummond, M. S. (1990). Derivation of some modern arc magmas by melting of young subducted lithosphere. *Nature, 662 – 665.*

Dempster, T. J., & Rogers, G. (2002). Timing of deposition, orogenesis and

glaciation within the Dalradian rocks of Scotland: constraints from U–Pb zircon ages. *Journal of the Geological Society, London,* 83– 94.

Dewey, J. F., & Ryan, P. (1990). The Ordovician evolution of the South Mayo Trough, western Ireland. *Tectonics*.

Dewey, J.F. & Strachan, R.A. (2003). Changing Silurian–Devonian relative plate motion in the Caledonides: sinistral transpression to sinistral transtension. *Journal of the Geological Society, London*, 160, 219–229.

Dewey J.F. (2005). Orogeny can be very short . *Proceedings of the National Academy of Sciences of the United states of America* , 15286-15293.

Dewey, J. F., Dalziel, I. W., Reavy, R. J., & Strachan, R. A. (2015). The Neoproterozoic to Mid-Devonian evolution of Scotland: a review and unresolved issues. *Scottish Journal of Geology* , 5 - 30 .

England, P. C., & Thompson, A. B., (1984). Pressure - Temperature - Time Paths of Regional Metamorphism I. Heat Transfer during the Evolution of Regions of Thickened Continental Crust. *Journal of Petrology* , 894 - 928.

Flinn, D., & Oglethorpe, J. D. (2005). A history of the Shetland Ophiolite Complex. Scottish Journal of Geology, 141 - 148.

Fowler, M. B., Kocks, H., Darbyshire D.P.F., & Greenwood. P. B., (2008). Petrogenesis of high Ba–Sr plutons from the Northern Highlands Terrane of the British Caledonian Province. *Lithos*, 129 - 148 .

Fowler, M. B., Millar. I. L., Strachan, R.A., & Fallick, A.E. (2013). Petrogenesis of the Neoproterozoic West Highland Granitic Gneiss, Scottish Caledonides: cryptic mantle input to S-type granites? *Lithos*, 173 - 185 .

Fraser, G.L., Pattison, D. R. M., & Heaman, L. M. (2004). Age of the Ballachulish and Glencoe Igneous Complexes (Scottish Highlands), and paragenesis of zircon, monazite and baddeleyite in the Ballachulish Aureole. *Journal of the Geological Society* , 447 - 462.

Freeman, S.R. (1998). Direct dating of Mylonite evolution: a multi-disciplinary geochronological study from the Moine Thurst Zone, NW Scotland. (1998). *Journal of the Geological Society* , 745 - 758.

Friend, C. R. L., Strachan, R.A., & Kinny. P. D., (2008). U-Pb zircon dating of basement inliers within the Moine Supergroup, Scottish Caledonides: implications of Archean protolith ages. *Journal of the Geological Society* .

Fujimaki, H. (1986). Partition-Coefficients of Hf, Zr, and Ree between Zircon, Apatite, and Liquid. *Contributions to Mineralogy and Petrology* , 42 - 45 .

Gerya, T. V., Yuen, D. A., & Maresh, W. V. (2004). Thermomechanical modelling of slab detatchment. *Earth Planet Science Letters*, 101 – 116.

Goodenough, K.M., Millar, I., Strachan, R.A., Krabbendam, M. & Evans, J.A. (2011). Timing of regional deformation and development of the Moine Thrust Zone in the Scottish Caledonides: Constraints from the U–Pb geochronology of alkaline intrusions. *Journal of the Geological Society, London,* 168, 99–113.

Green, T., Blundy, J., Adam, J., & Yaxley, G. (2000). SIMS determination of trace element partition coefficients between garnet, clinopyroxene and hydrous basaltic liquids at 2–7.5 GPa and 1080–12008C. *Lithos*, 165 - 187.

Groome, D. R., & Hall, A. (1974). The geochemistry of the Devonian lavas of the northern Lorne Plateau, Scotland. *Mineralogical Magazine*, 621 - 640.

Hall. (1985). Geophysical constraints on crustal structure in the Dalradian region of Scotland . *Journal of the Geological Society* , 149 - 155.

Hall, Brewer, Mathews, & Warner. (1984). Crustal structure across the Caledonides from the WINCH seismic reflection profile: Influences on the

evolution of the Midland Valley of Scotland. *Earth and Environmental Science Transactions of the Royal Society of Edinburgh*.

Halliday, Aftalion, Parsons, Dickin, & Johnson. (1987). Syn-orogenic alkaline magmatism and its relationship to the Moine Thrust Zone and the thermal state of the Lithosphere in NW Scotland. *Journal of the Geological Society*, 611 - 617 .

Hammersrom, J. M., & Zen, E. A. (1986). Aluminum in hornblende: An empirical igneousgeobarometer. *American Mineralogist*.

Holdsworth, R., Strachan, R. & Harris, A. (1994). Precambrian rocks in northern Scotland east of the Moine Thrust: the Moine Supergroup. In: Gibbons, W. & Harris, A. L. (eds.) A Revised Correlation of Precambrian Rocks in the British Isles. Geological Society, London, Special Reports, 22, 23-32.

Holdsworth, Alsop, & Strachan. (2007). Tectonic stratigraphy and structural continuity of the northernmost Moine Thrust and Moine Nappe, Scottish Caledonides. *Journal of the Geological Society* , 121 - 142.

Holdsworth, R.A, Strachan R.A, Alsop, Grant, & Wilson. (2006). Thrust sequences and the significance of low-angle, out-of-sequence faults in the. *Journal of the Geological Society*, 801 - 814.

Holdsworth, R.E., Dempsey, E., Selby, D., Darling, J.R., Feely, M., Costanzo, A., Strachan, R.A., Waters, P., Finlay, A.J. & Porter, S.J., (2015). Silurian-Devonian magmatism, mineralization, regional exhumation and brittle strike-slip deformation along the Loch Shin Line, NW Scotland. *Journal of the Geological Society,* 748-762.

Horstwood, M. S., J, K., Gehrels, G., Jackson, S. E., McLean, N. M., Paton, C. Sylvester, P. (2016). Community-Derived Standards for LA-ICP-MS U-(Th) Pb Geochronology – Uncertainty Propagation, Age Interpretation and Data Reporting. *Geostandards and Geoanalytical Research* , 311 - 332 .

Hou, Z., Gao, Y., Qu, X., & Rui, Z. M. (2004). Origin of adakitic intrusives generated during mid-Miocene east-west extension in southern Tibet. *Earth and Planetary Science Letters* , 139 - 155.

Hutton, D.H.W. (1988). Granite emplacement mechanisms and tectonic controls from deformation studies. *Trans. R. Soc. Edinb. Earth Sci.* 79, 245– 255.
Hutton, D. H. W. (1992). Strike Slip Tectonics and Granite Petrogenesis . *Tectonics* , 960 - 967 .

Hutton, D. H. W, McErlean, M. (1991) Silurian and Early Devonian sinistral deformation of the Ratagain granite, Scotland: constraints on the age of Caledonian movements on the Great Glen fault system. Journal of the Geological Society, 1 – 4

Jackson, M.D., Blundy, J. & Sparks, R.S.J. (2018) Chemical differentiation, cold storage and remobilization of magma in the Earth's crust. *Nature*, 405–409

Kinny, Friend, Strachan, Wattand, & Burns. (1999). U–Pb geochronology of regional migmatites in East Sutherland, Scotland: evidence for crustal melting during the Caledonian orogeny. *Journal of the Geological Society*, 1143 - 1152.

Kinny, Strachan, Friend, Kocks, Rogers, & Paterson. (2003). U–Pb geochronology of deformed metagranites in central Sutherland, Scotland: evidence for widespread late Silurian metamorphism and ductile deformation of the Moine Supergroup during the Caledonian orogeny. *Journal of the Geological Society* , 259 - 269 .

Kirkland, S. P. (2008). Detrital zircon signature of the Moine Supergroup, Scotland: Contrasts and comparisons with other Neoproterozoic

successions within the circum-North Atlantic region. *Precambrian Research*, 332 - 350.

Klein, M., H, S., & Seck, H. (1997). Partitioning of high field-strength and rare-earth elements between amphibole and quartz-dioritic to tonalitic melts: an experimental study. *Chemical Geology*, 257 - 271.

Kneller, B. C. & Aftalion, M (1987). The isotopic and structural age of the Aberdeen Granite. Journal of the Geological Society of London.

Kocks, Strachan, & Evans. (2006). Heterogeneous reworking of Grampian metamorphic complexes during Scandian thrusting in the Scottish Caledonides: insights from the structural setting and U–Pb geochronology of the Strath Halladale Granite. *Journal of the Geological Society* , 525 - 538.

Kocks, Strachan, Evans, & Fowler. (2013). Contrasting magma emplacement mechanisms within the Rogart igneous complex, NW Scotland, record the switch from regional contraction to strike-slip during the Caledonian orogen. *Geological magazine*, 899 - 915.

Kolb, M., Quadt, A., Peycheva, I., Heinrich, C., Fowler, S., & Cvetkovic, V. (2012). Adakite-like and Normal Arc Magmas: Distinct Fractionation Paths in the East Serbian Segment of the Balkan–Carpathian Arc. *Journal of Petrology* , 421 – 451.

Krabbendam, M., Prave, A.R. & Cheer, D. (2008). A fluvial origin for the Neoproterozoic Morar Group, NW Scotland: Implications for TorridonMorar group correlation and the Grenville Orogen Foreland Basin. *Journal of the Geological Society,* 379–394

Lechmann, A, Burgm J-P, Ulmer, P., Guillong, M., Faridi, M. (2018). Metasomatized mantle as the source of Mid-Miocene-Quaternary volcanism in NW-Iranian Azerbaijan: Geochronological and geochemical evidence. *Lithos,* 311 – 328.

Macpherson, C., Dreher, C., & Thirlwall, M. (2006). Adakites without slab melting: High pressure differentiation of island arc magma, Mindanao, the Philippines. *Earth and Planetary Science Letters* , 581 - 593.

Mahood, G., & Hildreth, W. (1983). Large partition coefficients for trace elements in high-silica rhyolites. *Geochemica and cosmochemica Acta,* 11 - 30.

Martin, H., (1986). Effect of steeper Archean geothermal gradient on geochemistry of subduction-zone magmas. *Geology* 14, 753 – 756.

Martin, H. (1999), Adakitic magmas: modern analogues of Archean granitoids, *Lithos*, 411-429.

McDonough, W.F., Sun, S.-S., (1995). Composition of the Earth. *Chemical Geology*, 223 – 253

Mckenzie, D., & O'nions, R. (1991). Partial melt distributions from inversion of rare Earth element concentrations. *Journal of Petrology* , 1021- 1091.

Mendum J.R., & Noble, S.R. (2010). Mid-Devonian sinistral transpressional movements on the Great Glen Fault: the rise of the Rosemarkie Inlier and the Acadian Event in Scotland. *Geological Society of London*, 161 - 187.

Mendum, J. R., (2012) Late Caledonian (Scandian) and proto-Variscan (Acadian) orogenic events in Scotland: Journal of the Open University Geological Society, v. 33, n. 1, p. 37–51.

Merriman, R.J., Rex, D.C., Soper, N.J. & Peacor, D. (1995). The age of Acadian cleavage in northern England, UK: K-Ar and TEM analysis of a Silurian metabentonite. Proceedings of the Yorkshire Geological Society, 50, p. 255–265.

Miles, A. J., Woodcock, N. H. (2018). A combined geochronological approach to Investigating long lived granite magmatism, the Shap granite, UK. *Lithos,* 45 – 257.

Millar, I, Ritchie, D, Goodenough, K M, Noble, S, Kimbell, G. (2008). U-Pb zircon ages for the Loch Borralan and Flannan syenites, and their relationship to the Caledonian orogenic front [abstract]. [Poster] In: Highland Workshop, Murchison House, Edinburgh, 2008.

Millar, I (1999). Neoproterozoic extensional basic magmatism associated with the West Highland granite gneiss in the Moine Supergroup of NW Scotland. Journal of the Geological Society, 1153 – 1162

Molnar, P., England. P., Martinod, J. (1993). Mantle dynamics, uplift of the Tibetan Plateau, and the Indian Monsoon. *Reviews of Geophysics. 357 - 396.*

Mo, X, Niu, Y., Dong, G., & Zhao. Z. (2008). Contribution of syncollisional felsic magmatism to continental crust growth: A case study of the Paleogene Linzizong volcanic Succession in southern Tibet. *Chemical Geology* , 49 - 67.

Moyen, J-F., Nedelec, A., Jayanada, M., Martin, H (2003). Syntectonic granite emplacement at different structural levels: The Closepet granite, South India. *Journal of Stuctural Geology,* 611 – 631

Neill, I., Leiksetian, K., Allen, M. B., Navasardyan. G., Kuiper, K. (2015). Petrogenesis of mafic collision zone magmatism: The Armenian sector of the Turkish–Iranian Plateau. *Chemical Geology,* 24 – 41.

Neill, I. and Stephens, W. E. (2009) The Cluanie granodiorite, NW Highlands of Scotland: a late Caledonian pluton of trondhjemitic affinity. *Scottish Journal of Geology,* 117-130

Neilson, J.C., Kokelaar, B.P., Crowley, Q.G. (2009). Timing, relations and cause of plutonic activity of the Siluro-Devonian post-collision magmatic episode in the Grampian Terrane, Scotland, Journal of the Geological Society, London, 166, pp 545 561

Niu Y., Zhao. Z., & Mo. X. (2013). Continental collision zones are primary sites for net continental crust growth — A testable hypothesis. *Earth-Science Reviews* , 96 - 110 .

Oliver, G. H. J., Wilde, S. A., & Wan, Y. (2008). Geochronology and geodynamics of Scottish granitoids from the late Neoproterozoic break-up of Rodinia to Palaeozoic collision. *Journal of the Geological Society* , 661 - 674.

Park, R. G., Stewart, A. D. & Wright, D. T. (2002). The Hebridean terrane. In: Trewin, N. H. (ed.) Geology of Scotland, 4th edition. The Geological Society, Bath, 45-80.

Pankhurst, R. J., & Sutherland, D. S. (1982). Caledonian granites and diorites of Scotland and Ireland. In *Igneous rocks of the British Isles* (pp. 149 - 190). Chichester: Wiley.

Paterson, S. R., & Fowler, K. J. (1993). Re-examining pluton emplacement processes. *Journal of Structual Geology* , 191 - 206 .

Paterson, B. A., Stephens, W.E., Rogers, G., & Williams, I.S. (1992). The nature of zircon inheritance in two granite plutons. *Second Hutton Symposium: The Origin of Granites and Related Rocks*, 459-471.

Peacock, S. M., Rushmer, T., & Thomson, A. B. (1994). Partial melting of subducting oceanic crust . *Earth and Planetary Sceince Letters*, 227 - 244.

Petrus, J. A, & Kamber, B. A. (2012). A novel new approach to laser ablation ICP - MS U-Pb geochronology data reduction. *Geostandards and Geoanalytical Research*, 247 - 270.

Pidgeon R. T., & Aftalion. M. (1978). Cogenetic and inherited U-Pb systems in granites: Palaeozoic granites of Scotland and England. *Geological Journal Special Issue* , 183 - 220.

Pidgeon. R. T., & Compston. (1992). A SHRIMP ion microprobe study of inherited and magmatic zircons from four Scottish Caledonian granites. *Second Hutton Symposium: The Origin of Granites and Related Rocks*, 273 - 483.

Rapp, R. P., Watson, E. B., Miller, C. F. (1991). Partial melting of amphibolite/eclogite and the origin of Archean trondhjemites and tonalites. *Precambrian research*, 1 – 25.

Rapp, R. P, Watson E. B (1995). Dehydration Melting of Metabasalt at 8–32 kbar: Implications for Continental Growth and Crust-Mantle Recycling. Journal of Petrology, 891 – 931.

Rainbird, R. H., Hamilton, M. A. & Young, G. M. (2001). Detrital zircon geochronology and provenance of the Torridonian, NW Scotland. *Journal of the Geological Society,* 15 - 27.

Reavy, J. A. (1994). Caledonian plutonism and major lineaments in the SW Scottish Highlands. *Journal of the Geological Society* , 955 - 969.

Ribeiro, J., Maury, R., & Gregoire, M. (2016). Are Adakites Slab Melts or High-pressure Fractionated Mantle Melts? *Journal of Petrology* , 839 - 862.

Roberts, A. M. & Holdsworth, R. E. (1999). Linking onshore and offshore structures: Mesozoic extension in the Scottish Highlands. *Journal of the Geological Society*, 1061 - 1064.

Roberts, A. M., & Holdsworth, R. E., (1999). Linking onshore and offshore structures: Mesozoic extension in the Scottish Highlands. *Journal of the Geological Society*, 1061 - 1064.

Rogers, G., & Dunning. G. R. (1991). Geochronology of appinitic and related granitic magmatism in the W Highlands of Scotland: constraints on the timing of transcurrent fault movement. *Journal of the Geological Society*, 17 - 27.

Rogers, G. Marshall, & Astrin. (1989). Devonian and later movements on the Great Glen Fault Zone . *Journal of the Geological Society* , 369 - 372.

Rollinson, H. (1993). *Using geochemical data: Evaluation, presentation, interpretation.* New York : Wiley.

Royden, L. H, Burchfiel. B. C., Hilst R, V, D (2008). The Geological Evolution of the Tibetan Plateau. *Science*, 1054 – 1058.

Sajona, F., Ballon, H., Maury, R., Pubellier, M., Cotten, J., & Rangin, C. (1994). Magmatic response to abrupt changes in geodynamic settings: Pliocene—Quaternary calc-alkaline and Nb-enriched lavas from Mindanao (Philippines). *Tectonophysics* , 47 - 72 .

Sen, C., & Dunn, T. (1994). Dehydration melting of a basaltic composition amphibolite at 1.5 and 2.0 GPa: implications for the origin of adakites. *Contributions to Mineralogy and Petrology* , 394 - 409.

Sláma, J. Košler, D.J. Condon, J.L. Crowley, A. Gerdes, J.M. Hanchar, M.S.A. Horstwood, G.A. Morris, L. Nasdala, N. Norberg, U. Schaltegger, B. Schoene, M.N. Tubrett, M.J. Whitehouse (2008). Plešovice zircon – a new natural reference material for U–Pb and Hf isotopic microanalysis. *Chemical Geology, 1 - 35.*

Song, S.G., Wang, M., Wang, C., & Niu, Y. (2016). Magmatism during continental collision, subduction, exhumation and mountain collapse in collisional orogenic belts and continental net growth: A perspective. *Science China Earth Sciences*, 1284 - 1304.

Soper, N.J., Webb, B.C. & Woodcock, N.H. 1987. Late Caledonian (Acadian) transpression in north-west England: timing, geometry and geotectonic significance. Proceedings of the Yorkshire Geological Society, 46, 175–192, https://doi.org/10.1144/pygs.46.3.175

Soper, N. J. (1988). Timing and geometry of collision, terrane accretion and sinistral strike-slip events in the British Caledonides. *Geological Society of London* , 481 - 492 .

Soper N.J., & Hutton. (1984). Late Caledonian Sinistral Displacements in Britain: Implications for a Three-Plate Collision Model. *Tectonics*.

Spray, J. G., & Williams, G. D. (1980). The Sub - ophiolite metamorphic rocks of the Ballantrae Igenous Complex, SW Scotland. *Journal of the Geological Society of London* , 359 - 368.

Stall, V. (2007). Pre-Carboniferous metallogeny of the Canadian Appalachians. *Geological Association of Canada, Special Publications*, 793 - 818.

Stephenson, D., Mendum, J.R., Fettes, D.J. & Leslie, A.G. (2013). The Dalradian rocks of Scotland: an introduction. *Proceedings of the Geologists Association,* 124, 3-82.

Stewart, M., & Strachan, R.A (1999). Structure and early kinematic history of the Great Glen Fault Zone, Scotland. *Tectonics* vol 18, pp 326 – 342

Stewart, M., Strachan. R. A, Martin, M. W & Holdsworth. R. E. (2001). Constraints on early sinistral displacements along the Great Glen Fault Zone, Scotland: structural setting, U–Pb geochronology and emplacement of the syn-tectonic Clunes tonalite. *Journal of the Geological Society*, 821-830.

Strachan, R. A., Holdsworth, R. E., Krabbendam, M. & Alsop, G. I. (2010). The Moine Supergroup of NW Scotland: insights into the analysis of polyorogenic supracrustal sequences. In: Law, R., Butler, R. W. H., Holdsworth, R. E., Krabbendam, M. & Strachan, R. A. (eds.) Continental tectonics and mountain building: the legacy of Peach and Horne. 2628 Geological Society, London, Special Publications, 335, 233-254.

Strachan, R. A & Evans. J. (2008). Structural setting and U-Pb zircon geochronology of the Glen Scaddle Metagabbro: evidence for polyphase Scandian ductile deformation in the Caledonides of northern Scotland. *Geological Magazine*, 361 - 371.

Strachan, R.A., Prave, A.R., Kirkland, C.L. & Storey, C.D. (2013). U–Pb detrital zircon geochronology of the Dalradian Supergroup, Shetland Islands, Scotland: Implications for regional correlations and Neoproterozoic–Palaeozoic basin

Tanner, P. W. G. (1996). Significance of the early fabric in the contact aureole of the 590 Ma Ben Vuirich Granite, Perthshire, Scotland. *Journal of Scottish Geology* , 20 - 212 .

Tiepolo, M., Oberti, R., & Vannucci, R. (2002). Trace-element incorporation in titanite: Constraints from experimentally determined solid/liquid partition coefficients. *Chemical Geology* , 103 – 117.

Underhill, J.R, & Brodie, J. A. (1993). Structural geology of Easter Ross, Scotland: implications for movement on the Great Glen fault zone. *Journal of the Geological Society*, 515 - 527.

Van-Hunen, J, & Allen, M. B. (2011). Continental collision and slab break-off: A comparison of 3-D numerical models with observations. *Earth and Planetary Science letters*.

Verdel, W. H. (2011). A Paleogene extensional arc flare-up in Iran. *Tectonics* , 1 - 16.

Walker, S., Thirlwall, M. F., Strachan, R. A., Bird, A. F. (2015). Evidence from Rb–Sr mineral ages for multiple orogenic events in the Caledonides of Shetland, Scotland. Journal of the Geological Society of London, 173, 489-503,

Wang, C., Deng, J., Bagas, L., & Wang, Q. (2017). Zircon Hf–isotopic mapping for understanding crustal architecture and metallogenesis in the Eastern Qinling Orogen. *Gondwana Research*, 293 - 310.

Wang, Q., Xu, J., Jian, P., Wei, Z., Zhao, Z., Li, C. Ma, J. (2005). Petrogenesis of Adakitic Porphyries in an Extensional Tectonic Setting, Dexing, South China: Implications for the Genesis of Porphyry Copper Mineralization. *Journal of Petrology* , 119 - 144.

Widdman, P., Davies, J. H. F. L & Schaltegger. (2019). Calibrating chemical abrasion: Its effects on zircon crystal structure, chemical composition and U-Pb age. *Chemical Geology* , 1 - 10 .

Wolf, M. B., Wylie, P. J. (1994). Dehydration-melting of amphibolite at 10 kbar: the effects of temperature and time. Contributinos to Mineralogy and Petrology. 369 – 383.

Woodcock, N. H., Soper, N. J & Miles, A. J. (2019). Age of the Acadian deformation and Devonian granites in northern England reviewed *Proceednigs of the Yorkshire Geological Society*, 62, 238 – 253.

Winter, J. D (2014). *An Introduction to Igneous and Metmorphic Petrology*. Prentice Hall.

Yogadzinski, G., Lees, J., Churikova, T., & Dorendorf, F. (2001). Geochemical evidence for the melting of subducting oceanic lithosphere at plate edges. *Nature*, 500 - 504.